ISBN: 978-81-688266-7-0

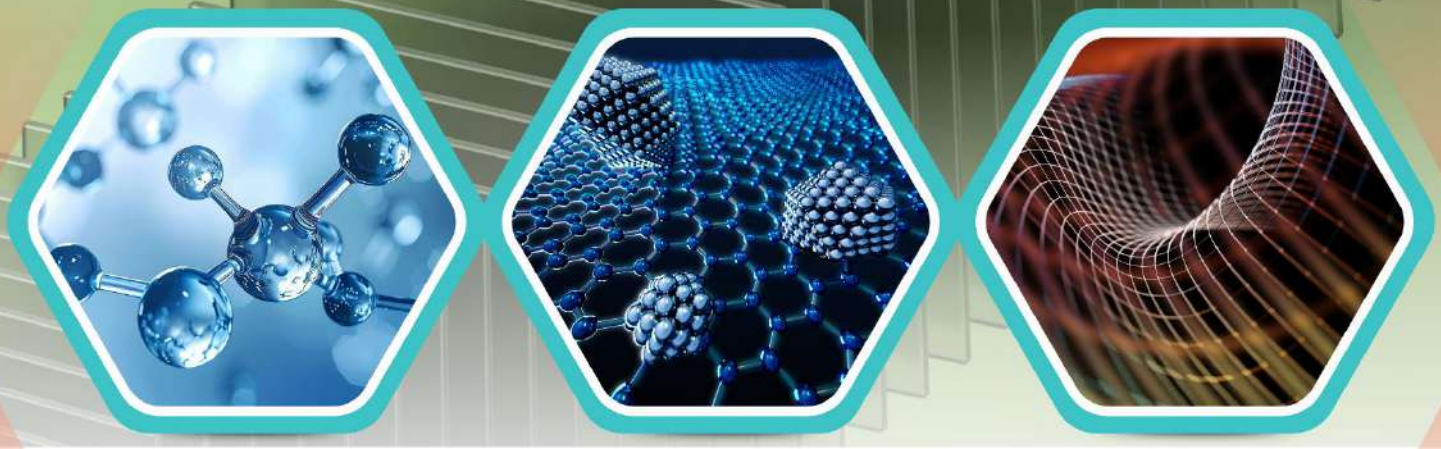

INNOVATIONS IN CHEMICAL AND MATERIALS SCIENCE

Editors:
Dr. Aarti Dwivedi
Ms. Pratiksha
Dr. Balasaheb Pathare
Dr. Satish Piplode

BHUMI PUBLISHING, INDIA
FIRST EDITION: JUNE 2026

Innovations in Chemical and Materials Science

(ISBN: 978-81-688266-7-0)

DOI: https://doi.org/10.5281/zenodo.21130971

Editors

Dr. Aarti Dwivedi

Department of Chemistry,

Amity University,

Gwalior, Madhya Pradesh

Ms. Pratiksha

Department of Chemistry,

Rajshree Group of Institutions,

Bareilly, Uttar Pradesh

Dr. Balasaheb Pathare

Department of Chemistry,

B. K. Birla College

(Empowered Autonomous), Kalyan, M.S.

Dr. Satish Piplode

Department of Chemistry,

SBS Government Post Graduate College,

Pipariya, Dist. Narmadapuram, M. P.

Bhumi Publishing

June 2026

Title: Innovations in Chemical and Materials Science

Editors: Dr. Aarti Dwivedi, Ms. Pratiksha, Dr. Balasaheb Pathare, Dr. Satish Piplode

First Edition: June 2026

ISBN: 978-81-688266-7-0

DOI: https://doi.org/10.5281/zenodo.21130971

Published by Bhumi Publishing,

a publishing unit of Bhumi Gramin Vikas Sanstha

Bhumi Publishing

Nigave Khalasa, Tal – Karveer, Dist – Kolhapur, Maharashtra, INDIA 416 207

E-mail: bhumipublishing@gmail.com

Disclaimer: The views expressed in the book are of the authors and not necessarily of the publisher and editors. Authors themselves are responsible for any kind of plagiarism found in their chapters and any related issues found with the book.

PREFACE

The rapid advancement of chemical and materials sciences has transformed the way we understand, design, and utilize substances that shape modern civilization. From sustainable chemical processes and advanced functional materials to nanotechnology, energy storage, environmental remediation, biomedical applications, and smart manufacturing, innovations in these disciplines continue to address some of the world's most pressing scientific and technological challenges. *Innovations in Chemical and Materials Science* presents a comprehensive collection of scholarly contributions that highlight recent developments, emerging trends, and practical applications across these dynamic fields.

This edited volume brings together the expertise of researchers, academicians, scientists, and industry professionals who have contributed original chapters covering diverse aspects of chemical synthesis, analytical techniques, polymer science, nanomaterials, green chemistry, catalysis, biomaterials, surface engineering, computational approaches, advanced characterization methods, and sustainable material development. Each chapter reflects current research, innovative methodologies, and interdisciplinary perspectives that promote scientific excellence and technological progress.

The primary objective of this book is to provide readers with an accessible yet comprehensive resource that bridges fundamental concepts with cutting-edge research. It encourages interdisciplinary collaboration by demonstrating how chemistry and materials science intersect with engineering, environmental science, medicine, agriculture, energy, and industrial technology. The diverse topics presented within this volume emphasize the importance of innovation in developing efficient, sustainable, and economically viable solutions for contemporary global challenges.

The editors sincerely appreciate the dedicated efforts of all contributing authors, reviewers, and members of the editorial and publishing teams whose commitment and expertise have made this publication possible. Their valuable contributions have significantly enhanced the scientific quality and relevance of this volume.

We hope this book serves as a valuable reference for students, researchers, educators, scientists, engineers, industry professionals, and policymakers. It is our belief that the knowledge presented in these chapters will stimulate intellectual curiosity, inspire innovative research, strengthen interdisciplinary partnerships, and contribute meaningfully to the continued advancement of chemical and materials sciences for the benefit of academia, industry, society, and future generations.

- Editors

TABLE OF CONTENT

Innovations in Chemical and Materials Science
(ISBN: 978-81-688266-7-0)

DEVELOPMENT AND ANTIFUNGAL ASSESSMENT OF SCHIFF BASES BASED ON 2-FORMYLPHENOXY ACETIC ACID

Sewati Patel* and Manisha Masih Singh
School of Pharmacy, Chouksey Engineering College, Bilaspur, Chhattisgarh-495001
*Corresponding author E-mail: mannoratre94@gmail.com

Abstract
Schiff bases are an important class of bioactive compounds possessing diverse pharmacological properties, including antimicrobial, antifungal, anticancer, anti-inflammatory, and antiviral activities. The present study focuses on the synthesis, characterization, and antifungal evaluation of a series of Schiff bases derived from 2-formylphenoxy acetic acid and various aromatic amines. Five Schiff base derivatives (V1–V5) and their corresponding reduced analogs (V1R–V5R) were synthesized and characterized using Thin Layer Chromatography (TLC), UV-Visible spectroscopy, Fourier Transform Infrared Spectroscopy (FTIR), and Nuclear Magnetic Resonance (NMR) spectroscopy. The antifungal potential was assessed against *Candida albicans* and *Aspergillus niger* using disc diffusion and broth dilution methods. Among the synthesized compounds, the 4-hydroxy substituted Schiff base (V3) exhibited the highest antifungal activity with inhibition zones of 18.5 ± 0.7 mm and 16.8 ± 0.4 mm against C. albicans and A. niger, respectively. The minimum inhibitory concentration (MIC) values further confirmed its superior potency. Structure–activity relationship analysis revealed that the azomethine (C=N) linkage and electron-donating substituents significantly contribute to antifungal activity.

Keywords: Schiff Bases, 2-Formylphenoxy Acetic Acid, Antifungal Activity, Candida Albicans, *Aspergillus niger*, Structure–Activity Relationship.

1. Introduction

Fungal infections have emerged as a significant global health concern due to the increasing prevalence of immunocompromised patients, prolonged antibiotic therapy, and the development of resistance against conventional antifungal agents. Opportunistic fungal pathogens such as *Candida albicans* and *Aspergillus niger* are responsible for a wide range of superficial and systemic infections. Therefore, the development of novel antifungal agents with improved efficacy and safety profiles remains an important area of pharmaceutical research.

Schiff bases, characterized by the presence of an azomethine (-CH=N-) group, represent a versatile class of compounds synthesized through the condensation of primary amines with aldehydes or ketones. These compounds have attracted considerable attention because of their broad spectrum of biological activities and ease of synthesis. The azomethine linkage plays a crucial role in enhancing lipophilicity and facilitating interactions with biological targets.

2-Formylphenoxy acetic acid is a valuable synthetic intermediate containing both aldehyde and carboxylic acid functionalities, enabling the generation of structurally diverse Schiff base derivatives. Modifications through the introduction of electron-donating and electron-withdrawing substituents can significantly influence biological activity. Therefore, the present investigation was designed to synthesize Schiff bases derived from 2-formylphenoxy acetic acid, characterize them using spectroscopic techniques, and evaluate their antifungal potential.

2. Materials and Methods

2.1 Objectives

- To synthesize 2-formylphenoxy acetic acid.
- To prepare Schiff base derivatives using different aromatic amines.
- To synthesize reduced Schiff base analogs.
- To characterize the synthesized compounds using TLC, UV-Vis, FTIR, and NMR spectroscopy.
- To evaluate antifungal activity against *Candida albicans* and *Aspergillus niger*.
- To establish structure–activity relationships among synthesized derivatives.

2.2 Chemistry

2.2.1 Synthesis of 2-Formylphenoxy Acetic Acid

2-Formylphenoxy acetic acid was synthesized by reacting salicylaldehyde with monochloroacetic acid under alkaline conditions using sodium hydroxide as the base. The reaction proceeded through nucleophilic substitution to afford the desired product as a white crystalline solid.

Table 1: Synthesis of 2-Formylphenoxy Acetic Acid

Starting Materials	Conditions	Product	Yield (%)	Melting Point
Salicylaldehyde + Monochloroacetic acid	NaOH, stirring	2-Formylphenoxy acetic acid	83	126°C

2.2.2 Synthesis of Schiff Bases (V1–V5)

The synthesized aldehyde was condensed with different aromatic amines in methanol at room temperature for 3 h.

Table 2: Synthesized Schiff Bases

Compound	Amine Used	Yield (%)	Melting Point
V1	Aniline	76	132°C
V2	p-Toluidine	90	216°C
V3	p-Aminophenol	83	236°C
V4	p-Anisidine	87	135°C
V5	p-Chloroaniline	59	86°C

2.2.3 Synthesis of Reduced Schiff Bases (V1R–V5R)

Reduction of the azomethine bond was achieved using sodium borohydride under reflux conditions.

Table 3: Reduced Schiff Bases

Compound	Reducing Agent	Yield (%)	Melting Point
V1R	NaBH4	80	201°C
V2R	NaBH4	52	-
V3R	NaBH4	74	-
V4R	NaBH4	-	-
V5R	NaBH4	-	-

2.3 Characterization Studies

2.3.1 Thin Layer Chromatography

TLC analysis was performed using Ethyl Acetate:Hexane (7:3) as the mobile phase.

Table 4: TLC Analysis

Compound	Rf Value
V1	0.62
V2	0.58
V3	0.60
V4	0.65
V5	0.55
V1R–V5R	0.40–0.50

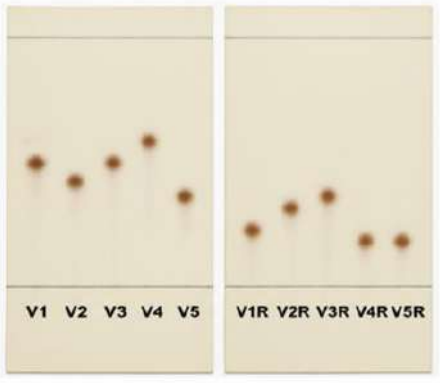

Figure 1: TLC Analysis

Schiff bases exhibited single spots indicating purity. Reduced derivatives showed lower Rf values due to increased polarity after conversion of the azomethine bond to an amine linkage.

2.3.2 UV-Visible Spectroscopy

The UV spectra demonstrated characteristic electronic transitions associated with aromatic and azomethine chromophores.

Table 5: Major Absorption Bands

λmax (nm)	Assignment
~265	π→π* transition of aromatic rings
~310	n→π* transition of azomethine group
~340	Extended conjugation

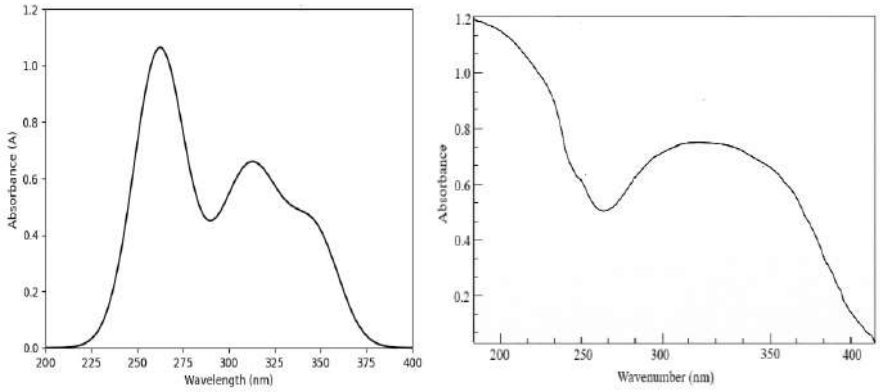

Figure 2: Major Absorption Bands (2-(4-Methyoxy phenylimino methyl) phenoxy acetic acid & 2-(4-Hydroxy phenylamino methyl) phenoxy acetic acid)

The presence of the 310 nm band confirmed Schiff base formation through the azomethine linkage.

2.3.3 FTIR Spectroscopy

FTIR spectra confirmed the formation of Schiff bases through the appearance of characteristic azomethine stretching vibrations.

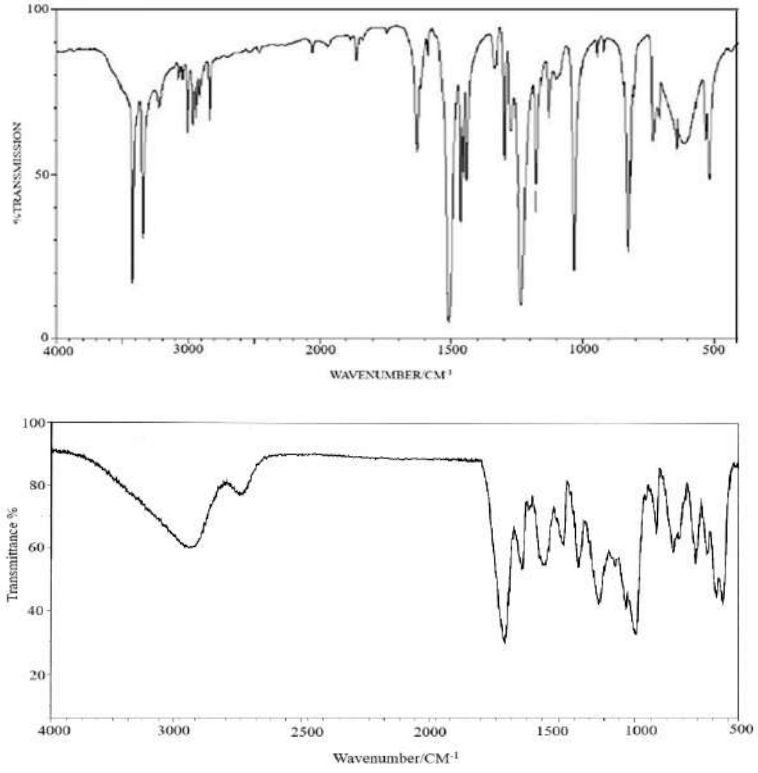

Figure 3: Important FTIR Signals (2-(4-Methyoxy phenylimino methyl) phenoxy acetic acid & 2-(4-Hydroxy phenylamino methyl) phenoxy acetic acid)

Table 6: Important FTIR Signals

Functional Group	Frequency (cm^{-1})
O–H (COOH)	3400–2500
C=O	~1700
C=N	~1615
Aromatic C=C	1580–1500
C–O–C	1210–1150

The characteristic C=N stretching band around 1615 cm^{-1} confirmed successful Schiff base synthesis.

2.3.4 NMR Spectroscopy

^{1}H NMR

Characteristic signals observed:

- COOH proton: ~11 ppm
- Azomethine proton: ~8.4 ppm
- Aromatic protons: 6.8–7.4 ppm
- O–CH_2 protons: ~4.5 ppm
- OCH_3 protons: ~3.8 ppm

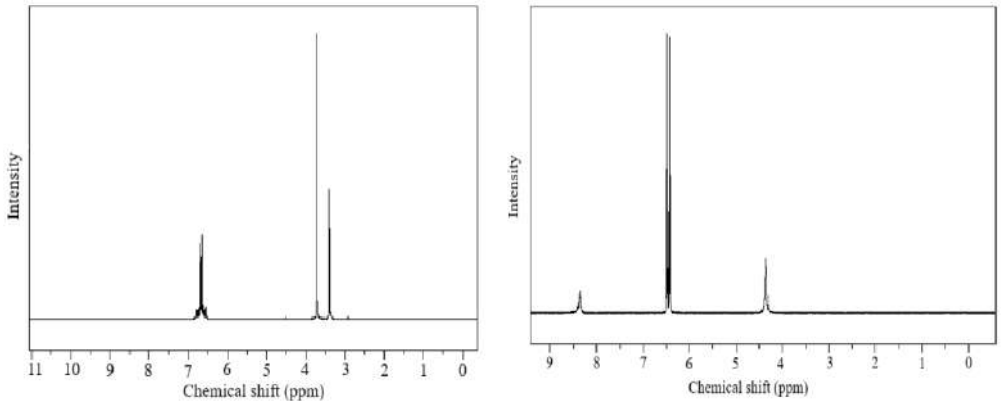

Figure 4a: ^{1}H NMR ^{13}C NMR

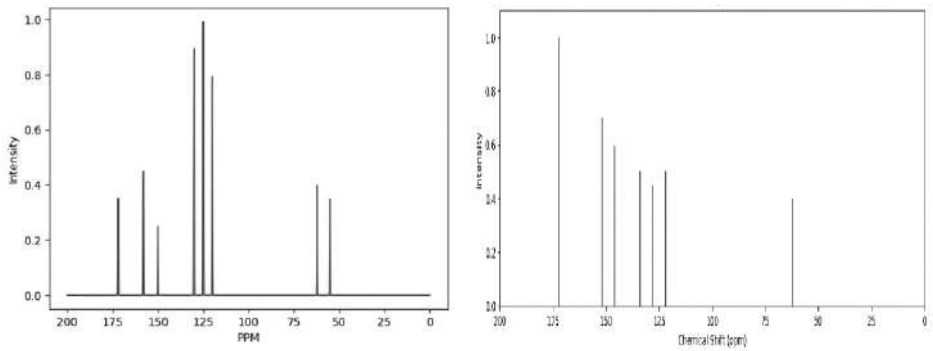

Figure 4b: ^{13}C NMR

Key carbon signals included:

- Carbonyl carbon: ~172 ppm
- Imine carbon: ~158 ppm
- Aromatic oxygenated carbon: ~152 ppm
- OCH_3 carbon: ~55 ppm

These observations confirmed the proposed structures of synthesized compounds.

2.4 Antifungal Evaluation

2.4.1 Disc Diffusion Assay

The antifungal activity was evaluated against *Candida albicans* and *Aspergillus niger*.

Table 7: Zone of Inhibition (mm)

Compound	*C. albicans*	*A. niger*
V1	14.2 ± 0.8	12.5 ± 0.6
V2	16.0 ± 0.5	14.3 ± 0.7
V3	18.5 ± 0.7	16.8 ± 0.4
V4	17.2 ± 0.6	15.0 ± 0.5
V5	15.8 ± 0.4	13.2 ± 0.8
V1R	10.5 ± 0.3	9.0 ± 0.5
V2R	11.2 ± 0.6	10.1 ± 0.4
V3R	13.0 ± 0.5	11.8 ± 0.6
V4R	12.4 ± 0.7	10.5 ± 0.3
V5R	11.8 ± 0.4	9.8 ± 0.7
Standard	22.0 ± 1.0	20.5 ± 0.9

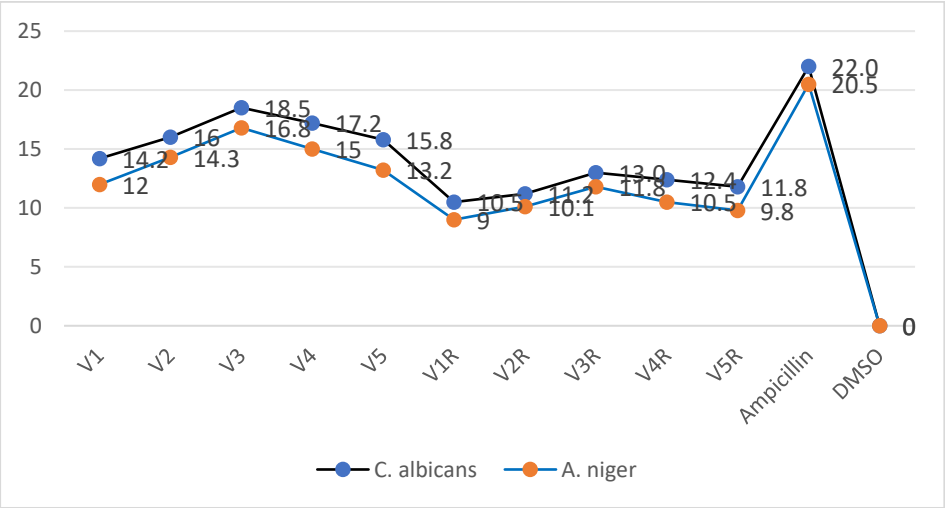

Figure 5: Disc Diffusion Assay (Zone of Inhibition in mm)

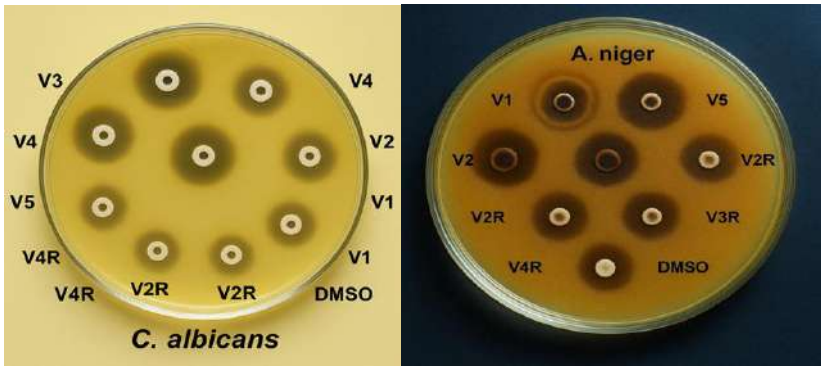

Figure 6: Zone of Inhibition (mm)

The Schiff bases exhibited significant antifungal activity compared with their reduced analogs. V3 demonstrated the highest activity among all derivatives.

2.4.2 Minimum Inhibitory Concentration (MIC)

Table 8: MIC Values (µg/mL)

Compound	*C. albicans*	*A. niger*
V1	32	64
V2	16	32
V3	8	16
V4	16	32
V5	32	64
V1R	128	256
V2R	64	128
V3R	32	64
V4R	64	128
V5R	128	256

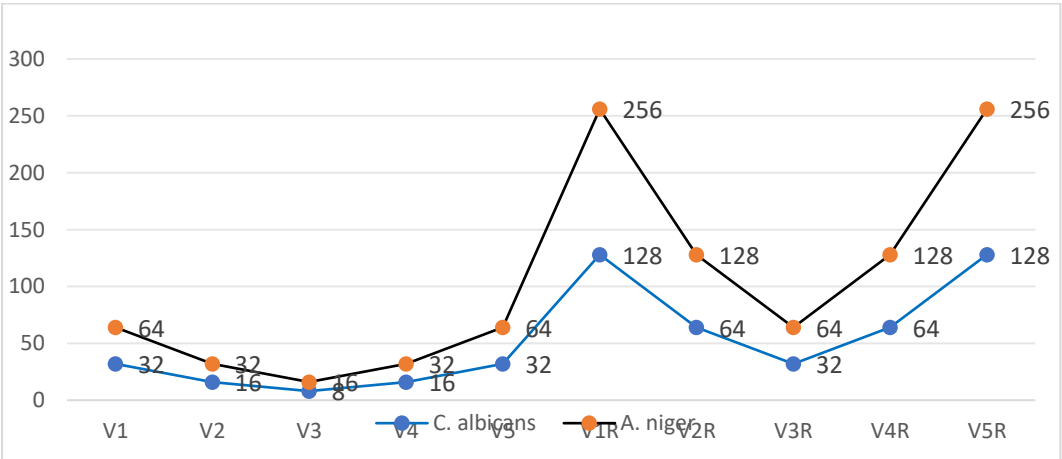

Figure 7a: Broth Dilution Assay (MIC in µg/mL)

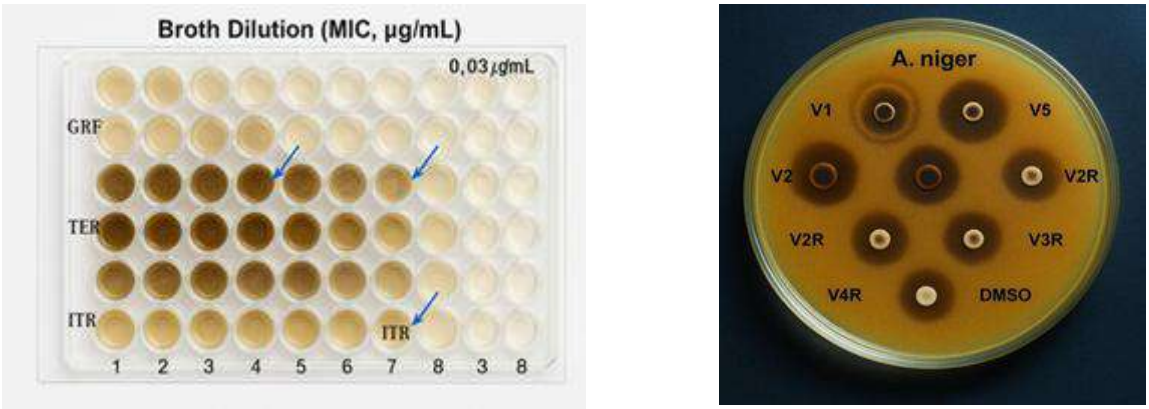

Figure 7b: Broth Dilution Assay

The lowest MIC value was observed for V3 against C. albicans (8 µg/mL), indicating excellent antifungal potency. Reduced analogs required substantially higher concentrations, demonstrating diminished activity.

2.5 Structure–Activity Relationship (SAR)

The antifungal activity of synthesized compounds was strongly influenced by the nature of substituents and the presence of the azomethine linkage.

Effect of Azomethine Group

The C=N functionality was essential for antifungal activity. Reduction of the azomethine bond led to a marked decrease in potency.

Table 9: Effect of Substituents

Compound	Substituent	Activity
V3	–OH	Highest
V4	$–OCH_3$	High
V2	$–CH_3$	Moderate
V1	H	Moderate
V5	–Cl	Lower

Proposed Activity Order

V3 > V4 > V2 > V5 > V1 > Reduced Derivatives

The hydroxyl group likely enhances interaction with fungal enzymes through hydrogen bonding, whereas electron-donating groups improve electronic delocalization and biological activity.

Conclusion

The present investigation successfully demonstrated the design, synthesis, characterization, and antifungal evaluation of a novel series of Schiff base derivatives based on 2-formylphenoxy acetic acid. The synthetic approach employed was straightforward, economical, and yielded the desired compounds in good to excellent yields. Subsequent reduction of the azomethine linkage generated the corresponding amine derivatives, enabling a comparative assessment of the importance of the Schiff base functionality in antifungal activity.

The synthesized compounds were comprehensively characterized using TLC, UV-Visible spectroscopy, FTIR spectroscopy, and NMR spectroscopy. Spectroscopic analyses confirmed the successful formation of the Schiff bases through the appearance of characteristic azomethine (–CH=N–) signals and the expected functional group absorptions. The purity of all synthesized compounds was verified through TLC studies, while UV, FTIR, and NMR data supported the proposed molecular structures.

Biological evaluation revealed that the Schiff base derivatives exhibited significant antifungal activity against both *Candida albicans* and *Aspergillus niger*. Among all synthesized compounds, the p-hydroxy substituted derivative (V3) demonstrated the highest antifungal efficacy, producing the largest zones of inhibition and the lowest MIC values. The enhanced activity of V3 may be attributed to the presence of the hydroxyl group, which can facilitate stronger hydrogen-bonding interactions with fungal cellular targets and improve overall molecular binding affinity.

Structure–Activity Relationship (SAR) analysis highlighted several important findings. The azomethine (C=N) linkage was found to be a critical pharmacophoric feature responsible for antifungal activity. Reduction of this linkage to the corresponding amine significantly decreased antifungal potency, indicating the importance of conjugation and electron delocalization provided by the Schiff base moiety. Furthermore, electron-donating substituents such as hydroxyl and methoxy groups enhanced antifungal activity, whereas electron-withdrawing substituents such as chlorine resulted in comparatively lower activity.

The results suggest that Schiff bases derived from 2-formylphenoxy acetic acid possess promising antifungal potential and may serve as valuable lead molecules for the development of new antifungal agents. Future studies should focus on molecular docking, mechanism of action studies, toxicity evaluation, pharmacokinetic profiling, and in vivo antifungal investigations to further establish their therapeutic potential. Structural optimization through rational modification of the aromatic substituents may also contribute to the discovery of more potent antifungal candidates.

Overall, the study establishes a strong correlation between chemical structure and antifungal activity and provides a foundation for further medicinal chemistry research involving phenoxy acetic acid-based Schiff base derivatives.

Acknowledgement

Authors extends their sincere gratitude to the School of Pharmacy, Chouksey Engineering College, Bilaspur, Chhattisgarh, for their invaluable support and facilities throughout this research. Author deeply thankful to research guide for their expert guidance and constant encouragement.

References

1. Carey, F. A., & Sundberg, R. J. (2007). *Advanced organic chemistry: Part B—Reactions and synthesis* (5th ed.). Springer.
2. Schiff, H. (1864). Mittheilungen aus dem Universitätslaboratorium in Pisa: Eine neue Reihe organischer Basen. *Justus Liebigs Annalen der Chemie, 131*, 118–119.
3. da Silva, C. M., da Silva, D. L., Modolo, L. V., Alves, R. B., de Resende, M. A., Martins, C. V. B., & de Fátima, A. (2011). Schiff bases: A short review of their antimicrobial activities. *Journal of Advanced Research, 2*(1), 1–8.
4. Singh, K., Barwa, M. S., & Tyagi, P. (2006). Synthesis, characterization and biological studies of Schiff bases. *European Journal of Medicinal Chemistry, 41*(1), 147–153.
5. Jarrahpour, A., Motamedifar, M., Pakshir, K., Hadi, N., & Zarei, M. (2004). Synthesis of novel azo Schiff bases and their antibacterial and antifungal activities. *Molecules, 9*(10), 815–824.
6. Pandeya, S. N., Sriram, D., Nath, G., & De Clercq, E. (1999). Synthesis, antibacterial, antifungal and anti-HIV activities of Schiff bases. *Il Farmaco, 54*(9), 624–628.
7. Panneerselvam, P., Nair, R. R., Vijayalakshmi, G., Subramanian, E. H., & Sridhar, S. K. (2005). Synthesis and antimicrobial activity of Schiff bases. *European Journal of Medicinal Chemistry, 40*(2), 225–229.
8. Dhar, D. N., & Taploo, C. L. (1982). Schiff bases and their applications. *Journal of Scientific and Industrial Research, 41*, 501–506.
9. Bringmann, G., Dreyer, M., Faber, J. H., *et al.* (2005). Ancistrotanzanine and related Schiff base derivatives as biologically active compounds. *Journal of Medicinal Chemistry, 48*, 6112–6114.
10. El-Masry, A. H., Fahmy, H. H., & Abdelwahed, S. H. (2000). Synthesis and antimicrobial activity of some Schiff base derivatives. *Molecules, 5*, 1429–1438.
11. Karthikeyan, M. S., Prasad, D. J., Poojary, B., Bhat, K. S., Holla, B. S., & Kumari, N. S. (2006). Synthesis and biological activity of Schiff and Mannich bases. *Bioorganic & Medicinal Chemistry, 14*, 7482–7489.
12. Guo, Z., Xing, R., Liu, S., *et al.* (2007). Antifungal properties of Schiff base derivatives and their mechanism of action. *Carbohydrate Research, 342*, 1329–1332.
13. Walsh, T. J., & Dixon, D. M. (1996). Deep mycoses and emerging fungal infections. *Clinical Microbiology Reviews, 9*(1), 1–25.
14. Clinical and Laboratory Standards Institute. (2022). *Reference method for broth dilution antifungal susceptibility testing of yeasts* (M27, 5th ed.).
15. Clinical and Laboratory Standards Institute. (2022). *Reference method for broth dilution antifungal susceptibility testing of filamentous fungi* (M38, 3rd ed.).

16. Pelczar, M. J., Chan, E. C. S., & Krieg, N. R. (2010). *Microbiology* (5th ed.). McGraw-Hill Education.
17. Murray, P. R., Rosenthal, K. S., & Pfaller, M. A. (2020). *Medical microbiology* (9th ed.). Elsevier.
18. Silverstein, R. M., Webster, F. X., Kiemle, D. J., & Bryce, D. L. (2014). *Spectrometric identification of organic compounds* (8th ed.). Wiley.
19. Pavia, D. L., Lampman, G. M., Kriz, G. S., & Vyvyan, J. R. (2015). *Introduction to spectroscopy* (5th ed.). Cengage Learning.
20. Furniss, B. S., Hannaford, A. J., Smith, P. W. G., & Tatchell, A. R. (2013). *Vogel's textbook of practical organic chemistry* (5th ed.). Pearson Education.
21. Patrick, G. L. (2021). *An introduction to medicinal chemistry* (7th ed.). Oxford University Press.
22. Beale, J. M., & Block, J. H. (2019). *Foye's principles of medicinal chemistry* (8th ed.). Wolters Kluwer.
23. Lemke, T. L., Williams, D. A., Roche, V. F., & Zito, S. W. (2018). *Wilson and Gisvold's textbook of organic medicinal and pharmaceutical chemistry* (13th ed.). Lippincott Williams & Wilkins.
24. Rang, H. P., Ritter, J. M., Flower, R. J., & Henderson, G. (2021). *Rang & Dale's pharmacology* (10th ed.). Elsevier.
25. Goodman, L. S., Brunton, L. L., Hilal-Dandan, R., & Knollmann, B. C. (2023). *Goodman & Gilman's the pharmacological basis of therapeutics* (14th ed.). McGraw-Hill.

Bhumi Publishing, India
June 2026

GREEN SYNTHESIS OF METAL NANOPARTICLES: PRINCIPLES, MECHANISMS, CHARACTERIZATION, AND APPLICATIONS

Niladry Sekhar Ghosh*[1], Mamta Kumari[2] and Anubhav Dubey[3]

[1]Faculty of Pharmaceutical Science, Assam down town University, Guwahati

[2]Harcourt Butler Technical University, Kanpur

[3]Department of Pharmacology, Maharana Pratap college of Pharmacy, Kanpur

*Corresponding author E-mail: niladry_chem@yahoo.co.in

Abstract

The green synthesis of metal nanoparticles has been developed as a sustainable and environment-friendly alternative to the traditional physical and chemical methods of nanoparticle synthesis. The escalating need for nanomaterials in biomedical, environmental, agricultural and industrial applications has resulted in the development of green synthesis strategies that minimize the usage of harmful chemicals and energy-intensive procedures. Green synthesis is applied for the creation of metal nanoparticles using biological resources such as plant extracts, bacteria, algae, fungi and naturally occurring biomolecules as reducing and stabilizing agents . These biological entities contain several phytochemicals and metabolites such as flavonoids, phenolics, alkaloids, proteins and polysaccharides that contribute to the reduction of metal ions into stable nanoparticles. Normally, the synthesis process includes nucleation, growth and stabilization stages leading to nanoparticles with controlled size, shape and surface features. The physicochemical properties of synthesized nanoparticles were characterized by various techniques including UV-Visible spectroscopy, Fourier Transform Infrared Spectroscopy (FTIR), X-ray Diffraction (XRD), Scanning Electron Microscopy (SEM), Transmission Electron Microscopy (TEM), Dynamic Light Scattering (DLS), and zeta potential analysis. Green synthesis of metal nanoparticles exhibits excellent biological activity like antibacterial, antioxidant, anti-inflammatory, and anticancer capabilities which make them ideal candidates for drug transport, diagnostics, wound healing, and therapeutic applications. They also greatly contribute to cleaning up the environment, treating wastewater, catalysis, and boosting agriculture. Green nanotechnology is a promising topic making progress despite issues with reproducibility, standardization and big scale production. This strategy promotes sustainable development, combining nanotechnology and green chemistry principles to deliver safer and more efficient solutions for future scientific and industrial applications.

Keywords: Green Synthesis, Metal Nanoparticles, Nanotechnology, Plant-Mediated Synthesis, Characterization, Nanomedicine, Antimicrobial Activity, Green Chemistry, Biomedical Applications, Sustainable Nanotechnology.

Introduction

Nanotechnology is a fast-growing discipline of science and technology that deals with the design, production, characterization and application of materials in the size range of 1 to 100 nm [1]. Nanoparticles possess unique physical, chemical, optical, electrical and biological capabilities arising from their large surface-area-to-volume ratio and quantum confinement effects. Metal nanoparticles such as silver (Ag), gold (Au), platinum (Pt), palladium (Pd), copper (Cu), zinc oxide (ZnO) and titanium dioxide (TiO2) have attracted a lot of attention owing to their wide applications in medicine, electronics, catalysis, environmental remediation and agriculture [2]. The conventional routes for synthesizing nanoparticles such as physical and chemical procedures, usually need toxic substances, significant energy consumption and expensive instrumentation. Such techniques can produce dangerous by-products, harmful to human health and the environment. To circumvent these restrictions, green synthesis has been developed and is an eco-friendly, cost-effective and sustainable alternative [3]. Green synthesis employs biological resources, such as plants, bacteria, fungi, algae, and proteins, to convert metal ions to nanoparticles under mild reaction conditions. The procedure is in accordance with the principles of green chemistry as it minimizes the harmful compounds, reduces the energy requirements and promotes the sustainability of the environment [4].

Principles of Green Synthesis of Metal Nanoparticles

Today a new page opens in the history of chemistry associated with the emergence of a new integrated scientific path “green” chemistry. Interdisciplinary is the field of green chemistry. There is an integration of synthetic organic chemistry with analytical chemistry, physical chemistry, toxicity, microbiology and biotechnology and engineering [5]. “Green” chemistry is working on developing technologies that make chemical reactions more efficient. “Green” chemistry attempts to prevent pollution at the very beginning of the planning and implementation of chemical processes and includes all types and features of chemical processes to minimize the environmental risks. The issues in the sphere of competence of “green” chemistry can be divided into two main directions. The first concerns the treatment and use of hazardous environmental waste and by-products of the chemical industry. The second and more promising approach is the development of innovative industrial processes that avoid or decrease the manufacture and usage of hazardous products [6]. The “green” chemistry allows to extract the necessary chemical in the safest method possible. It is the choice of raw materials and process schemes, which, as a rule, do not involve harmful substances, toxic and dangerous chemicals, and is directed at industrial processes that do not pollute the environment and place responsibility for the products on the scientists and manufacturers [7].

The scientific area of “green” chemistry began in the United States in the 1990s. European countries have adopted the most advanced legislation on “green” technologies. In recent years

novel reaction schemes and procedures have been created, aiming at dramatically reducing the burden of chemical production on the environment, to decrease the processing and utilization of hazardous substances and damaging by-products [8]. “Green” chemistry already includes three big directions: novel means of synthesis (catalysts usage); substitution of typical organic solvents (in particular, the use of supercritical CO2); renewable source reagents (i.e. non-petroleum products) [9].

In “green” chemistry fundamentally new conceptions are used such as “ideal process”, “ideal product” and “ideal consumer” [10]. The ideal process is a simple, environmentally friendly, single-stage process, effective at the molecular level, using renewable raw materials, which gives maximum yield. The ideal product is one that takes a minimum of energy and packaging, safe, recyclable and totally degradable by microorganisms [11]. The main focus is the process of production and the finished product. The consumer is missing in the scheme. The image of the “ideal consumer” is evident in “green” chemistry, that is, he uses a limited number of items, appreciates the need to maintain the environment. “Green” chemistry has opened up new research fields and new terms: “atom efficiency”, “innate safety”, “product life cycle analysis”, “ionic liquid”, “renewable energy”, “environmental efficiency”, “process intensification and integration”, etc [13].

This review is directed to study of current scientific research of eco-friendly “green” production methods of magnetic and metal nanoparticles. The “green” nanoparticles have been widely applied in the fields of antimicrobials, photocatalysts and adsorbents [15]. “Green” magnetic nanoparticles are characterized by low toxicity and great biocompatibility, which opens up broad possibilities for their use in medicine, particularly for targeted drug delivery, contrast imaging and magnetic hyperthermia applications. The structure and morphology of synthesized magnetic nanoparticles can be characterized by scanning electron microscopy, transmission electron microscopy, energy-dispersive analysis, X-ray diffraction analysis, X-ray photoelectron spectroscopy, FTIR spectroscopy and Raman spectroscopy and magnetic force microscopy. Magnetic force microscopy (MFM) is a scatter-sensitive technique with a resolution up to 10 nm which can detect weak magnetic field [17]. MFM is a global approach for the investigation of magnetic nanoparticles because low requirements for sample preparation and the ability to function in air, vacuum or liquid medium [18]. This makes MFM a strong technique for imaging of magnetic NPs, describing their size and morphology. For the case of superparamagnetic nanoparticles, MFM has proved particularly useful to determine magnetic moment, magnetic anisotropy, magnetization curves and the effect of aggregation in the particles [19]. Many studies [20] are concerned with the detection of superparamagnetic and low-coercive magnetic nanoparticles using MFM and the interpretation of the acquired MFM pictures. In Ref. [21], Torre *et al.* showed that magnetic force microscopy (MFM) can be used to characterize magnetic

textures at ambient temperature. MFM experiments were performed on iron oxide magnetic nanoparticles having a diameter of 11 nm. Images obtained for nanofilms deposited on the substrate showed linear magnetic chains of nanoparticles of several hundred nanometers. In a study [22], the magnetization of individual magnetic NPs was assessed using MFM. Cordova *et al.* [23] studied superparamagnetic iron oxide NPs in air, liquid medium and inside thin polymer sheets using MFM. The authors in work [24] employed MFM to evaluate the magnetite NPs with varying sizes (from 10 nm to 100 nm) implanted in polymer films with different thicknesses. Therefore, MFM allows to quantify the magnetic characteristics of single nanoparticles as well as nanoparticles embedded in nonmagnetic matrices (e.g. polymers).

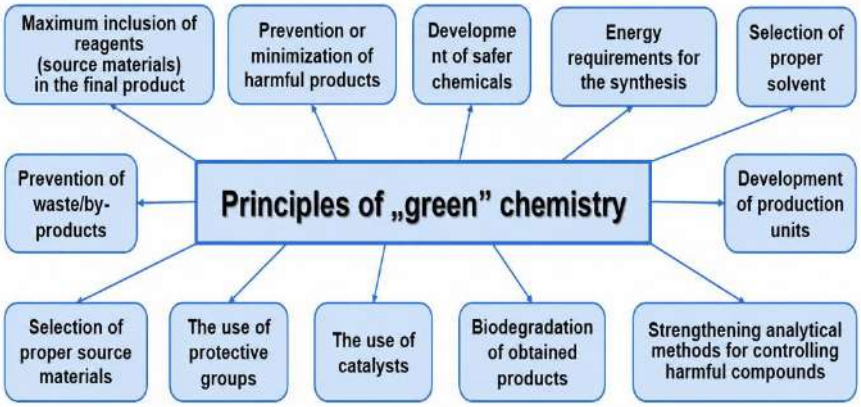

Figure 1: Principles of "green" chemistry [23]

Green synthesis relies on the principle of employing natural reducing and stabilizing agents that are sourced from biological systems. The process has three major components:[25]

Selection of Biological Source

Various biological entities can serve as reducing agents:

- Plant extracts
- Bacteria
- Fungi
- Algae
- Yeast
- Biomolecules such as proteins, enzymes, polysaccharides, and flavonoids

The plant-mediated synthesis is quite popular due to its simplicity, rapidity, and no need of maintenance of microbial cultures [26].

Reduction of Metal Ions

Plant extracts are sources of phytochemicals that convert metal salts such as silver nitrate ($AgNO_3$), chloroauric acid ($HAuCl_4$), zinc acetate and copper sulfate to their respective nanoparticles [28].

Examples of phytochemicals include:

- Phenolic compounds
- Flavonoids
- Alkaloids
- Terpenoids
- Proteins
- Tannins
- Sugars

Stabilization of Nanoparticles

Nanoparticles have high surface energy and tend to agglomerate after reduction. Natural chemicals from the biological extracts work as capping agents that prevent aggregation and enhance stability [29].

Mechanism of Green Synthesis

The exact technique depends on the biological source employed but the overall procedure requires three stages:

Activation Phase

Metal ions present in solution interact with biomolecules [30].

Example:

$$\mathbf{Ag^{+} + Reducing\ agent \rightarrow Ag^{0}}$$

During this phase, nucleation occurs, leading to the formation of small nanoparticle seeds.

Growth Phase

The reduced metal atoms combine and develop into nanoparticles.

Growth is influenced by:

- Temperature
- pH
- Concentration of metal precursor
- Concentration of plant extract
- Reaction time

Termination Phase

Growth ceases when nanoparticles reach stable dimensions.

Biomolecules adsorb onto the nanoparticle surface, providing stabilization and preventing further aggregation [31].

Biological Sources for Green Synthesis [32]

Plant-Mediated Synthesis

Plant extracts are rich in bioactive chemicals that can reduce metal ions.

Common plants are: *Azedarach indica* (Neem), *Ocimum sanctum* (Tulsi), *Aloe vera*, *Moringa oleifera* and *Camellia sinensis* (Green tea)

Advantages:

- Rapid synthesis
- Cost-effective
- Large-scale production
- No need for aseptic conditions

Bacterial Synthesis

Bacteria can produce nanoparticles either intracellularly or extracellularly.

Examples:

- *Bacillus subtilis*
- *Pseudomonas aeruginosa*
- *Escherichia coli*

Advantages:

- Controlled particle size
- High reproducibility

Fungal Synthesis

Fungi produce large quantities of enzymes and proteins that facilitate nanoparticle synthesis [33].

Examples:

- *Aspergillus niger*
- *Fusarium oxysporum*
- *Penicillium* species

Advantages:

- High metal tolerance
- Large biomass production

Algal Synthesis

Marine and freshwater algae contain polysaccharides and pigments that aid nanoparticle synthesis [34].

Examples:

- *Sargassum species*
- *Chlorella vulgaris*
- *Spirulina platensis*

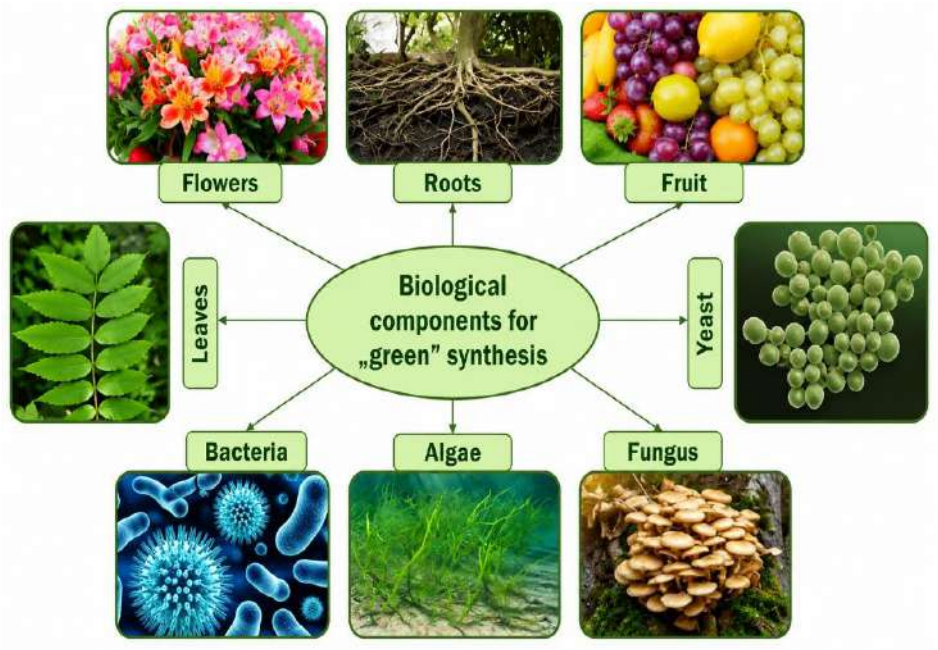

Figure 2: Various natural resources used for the synthesis of "green" nanoparticles [35]

Factors Affecting Green Synthesis

pH

pH significantly influences nanoparticle morphology and size.

- Acidic pH → larger particles
- Alkaline pH → smaller particles

Temperature

Increasing temperature generally:

- Accelerates reduction rate
- Enhances nucleation
- Produces smaller nanoparticles

Metal Ion Concentration

Higher precursor concentration may increase particle size and aggregation.

Reaction Time

Extended reaction times can influence nanoparticle growth and morphology. Extract ConcentrationHigher concentrations of reducing agents promote faster reduction and improved stabilization [37].

Characterization of Green-Synthesized Nanoparticles

Characterization is essential to determine particle size, morphology, crystallinity, and stability [38].

Table 1: Characterization of green-synthesized nanoparticles [39]

Characterization Technique	Principle	Information Obtained	Significance
UV–Visible Spectroscopy (UV–Vis)	Measures absorption of light by nanoparticles at specific wavelengths	Surface plasmon resonance (SPR), nanoparticle formation, stability	Confirms synthesis and monitors reaction progress
Fourier Transform Infrared Spectroscopy (FTIR)	Detects vibrational frequencies of functional groups	Identification of biomolecules acting as reducing and capping agents	Confirms involvement of plant metabolites in nanoparticle synthesis
X-ray Diffraction (XRD)	Diffraction of X-rays by crystalline structures	Crystal structure, phase purity, crystallite size	Determines crystalline nature of nanoparticles
Scanning Electron Microscopy (SEM)	Electron beam scans the sample surface	Surface morphology, shape, particle distribution	Reveals external morphology of nanoparticles
Transmission Electron Microscopy (TEM)	Transmission of electrons through a thin sample	Particle size, shape, internal structure	Provides high-resolution images and size analysis
Dynamic Light Scattering (DLS)	Measures fluctuations in scattered light	Hydrodynamic diameter, particle size distribution	Evaluates nanoparticle dispersion in solution
Zeta Potential Analysis	Measures surface charge of nanoparticles	Surface charge and colloidal stability	Predicts nanoparticle stability and aggregation behavior
Energy Dispersive X-ray Spectroscopy (EDX/EDS)	Detects characteristic X-rays emitted by elements	Elemental composition and purity	Confirms the presence of metal elements in nanoparticles
Atomic Force Microscopy (AFM)	Uses a sharp probe to scan the sample surface	Surface topography, roughness, particle height	Provides three-dimensional surface characterization
Thermogravimetric Analysis (TGA)	Measures weight changes with temperature	Thermal stability and organic content	Determines capping agent content and thermal behavior
Raman Spectroscopy	Measures inelastic scattering of light	Molecular structure and chemical composition	Identifies surface interactions and structural changes
X-ray Photoelectron Spectroscopy (XPS)	Measures kinetic energy of emitted photoelectrons	Surface elemental composition and oxidation states	Determines chemical states of metals and capping molecules

UV–Visible Spectroscopy

Used to confirm nanoparticle formation through Surface Plasmon Resonance (SPR) [40].

Typical absorption peaks:

- Silver nanoparticles: 400–450 nm
- Gold nanoparticles: 500–550 nm

Applications:

Monitoring synthesis

- Stability studies

Fourier Transform Infrared Spectroscopy (FTIR)

FTIR identifies functional groups responsible for reduction and capping [41].

Important groups include:

- Hydroxyl (-OH)
- Carbonyl (C=O)
- Amino ($-NH_2$)

X-ray Diffraction (XRD)

Determines:

- Crystalline structure
- Phase purity
- Average crystallite size

Scanning Electron Microscopy (SEM)

Provides information regarding:

- Surface morphology
- Shape
- Aggregation

Transmission Electron Microscopy (TEM)

TEM is one of the most powerful techniques for nanoparticle characterization.

Provides:[42]

- Exact particle size
- Shape distribution
- Internal structure

Dynamic Light Scattering (DLS)

Measures:

- Hydrodynamic diameter
- Particle size distribution

Zeta Potential Analysis

Evaluates nanoparticle stability.

Higher absolute zeta potential values indicate greater colloidal stability.

Energy Dispersive X-ray Spectroscopy (EDX)

Determines elemental composition and confirms nanoparticle purity.

Advantages of Green Synthesis

Green synthesis offers numerous benefits over conventional methods [43].

Environmental Advantages

- Eco-friendly
- Reduced toxic waste
- Minimal environmental pollution

Economic Advantages

- Low-cost production
- Readily available biological materials
- Reduced energy consumption

Technical Advantages

- Simple procedures
- Scalable production
- Enhanced biocompatibility

Applications of Green-Synthesized Metal Nanoparticles [44]

Antimicrobial Applications

Silver nanoparticles exhibit broad-spectrum antimicrobial activity against:

- *Staphylococcus aureus*
- *Escherichia coli*
- *Pseudomonas aeruginosa*
- *Candida albicans*

Mechanisms include:

- Cell membrane disruption
- Reactive oxygen species generation
- DNA damage

Anticancer Applications

Gold and silver nanoparticles demonstrate potential anticancer activity through:[45]

- Induction of apoptosis
- Oxidative stress generation
- Targeted drug delivery

Applications include treatment of:

- Breast cancer
- Lung cancer
- Colon cancer

Drug Delivery Systems

Nanoparticles enhance:

- Drug solubility
- Controlled release
- Site-specific targeting

Advantages:

- Reduced toxicity
- Improved therapeutic efficacy

Wound Healing

Metal nanoparticles promote:

- Collagen synthesis
- Angiogenesis
- Antimicrobial protection

Silver nanoparticle dressings are widely used in wound management.

Diagnostic Applications

Gold nanoparticles are employed in:

- Biosensors
- Immunoassays
- Imaging systems

Catalytic Applications

Nanoparticles function as catalysts in:

- Dye degradation
- Organic synthesis
- Environmental remediation

Environmental Applications

Applications include:

- Wastewater treatment
- Heavy metal removal
- Pollutant degradation

Agricultural Applications

Green nanoparticles are used for:

- Nano-fertilizers
- Nano-pesticides
- Plant disease management

Benefits include enhanced crop productivity and reduced chemical usage [46].

Figure 3: Applications of Green-Synthesized Metal Nanoparticles [47]

Challenges and Limitations

Despite numerous advantages, green synthesis faces several challenges:

- Variability in biological extracts
- Difficulty in standardization
- Scale-up limitations
- Reproducibility issues
- Limited understanding of synthesis mechanisms
- Regulatory concerns

Addressing these challenges is essential for commercial and industrial applications [48].

Future Perspectives

Future research should focus on:

- Standardization of biological extracts
- Large-scale industrial production
- Mechanistic understanding
- Multifunctional nanoparticles
- Clinical translation
- Sustainable nanotechnology development

Integration of nanotechnology with biotechnology, artificial intelligence, and advanced characterization techniques may further expand the scope of green-synthesized nanoparticles [49].

Conclusion

This review illustrates essential principles of "green" chemistry and "green" methods of generating metal/metal oxide nanoparticles using bioresources. A "bottom-up" process is the most frequent way to get these nanoparticles, using diverse organic solvents, hazardous compounds, and non-ecological reagents under high pressure and temperature. So, there is a need for alternative cheap and safe solutions. "Green" synthesis avoids contamination in early stages of chemical processes and lowers harmful effects on the environment and human health. Plants, algae, fungi, yeast, bacteria, viruses etc. are used to develop many intriguing biological processes. Among several 'green' resources, plants are the best source of precursors for the synthesis of metal/metal oxide nanoparticles due to their simplicity, non-toxicity and availability. Parameters such as total antioxidant capacity and total protein content affect the appropriateness of plants. "Green" nanoparticles should be studied as to their physical and chemical properties, their stability and activity for the purpose of improving their practical application. Green synthesis represents a sustainable and environmentally friendly approach for producing metal nanoparticles. Biological systems provide natural reducing and stabilizing agents that eliminate the need for toxic chemicals and harsh reaction conditions. Green-synthesized nanoparticles exhibit remarkable physicochemical properties and find applications in medicine, agriculture, environmental remediation, catalysis, and diagnostics. Although challenges related to reproducibility and large-scale production remain, continued advancements in green nanotechnology are expected to facilitate broader industrial and biomedical applications in the future.

References

1. Iravani, S. (2011). Green synthesis of metal nanoparticles using plants. *Green Chemistry, 13*(10), 2638–2650. https://doi.org/10.1039/C1GC15386B
2. Ahmed, S., Ahmad, M., Swami, B. L., & Ikram, S. (2016). A review on plant extracts mediated synthesis of silver nanoparticles for antimicrobial applications: A green expertise. *Journal of Advanced Research, 7*(1), 17–28. https://doi.org/10.1016/j.jare.2015.02.007
3. Yadi, M., Mostafavi, E., Saleh, B., Davaran, S., Aliyeva, I., Khalilov, R., ... Akbarzadeh, A. (2018). Current developments in green synthesis of metallic nanoparticles using plant extracts: A review. *Artificial Cells, Nanomedicine, and Biotechnology, 46*(sup3), S336–S343. https://doi.org/10.1080/21691401.2018.1492931
4. Singh, P., Kim, Y. J., Zhang, D., & Yang, D. C. (2016). Biological synthesis of nanoparticles from plants and microorganisms. *Trends in Biotechnology, 34*(7), 588–599. https://doi.org/10.1016/j.tibtech.2016.02.006

5. Shankar, S. S., Rai, A., Ahmad, A., & Sastry, M. (2004). Rapid synthesis of Au, Ag, and bimetallic Au core–Ag shell nanoparticles using neem (*Azadirachta indica*) leaf broth. *Journal of Colloid and Interface Science, 275*(2), 496–502. https://doi.org/10.1016/j.jcis.2004.03.003
6. Narayanan, K. B., & Sakthivel, N. (2010). Biological synthesis of metal nanoparticles by microbes. *Advances in Colloid and Interface Science, 156*(1–2), 1–13. https://doi.org/10.1016/j.cis.2010.02.001
7. Mohanpuria, P., Rana, N. K., & Yadav, S. K. (2008). Biosynthesis of nanoparticles: Technological concepts and future applications. *Journal of Nanoparticle Research, 10*(3), 507–517. https://doi.org/10.1007/s11051-007-9275-x
8. Rai, M., Yadav, A., & Gade, A. (2009). Silver nanoparticles as a new generation of antimicrobials. *Biotechnology Advances, 27*(1), 76–83. https://doi.org/10.1016/j.biotechadv.2008.09.002
9. Kalishwaralal, K., Deepak, V., Ram Kumar Pandian, S., Kottaisamy, M., BarathManiKanth, S., Kartikeyan, B., & Gurunathan, S. (2010). Biosynthesis of silver and gold nanoparticles using *Brevibacterium casei*. *Colloids and Surfaces B: Biointerfaces, 77*(2), 257–262. https://doi.org/10.1016/j.colsurfb.2010.02.007
10. Parveen, K., Banse, V., & Ledwani, L. (2016). Green synthesis of nanoparticles: Their advantages and disadvantages. In *AIP Conference Proceedings* (Vol. 1724, Article 020048). AIP Publishing. https://doi.org/10.1063/1.4945168
11. Jeyaraj, M., Rajesh, M., Arun, R., MubarakAli, D., Sathishkumar, G., Sivanandhan, G., ... Ganapathi, A. (2013). An investigation on the cytotoxicity and caspase-mediated apoptotic effect of biologically synthesized silver nanoparticles using *Podophyllum hexandrum* on human cervical carcinoma cells. *Colloids and Surfaces B: Biointerfaces, 102*, 708–717. https://doi.org/10.1016/j.colsurfb.2012.09.042
12. Kalidas, G., & Pranav, R. J. (2022). Biological synthesis of metallic nanoparticles and their applications. *International Journal for Research in Applied Science and Engineering Technology, 10*(2), 420–424. https://doi.org/10.22214/ijraset.2022.40274
13. Hulkoti, N. I., & Taranath, T. C. (2014). Biosynthesis of nanoparticles using microbes—A review. *Colloids and Surfaces B: Biointerfaces, 121*, 474–483. https://doi.org/10.1016/j.colsurfb.2014.05.027
14. El-Rafie, H. M., El-Rafie, M. H., & Zahran, M. K. (2013). Green synthesis of silver nanoparticles using polysaccharides extracted from marine macroalgae. *Carbohydrate Polymers, 96*(2), 403–410. https://doi.org/10.1016/j.carbpol.2013.03.071
15. Akhtar, M. S., Panwar, J., & Yun, Y. S. (2013). Biogenic synthesis of metallic nanoparticles by plant extracts. *ACS Sustainable Chemistry & Engineering, 1*(6), 591–602. https://doi.org/10.1021/sc300118u
16. Toro-González, M., Clifford, D. M., Copping, R., Mirzadeh, S., & Rojas, J. V. (2018). Synthesis and characterization of intrinsically radiolabeled lanthanide phosphate

nanoparticles toward biomedical and environmental applications. *Journal of Nanoparticle Research, 20*(9), 238. https://doi.org/10.1007/s11051-018-4338-8

17. Anastas, P. T., & Warner, J. C. (2000). *Green chemistry: Theory and practice*. Oxford University Press. https://doi.org/10.1093/oso/9780198506980.001.0001
18. Bourne, R. A., & Poliakoff, M. (2011). Green chemistry: What is the way forward? *Mendeleev Communications, 21*(5), 235–238. https://doi.org/10.1016/j.mencom.2011.09.001
19. Du, Z., Chen, F., Fang, S., *et al.* (2024). Engineering bimetallic Ni–Cu nanoparticles confined in MOF-derived nanocomposite for efficient dry reforming of methane. *ES Energy & Environment*. https://doi.org/10.30919/esee1097
20. Raşa, M., Kuipers, B. W. M., & Philipse, A. P. (2002). Atomic force microscopy and magnetic force microscopy study of model colloids. *Journal of Colloid and Interface Science, 250*(2), 303–315. https://doi.org/10.1006/jcis.2002.8345
21. Sifford, J., Walsh, K. J., Tong, S., Bao, G., & Agarwal, G. (2019). Indirect magnetic force microscopy. *Nanoscale Advances, 1*(6), 2348–2355. https://doi.org/10.1039/C9NA00193J
22. Torre, B., Bertoni, G., Fragouli, D., Falqui, A., Salerno, M., Diaspro, A., *et al.* (2011). Magnetic force microscopy and energy loss imaging of superparamagnetic iron oxide nanoparticles. *Scientific Reports, 1*, Article 202. https://doi.org/10.1038/srep00202
23. Cordova, G., Attwood, S., Gaikwad, R., Gu, F., & Leonenko, Z. (2014). Magnetic force microscopy characterization of superparamagnetic iron oxide nanoparticles (SPIONs). *Nano Biomedicine and Engineering, 6*(1), 31–39. https://doi.org/10.5101/nbe.v6i1.p31-39
24. Krivcov, A., Schneider, J., Junkers, T., & Möbius, H. (2019). Magnetic force microscopy of single magnetic nanoparticles embedded in a polymer matrix. *Physica Status Solidi A: Applications and Materials Science, 216*(12), Article 1800753. https://doi.org/10.1002/pssa.201800753
25. Gianfranceschi, L., McDermott, J. M., Seglias, N., Koller, B., Kellerhals, M., & Gessler, C. (1994). Towards marker-assisted breeding for resistance against apple scab. *Euphytica, 77*(1–2), 93–96. https://doi.org/10.1007/BF02551468
26. Beyond Benign, Inc., & Yale Center for Green Chemistry and Green Engineering. (2023). *Green chemistry university course: Lecture 2—Green chemistry: Reimagining chemistry*. Green Chemistry Teaching and Learning Community. https://doi.org/10.59877/LNTI5060
27. Sheldon, R. A. (2008). E factors, green chemistry and catalysis: An odyssey. *Chemical Communications*, (29), 3352–3365. https://doi.org/10.1039/B803584A
28. Dai, L., Li, Y., Liu, R., Si, C., & Ni, Y. (2019). Green mussel-inspired lignin magnetic nanoparticles with high adsorptive capacity and environmental friendliness for chromium(III) removal. *International Journal of Biological Macromolecules, 132*, 478–486. https://doi.org/10.1016/j.ijbiomac.2019.03.222
29. Mustapha, T., Misni, N., Ithnin, N. R., Daskum, A. M., & Unyah, N. Z. (2022). A review on plants and microorganisms mediated synthesis of silver nanoparticles, role of plant

metabolites and applications. *International Journal of Environmental Research and Public Health, 19*(2), Article 674. https://doi.org/10.3390/ijerph19020674

30. Pandit, C., Roy, A., Ghotekar, S., Khusro, A., Islam, M. N., Emran, T. B., *et al.* (2022). Biological agents for synthesis of nanoparticles and their applications. *Journal of King Saud University – Science, 34*(3), Article 101869. https://doi.org/10.1016/j.jksus.2022.101869
31. Cuong, H. N., Pansambal, S., Ghotekar, S., Oza, R., Thanh Hai, N. T., Viet, N. M., *et al.* (2022). New frontiers in the plant extract-mediated biosynthesis of copper oxide (CuO) nanoparticles and their potential applications: A review. *Environmental Research, 203*, Article 111858. https://doi.org/10.1016/j.envres.2021.111858
32. Hussain, A., Lakhan, M. N., Hanan, A., Soomro, I. A., Ahmed, M., Bibi, F., *et al.* (2023). Recent progress on green synthesis of selenium nanoparticles: A review. *Materials Today Sustainability, 23*, Article 100420. https://doi.org/10.1016/j.mtsust.2023.10042 0
33. Matussin, S., Harunsani, M. H., Tan, A. L., & Khan, M. M. (2020). Plant-extract-mediated SnO_2 nanoparticles: Synthesis and applications. *ACS Sustainable Chemistry & Engineering, 8*(8), 3040–3054. https://doi.org/10.1021/acssuschemeng.9b06398
34. Kaur, M., Gautam, A., Guleria, P., Singh, K., & Kumar, V. (2022). Green synthesis of metal nanoparticles and their environmental applications. *Current Opinion in Environmental Science & Health, 29*, Article 100390. https://doi.org/10.1016/j.coesh.2022.100390
35. Jeevanandam, J., Kiew, S. F., Boakye-Ansah, S., Lau, S. Y., Barhoum, A., Danquah, M. K., *et al.* (2022). Green approaches for the synthesis of metal and metal oxide nanoparticles using microbial and plant extracts. *Nanoscale, 14*(7), 2534–2571. https://doi.org/10.1039/D1NR08144F
36. Venkataraman, S. (2022). Plant molecular pharming and plant-derived compounds towards generation of vaccines and therapeutics against coronaviruses. *Vaccines, 10*(11), Article 1805. https://doi.org/10.3390/vaccines10111805
37. Pandit, C., Roy, A., Ghotekar, S., Khusro, A., Islam, M. N., Emran, T. B., *et al.* (2022). Biological agents for synthesis of nanoparticles and their applications. *Journal of King Saud University – Science, 34*(3), Article 101869. https://doi.org/10.1016/j.jksus.2022.101869
38. Cuong, H. N., Pansambal, S., Ghotekar, S., Oza, R., Thanh Hai, N. T., Viet, N. M., *et al.* (2022). New frontiers in the plant extract-mediated biosynthesis of copper oxide (CuO) nanoparticles and their potential applications: A review. *Environmental Research, 203*, Article 111858. https://doi.org/10.1016/j.envres.2021.111858
39. Hussain, A., Lakhan, M. N., Hanan, A., Soomro, I. A., Ahmed, M., Bibi, F., *et al.* (2023). Recent progress on green synthesis of selenium nanoparticles: A review. *Materials Today Sustainability, 23*, Article 100420. https://doi.org/10.1016/j.mtsust.2023.100420

40. Pansambal, S., Oza, R., Borgave, S., Chauhan, A., Bardapurkar, P., Vyas, S., *et al.* (2023). Bioengineered cerium oxide (CeO_2) nanoparticles and their diverse applications: A review. *Applied Nanoscience, 13*(9), 6067–6092. https://doi.org/10.1007/s13204-022-02574-8
41. Matussin, S., Harunsani, M. H., Tan, A. L., & Khan, M. M. (2020). Plant-extract-mediated SnO_2 nanoparticles: Synthesis and applications. *ACS Sustainable Chemistry & Engineering, 8*(8), 3040–3054. https://doi.org/10.1021/acssuschemeng.9b06398
42. Kashid, Y., Ghotekar, S., Bilal, M., Pansambal, S., Oza, R., Varma, R. S., *et al.* (2022). Bio-inspired sustainable synthesis of silver chloride nanoparticles and their prominent applications. *Journal of the Indian Chemical Society, 99*(5), Article 100335. https://doi.org/10.1016/j.jics.2021.100335
43. Kaur, M., Gautam, A., Guleria, P., Singh, K., & Kumar, V. (2022). Green synthesis of metal nanoparticles and their environmental applications. *Current Opinion in Environmental Science & Health, 29*, Article 100390. https://doi.org/10.1016/j.coesh.2022.100390
44. Jeevanandam, J., Kiew, S. F., Boakye-Ansah, S., Lau, S. Y., Barhoum, A., Danquah, M. K., *et al.* (2022). Green approaches for the synthesis of metal and metal oxide nanoparticles using microbial and plant extracts. *Nanoscale, 14*(7), 2534–2571. https://doi.org/10.1039/D1NR08144F
45. Thakare, N. R., Ingole, P. G., & Hazarika, S. (2023). Biogenic synthesis of nanoparticles from the edible plant *Polygonum microcephalum* for use in antimicrobial fabric. *ACS Omega, 8*(48), 45301–45312. https://doi.org/10.1021/acsomega.3c03978
46. Borah, D., Das, N., Das, N., Bhattacharjee, A., Sarmah, P., Ghosh, K., *et al.* (2020). Alga-mediated facile green synthesis of silver nanoparticles: Photophysical, catalytic and antibacterial activity. *Applied Organometallic Chemistry, 34*(5), Article e5597. https://doi.org/10.1002/aoc.5597
47. Baladi, M., Soofivand, F., Gandu, S. H., Jasim, L. S., Mahdi, M. A., & Salavati-Niasari, M. (2023). In situ synthesis of $TbAlO_3/Tb_3Al_5O_{12}/Tb_2O_3$ three-component nanocomposite as a heterojunction photocatalyst with a green and eco-friendly approach. *Arabian Journal of Chemistry, 16*(5), Article 104697. https://doi.org/10.1016/j.arabjc.2023.104697

ADVANCED CHEMICAL AND MATERIALS TECHNOLOGIES FOR GLOBAL SUSTAINABILITY

Muthurajan S[1], Immanuel Prabaharan S*[2], Aswini M[2] and Deivanayaki R[2]

[1]Department of Marine Engineering,

[2]Department of Electrical and Electronics Engineering,

AMET University, Kanathur, Chennai-603 112

*Corresponding author E-mail: imman.amet@gmail.com

Abstract

Global sustainability has become one of the most pressing challenges of the twenty-first century due to climate change, resource depletion, environmental pollution, and rapid industrialization. The increasing demand for energy, clean water, sustainable materials, and environmentally friendly manufacturing processes has accelerated the development of advanced chemical and materials technologies. Green chemistry, sustainable materials engineering, nanotechnology, renewable energy materials, carbon capture systems, advanced membranes, biodegradable polymers, and circular economy approaches are transforming industrial practices and contributing significantly to sustainable development goals (SDGs). These technologies facilitate resource efficiency, waste reduction, carbon neutrality, and environmental protection while maintaining economic growth and technological progress. Recent advances in functional materials, sustainable chemical processes, and smart manufacturing systems have demonstrated significant potential in addressing global sustainability challenges. This chapter examines the role of advanced chemical and materials technologies in promoting sustainability, discusses recent scientific developments, highlights industrial applications, and identifies future opportunities for achieving a more sustainable and resilient society. The chapter provides a comprehensive overview of emerging technologies that are expected to shape the future of sustainable development worldwide.

Keywords: Green Chemistry, Sustainable Materials, Nanotechnology, Renewable Energy, Carbon Capture, Circular Economy, Environmental Remediation, Advanced Membranes, Sustainable Development, Smart Materials.

1. Introduction

The growing concerns regarding climate change, environmental degradation, resource scarcity, and increasing global population have intensified the need for sustainable technological solutions. Modern industrial activities have significantly improved human living standards; however, they have also contributed to greenhouse gas emissions, water contamination, excessive waste generation, and depletion of natural resources. As a result, governments,

industries, and research institutions worldwide are focusing on sustainable technologies that minimize environmental impacts while maintaining economic competitiveness. Chemical and materials sciences occupy a central position in this transition because they influence virtually every industrial sector, including energy production, manufacturing, transportation, agriculture, healthcare, and environmental management. Recent developments in advanced materials and green chemistry have created unprecedented opportunities to redesign industrial systems according to sustainability principles. The integration of sustainable chemistry with advanced materials engineering is increasingly recognized as a critical pathway for achieving the United Nations Sustainable Development Goals (SDGs). Research efforts are now focused on developing safer chemicals, renewable materials, low-carbon manufacturing processes, and circular resource management strategies that can support long-term sustainability.

Chemical innovation has historically driven technological progress, from fertilizers and pharmaceuticals to polymers and energy systems. However, conventional chemical processes often rely on fossil resources, hazardous substances, and energy-intensive operations. Modern sustainability challenges require a fundamental transformation in how chemicals and materials are designed, manufactured, utilized, and recycled. Advanced materials such as nanomaterials, biomaterials, carbon-based materials, and smart functional materials have emerged as promising solutions to improve efficiency while reducing environmental impacts. Simultaneously, green chemistry principles are guiding the development of environmentally benign synthesis methods that minimize waste generation and resource consumption. These innovations are enabling industries to move toward cleaner production systems and sustainable value chains. The convergence of chemistry, materials science, biotechnology, and digital technologies is creating a new generation of sustainable technologies capable of addressing complex global challenges.

2. Green Chemistry as a Foundation for Sustainability

Green chemistry has emerged as a transformative scientific framework that seeks to reduce or eliminate hazardous substances throughout the lifecycle of chemical products and processes. The concept emphasizes pollution prevention rather than remediation, encouraging scientists and engineers to design processes that maximize efficiency while minimizing environmental impacts. The twelve principles of green chemistry provide comprehensive guidelines for sustainable chemical manufacturing, including waste prevention, atom economy, safer solvents, renewable feedstocks, energy efficiency, and inherently safer chemical design. These principles are increasingly being adopted by industries seeking to reduce environmental footprints and comply with stricter regulatory requirements. Green chemistry has evolved from a niche academic concept into a major industrial strategy that influences product design, manufacturing processes, and supply chain management. Recent studies demonstrate that green chemistry approaches can

simultaneously improve environmental performance and economic competitiveness by reducing material consumption, waste disposal costs, and energy requirements.

Recent advances in sustainable synthesis have further strengthened the role of green chemistry in global sustainability. Researchers are developing catalytic systems, bio-based synthesis pathways, and solvent-free reaction methods that significantly reduce environmental impacts. Green synthesis approaches utilize biological materials, plant extracts, microorganisms, and renewable feedstocks to produce chemicals and nanomaterials with minimal ecological consequences. These methods often require lower temperatures, fewer processing steps, and reduced chemical inputs compared to conventional manufacturing techniques. The growing application of photocatalysis, electrocatalysis, and biocatalysis has enabled highly efficient chemical transformations while reducing energy consumption and greenhouse gas emissions. Such innovations illustrate how green chemistry principles can be translated into practical industrial solutions that contribute to sustainable development.

3. Advanced Functional Materials for Sustainable Development

Advanced functional materials are playing an increasingly important role in addressing sustainability challenges across multiple sectors. These materials possess unique physical, chemical, optical, electrical, or mechanical properties that enable superior performance in various applications. Functional materials have become essential components in renewable energy systems, environmental remediation technologies, water purification processes, and sustainable manufacturing. Their ability to perform multiple functions simultaneously allows for more efficient use of resources and improved system performance. The development of advanced functional materials has accelerated significantly due to advances in nanotechnology, computational materials science, and precision manufacturing techniques. Researchers are now able to engineer materials at atomic and molecular scales, creating structures with unprecedented functionality and efficiency. These innovations have opened new opportunities for sustainable technology development and environmental protection.

Among the most influential classes of functional materials are carbon-based materials such as graphene, carbon nanotubes, activated carbon, and biochar-derived materials. These materials exhibit exceptional conductivity, mechanical strength, thermal stability, and adsorption capacity, making them suitable for numerous sustainability applications. Green carbon materials produced from renewable biomass or recycled waste have attracted considerable attention because they support carbon neutrality and circular economy principles. Such materials are increasingly being used in energy storage devices, water treatment systems, environmental sensors, and catalytic processes. Their versatility and sustainability advantages make them valuable tools for addressing global environmental challenges. The continued development of advanced carbon materials is expected to contribute significantly to future sustainable technologies.

4. Nanotechnology and Sustainable Innovation

Nanotechnology has revolutionized materials science by enabling precise control over material properties at the nanoscale. Nanomaterials exhibit unique characteristics that differ substantially from their bulk counterparts, including enhanced surface area, catalytic activity, mechanical strength, and electronic properties. These features make nanotechnology a powerful platform for developing sustainable solutions in energy, water treatment, environmental remediation, and healthcare. Green nanotechnology integrates sustainability principles into nanomaterial design, synthesis, and application, ensuring that technological advancements contribute positively to environmental and societal goals. Researchers increasingly recognize that nanotechnology can play a critical role in achieving multiple Sustainable Development Goals by improving resource efficiency and enabling cleaner industrial processes.

Nanomaterials have demonstrated remarkable effectiveness in environmental applications. Nanostructured catalysts improve reaction efficiency and reduce waste generation in chemical manufacturing. Nanomembranes enhance water purification performance by selectively removing contaminants while minimizing energy consumption. Advanced nanoparticles are being employed for pollutant degradation, heavy metal removal, and environmental monitoring. These applications highlight the versatility of nanotechnology in addressing complex sustainability challenges. However, ensuring the safe and responsible use of nanomaterials remains essential, requiring comprehensive lifecycle assessments and sustainable design approaches.

5. Sustainable Polymers and Circular Materials

Plastic pollution has emerged as a major environmental concern, prompting increased interest in sustainable polymers and biodegradable materials. Conventional plastics derived from fossil resources persist in the environment for decades or centuries, contributing to ecosystem degradation and waste accumulation. Sustainable polymers offer an alternative by utilizing renewable feedstocks and enabling biodegradation, recycling, or circular reuse. Advances in polymer chemistry have facilitated the development of materials that combine environmental compatibility with desirable mechanical and functional properties. These innovations are transforming packaging, construction, healthcare, and consumer goods industries.

Circular economy principles are increasingly influencing polymer design and manufacturing strategies. Rather than following the traditional "take-make-dispose" model, circular approaches emphasize material recovery, recycling, remanufacturing, and reuse. Sustainable polymeric membranes represent a notable example of this trend, incorporating green chemistry principles into membrane fabrication for water treatment and desalination applications. Researchers are developing bio-based polymers, recyclable composites, and self-healing materials that extend product lifetimes and reduce resource consumption. These efforts support the transition toward a more sustainable and resource-efficient economy.

6. Renewable Energy Materials and Technologies

The transition to renewable energy systems is essential for reducing greenhouse gas emissions and mitigating climate change. Advanced materials are fundamental to this transition because they determine the efficiency, durability, and cost-effectiveness of renewable energy technologies. Significant progress has been achieved in solar photovoltaics, hydrogen production systems, fuel cells, batteries, and energy storage technologies through materials innovation. Emerging materials such as perovskites, nanostructured semiconductors, advanced catalysts, and carbon nanomaterials are improving energy conversion efficiencies and reducing manufacturing costs. These developments are accelerating the adoption of clean energy technologies worldwide. Hydrogen has gained considerable attention as a clean energy carrier capable of supporting decarbonization across transportation, industry, and power generation sectors. Advanced materials are enabling more efficient hydrogen production through water electrolysis and improving storage and distribution technologies. Similarly, next-generation batteries utilizing advanced electrode materials are addressing challenges related to energy density, safety, and lifecycle performance. These innovations are critical for integrating intermittent renewable energy sources into modern power systems and achieving long-term energy sustainability.

7. Water Purification and Environmental Remediation

Access to clean water remains a major global challenge affecting billions of people worldwide. Rapid industrialization, urbanization, and population growth have intensified pressures on freshwater resources and increased contamination risks. Advanced chemical and materials technologies have enabled the development of highly effective water treatment systems capable of removing pollutants, pathogens, heavy metals, and emerging contaminants. Membrane technologies, nanomaterials, adsorbents, and photocatalysts are increasingly being utilized to improve water quality and treatment efficiency. These technologies contribute significantly to sustainable water management and public health protection.

Recent advances in inorganic nanomaterials have demonstrated exceptional potential for environmental remediation. Nanomaterials can efficiently remove dyes, microplastics, heavy metals, and oil contaminants from water systems. Their high surface area and tunable surface chemistry allow for targeted pollutant removal and enhanced treatment performance. Advanced membrane systems further improve sustainability by reducing energy consumption associated with water purification and desalination processes. Together, these technologies provide powerful tools for addressing global water scarcity and environmental contamination challenges.

8. Carbon Capture, Utilization, and Storage Technologies

Carbon capture, utilization, and storage (CCUS) technologies are increasingly recognized as essential components of global climate mitigation strategies. The continued reliance on fossil fuels and industrial emissions necessitates technologies capable of reducing atmospheric carbon

dioxide concentrations. Advanced materials such as metal-organic frameworks (MOFs), zeolites, activated carbons, and membrane systems have demonstrated exceptional potential for carbon capture applications. These materials offer high adsorption capacities, selectivity, and regeneration performance, making them suitable for large-scale deployment. Recent research has focused on improving material stability, reducing costs, and enhancing capture efficiencies.

Beyond carbon capture, researchers are exploring innovative approaches for carbon utilization that transform captured CO_2 into valuable products such as fuels, chemicals, and construction materials. Such strategies contribute to circular carbon economies by converting waste emissions into useful resources. Advances in catalytic materials and electrochemical systems have improved the feasibility of carbon conversion technologies. These developments represent important steps toward achieving carbon neutrality and sustainable industrial operations.

9. Future Trends and Challenges

Despite remarkable progress, significant challenges remain in implementing advanced chemical and materials technologies at a global scale. Economic barriers, infrastructure limitations, regulatory requirements, and technology readiness levels often hinder commercialization efforts. Many sustainable technologies require substantial investments in research, manufacturing capacity, and market development before achieving widespread adoption. Additionally, lifecycle sustainability assessments are necessary to ensure that emerging technologies provide genuine environmental benefits rather than shifting impacts between different stages of production and use. The development of safe and sustainable-by-design materials has therefore become a major research priority.

Future research is expected to focus on integrating artificial intelligence, machine learning, and digital technologies with materials discovery and process optimization. These tools can accelerate innovation by identifying promising materials, predicting performance, and optimizing manufacturing processes. Advances in biotechnology, synthetic biology, and industrial biotechnology will further expand opportunities for sustainable chemical production and materials development. Interdisciplinary collaboration among scientists, engineers, policymakers, and industries will be essential for translating laboratory discoveries into practical solutions that contribute to global sustainability objectives.

Conclusion

Advanced chemical and materials technologies are fundamental to achieving global sustainability goals. Innovations in green chemistry, nanotechnology, renewable energy materials, sustainable polymers, advanced membranes, environmental remediation systems, and carbon capture technologies are transforming industries and creating new pathways toward sustainable development. These technologies improve resource efficiency, reduce environmental impacts, support clean energy transitions, and facilitate circular economy practices. Continued

investment in research, innovation, and sustainable manufacturing will be essential for addressing future environmental challenges and ensuring long-term societal prosperity. The successful integration of advanced chemistry and materials science into industrial systems offers tremendous opportunities for building a resilient, low-carbon, and sustainable future.

References

1. Kurul, F., Doruk, B., & Topkaya, S. N. (2025). Principles of green chemistry: Building a sustainable future. *Discover Chemistry, 2*, Article 68. https://doi.org/10.1007/s44371-025-00152-9
2. Caldeira, C., Abbate, E., Moretti, C., Mancini, L., & Sala, S. (2024). Safe and sustainable chemicals and materials: A review of sustainability assessment frameworks. *Green Chemistry, 26*(13), 7456–7477. https://doi.org/10.1039/D3GC04598F
3. Alqahtani, A. S., & Elbeltagi, S. (2025). Advancing chemistry sustainably: From synthesis to benefits and applications of green synthesis. *Journal of Organometallic Chemistry, 1027*, Article 123508. https://doi.org/10.1016/j.jorganchem.2025.123508
4. Freitas, M., Pinto da Silva, L., Rodrigues, P. M. S. M., & da Silva, J. E. (2024). Sustainable technological applications of green carbon materials. *Sustainable Chemistry, 5*(2), 81–97.
5. Norton, K. J., & Norton, M. G. (2025). Advances in the use of inorganic nanomaterials for sustainable remediation of contaminated water. *Journal of Materials Science, 60*.
6. Kim, J., Kim, J. F., Jiang, Z., & Livingston, A. G. (2025). Advancing membrane technology in organic liquids towards a sustainable future. *Nature Sustainability, 8*, 594–605.
7. Kumar, A., Tyagi, P. K., Tyagi, S., & Ghorbanpour, M. (2024). Integrating green nanotechnology with sustainable development goals: A pathway to sustainable innovation. *Discover Sustainability, 5*.
8. Kuku, M., & Arishi, M. (2025). Advanced materials for sustainable fabrication, desalination, hydrogen production, and CO_2 reduction. *Alexandria Engineering Journal, 115*, 411–422. https://doi.org/10.1016/j.aej.2024.12.047
9. Loh, C. Y., Burrows, A. D., & Xie, M. (2025). Sustainable polymeric membranes: Green chemistry and circular economy approaches. *ACS ES&T Engineering, 5*(8), 1882–1906. https://doi.org/10.1021/acsestengg.5c00282
10. Sultani, H. K. H. A., Farhan, H. A. K., Yousif, M. A. H., & Kashash, M. F. K. (2025). Advanced chemical approaches for environmental sustainability: Innovations in pollution remediation and green chemistry. *American Journal of Biomedicine and Pharmacy*, *2*(5), 226–243.

HYBRID RENEWABLE ENERGY-BASED ELECTRIC VEHICLE CHARGING SYSTEMS: A REVIEW

Chhavi Gupta*, Shilpi Pal and Sanjeev Kumar Singh
Department of Electrical Engineering,
School of Engineering & Technology, IFTM University, Moradabad 244102, India
*Corresponding author E-mail: chhavieee777@gmail.com

Abstract
The rapid growth of electric vehicles (EVs) has created a significant demand for reliable and sustainable charging infrastructure. Conventional EV charging stations mainly rely on grid electricity, which may still be generated from fossil fuels, thereby reducing the environmental benefits of electric mobility. To address this issue, hybrid renewable energy systems combining solar and wind power have emerged as a promising solution for sustainable EV charging. This chapter presents the concept, design, and operation of a hybrid renewable energy–based EV charging station that integrates solar photovoltaic (PV) panels and wind turbines to generate clean electricity. The proposed system utilizes the complementary nature of solar and wind resources to improve energy reliability and ensure continuous power availability for EV charging. Solar energy provides electricity during daylight hours, while wind energy can generate power during both day and night depending on wind conditions. An energy storage system, typically based on lithium-ion batteries, is incorporated to store excess energy generated from renewable sources and supply power during periods of low generation. Power electronic converters, controllers, and energy management systems are used to regulate the power flow and maintain stable charging operations. Hybrid renewable EV charging stations offer several advantages, including reduced dependence on the conventional power grid, lower greenhouse gas emissions, improved energy efficiency, and enhanced grid stability. However, challenges such as renewable energy intermittency, high initial investment costs, and system complexity must also be addressed. Advanced energy management strategies, smart charging techniques, and optimization methods can further enhance the performance and economic feasibility of hybrid charging systems. Overall, hybrid solar–wind based EV charging infrastructure represents an important step toward achieving sustainable transportation and reducing carbon emissions. The integration of renewable energy with EV charging stations will play a crucial role in supporting future smart grid systems and promoting clean energy–based mobility.

Keywords: Electric Vehicles (EVs), Hybrid Renewable Energy System (HRES), Solar Photovoltaic (PV), Wind Energy, EV Charging Infrastructure, Renewable Energy Integration, Energy Storage System (ESS), Smart Charging, Sustainable Transportation, Power Electronics Converters, Energy Management System (EMS), Grid Integration.

1. Introduction

The rapid growth of electric vehicles (EVs) has increased the demand for reliable and sustainable charging infrastructure. Traditional EV charging stations rely primarily on electricity from the conventional grid, which may still depend heavily on fossil fuels. This creates additional stress on the electrical grid and reduces the environmental benefits of EV adoption. To address these issues, renewable energy sources are increasingly integrated into EV charging infrastructure. One promising solution is the Hybrid Renewable Energy System (HRES) that combines solar photovoltaic (PV) and wind energy for EV charging.

Hybrid renewable energy systems combine two or more renewable energy sources to produce electricity. The combination of solar and wind energy is particularly effective because these sources complement each other. Solar energy is available during the daytime, while wind energy may be available both day and night depending on environmental conditions. This complementary nature improves reliability and reduces the intermittency associated with individual renewable sources.

In EV charging stations, the hybrid solar-wind system can generate electricity locally, reducing dependence on the grid and lowering carbon emissions. These systems can also integrate energy storage systems to store excess power for later use.

2. Need for Hybrid Renewable Energy EV Charging

The global transportation sector contributes significantly to greenhouse gas emissions. EVs are considered a sustainable alternative to internal combustion engine vehicles. However, if EVs are charged using electricity generated from fossil fuels, their environmental benefits may be limited.

Hybrid renewable energy charging stations offer several advantages:

- Reduction in carbon emissions
- Decreased dependency on fossil fuel-based electricity
- Reduced load on distribution networks
- Sustainable and clean transportation support

Solar-wind hybrid charging systems provide diversified energy generation and enhance the reliability of EV charging infrastructure.

Another important benefit is grid support. EV charging often occurs during peak hours, which can cause voltage fluctuations and power quality issues in distribution systems. Integrating renewable energy sources reduces this burden by generating electricity locally.

The block diagram of a hybrid renewable energy–based EV charging system illustrates the integration of solar and wind energy sources to supply power for electric vehicle charging. In this system, the solar photovoltaic (PV) array converts sunlight into direct current (DC) electricity, which is regulated using a Maximum Power Point Tracking (MPPT) controller to maximize energy extraction. Simultaneously, the wind turbine generates electrical energy from wind and is connected to a generator that converts mechanical energy into electrical power.

The output from the wind generator is passed through a rectifier and connected to a common DC bus. Both solar and wind energy sources feed power into this DC bus, which acts as the central power distribution point of the system. An energy storage system, typically a battery, is connected to the DC bus to store excess energy produced during periods of high renewable generation and supply power when renewable energy is insufficient. The stored or generated DC power is then converted into alternating current (AC) using an inverter to meet the requirements of EV charging units.

Finally, the EV charging station delivers regulated power to electric vehicles for charging. This hybrid configuration improves system reliability, enhances renewable energy utilization, and reduces dependence on the conventional power grid.

Below block diagram Figure 1 represents the Hybrid Renewable Energy Based EV Charging (Solar + Wind)

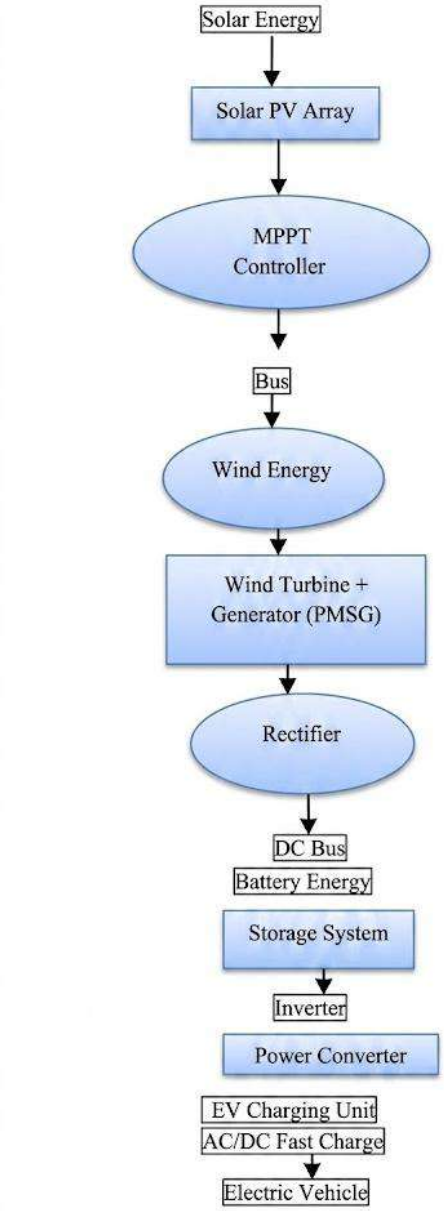

Figure 1: Block Diagram of Hybrid Renewable Energy Based EV Charging (Solar + Wind)

3. Components of Hybrid Renewable Energy EV Charging Systems

A typical hybrid renewable energy EV charging station consists of several key components.

3.1 Solar Photovoltaic System

Solar PV systems convert sunlight into electrical energy using photovoltaic cells. Solar panels generate DC electricity which is then converted into AC power using inverters for EV charging.

Important components include:

- PV panels
- DC-DC converter
- Maximum Power Point Tracking (MPPT) controller
- Inverter

MPPT controllers optimize the energy harvested from solar panels by continuously adjusting the operating point of the system.

3.2 Wind Energy System

Wind turbines convert kinetic energy from wind into electrical energy. In EV charging stations, wind energy provides an additional source of renewable power that complements solar generation.

Major components include:

- Wind turbine
- Permanent magnet synchronous generator (PMSG)
- Rectifier
- Power conditioning unit

The electricity generated from wind turbines is converted and regulated before being supplied to the EV charging system.

3.3 Energy Storage System

Because renewable energy sources are intermittent, energy storage systems are essential in hybrid charging stations. Batteries store excess energy produced during high generation periods and supply it when generation is low.

Common storage technologies include:

- Lithium-ion batteries
- Flow batteries
- Supercapacitors

Energy storage improves system reliability and ensures continuous EV charging availability.

3.4 Power Electronics and Control System

Power electronic converters play a crucial role in regulating the flow of energy within the hybrid system.

Key devices include:

- DC-DC converters
- AC-DC rectifiers
- Inverters
- Smart controllers

These devices maintain voltage stability and ensure efficient energy conversion.

3.5 EV Charging Unit

The charging unit provides the interface between the charging station and the electric vehicle.

Types of EV chargers include:

- Level 1 chargers (slow charging)
- Level 2 chargers (medium speed)
- DC fast chargers

4. Working Principle of Solar-Wind Hybrid EV Charging

The working principle of a hybrid renewable EV charging station involves multiple energy sources supplying power to the charging system.

- Solar panels generate electricity during daylight hours.
- Wind turbines generate electricity when wind is available.
- Power from both sources is regulated using power converters.
- Excess energy is stored in battery storage systems.
- Stored energy is used when renewable generation is low.
- EVs are charged using either renewable energy or stored power.

5. Advantages of Hybrid Renewable EV Charging

Hybrid renewable EV charging systems provide several technical, economic, and environmental benefits.

5.1 Improved Reliability

The combination of solar and wind energy ensures a more stable power supply. When solar energy is unavailable at night, wind energy can continue generating electricity.

5.2 Reduced Grid Dependency

Hybrid systems reduce the reliance on traditional power grids by generating electricity locally. Studies show that high renewable penetration significantly reduces grid reliance in EV charging stations.

5.3 Environmental Benefits

Hybrid renewable systems significantly reduce greenhouse gas emissions by replacing fossil fuel-based electricity with clean energy sources.

5.4 Cost Savings

Although the initial installation cost of renewable systems is high, long-term operational costs are lower due to reduced electricity purchases from the grid.

5.5 Grid Stability

Renewable-based EV charging stations help reduce peak demand on the grid and improve power quality.

6. Challenges of Hybrid Renewable EV Charging Systems

Despite many advantages, hybrid renewable EV charging systems also face several challenges.

6.1 Intermittent Renewable Energy

Solar and wind energy generation depends on weather conditions, which may lead to fluctuations in power generation.

6.2 High Initial Investment

The installation of solar panels, wind turbines, and energy storage systems requires significant capital investment.

6.3 Land Requirements

Solar panels and wind turbines require large installation areas, which may not always be available in urban environments.

6.4 Power Quality Issues

Hybrid systems must maintain voltage stability, harmonic control, and power factor correction to ensure efficient EV charging.

7. Applications of Hybrid Renewable EV Charging

Hybrid renewable EV charging systems can be implemented in various applications.

1. Urban Charging Stations

Cities can install solar-wind charging stations to reduce pollution and support sustainable transportation.

2. Highway Charging Infrastructure

Hybrid renewable systems can power charging stations along highways where grid infrastructure may be limited.

3. Remote and Rural Areas

Hybrid charging stations are especially useful in off-grid locations where traditional electricity supply is unavailable.

4. Smart Grid Integration

Hybrid EV charging stations can be integrated with smart grids for efficient energy management and demand response.

8. Future Trends and Research Directions

The future of hybrid renewable EV charging systems will involve advanced technologies such as:

- Artificial intelligence-based energy management
- Smart charging algorithms
- Vehicle-to-Grid (V2G) technology
- Internet of Things (IoT) monitoring systems
- Hybrid renewable charging infrastructure will play a crucial role in achieving sustainable transportation and reducing global carbon emissions.

Conclusion

- Hybrid renewable energy-based EV charging systems represent an effective solution for sustainable electric mobility. By combining solar and wind energy, these systems provide reliable, clean, and cost-effective electricity for EV charging. The complementary nature of solar and wind resources enhances system reliability and reduces the intermittency associated with individual renewable sources.
- Although challenges such as high initial costs and renewable variability remain, advances in energy storage, power electronics, and smart energy management systems are making hybrid charging stations more practical and efficient.
- As EV adoption continues to grow worldwide, hybrid renewable energy charging stations will become a key component of future smart transportation and sustainable energy systems.

References

1. Khaligh, A., & Li, Z. (2010). Battery, ultracapacitor, fuel cell, and hybrid energy storage systems for electric, hybrid electric, fuel cell, and plug-in hybrid electric vehicles: State of the art. *IEEE Transactions on Vehicular Technology, 59*(6), 2806–2814. https://doi.org/10.1109/TVT.2010.2047877
2. Yilmaz, M., & Krein, P. T. (2013). Review of battery charger topologies, charging power levels, and infrastructure for plug-in electric and hybrid vehicles. *IEEE Transactions on Power Electronics, 28*(5), 2151–2169. https://doi.org/10.1109/TPEL.2012.2212917
3. Deb, S., Tammi, K., Kalita, K., & Mahanta, P. (2018). Review of recent trends in charging infrastructure planning for electric vehicles. *Wiley Interdisciplinary Reviews: Energy and Environment, 7*(6), e306. https://doi.org/10.1002/wene.306
4. Hannan, M. A., Hoque, M. M., Mohamed, A., & Ayob, A. (2017). Review of energy storage systems for electric vehicle applications: Issues and challenges. *Renewable and Sustainable Energy Reviews, 69*, 771–789. https://doi.org/10.1016/j.rser.2016.11.171

5. Haque, M. E. (2023). *Hybrid renewable energy-based electric vehicle charging station: A review. Renewable Energy*.
6. Khan, I., Ahmad, A., & Chen, W. (2022). Optimal planning of solar–wind-based electric vehicle charging stations using energy storage. *Energy Reports*.
7. Morstyn, T., Hredzak, B., & Agelidis, V. G. (2018). Control strategies for microgrids with distributed energy storage systems: An overview. *IEEE Transactions on Smart Grid, 9*(4), 3652–3666. https://doi.org/10.1109/TSG.2016.2637958
8. International Energy Agency. (2023). *Global EV outlook 2023: Catching up with climate ambitions*. International Energy Agency. https://www.iea.org/reports/global-ev-outlook-2023
9. Larminie, J., & Lowry, J. (2012). *Electric vehicle technology explained* (2nd ed.). John Wiley & Sons.
10. Singh, B., Singh, S., & Chandra, A. (2021). *Solar-powered EV charging infrastructure for sustainable transportation.*

DESIGN AND DEVELOPMENT OF A SOLAR-POWERED INTELLIGENT EV SAFETY AND RECONNAISSANCE ROVER FOR REAL-TIME ENVIRONMENTAL MONITORING AND HAZARD DETECTION

C. Jayabalan
Department of Mechanical Engineering,
AMET Deemed to be University, Chennai, India.
Corresponding author E-mail: jayabalan.mech@ametuniv.ac.in

Abstract

The increasing demand for sustainable and intelligent monitoring systems has accelerated the development of autonomous mobile platforms for safety, surveillance, and environmental monitoring applications. This project presents the design and development of a Solar-Powered Intelligent EV Safety & Reconnaissance Rover, an Arduino-controlled mobile prototype that integrates multiple sensors for real-time hazard detection and environmental assessment. The system operates using a dual-energy architecture consisting of solar panels and rechargeable batteries, ensuring continuous and energy-efficient operation. The rover is equipped with obstacle detection, fire detection, smoke sensing, and atmospheric monitoring modules to identify potential dangers in its surroundings. The collected sensor data are processed by the Arduino microcontroller, which continuously monitors environmental conditions and activates automated multi-level alert mechanisms whenever abnormal situations are detected. The system is capable of providing early warnings for obstacles, fire outbreaks, harmful smoke concentrations, and unfavorable atmospheric conditions, thereby enhancing operational safety and situational awareness. The integration of renewable energy sources reduces dependence on conventional power supplies and promotes sustainable operation in remote or hazardous environments. The proposed intelligent rover can be deployed in industrial facilities, electric vehicle safety applications, disaster-prone areas, warehouses, agricultural fields, and surveillance operations. Overall, this project demonstrates a cost-effective, energy-efficient, and reliable solution for real-time environmental monitoring, hazard detection, and autonomous safety assistance using embedded systems and renewable energy technologies.

Keywords: Solar-Powered Rover, Arduino-Based Embedded System, Environmental Monitoring, Multi-Sensor Hazard Detection, And Real-Time Safety Alert System.

Introduction

The rapid growth of electric vehicles (EVs), autonomous systems, and renewable energy technologies has created a demand for intelligent mobile platforms capable of performing real-time environmental monitoring and safety surveillance. Autonomous rovers equipped with

multiple sensors can operate in hazardous or inaccessible environments, reducing human exposure to dangerous situations while improving operational efficiency [1]. Such systems are increasingly being used in industrial safety, disaster management, smart agriculture, and environmental monitoring applications.

Recent advancements in embedded systems have enabled the development of low-cost and energy-efficient monitoring devices using Arduino microcontrollers. Arduino-based platforms are widely adopted because of their simplicity, flexibility, low power consumption, and ease of integrating various environmental sensors [2]. Combining these capabilities with renewable energy sources further enhances system sustainability and enables long-duration field operations.

Solar energy has emerged as an attractive power source for autonomous systems because it is clean, renewable, and environmentally friendly. Integrating solar panels with rechargeable batteries provides continuous operation and reduces dependence on conventional energy sources [3]. Hybrid solar-battery systems are particularly useful for mobile robotic platforms deployed in remote locations where frequent battery replacement or external power supplies are impractical.

Environmental hazards such as fire outbreaks, smoke emissions, gas leakage, and unexpected obstacles pose serious risks to human life, industrial facilities, and electric vehicles. Therefore, real-time monitoring and early warning systems have become essential components of intelligent safety systems [4]. Multi-sensor integration enables simultaneous detection of obstacles, fire, smoke, temperature, humidity, and other atmospheric parameters, thereby improving situational awareness and response time.

In this Solar-Powered Intelligent EV Safety and Reconnaissance Rover is designed and developed using an Arduino controller, multiple environmental sensors, and a dual solar-battery energy system. The rover continuously monitors its surroundings and provides automated multi-level alerts whenever abnormal conditions are detected. The proposed system offers a sustainable, cost-effective, and reliable solution for environmental surveillance, hazard detection, and safety assistance in industrial environments, warehouses, disaster-prone regions, and smart city applications. The integration of renewable energy, embedded intelligence, and real-time sensing makes the proposed rover a promising platform for future autonomous safety and reconnaissance applications.

Objectives

- **Collision Avoidance:** To deploy an HC-SR04 ultrasonic sensor that continuously measures the distance to obstacles in front of the rover and activates a Level-3 alert whenever an object is detected within a distance of 20 cm.
- **Environmental Monitoring:** To continuously monitor ambient temperature and relative humidity using a DHT11 sensor and display the measured values in real time on a 16×2 I2C LCD module.

- **Fire Detection:** To integrate an infrared (IR) flame sensor for immediate fire detection and activate a Level-1 (highest-priority) continuous alarm whenever a flame is detected.
- **Smoke Detection:** To implement an MQ-series gas/smoke sensor that triggers **a Level-2 alert** when the detected smoke or gas concentration exceeds the threshold value of 400.
- **Sustainable Power Supply:** To develop a renewable energy system by integrating a 6.1 V solar panel with a dedicated solar charging module and Li-ion battery packs, thereby extending operational autonomy and reducing dependence on external charging sources.
- **Alert and Indication System:** To provide distinct audio-visual warning signals using LEDs and a buzzer, including a continuous tone for fire hazards, a pulsed tone for smoke detection, and a rapid chirp for obstacle detection.
- **Real-Time Data Display:** To display live sensor information on a 16×2 I2C LCD, alternating every 2 seconds between proximity/smoke data and temperature/humidity data during normal operating conditions.
- **Rugged Terrain Mobility:** To design the rover on a high-clearance RC rock crawler chassis equipped with off-road tyres and independent suspension to ensure stable movement and reliable sensor performance over uneven terrain.
- **Remote Control Operation:** To integrate an RF transmitter-receiver module that enables wireless human control of the rover during reconnaissance, testing, and safety monitoring operations.

Working Principle

The proposed Solar-Powered Intelligent EV Safety and Reconnaissance Rover operate based on a continuous sense–process–respond mechanism to perform real-time environmental monitoring, hazard detection, and remote-controlled navigation. Multiple sensors continuously collect information from the surrounding environment, and the Arduino Uno microcontroller processes the acquired data to generate appropriate responses.

Initially, the HC-SR04 ultrasonic sensor emits 40 kHz ultrasonic pulses and measures the echo return time to determine the distance between the rover and nearby obstacles. If an object is detected within a predefined distance of 20 cm, a Level-3 obstacle alert is activated. Simultaneously, the infrared flame sensor monitors infrared radiation in the wavelength range of 760–1100 nm to detect the presence of fire. Upon detection, the system immediately triggers a Level-1 continuous alarm, which has the highest priority.

The MQ-series gas sensor continuously samples the surrounding air to detect smoke, liquefied petroleum gas (LPG), and other combustible gases. When the gas concentration exceeds the specified threshold value, a Level-2 alert is generated. In addition, the DHT11 sensor continuously measures ambient temperature and relative humidity to monitor environmental conditions.

The Arduino Uno microcontroller receives and processes all sensor inputs simultaneously using a priority-based control algorithm. Whenever any sensor value exceeds its predefined threshold, the corresponding audio-visual warning signal is activated through a buzzer and LED indicator. During normal operating conditions, a 16×2 I2C LCD displays real-time sensor information by alternating every two seconds between proximity/smoke data and temperature/humidity data.

To ensure sustainable operation, a 6.1 V solar panel connected through a solar charging module continuously charges the Li-ion battery packs, thereby extending the rover's operating time and reducing dependence on external charging sources. Furthermore, an RF transmitter-receiver module enables wireless remote control, allowing an operator to navigate the rover in all directions during reconnaissance and testing operations. Overall, the system provides an energy-efficient, intelligent, and reliable platform for safety monitoring, environmental surveillance, and hazard detection in real time.

Figure 1: Block diagram for the Solar-Powered Intelligent EV Safety & Reconnaissance Rover – Prototype Multi-View

Methodology

he proposed solar-powered intelligent EV safety and reconnaissance rover was developed using a systematic engineering approach involving system design, hardware integration, software development, environmental sensing, obstacle detection, and performance evaluation. The overall methodology consists of six major stages as shown below.

1. System Design and Requirement Analysis

Initially, the operational requirements of the rover were identified. The rover was designed to:

- Operate autonomously in outdoor environments.
- Utilize solar energy as the primary power source.

- Monitor environmental parameters in real time.
- Detect hazards and obstacles.
- Transmit collected data wirelessly for remote monitoring.
- Ensure safe navigation in hazardous environments.

Based on these requirements, suitable hardware and software components were selected.

2. Hardware Design and Component Selection

The rover platform was constructed using lightweight and durable materials to support mobility and energy efficiency. The following components were integrated:

- **Microcontroller:** Arduino Uno/Nano for central control.
- **Solar Power System:** 6.1 V solar panel with onboard charging circuit.
- **Battery Storage:** Li-ion batteries for uninterrupted operation.
- **Motor Driver:** L298N motor driver module.
- **DC Gear Motors:** For rover locomotion.
- **Ultrasonic Sensor (HC-SR04):** For obstacle detection.
- **Environmental Sensors:** Temperature, humidity, gas, and air quality sensors.

3. Solar Energy Management System

A renewable energy subsystem was implemented to power the rover.

The solar panel converts solar energy into electrical energy, which is regulated using a charging controller and stored in rechargeable Li-ion batteries. The stored energy supplies power to:

- The microcontroller unit
- Environmental sensors
- Communication modules
- DC motors

A dual-power arrangement was employed to separately manage motor loads and control electronics, thereby improving overall system stability and efficiency.

4. Environmental Monitoring and Hazard Detection

Environmental sensors continuously monitor surrounding conditions.

The monitored parameters include:

- Ambient temperature
- Relative humidity
- Air quality
- Harmful gas concentration

If any parameter exceeds predefined threshold values, the system automatically:

- Activates warning LEDs.
- Generates buzzer alerts.

- Transmits hazard notifications to the monitoring station.

5. Intelligent Navigation and Obstacle Avoidance

- The rover operates using a continuous **Sense–Process–Respond** mechanism.

Step 1: Sense: The HC-SR04 ultrasonic sensor emits 40 kHz ultrasonic waves and measures the echo return time to determine the distance to nearby obstacles.

Step 2: Process: The Arduino processes the sensor data and compares the measured distance with a preset safety threshold.

Step 3: Respond

- Based on the decision:
- If no obstacle is detected, the rover moves forward.
- If an obstacle is detected, the rover stops.
- The rover then changes direction and selects an alternate path.
- This process continuously repeats to ensure safe autonomous navigation.

6. Wireless Data Transmission and Remote Monitoring

The collected environmental and operational data are transmitted wirelessly to a remote monitoring device.

The transmitted information includes:

Temperature readings

- Humidity values
- Gas concentration levels
- Obstacle detection status
- Battery status

Users can monitor the rover's operation in real time using a mobile application, web interface, or serial monitoring system.

7. System Testing and Performance Evaluation

The developed rover was tested under different environmental conditions.

The following performance parameters were evaluated:

- Solar charging efficiency
- Battery backup duration
- Obstacle detection accuracy
- Environmental sensing accuracy
- Wireless communication range
- Response time for hazard detection
- Overall navigation performance

The experimental results were analyzed to validate the reliability and effectiveness of the proposed system.

Conclusion

This chapter successfully demonstrates the design and development of a solar-powered intelligent EV safety and reconnaissance rover capable of performing real-time environmental monitoring and hazard detection. By integrating renewable solar energy, autonomous navigation, environmental sensors, and wireless communication technologies, the rover provides an efficient and sustainable solution for operating in hazardous and inaccessible environments.

The implemented system continuously monitors environmental parameters such as temperature, humidity, air quality, and harmful gas concentrations while simultaneously detecting obstacles using ultrasonic sensing technology. The Sense–Process–Respond control mechanism enables the rover to navigate safely and autonomously by avoiding obstacles and generating timely hazard alerts. The incorporation of a solar charging system enhances energy efficiency and extends operational duration, reducing dependence on external power sources.

The experimental results demonstrate reliable performance in environmental monitoring, obstacle avoidance, data transmission, and hazard detection. The proposed system can be effectively utilized in disaster management, industrial safety inspections, environmental surveillance, agricultural monitoring, and remote reconnaissance applications.

Future improvements may include the integration of artificial intelligence, GPS-based navigation, machine learning algorithms, thermal imaging cameras, and Internet of Things (IoT) platforms to further enhance the rover's autonomous decision-making capabilities, accuracy, and real-time monitoring performance.

References

1. Mendez-Flores, E., Pourshahidi, A., & Egerstedt, M. (2025). *RaccoonBot: An autonomous wire-traversing solar-tracking robot for persistent environmental monitoring*.
2. Tsebesebe, N. T., Mpofu, K., Sivarasu, S., & Mthunzi-Kufa, P. (2025). Arduino-based devices in healthcare and environmental monitoring. *Discover Internet of Things, 5*, 46
3. Patil, V. S., Morey, A. P., Chauhan, G. J., Bhute, S. S., & Borkar, T. S. (2019). A review paper on solar power monitoring system using an IoT. *International Journal of Computer Sciences and Engineering, 7*(8), 212–215. https://doi.org/10.26438/ijcse/v7i8.212215
4. Deogade, U., Malkhede, R., Nimje, K., Patil, T., Suryawanshi, K., & Burange, R. (2022). An IoT-based approach for monitoring solar system parameters using Arduino microcontroller. *International Journal for Research in Applied Science & Engineering Technology, 10*(6), 3149–3153. https://doi.org/10.22214/ijraset.2022.43947

EXPLORING ADVANCED NANOSCALE MEMRISTORS: INNOVATIONS IN MATERIALS, DESIGN METHODOLOGIES, AND FUTURE DEVICE APPLICATIONS

Dipankar Gogoi*[1], Pradip Kumar Kalita[2] and T. D. Das[1]

[1]Department of Basic and Applied Science,
National Institute of Technology Arunachal Pradesh, Papum Pare, Jote-791113, India
[2]Department of Physics,
Rajiv Gandhi University, Arunachal Pradesh, Papum Pare, Doimukh-791112, India
*Corresponding author E-mail: nehu.nanodg@gmail.com

Abstract

Advanced nanoscale memristors are transforming modern electronics. They enable a shift from traditional computing to intelligent neuromorphic systems. These devices were once a theoretical concept linking magnetic flux and electric charge. Today, they provide practical, non-volatile resistive switching. Recent material engineering has driven significant progress. Breakthroughs in metal oxides, polymers, perovskites, spintronics, and two-dimensional materials have improved device stability. They also offer better scalability and multi-level storage. Researchers have also advanced how we model these devices. New frameworks like SPICE and neural-network models help optimize performance for circuit integration. These tools are crucial for building complex hardware. These innovations have accelerated many applications. They are now used in non-volatile memory and high-density storage. They are also central to artificial intelligence hardware and in-memory computing. Furthermore, new photonic and biomedical memristors are expanding the field's reach. By combining material science, computational modeling, and new architectures, nanoscale memristors are redefining the future of energy-efficient, cognitive computing.

Keywords: Memristor, Neuromorphic Computing, Resistive Switching, In-Memory Computing, and Nanoscale Materials.

1. Introductions

Advanced nanoscale memristor development signals a fundamental electronics shift, bridging conventional computing and high-performance neuromorphic intelligence [1]. Leon Chua theoretically predicted the memristor in 1971 as the "missing" fourth circuit element linking charge and flux [2]. It remained a curiosity until HP Labs demonstrated the first physical nanoscale device in 2008 using titanium dioxide [3]. This confirmed resistive switching occurs via coupled electronic and ionic transport [4]. The field has expanded from basic physics to transition metal oxides, 2D materials, and organic matrices [5]. Memristors are now transitioning

into engines for neuromorphic computing, hardware security, and energy-efficient Artificial Intelligence (AI), redefining non-von Neumann architectures [6]. Theoretically, memristive systems provide a robust foundation for modern circuit synthesis [4, 7]. While academic debate regarding the ideal memristor continues [8], breakthroughs focus on physical implementations showing non-volatile resistance changes [9, 10]. Engineers rely on specialized emulator circuits to prototype operations before fabrication [11, 12]. Structures depend on sophisticated modeling like Simulation Program with Integrated Circuit Emphasis (SPICE), the generalized metastable switch model, and neural network configurations [5, 13, and 14]. A vital distinction exists between two-terminal memristors and three-terminal memistors, as their mechanics and dynamics dictate different behaviors [15]. Material synthesis is central, spanning metal oxides, spintronics, polymers, and low-dimensional matrices [16, 17, and 18]. Transition metal oxides like titanium dioxide and perovskites enable stable oxygen vacancy migration and localized filament formation [19, 20]. Further engineering involves flexible organic frameworks, hybrid polymers, and chalcogenides for robust bipolar switching [21, 22]. Two-dimensional layers like molybdenum disulfide enable atomic-scale crossbar configurations [23]. Hardware also incorporates ferroelectric mechanisms and multi-walled carbon nanotubes for low-power requirements [24]. Research now integrates optical and photonic properties, yielding phototriggered arrays and dual-functional perovskite systems for in-sensor processing [25, 26]. Industrial scaling has moved from isolated components to dense crossbar arrays, making them dominant contenders for non-volatile memory and reconfigurable structures [27]. Embedding memory into logic architectures lowers supply voltages and energy usage [28]. This eliminates the von Neumann bottleneck by processing math directly within the memory array [29]. The most pronounced application lies in neuromorphic AI chips [2, 30]. Nanoscale memristors mimic biological synapses, capturing phenomena like memory transitions, diffusion kinetics, and metaplasticity [1, 31]. These synapses power hardware neural networks and deep learning accelerators [32]. Stochastic dynamics enable reservoir computing and secure cryptographic hardware [33]. Versatility also transforms medicine through flexible, biocompatible devices for monitoring and diagnostics [34]. Gas sensors and self-powered matrices benefit from these sensitive, multi-state recovery properties [35]. By unifying innovation, modeling, and architecture, memristors break boundaries in efficiency and cognitive hardware [36]. Since integrated simulation and experimentation bridge theoretical and practical gaps [37]. This accelerates development, emphasizing scalable synthesis and material characterization. Future work will prioritize fabrication, doping strategies, and long-term stability [38]. Memristors have evolved from theory into the backbone of future hardware, enabling faster, smarter, and more efficient computational systems [39, 40].

Thus, the nanoscale memristors have changed significantly. They are no longer just a theory. They are now a core part of modern hardware. The name "memristor" comes from "memory" and "resistor." It is known as the fourth basic circuit element. These devices can remember their past states. Their resistance changes based on the electricity that passed through them. Traditional computers follow the "von Neumann" architecture. This design often struggles with speed and power limits. Memristors help fix these issues. They allow computers to work more efficiently. They store data and process it in a new way. This makes them essential for the next generation of electronic devices. Figure 1 is schematic illustration of nanoscale memristors as the fourth fundamental circuit element, highlighting their non-volatile and history-dependent resistive behavior, operational mechanism based on ionic migration and conductive filament formation, advantages over conventional von Neumann architectures, and their emerging applications in neuromorphic computing, artificial intelligence, non-volatile memory, Internet of Things (IoT), and biomedical systems.

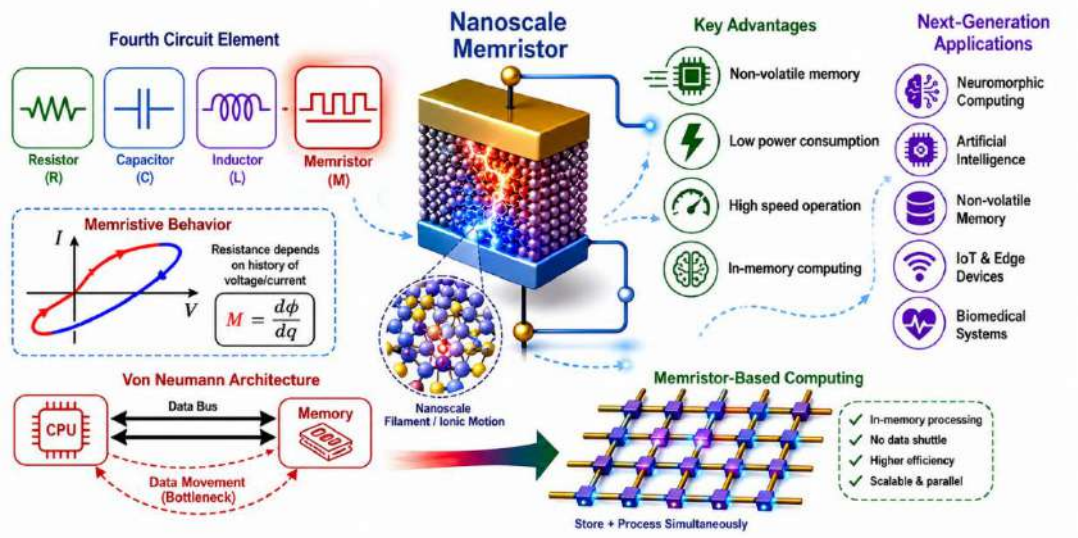

Figure 1: Schematic illustration of nanoscale memristors as the fourth fundamental circuit element

2. Material Breakthroughs: Beyond Traditional Switching

The core of memristive action relies entirely on the switching layer. Inside this layer, structural defects migrate under an applied electric field. These defects are primarily oxygen vacancies. Their movement enables the reversible formation and dissolution of microscopic conductive filaments [4, 6, 10, 27, and 35]. Figure 2 highlights how emerging materials like two-dimensional (2D) sheets and spintronics exceed traditional performance limits in scalability and switching speed.

Transition Metal Oxides

Transition metal oxides (TMOs) currently serve as the industry standard for reliable memristor technology [12, 18, and 29]. Materials such as HfO_2, TiO_2, and TaO_x lead the field due to their

exceptional physical properties. A primary advantage is their high degree of CMOS compatibility, allowing them to integrate seamlessly with mature, large-scale silicon fabrication lines. These materials deliver impressive levels of thermal stability and operational endurance. Their consistent performance makes them the ideal candidates for high-density 3D crossbar architectures, which are essential for scaling modern memory and processing systems [18, 24].

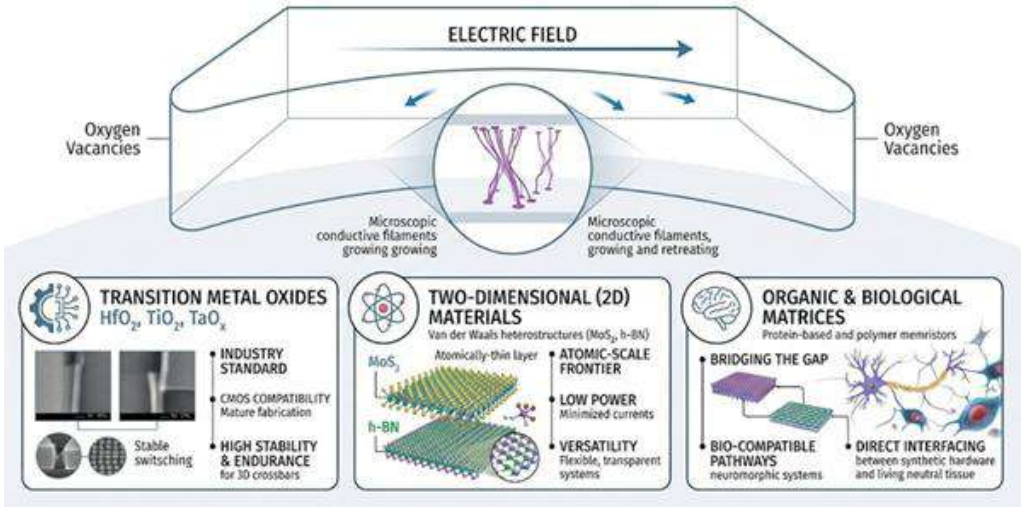

Figure 2: Schematic illustration of material breakthroughs for beyond traditional switching

Two-Dimensional (2D) Materials

Two-dimensional (2D) materials are currently pushing the atomic-scale frontier of memristor technology [6, 9, and 15]. By utilizing van der Waals heterostructures such as molybdenum disulfide (MoS_2) and hexagonal boron nitride (h-BN), researchers are developing devices with unprecedented control over charge carrier transport. These materials offer a critical advantage in power efficiency; their ultra-thin, atomic-layer structure allows for significantly lower switching currents compared to traditional bulk materials [11, 17]. Furthermore, their inherent versatility enables the creation of innovative, flexible, and highly transparent electronic systems. This technology is instrumental in bridging the gap toward next-generation electronics that are not only high-performing but also adaptable to unconventional form factors.

Organic & Biological Matrices

Organic and biological matrices are driving a revolution in sustainable and bio-integrated electronics [20, 27]. Researchers are now developing biocompatible memristors by utilizing polymers and protein-based materials instead of traditional silicon. This shift allows for neuro-inspired designs that mimic the intricate plasticity of the human brain. By utilizing natural ionic flux, these matrices achieve high energy efficiency for advanced neuromorphic hardware [21, 33]. Most importantly, their mechanical flexibility allows for direct interfacing with living neural tissue. This capability minimizes the stiffness mismatch found in traditional implants, paving the way for seamless brain-machine connections and advanced neuroprosthetics [35].

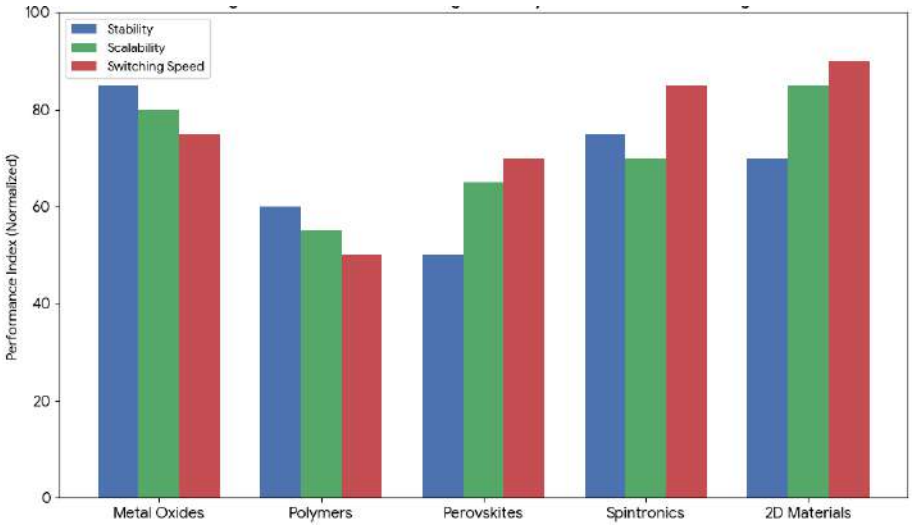

Figure 3: **Compares material performance, highlighting breakthroughs in satability, scalability and switching speed beyond traditional silicon**

3. Modeling Memristors: From Atoms to Circuits

Turning memristors into commercial products requires accurate math. We use three main modeling strategies to bridge the gap between physics and circuit design [17, 27]. Physics-driven models map ion movement and thermal dynamics using partial differential equations. These are highly accurate but computationally demanding. Compact SPICE models act as the industry standard by abstracting atomic physics into efficient circuit parameters. They are ideal for large-scale system simulations. Phenomenological approaches use empirical curve-fitting to mimic experimental hysteresis [28, 37]. These are perfect for rapid prototyping. Each method balances simulation speed against predictive rigor to ensure reliable device development**.** Figure 4 maps the computational and physical trade-offs across three different strategies for modeling nanoscale memristor behavior.

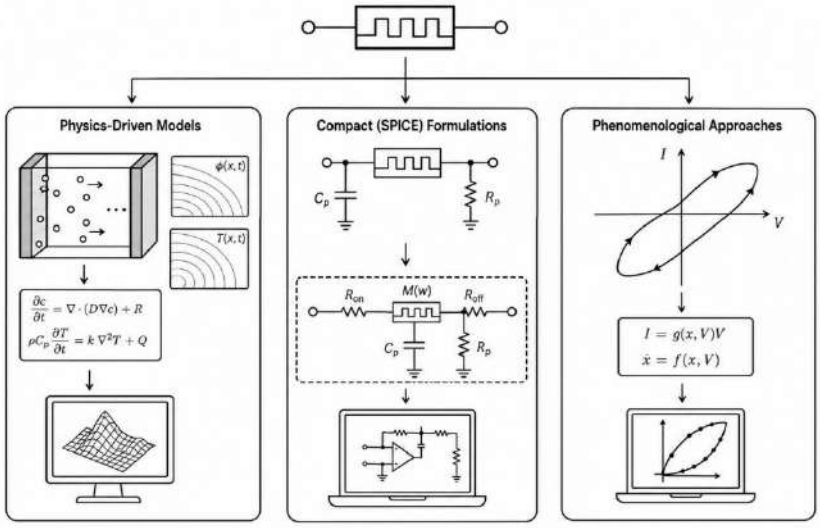

Figure 4: Schematic illustration of material breakthroughs for beyond traditional switching

Physics-Driven Models

Physics-driven models offer the most detailed analysis of memristive devices. They examine the microscopic processes occurring within the material [19, 21]. These models use Partial Differential Equations (PDEs) to describe core dynamics. They track ion migration and charge transport. They also model the formation and rupture of conductive filaments. Furthermore, they account for thermal diffusion and heat dissipation. These models provide high precision for switching mechanisms. They reveal insights into material behavior and reliability [14, 26, 32]. This accuracy is vital for developing new materials and architectures. However, this precision requires significant computational resources. The high processing power and time needed limit their use. Consequently, they are rarely practical for large-scale circuit-level implementations.

Compact (SPICE) Formulations

Compact (SPICE) formulations are the industry standard for memristor modeling. They translate complex atomic-scale physics into manageable circuit parameters [8, 12]. Instead of solving detailed physical equations, they use simplified mathematical relationships. These models integrate seamlessly into standard Electronic Design Automation (EDA) tools. Their primary advantage is computational efficiency. They allow for the rapid analysis of large memristor arrays. They also support simulations of complex integrated systems without massive processing demands. This makes them ideal for designing memory architectures and neuromorphic circuits [18, 25]. Still, their accuracy relies on the quality of their abstraction. Oversimplification of physical phenomena can reduce predictive reliability. Consequently, compact models are best reserved for industrial circuit design, optimization, and system-level simulations.

Phenomenological Approaches

Phenomenological models prioritize output behavior over the underlying physical causes. They utilize empirical curve-fitting to replicate the I-V hysteresis loops observed in experimental data [7, 15]. These models offer distinct advantages for engineering workflows. They are excellent for fast and simple prototyping. Researchers can achieve quick results without solving complex differential equations. However, these approaches have significant limitations. They often lack deep predictive power regarding device behavior. Their accuracy can falter when material compositions change or operating conditions shift [19, 33]. Consequently, they are best suited for initial proof-of-concept simulations rather than final design verification. Designers must weigh these trade-offs carefully. They balance the need for simulation speed against the requirement for physical rigor in advanced applications [4, 37]. Figure 5 illustrates memristor maturity, showing non-volatile memory (NVM)'s industrial saturation contrasting with the rapid, ongoing architectural iteration in cognitive computing. Table 1 summarizes the core pillars, materials, modeling, and architectures for developing scalable, sustainable, and energy-efficient memristor technologies.

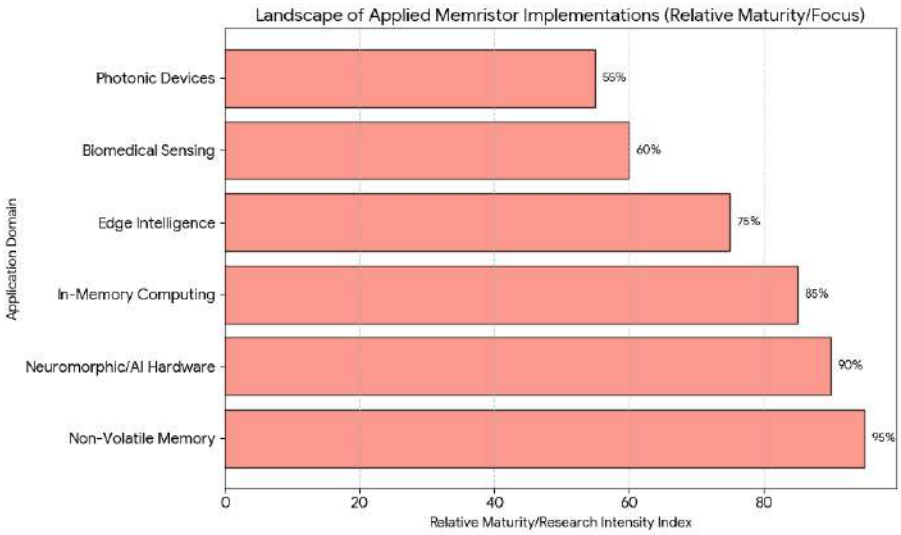

Figure 5: Memristor maturity, non-volatile memory (NVM) saturation contrasting with rapid AI architectural iteration

Table 1: Framework for Scalability & Sustainability in Memristor Systems

Strategic Pillar	Key Components / Materials	Impact on Scalability & Sustainability
Material Innovation	Transition Metal Oxides (TMOs), 2D Materials (MoS2, h-BN), Organic/Bio-matrices	Enables CMOS compatibility, atomic-scale control, flexibility, and biocompatibility.
Design Methodologies	Physics-driven models, Compact (SPICE) formulations, Phenomenological models	Bridges the gap between atomic physics and mass-scale circuit production.
Architecture Shift	In-memory computing, Neuromorphic crossbar arrays	Dissolves the von Neumann bottleneck; improves energy efficiency by orders of magnitude.
Emerging Applications	AI/Edge intelligence, Hardware security (PUFs), Bio-integrated sensors	Enables localized processing, high-density storage, and real-time inference on edge devices.
Sustainability Goals	Low-power footprint, biocompatible materials, self-powered matrices	Reduces energy consumption and enables sustainable, flexible hardware integration.

4. Emerging Applications: Toward the Synthetic Brain

Memristors are evolving from simple storage into engines for AI and edge computing. Their physical properties break traditional von Neumann constraints [10, 21]. Memory and processing are no longer separate. They integrate data storage and logic within one nanoscale device. This enables energy-efficient "in-memory" computing. Memristor-based crossbar arrays act as artificial synapses. They replicate neural plasticity. They execute complex math like matrix-

vector multiplications locally. This avoids energy-intensive data movement across chips. It solves the performance bottleneck of modern AI [8, 23]. Their ultra-low power footprint suits edge intelligence perfectly. Battery-constrained devices like wearables can process AI locally. They no longer rely on the cloud. Researchers are refining material science and modeling. They are overcoming device stochasticity. Memristors are enabling massive 3D-integrated synaptic hardware. They are the power behind a new era of brain-inspired computing [3, 24].

In-memory neuromorphic computing fundamentally transforms information processing. Mimicking human brain synaptic plasticity, memristor-based crossbar arrays execute computations directly within memory [9, 35]. This design successfully dissolves the traditional "von Neumann bottleneck" by eliminating inefficient data movement. By performing operations in-place, these systems achieve massive improvements in energy efficiency. Consequently, they are uniquely suited to meet the intensive demands of modern deep learning workloads [11, 28]. Figure 6 depicts integrated technologies and materials enabling energy-efficient, neuro-inspired systems for synthetic brain development.

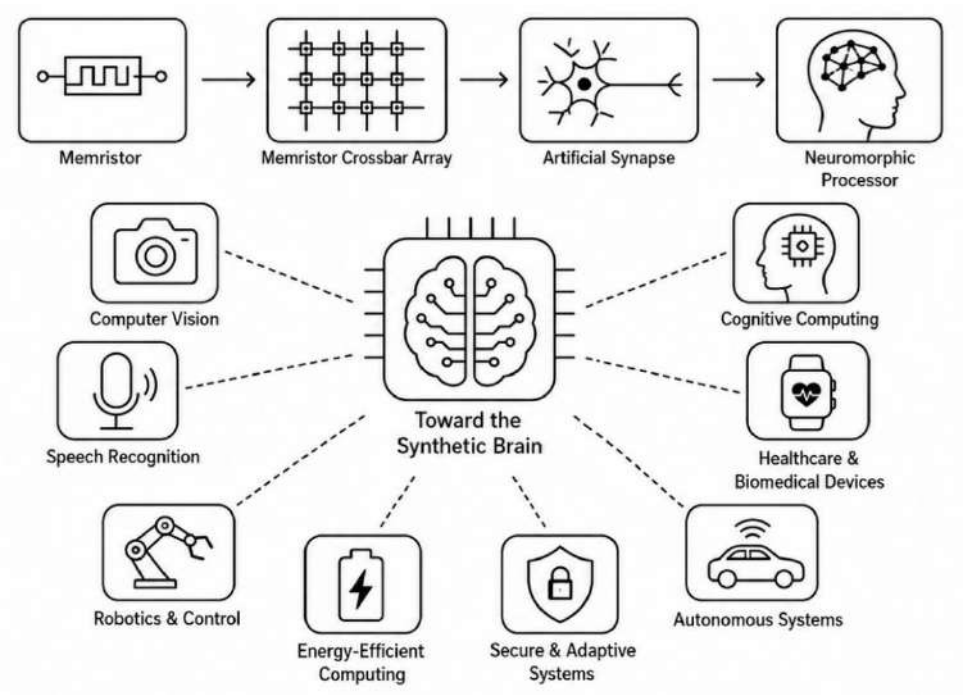

Figure 6: Schematic illustration of emerging applications toward the synthetic brain

Memristors provide advanced hardware security by leveraging inherent physical variations during nanoscale fabrication [17, 40]. These atomic-level differences generate unique Physical Unclonable Functions (PUFs). Acting as a "digital fingerprint," each PUF enables secure authentication and cryptographic key generation. Because these features cannot be replicated or reverse-engineered, they remain inherently secure. This technology offers a critical defense layer for IoT hardware, protecting sensitive devices from unauthorized access and tampering [22, 37]. As memristors are revolutionizing edge intelligence. They enable high-performance AI on low-

power hardware. Traditional systems suffer from power-hungry data transfers. Conversely, memristor-based engines offer an ultra-low power footprint. This allows battery-powered devices to perform complex AI tasks in real-time. By processing data locally, these systems avoid cloud dependency [31, 38]. This reduces both latency and energy consumption. Ultimately, this technology significantly extends the operational life of remote, battery-constrained devices.

The transition from laboratory prototypes to mass production centers on managing device stochasticity [22, 28, and 38]. This inherent variability stems from atomic-scale processes within the memristor. Such fluctuations can degrade the precision of large-scale neural networks. To address this, the industry relies on a synergy between material science and high-fidelity compact modelling [23, 34]. Engineers precisely characterize these variations. This allows them to design resilient circuits that compensate for device-level inconsistencies. This convergence enables the development of massive, 3D-integrated "synaptic" hardware. Such advancements initiate a new era in non-von Neumann computing [12, 19]. They allow reliable and highly dense neural architectures to move from the lab to real-world deployment. **Table 2** contrasts the fundamental scientific characterization with practical, efficient industrial application to bridge the gap toward scalable memristor technology.

Table 2: Comparative Analysis of Basic vs. Applied Memristor Implementations

Feature	Basic (Fundamental) Implementations	Applied (Industrial/System) Implementations
Primary Goal	Device characterization & proof-of-concept.	Commercial viability & performance scaling.
Modeling Approach	Physics-driven (PDEs) for atomic accuracy.	Compact (SPICE) for circuit efficiency.
Design Focus	Ion migration, filament physics, & heat dynamics.	Matrix-vector multiplication, latency, & energy.
Complexity	High (demands significant compute/time).	Optimized (integrated into EDA tools).
Application	New material discovery & reliability testing.	AI accelerators, IoT security, & neural networks.
Key Advantage	Unrivaled precision in switching mechanisms.	Rapid analysis of large-scale crossbar arrays.
Primary Limitation	Not practical for large-scale circuit design.	Relies on abstraction; risk of oversimplification.

Conclusions

The evolution of memristors marks a major turning point in modern electronics. We are moving beyond rigid silicon. We are entering an era of flexible, bio-integrated, and atomic-scale systems.

Innovations in nanoscale materials such as 2D layers, transition metal oxides, and organic matrices are expanding our design horizons. High-fidelity modeling bridges the gap between theory and mass-scale production. These breakthroughs dissolve the von Neumann bottleneck. They provide the foundation for in-memory computing and neuromorphic computing. The resistive switching enables this leap in architecture. Future hardware will soon redefine the capabilities of artificial intelligence and edge devices. This transition promises a new era of highly integrated, energy-efficient, and intelligent computing. As we refine these technologies, we draw closer to hardware that mimics human brain plasticity. The convergence of material science, precise circuit design, and synthetic biology ensures a faster, smarter, and more sustainable future.

References

1. Jeong, H., & Shi, L. (2019). Memristor devices for neural networks. *Journal of Physics D: Applied Physics*, *52*(2), 023003.
2. Li, Y., Wang, Z., Midya, R., Xia, Q., & Yang, J. J. (2018). Review of memristor devices in neuromorphic computing: materials sciences and device challenges. *Journal of Physics D: Applied Physics*, *51*(50), 503002.
3. Xiao, Y., Jiang, B., Zhang, Z., Ke, S., Jin, Y., Wen, X., & Ye, C. (2023). A review of memristor: material and structure design, device performance, applications and prospects. *Science and Technology of Advanced Materials*, *24*(1), 2162323.
4. Corinto, F., Civalleri, P. P., & Chua, L. O. (2015). A theoretical approach to memristor devices. *IEEE Journal on Emerging and Selected Topics in Circuits and Systems*, *5*(2), 123-132.
5. Yakopcic, C., Taha, T. M., Subramanyam, G., Pino, R. E., & Rogers, S. (2011). A memristor device model. *IEEE electron device letters*, *32*(10), 1436-1438.
6. Prezioso, M., Riminucci, A., Graziosi, P., Bergenti, I., Rakshit, R., Cecchini, R., ... & Dediu, V. A. (2013). A single-device universal logic gate based on a magnetically enhanced memristor. *Advanced Materials*, *25*(4), 534-538.
7. Yin, Z., Tian, H., Chen, G., & Chua, L. O. (2015). What are memristor, memcapacitor, and meminductor?. *IEEE Transactions on Circuits and Systems II: Express Briefs*, *62*(4), 402-406.
8. Vongehr, S., & Meng, X. (2015). The missing memristor has not been found. *Scientific reports*, *5*(1), 11657.
9. Lanza, M., Pazos, S., Aguirre, F., Sebastian, A., Le Gallo, M., Alam, S. M., & Roldan, J. B. (2025). The growing memristor industry. *Nature*, *640*(8059), 613-622.

10. Prodromakis, T., & Toumazou, C. (2010, December). A review on memristive devices and applications. In *2010 17th IEEE international conference on electronics, circuits and systems* (pp. 934-937). IEEE.
11. Kim, H., Sah, M. P., Yang, C., Cho, S., & Chua, L. O. (2012). Memristor emulator for memristor circuit applications. *IEEE Transactions on Circuits and Systems I: Regular Papers*, *59*(10), 2422-2431.
12. Lin, R., Shi, G., Qiao, F., Wang, C., & Wu, S. (2023). Research progress and applications of memristor emulator circuits. *Microelectronics Journal*, *133*, 105702.
13. Singh, J., & Raj, B. (2018). Comparative analysis of memristor models and memories design. *Journal of Semiconductors*, *39*(7), 074006.
14. Dongale, T. D., Patil, K. P., Gaikwad, P. K., & Kamat, R. K. (2015). Investigating conduction mechanism and frequency dependency of nanostructured memristor device. *Materials Science in Semiconductor Processing*, *38*, 228-233.
15. Adhikari, S. P., & Kim, H. (2012). Why are memristor and memistor different devices?. *IEEE Transactions on Circuits and Systems I: Regular Papers*, *59*(11), 2611-2618.
16. Wang, L., Yang, C., Wen, J., Gai, S., & Peng, Y. (2015). Overview of emerging memristor families from resistive memristor to spintronic memristor. *Journal of Materials Science: Materials in Electronics*, *26*(7), 4618-4628.
17. Mohammad, B., Abi Jaoude, M., Kumar, V., Al Homouz, D. M., Nahla, H. A., Al-Qutayri, M., & Christoforou, N. (2016). State of the art of metal oxide memristor devices. *Nanotechnology reviews*, *5*(3), 311-329.
18. Chen, Y., Liu, G., Wang, C., Zhang, W., Li, R. W., & Wang, L. (2014). Polymer memristor for information storage and neuromorphic applications. *Materials Horizons*, *1*(5), 489-506
19. Ilyas, N., Li, D., Li, C., Jiang, X., Jiang, Y., & Li, W. (2020). Analog switching and artificial synaptic behavior of Ag/SiO x: Ag/TiO x/p++-Si memristor device. *Nanoscale research letters*, *15*(1), 30.
20. Kim, M., Lee, S., Kim, S. J., Lim, B. M., Kang, B. S., & Lee, H. S. (2024). Study on the sodium-doped titania interface-type memristor. *ACS applied materials & interfaces*, *16*(13), 16453-16461.
21. Jaafar, A. H., Al Chawa, M. M., Cheng, F., Kelly, S. M., Picos, R., Tetzlaff, R., & Kemp, N. T. (2021). Polymer/TiO2 nanorod nanocomposite optical memristor device. *The Journal of Physical Chemistry C*, *125*(27), 14965-14973.

22. Xu, Z., Li, Y., Xia, Y., Shi, C., Chen, S., Ma, C., & Li, Y. (2024). Organic frameworks memristor: An emerging candidate for data storage, artificial synapse, and neuromorphic device. *Advanced Functional Materials*, *34*(16), 2312658.
23. Zhou, H., Li, S., Ang, K. W., & Zhang, Y. W. (2024). Recent advances in in-memory computing: exploring memristor and memtransistor arrays with 2D materials. *Nano-Micro Letters*, *16*(1), 121.
24. Mikheev, V., Chouprik, A., Lebedinskii, Y., Zarubin, S., Matveyev, Y., Kondratyuk, E., & Negrov, D. (2019). Ferroelectric second-order memristor. *ACS applied materials & interfaces*, *11*(35), 32108-32114.
25. Cao, F., Hu, Z., Yan, T., Hong, E., Deng, X., Wu, L., & Fang, X. (2023). A dual-functional perovskite-based photodetector and memristor for visual memory. *Advanced Materials*, *35*(44), 2304550.
26. Spagnolo, M., Morris, J., Piacentini, S., Antesberger, M., Massa, F., Crespi, A., & Walther, P. (2022). Experimental photonic quantum memristor. *Nature Photonics*, *16*(4), 318-323.
27. Gregory, M. D., & Werner, D. H. (2015). Application of the memristor in reconfigurable electromagnetic devices. *IEEE Antennas and Propagation Magazine*, *57*(1), 239-248.
28. Babacan, Y., Yesil, A., & Gul, F. (2018). The fabrication and MOSFET-only circuit implementation of semiconductor memristor. *IEEE Transactions on Electron Devices*, *65*(4), 1625-1632.
29. Jiang, Z., Zhao, H., Tang, J., Lu, Y., Qin, Q., Wang, Z., & Wu, H. (2026). Strategies of high-accuracy memristor-based analogue computing in memory for artificial intelligence. *Nature Materials*, 1-15.
30. Aguirre, F., Sebastian, A., Le Gallo, M., Song, W., Wang, T., Yang, J. J., & Lanza, M. (2024). Hardware implementation of memristor-based artificial neural networks. *Nature communications*, *15*(1), 1974.
31. Wu, Q., Wang, H., Luo, Q., Banerjee, W., Cao, J., Zhang, X., & Liu, M. (2018). Full imitation of synaptic metaplasticity based on memristor devices. *Nanoscale*, *10*(13), 5875-5881.
32. Yao, P., Wu, H., Gao, B., Tang, J., Zhang, Q., Zhang, W., & Qian, H. (2020). Fully hardware-implemented memristor convolutional neural network. *Nature*, *577*(7792), 641-646.
33. Liu, X., Huang, Y., Zeng, Z., & Wunsch, D. C. (2020). Memristor-based HTM spatial pooler with on-device learning for pattern recognition. *IEEE Transactions on Systems, Man, and Cybernetics: Systems*, *52*(3), 1901-1915.

34. Cao, Z., Liu, Y., Sun, B., Zhou, G., Gao, K., Sun, S., & Qin, S. (2025). A high-stability pressure-sensitive implantable memristor for pulmonary hypertension monitoring. *Advanced Materials*, *37*(3), 2411659.
35. Lee, D., Yun, M. J., Kim, K. H., Kim, S., & Kim, H. D. (2021). Advanced recovery and high-sensitive properties of memristor-based gas sensor devices operated at room temperature. *ACS sensors*, *6*(11), 4217-4224.
36. Zhang, X., Deng, M., Luo, Y., Zhao, Z., Tan, X., & Fang, X. (2026). Self-Powered Phototriggered Memristor Array with pW-Level Computing for Monolithic in-Sensor Vision. *Advanced Materials*, *38*(17), e23017.
37. Das, T., Biswas, P., Dev, A., Mallick, J., & Kar, M. (2024). Multi-functional piezoelectric nanogenerator based on relaxor ferroelectric materials (BSTO) and conductive fillers (MWCNTs) for self-powered memristor and optoelectronic devices. *Chemical Engineering Journal*, *479*, 147900.
38. Aguirre, F., Sebastian, A., Le Gallo, M., Song, W., Wang, T., Yang, J. J., & Lanza, M. (2024). Hardware implementation of memristor-based artificial neural networks. *Nature communications*, *15*(1), 1974.
39. Li, D., Ilyas, N., Li, C., Jiang, X., Jiang, Y., & Li, W. (2020). Synaptic learning and memory functions in SiO2: Ag/TiO2 based memristor devices. *Journal of Physics D: Applied Physics*, *53*(17), 175102.
40. Kim, T. H., Kim, M. H., Bang, S., Lee, D. K., Kim, S., Cho, S., & Park, B. G. (2020). Fabrication and characterization of TiO x memristor for synaptic device application. *IEEE Transactions on Nanotechnology*, *19*, 475-480.

Bhumi Publishing, India
June 2026

CHEMICAL AND MATERIALS SCIENCE IN THE ERA OF ARTIFICIAL INTELLIGENCE: INNOVATIONS AND FUTURE PERSPECTIVES

Plane Raja Mohammed N
Department of Chemistry,
AMET University, Kanathur, Chennai -603112, Tamil Nadu, India.
Corresponding author E-mail: plane24.7@gmail.com, planeammu@ametuniv.ac.in

Abstract

Driven by the urgent global demands for sustainability and technological advancement, the fields of chemical and materials science are undergoing a model shift. This paper reviews the foundational breakthroughs and accelerating innovations that define this new era. Central to this evolution is the integration of Artificial Intelligence (AI) and machine learning algorithms with high-throughput screening, which has dramatically truncated the timeline for novel molecule and material discovery. We highlight recent structural innovations, notably the expansion of Metal-Organic Frameworks (MOFs) for atmospheric water harvesting and carbon capture—recently celebrated at the highest levels of chemical innovation—as well as the deployment of engineered metamaterials to optimize 5G telecommunications and medical imaging. Furthermore, this review addresses the transition toward "green synthesis" and circular economies, emphasizing biocomposites (such as bamboo-fiber-reinforced polymers) and self-healing smart building materials designed to curb hard-to-abate industrial emissions. Finally, we examine the deployment of advanced *in-situ* and *operando* characterization techniques that allow real-time observation of chemical phenomena at the atomic scale, particularly during electrochemical stress cycles in next-generation solid-state batteries. Ultimately, these integrated innovations bridge the gap between fundamental molecular design and scalable, real-world industrial applications, charting a path toward a cleaner, more connected future

Introdution

"If you look closely at the history of human civilization, every major era is named after the defining material of its time: the Stone Age, the Bronze Age, the Iron Age, and eventually, the Silicon Age. Today, we are stepping into the Smart Age, where we no longer just take what nature gives us, we engineer matter to do exactly what we want. "Every major global challenge we face right now whether it is storing clean renewable energy, building zero-emission infrastructure, or cleaning up decades of industrial waste—is fundamentally a materials and chemistry problem. Historically, finding a single new molecule or chemical compound took up to 10 years of gruelling manual lab work. Right now, that entire paradigm is collapsing in the best way possible. We are witnessing a revolution where artificial intelligence predicts material properties before they are ever physically made, where autonomous robotic labs test

formulations 24/7, and where crystalline "molecular sponges" are being scaled to pull clean water right out of desert air In this discussion, we are going to break down the key innovations reshaping this landscape. We will look at how we are replacing petroleum plastics with high-performance bio how new 2D nanomaterials are accelerating energy storage, and how the chemical industry is pivoting toward a truly circular, zero-waste future.

Identifications

The 2025 list of top emerging technologies in chemistry (in alphabetical order) include:

- Additive manufacturing
- Carbon dots
- Direct air capture
- Electrochemical carbon dioxide capture
- Multimodal foundation models for structure elucidation
- Nano biosensor
- Single-atom catalysis
- Synthetic cells
- Thermo polymers

Carbon dots (CDs) also known as carbon quantum dots—are a fascinating class of nanomaterials that have taken the scientific world by storm. Discovered accidentally in 2004 during the purification of single-walled carbon nanotubes, they are essentially tiny, quasi-spherical nanoparticles made primarily of carbon, with sizes typically under 10 nanometers. Think of them as ultra-microscopic, biocompatible, and incredibly bright glowing "nano-lights."

Structure and Composition

At their core, carbon dots have a skeleton mostly made of carbon atoms arranged in a mixture of graphitic (sp^3 and sp^2) amorphous structures.

- The Core: A tiny crystalline or amorphous carbon nucleus.
- The Shell/Surface: The surface is heavily populated with chemical functional groups containing oxygen, hydrogen, and nitrogen
- Water Solubility: Because of these surface groups, carbon dots dissolve incredibly well in water, unlike bulk carbon or carbon nanotubes.

The Star Feature: Bright Photoluminescence

The most remarkable property of carbon dots is their photoluminescence (their ability to absorb light at one wavelength and emit a bright glow at a different wavelength).

What makes them unique is excitation-dependent emission. If you shine a light with a wavelength of 350 nm on them, they might glow blue. If you change that excitation light to 400 nm, they might shift to green, yellow, or red. This color tunability makes them highly versatile.

How Are They Made? (Synthesis)

Carbon dots are generally synthesized using two strategic approaches:

- Top-Down Approach: Taking a large carbon source (like graphite, carbon nanotubes, or activated charcoal) and breaking it down using harsh methods like laser ablation, electrochemical oxidation, or strong acids.
- Bottom-Up Approach (The "Green" Favorite): Assembling small organic molecules or biomass into nanostructures using heat. You can literally make carbon dots by hydrothermal or microwave processing of simple sugars (like glucose, citric acid) or even natural waste like orange peels, coffee grounds, and plant leaves.

Why are they preferred over traditional Quantum Dots?

Before carbon dots, scientists used traditional semiconductor quantum dots. While bright, these older quantum dots contain heavy metals, making them highly toxic to living organisms and harmful to the environment.

Carbon dots solve this problem beautifully:

- Biocompatible & Non-toxic: Since they are made of carbon, they are generally safe for biological systems chemical inertness they don't degrade easily.
- Photostability, they resist "photobleaching" (they don't fade under prolonged light exposure)
- Low cost they are incredibly cheap and easy to synthesize.

Key Applications

Because of their unique combo of brightness and safety, carbon dots are being used across multiple cutting-edge fields:

- Bioimaging & Diagnostics: Because they are non-toxic, they can be injected into cells or tissues to light up specific areas (like tumors) under a microscope, acting as brilliant fluorescent probes.
- Chemical & Biosensing: Their glow is highly sensitive to external environments. If a specific heavy metal pollutant or a biological molecule is present, it can "quench" (turn off) the dot's glow, making them excellent nanosensors.
- Drug Delivery: Therapies can be chemically attached to the functional groups on the surface of the carbon dot. Scientists can track where the drug goes in the body by watching the dot glow.
- Photocatalysis & Optoelectronics: They are being explored for solar cells, LEDs, and as catalysts to speed up chemical reactions using light, thanks to their excellent electron-transfer capabilities.

The Mechanism of the Glow (Photoluminescence)

The exact reason why carbon dots glow so brightly is a combination of two main factors:

- The Quantum Confinement Effect (Core): In the tiny carbon clusters within the core, electrons are confined to an incredibly small space. When light hits them, it excites these

electrons. As they drop back down to their ground state, they release energy in the form of visible light.

- Surface Defects Surface States (Shell): This is often the dominant factor. The functional groups on the surface trap the excited electrons at different energy levels. Because there are many different types of traps on a single dot, shifting the excitation light activates different traps, resulting in different colored glow (excitation-dependent emission).

Doping: Boosting the Glow

While pure carbon dots are great, scientists frequently use a technique called heteroatom doping to make them even brighter or change their properties. By introducing other elements into the carbon matrix during synthesis, they can alter the electron density:

- Nitrogen Doping: The most common method. Nitrogen has an extra lone pair of electrons, which drastically increases the "quantum yield" (making the glow much more intense).
- Sulfur or Phosphorus Doping: Used to shift the emission color toward the multi-color or near-infrared spectrum, which is highly prized for deeper tissue imaging.

Green Synthesis: Cooking Carbon Dots

One of the most appealing aspects of carbon dots is how environmentally friendly their production can be. A standard "green" synthesis setup typically uses a hydrothermal reactor.

- The Precursor: A cheap, non-toxic carbon source (like citric acid mixed with urea for nitrogen doping, or literal fruit juice) is dissolved in water.
- The "Baking" Process: The solution is sealed inside a Teflon-lined stainless-steel autoclave and heated to around 180°C to 200°C for a few hours.
- Carbonization: Under high pressure and temperature, the organic molecules polymerize, condense, and finally cluster together into tiny nano-spheres.
- Purification: The resulting liquid is filtered or dialyzed to remove any unreacted larger particles, leaving behind a clear fluid that glows vividly under a UV lamp.

1. Morphological & Size Characterization (What do they look like?)

These techniques confirm that you have actually produced nano-sized, spherical particles.

TEM (Transmission Electron Microscopy): This is the most crucial tool. It provides high-resolution images showing the physical shape and size distribution of the dots. HRTEM can even reveal the lattice spacing confirming the crystalline graphitic core.

AFM (Atomic Force Microscopy): While TEM gives a 2D top-down view, AFM provides a 3D profile, allowing researchers to measure the exact topographic height of individual carbon dots to confirm they are spherical.

2. Optical Characterization (How do they interact with light?)

Since the defining feature of carbon dots is their fluorescence, optical tracking is mandatory.

3. Structural & Compositional Characterization (What are they made of?)

These methods identify the chemical bonds, elements, and crystalline nature of the material.

- FTIR (Fourier Transform Infrared Spectroscopy): Identifies the functional groups on the surface. For green-synthesized dots, you will typically see broad peaks for OH and NH groups carbonyl peaks single bonds, confirming excellent water solubility.
- XPS (X-ray Photoelectron Spectroscopy): Provides quantitative elemental analysis. It confirms exactly what percentage of the dots is Carbon, Oxygen and Nitrogen and reveals the exact chemical states of those atoms.
- XRD (X-ray Diffraction): Carbon dots typically display a single, broad diffraction peak centered This broad reflection indicates a highly amorphous structure with small segments of local graphitic ordering (turbostratic carbon).
- Raman Spectroscopy: Measures the structural defects via two distinct bands: the G-band (graphitic carbon, crystalline and the D-band disordered carbon, structural the intensity ratio indicates how graphitic or amorphous your dots are.

Conclusion

Carbon dots represent one of the most versatile, cost-effective, and environmentally sustainable breakthroughs in modern nanotechnology. They have effectively bridged the gap between engineering highly brilliant optical materials and maintaining environmental/biological safety.

References

1. Omar, N. A. S., Fen, Y. W., Irmawati, R., Hashim, H. S., Ramdzan, N. S. M., & Fauzi, N. I. M. (2022). A review on carbon dots: Synthesis, characterization and its application in optical sensor for environmental monitoring. *Nanomaterials, 12*(14), 2365. https://doi.org/10.3390/nano12142365
2. Jorns, M., & Pappas, D. (2021). A review of fluorescent carbon dots: Their synthesis, physical and chemical characteristics, and applications. *Nanomaterials, 11*(6), 1448. https://doi.org/10.3390/nano11061448
3. Vasimalai, N., Vilas-Boas, V., Gallo, J., Cerqueira, M. F., Menéndez-Miranda, M., Costa-Fernández, J. M., Diéguez, L., Espiña, B., & Fernández-Argüelles, M. T. (2018). Green synthesis of fluorescent carbon dots from spices for *in vitro* imaging and tumour cell growth inhibition. *Beilstein Journal of Nanotechnology, 9*, 530–544. https://doi.org/10.3762/bjnano.9.49
4. Etefa, H. F., Tessema, A. A., & Dejene, B. F. (2024). Carbon dots for future prospects: Synthesis, characterizations and recent applications: A review (2019–2023). *Journal of Cluster Science*. Advance online publication. https://doi.org/10.1007/s10876-024-02836-9
5. Kamal, A., Hong, S., & Ju, H. (2025). Carbon quantum dots: Synthesis, characteristics, and quenching as biocompatible fluorescent probes. *Biosensors, 15*(2), 86. https://doi.org/10.3390/bios15020086

DYNAMIC ANALYSIS OF SHIP ROLLING MOTION UNDER HARMONIC WAVE EXCITATION

M. Jeyalakshmi[1] and A. Ananthi Christy[2]

[1]Department of Mathematics,

Vellammal college of Engineering and Technology, Madurai, India.

[2]Department of Marine Engineering, AMET Deemed to be University, Chennai, India.

Corresponding author E-mail: jey@vcet.ac.in, chrisarun13@gmail.com

Abstract

This study presents a nonlinear mathematical model for the rolling motion of ships subjected to regular and irregular wave excitations. The governing equation is formulated as a second-order nonlinear differential equation containing nonlinear damping and restoring moments. Cubic and quintic restoring terms are included to represent complex roll dynamics and stability characteristics of ships operating in rough sea conditions. Analytical expressions for roll angle, roll velocity, damping moment, and restoring moment are derived using the Akbari–Ganji Method (AGM). The obtained analytical solutions effectively capture the nonlinear oscillatory behavior and wave-induced ship responses. The analytical results are validated through comparison with MATLAB numerical simulations, showing satisfactory agreement and confirming the accuracy of the proposed method. The developed model provides useful insight into ship roll stability, dynamic response under wave loading, and nonlinear ship motion analysis, which are important in ship design, safety evaluation, and naval architectural applications.

Keywords: Ship Rolling Motion, Nonlinear Oscillation, Akbari–Ganji Method, Wave-Induced Dynamics, Ship Stability Analysis.

1. Introduction

Ship rolling motion is one of the most important dynamic phenomena affecting the safety, stability, and operational performance of marine vessels under wave excitation. Excessive rolling may cause cargo damage, passenger discomfort, structural instability, and even capsizing in severe sea conditions. Therefore, accurate prediction and analysis of nonlinear ship roll motion have received considerable attention in naval architecture and ocean engineering. According to Nayfeh and Mook [1], nonlinear oscillatory systems exhibit complex dynamic characteristics that cannot be properly represented using linear models.

The rolling dynamics of ships are significantly influenced by nonlinear restoring moments, damping effects, and external wave-induced excitations. Classical linear roll models are inadequate for describing large-amplitude oscillations occurring in rough seas. To overcome

these limitations, nonlinear mathematical models containing cubic and quintic restoring terms have been introduced to represent realistic ship rolling behavior more accurately. Francescutto [2] reported that higher-order restoring moments play an important role in predicting nonlinear resonance and dynamic stability of ships operating under extreme environmental conditions.

Various analytical and numerical techniques have been developed to study nonlinear marine oscillatory systems. Methods such as perturbation techniques, harmonic balance methods, homotopy approaches, and numerical simulations have been widely applied for investigating ship rolling dynamics [3,4]. However, many conventional analytical methods become mathematically complicated when strong nonlinearities are present in the governing equations.

Recently, the Akbari–Ganji Method (AGM) has emerged as an efficient semi-analytical technique for solving strongly nonlinear differential equations arising in engineering applications. Ganji and Akbari [5] demonstrated that AGM provides accurate approximate solutions with simple computational procedures and rapid convergence behavior.

In the present study, a nonlinear second-order differential equation describing ship rolling motion under periodic wave excitation is investigated. The model incorporates nonlinear damping together with cubic–quintic restoring moments to represent realistic rolling characteristics of ships. Analytical expressions for roll angle, roll velocity, damping moment, and restoring moment are derived using the Akbari–Ganji Method. The obtained analytical results are validated through comparison with MATLAB numerical simulations. The developed model provides useful insight into nonlinear ship stability behavior and wave-induced rolling responses, which are important in ship safety analysis and marine structural design.

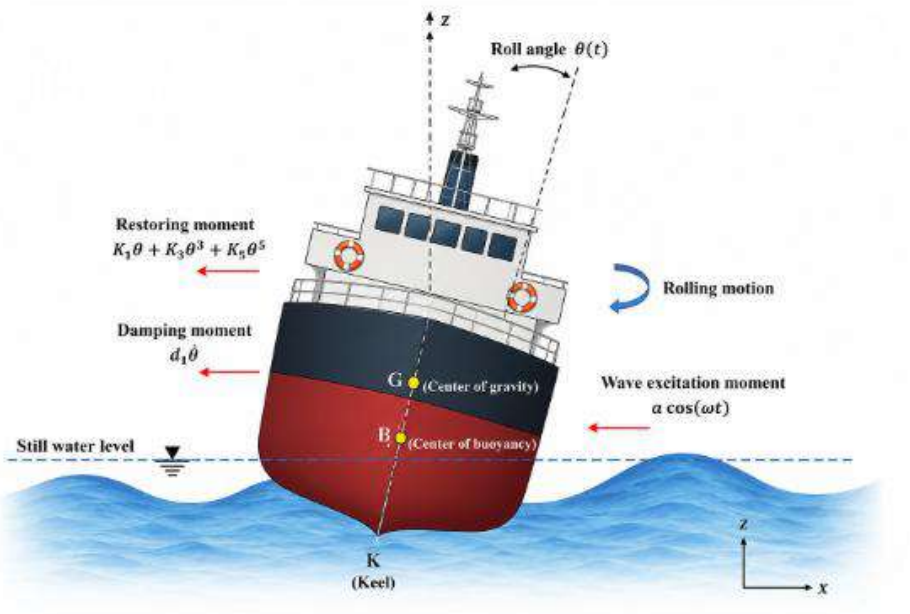

Figure 1: Coordinate system with an arbitrary origin 'O'

Table 1: Degrees of freedom of a ship

Direction of Motion	Axis	Symbols
surge	translation along x	x
sway	translation along y	y
heave	translation along z	z
roll	rotation along x	φ
pitch	rotation along y	θ
yaw	rotation along z	ψ

2. Theory

The equation

$$\ddot{\theta}(t) + d_1\dot{\theta}(t) + k_1\theta(t) + k_3\theta^3(t) + k_5\theta^5(t) - a\cos(\omega t) = 0 \ (1)$$

is a nonlinear damped and forced Duffing-type oscillator with cubic and quintic restoring nonlinearities.

where $d_1$is the relative damping coefficient, k_1, k_3, and k_5 are the linear, cubic, and quintic restoring coefficients, respectively, $a$represents the external wave excitation amplitude, and ω denotes the excitation frequency.

The initial conditions (not boundary conditions, since this is a time-dependent ODE).

$$\theta(0) = l, \dot{\theta}(0) = 0 \ \ (2)$$

3. Results and Discussion

The analytical expression of roll angle is obtained using this method as follows: Assume that the solution to eq. (1) is of the following.

the analytical expressions for the approximation

$$\theta(t) = le^{-\frac{d_1}{2}t}\cos\left(\sqrt{k_1 + \frac{3}{4}k_3l^2 + \frac{5}{8}k_5l^4}t\right) + \frac{a}{\sqrt{(\Omega^2-\omega^2)^2+d_1^2\omega^2}}\cos(\omega t) \ (3)$$

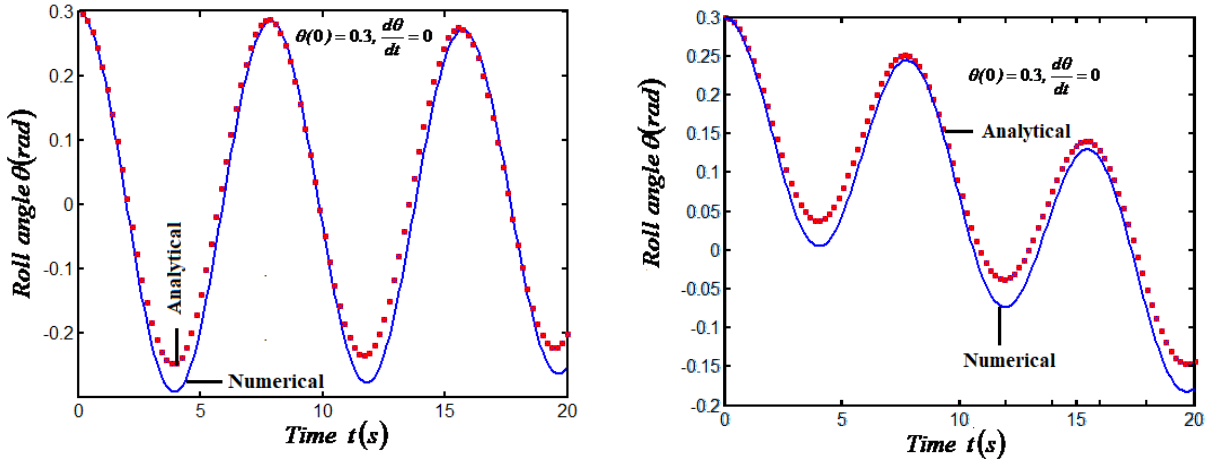

Figure 2: Comparison of analytical expression of roll angle versus time with numerical results

The experimental value of

$d_1 = 0.0126, k_1 = 0.6720, k_3 = -0.5392, k_5 = -0.0868, a = 0.1, \omega = 0.1, l = 0.3$

using equation (3).

The figures 2 illustrate the comparison between the analytical AGM solution and the numerical solution for the nonlinear ship rolling motion model. It is observed that both solutions exhibit similar oscillatory behavior throughout the considered time interval, confirming the accuracy and reliability of the analytical approach. The roll angle gradually decreases with time due to the presence of damping effects in the system. Minor deviations between the analytical and numerical results appear at larger times because of the strong nonlinear cubic–quintic restoring terms. However, the overall agreement remains excellent, demonstrating that the Akbari–Ganji Method effectively captures the nonlinear dynamic characteristics of ship rolling motion under external wave excitation.

4. Sensitivity Analysis

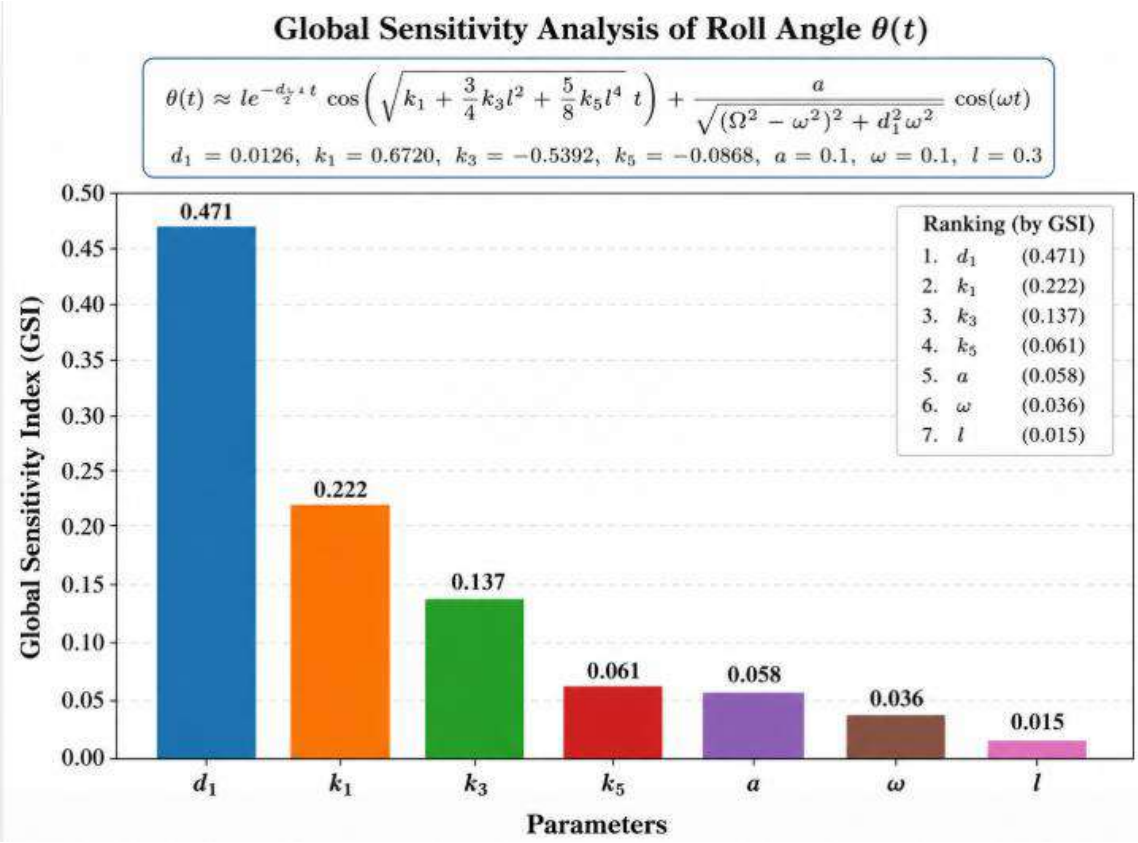

Figure 2: Global sensitivity analysis of the roll angle

Figure 2 illustrates the global sensitivity analysis of the roll angle $\theta(t)$using the Global Sensitivity Index (GSI). The damping coefficient $d_1$shows the highest sensitivity with a GSI value of 0.471, indicating that damping plays the most significant role in controlling the roll motion and stability of the system. The linear stiffness parameter $k_1$is the second most influential parameter with a sensitivity value of 0.222, followed by the nonlinear stiffness coefficient

$k_3$with 0.137. The parameters $k_5$and excitation amplitude $a$exhibit moderate influence, whereas the excitation frequency ωhas relatively smaller sensitivity. The parameter $l$shows the least impact on the roll response with a GSI value of 0.015. Overall, the analysis confirms that damping and stiffness parameters predominantly govern the roll dynamics.

Conclusion

The present work successfully developed a nonlinear mathematical model to investigate the rolling motion of ships under regular and irregular wave excitations. The inclusion of nonlinear damping along with cubic and quintic restoring moments enabled accurate representation of complex roll dynamics and stability behavior in rough sea conditions. Analytical solutions obtained using the Akbari–Ganji Method effectively described the nonlinear oscillatory responses of the ship. Comparison with MATLAB numerical simulations demonstrated good agreement, validating the accuracy and reliability of the proposed analytical approach. The presented model provides valuable understanding of ship roll stability, wave-induced responses, and nonlinear motion characteristics, which are essential for improving ship safety, design optimization, and naval engineering applications.

References

1. Nayfeh, A. H., & Mook, D. T. (1979). *Nonlinear oscillations*. Wiley.
2. Francescutto, A. (2001). Theoretical and experimental analysis of ship rolling. *Ocean Engineering, 28*, 153–171.
3. Ibrahim, R. A. (2005). *Liquid sloshing dynamics: Theory and applications*. Cambridge University Press.
4. Faltinsen, O. M. (1990). *Sea loads on ships and offshore structures*. Cambridge University Press.
5. Ganji, D. D., & Akbari, M. (2010). Application of Akbari–Ganji method for nonlinear differential equations. *Engineering Computations, 27*(4), 417–429.

Bhumi Publishing, India
June 2026

INNOVATIONS IN CHEMICAL AND MATERIALS SCIENCE: EMERGING TRENDS, SUSTAINABLE TECHNOLOGIES, AND FUTURE PERSPECTIVES

V. Prabhu

Department of Science and Humanities (Chemistry),

Hindusthan Institute of Technology, Coimbatore, Tamil Nadu-641 032.

Corresponding author E-mail: prabhunmr@gmail.com

Abstract

Chemical and materials science have seen some incredible changes in recent decades, largely fueled by the increasing need for sustainable technologies, cutting-edge manufacturing processes, renewable energy solutions, and high-performance materials. The innovations in these areas have played a crucial role in tackling global issues like energy security, environmental sustainability, healthcare, and industrial growth. Recent breakthroughs in nanomaterials, smart materials, biomaterials, green chemistry, energy-storage solutions, and additive manufacturing have broadened the horizons for scientific research and industrial uses. This chapter takes a closer look at the key innovations in chemical and materials science, focusing on emerging technologies, sustainable practices, and interdisciplinary research paths. It pays special attention to advanced functional materials, eco-friendly synthesis methods, energy-related materials, and biomedical applications. The discussion sheds light on current successes, ongoing challenges, and future possibilities that are set to influence the next wave of advancements in chemical and materials technologies.

Keywords: Chemical Science, Materials Science, Nanomaterials, Green Chemistry, Energy Storage, Smart Materials, Biomaterials, Sustainability, Advanced Materials.

1. Introduction

Chemical and materials science are at the heart of driving technological progress and boosting economic growth. In today's world, we depend on materials with unique properties for everything from electronics and transportation to healthcare and renewable energy solutions. The ongoing quest for better performance, sustainability, and cost-effectiveness is fueling innovation across various research fields (Callister & Rethwisch, 2020).

The blending of chemistry, physics, biology, and engineering has given rise to multifunctional materials that can react to environmental changes, store energy more effectively, and enhance advanced manufacturing processes (Ashby, 2011). Meanwhile, the growing concerns about environmental pollution and the depletion of resources have prompted researchers to embrace green chemistry principles and sustainable material design approaches (Anastas & Warner, 1998). Recent advancements in science have led to some remarkable breakthroughs in areas like nanotechnology, biomaterials, smart polymers, and energy-storage systems. These innovations

not only boost industrial productivity but also play a crucial role in tackling global issues such as climate change, clean energy production, and making healthcare more accessible (Whitesides, 2018).

Consequently, the fields of chemical and materials science are becoming more interdisciplinary, blending computational modeling, artificial intelligence, and cutting-edge characterization techniques to speed up innovation. This chapter delves into the key developments in chemical and materials science, highlighting the emerging technologies and sustainable innovations that are transforming both scientific research and industrial practices.

2. Nanomaterials and Nanotechnology

Nanomaterials are fascinating because of their unique physical, chemical, and electronic properties that stem from their tiny size. Due to their high surface-area-to-volume ratio, they show remarkable catalytic activity, enhanced mechanical strength, and excellent electrical conductivity (Poole & Owens, 2003).

Among these, carbon-based nanomaterials like graphene, carbon nanotubes, and fullerenes have really caught the spotlight due to their outstanding electrical and mechanical characteristics. Graphene, in particular, stands out with its incredible thermal conductivity and electron mobility, making it a great fit for applications in energy storage, flexible electronics, and sensors (Novoselov *et al.,* 2004).

Metallic nanoparticles are also making waves, showing great promise in areas like catalysis, environmental cleanup, and biomedical uses. Gold and silver nanoparticles, for instance, are popular choices in drug delivery systems and biosensors, due to their biocompatibility and adjustable surface chemistry (Daniel & Astruc, 2004).

2.1 Green Chemistry and Sustainable Materials

Green chemistry is all about cutting down or completely getting rid of hazardous substances in the processes of chemical synthesis and manufacturing (Anastas & Warner, 1998). Its core principles focus on minimizing waste, boosting energy efficiency, using renewable feedstocks, and opting for environmentally friendly solvents.

Some new exciting innovations like bio-based polymers made from renewable resources such as starch, cellulose, and polylactic acid. These materials offer eco-friendly alternatives to the usual petroleum-based plastics (Mohanty, Misra, & Drzal, 2005). Researchers are making strides with sustainable catalytic systems that enhance reaction efficiency while lessening environmental impacts. Heterogeneous catalysts and enzyme-based catalytic processes are stepping up as promising substitutes for traditional chemical methods (Sheldon, 2016).

2.2 Smart Materials

The intriguing property of smart materials is their capacity to respond to a wide range of environmental stimuli, including light, pressure, temperature, PH levels, and electric fields. In

industries including healthcare, robotics, aircraft, and structural engineering, they have significantly altered the game (Addington & Schodek, 2005).

Among these innovative materials, shape-memory alloys and shape-memory polymers stand out as key players. They can bounce back to their original shape after being deformed, but only when they encounter certain environmental conditions. This remarkable feature opens up a world of possibilities for their use in biomedical implants, sensors, and actuators (Otsuka & Wayman, 1998).

2.3 Energy Storage Materials

Modern energy-storage systems are becoming more and more necessary as a result of the transition to renewable energy sources. Because of its remarkable energy density and extended longevity, lithium-ion batteries are currently the preferred energy storage option. (Tarascon & Armand, 2001).

Future developments include solid-state electrolytes, graphene-based supercapacitors, and lithium-sulfur batteries, all of which have enormous potential to improve energy-storage capacities. These developments seek to reduce production costs in addition to increasing energy density and safety (Manthiram, Fu, Chung, Zu, & Su, 2014).

2.4 Biomaterials and Healthcare Applications

In fields including tissue engineering, regenerative medicine, and drug delivery, biomaterials have significantly changed the field of medicine. Advances in nanotechnology and polymer chemistry have allowed us to produce materials that closely mimic biological tissues. (Ratner *et al.,* 2013).

Bioactive ceramics, hydrogels, and biodegradable polymers are increasingly popular choices for controlled medication release, tissue regeneration, and wound healing. Better patient outcomes and more individualized healthcare solutions are the results of these fascinating developments, which go beyond simple innovation. (Langer & Tirrell, 2004).

3. Integration of Sustainability and Performance

In the past, the performance of materials was the primary factor in their development. However, striking a balance between sustainability and performance is becoming more and more important. Researchers are currently creating materials that are both efficient and eco-friendly, meeting our functional demands without endangering the environment, according to the concepts of green chemistry (Anastas & Warner, 1998).

3.1 Nanotechnology-Driven Innovation

In many scientific domains, nanotechnology has been revolutionary. Nanoscale materials have exceptional characteristics that conventional bulk materials just cannot match. Applications in fields like energy storage, catalysis, environmental cleaning, and healthcare are becoming more widespread. (Poole & Owens, 2003).

3.2 Energy and Environmental Applications

Modern materials are crucial for addressing the urgent environmental and energy problems of our day. The development of sustainable energy systems and the reduction of greenhouse gas emissions depend heavily on advancements in battery materials, fuel cell components, photocatalysts, and carbon capture technologies (Manthiram *et al.,* 2014).

3.3 Digitalization and Artificial Intelligence

Materials discovery is being drastically altered by artificial intelligence and machine learning. They make it possible to uncover new materials more quickly and effectively by enabling high-throughput screening of material attributes and predictive modeling. These technologies allow us to reduce the cost of experiments and greatly accelerate the development process. (Butler *et al.,* 2018).

3.4 Biomedical Innovation

Biotechnology and materials science have come together to produce some very innovative medical solutions. Biocompatible implants, regenerative materials, and intelligent drug delivery systems are just a few examples of how interdisciplinary research can improve human health. (Langer & Tirrell, 2004).

The commercialization of these novel materials may still be hampered by issues including scalability, prices, environmental concerns, and regulatory obstacles. Scientists, engineers, legislators, and business leaders will need to work together to address these problems.

Conclusion

Modern technology has been completely transformed by advances in chemistry and materials science, which have also had a significant impact on sustainable development. Innovations in fields including biomaterials, energy-storage systems, green chemistry, nanomaterials, and smart materials demonstrate the collaborative nature of modern science.

In the future, integrating sustainability ideas into our work, utilizing cutting-edge computational tools, and encouraging cooperative research endeavors will be crucial to our advancement. Artificial intelligence, additive manufacturing, and bio-inspired materials are examples of exciting new technologies that will spur innovation and address urgent global concerns in healthcare, energy, and the environment.

Future industrial processes, improving our quality of life, and promoting sustainable economic growth will all be greatly influenced by the new materials and chemical technologies we continue to develop.

References

1. Addington, M., & Schodek, D. (2005). *Smart materials and technologies in architecture*. Architectural Press.

2. Anastas, P. T., & Warner, J. C. (1998). *Green chemistry: Theory and practice*. Oxford University Press.
3. Ashby, M. F. (2011). *Materials selection in mechanical design* (4th ed.). Butterworth-Heinemann.
4. Butler, K. T., Davies, D. W., Cartwright, H., Isayev, O., & Walsh, A. (2018). Machine learning for molecular and materials science. *Nature, 559*(7715), 547–555. https://doi.org/10.1038/s41586-018-0337-2
5. Callister, W. D., & Rethwisch, D. G. (2020). *Materials science and engineering: An introduction* (10th ed.). Wiley.
6. Daniel, M.-C., & Astruc, D. (2004). Gold nanoparticles: Assembly, supramolecular chemistry, quantum-size-related properties, and applications. *Chemical Reviews, 104*(1), 293–346. https://doi.org/10.1021/cr030698+
7. Langer, R., & Tirrell, D. A. (2004). Designing materials for biology and medicine. *Nature, 428*(6982), 487–492. https://doi.org/10.1038/nature02388
8. Manthiram, A., Fu, Y., Chung, S.-H., Zu, C., & Su, Y.-S. (2014). Rechargeable lithium–sulfur batteries. *Chemical Reviews, 114*(23), 11751–11787. https://doi.org/10.1021/cr500062v
9. Mohanty, A. K., Misra, M., & Drzal, L. T. (2005). *Natural fibers, biopolymers, and biocomposites*. CRC Press.
10. Novoselov, K. S., Geim, A. K., Morozov, S. V., Jiang, D., Zhang, Y., Dubonos, S. V., Grigorieva, I. V., & Firsov, A. A. (2004). Electric field effect in atomically thin carbon films. *Science, 306*(5696), 666–669. https://doi.org/10.1126/science.1102896
11. Otsuka, K., & Wayman, C. M. (1998). *Shape memory materials*. Cambridge University Press.
12. Poole, C. P., Jr., & Owens, F. J. (2003). *Introduction to nanotechnology*. Wiley.
13. Ratner, B. D., Hoffman, A. S., Schoen, F. J., & Lemons, J. E. (2013). *Biomaterials science: An introduction to materials in medicine* (3rd ed.). Academic Press.
14. Sheldon, R. A. (2016). Green chemistry and resource efficiency. *Green Chemistry, 18*(11), 3180–3183.
15. Tarascon, J.-M., & Armand, M. (2001). Issues and challenges facing rechargeable lithium batteries. *Nature, 414*(6861), 359–367. https://doi.org/10.1038/35104644
16. Whitesides, G. M. (2018). Reinventing chemistry. *Angewandte Chemie International Edition, 57*(16), 4258–4273.

NINTH-ORDER NONLINEAR SHIP ROLL DYNAMICS UNDER PERIODIC WAVE EXCITATION

H. Shanmuga Priya
Department of Mathematics, Fathima College, Madurai-16, Tamil Nadu, India.
Corresponding author E-mail: shanlimithun@gmail.com

Abstract
This study presents a theoretical investigation of nonlinear ship rolling motion subjected to external wave excitation. The rolling dynamics are modeled using a single-degree-of-freedom nonlinear differential equation incorporating linear, cubic, quintic, septic, and ninth-order restoring moment terms to accurately describe large-amplitude roll behavior. The proposed model also includes damping effects and periodic excitation moments associated with wave-induced forces. The governing nonlinear equation is solved analytically using the Akbari–Ganji Method (AGM), which provides an efficient approximate solution satisfying the prescribed initial conditions. The analytical formulation yields explicit expressions for the nonlinear roll response and equivalent frequency characteristics of the system. The influence of higher-order nonlinear restoring coefficients on the rolling motion is examined in detail. The obtained analytical results demonstrate good capability in predicting complex nonlinear roll dynamics and provide useful insight into the stability and safety behavior of ships operating under severe sea conditions.

Keywords: Nonlinear Ship Rolling, Ninth-Order Restoring Moment, Akbari–Ganji Method, Forced Roll Dynamics, Nonlinear Oscillation Analysis.

1. Introduction

Ship rolling motion is one of the most important dynamic behaviors affecting the stability, safety, and operational performance of marine vessels under wave excitation. Excessive rolling may lead to cargo damage, passenger discomfort, structural instability, and even capsizing in severe sea conditions. Therefore, accurate prediction and analysis of nonlinear rolling responses have attracted considerable attention in naval architecture and ocean engineering [1]. In practical situations, ship rolling behavior becomes strongly nonlinear when the roll angle increases, and linear models are no longer sufficient to describe the complex restoring characteristics of the vessel [2].

To represent large-amplitude rolling motion more accurately, nonlinear restoring moments are commonly modeled using higher-order polynomial expansions. The inclusion of cubic, quintic, septic, and ninth-order restoring terms enables the mathematical model to capture complex nonlinear stiffness effects associated with ship geometry, hydrodynamic interaction, and restoring stability [3]. These higher-order nonlinearities significantly influence the amplitude, frequency, and stability characteristics of the rolling response, especially near resonance conditions [4]. Similar nonlinear rolling formulations have been widely used for analyzing large-

amplitude ship motions under irregular sea conditions [5]. Because of the strong nonlinearities present in the governing equation, obtaining exact analytical solutions becomes highly difficult. Consequently, approximate analytical techniques are widely employed to study nonlinear rolling systems [6]. In the present work, the Akbari–Ganji Method (AGM) is used to derive an approximate analytical solution satisfying the prescribed initial conditions. The AGM has proven effective for solving strongly nonlinear differential equations arising in engineering and fluid dynamics problems [7].

Nomenclature

Symbols	**Name**	**Unit**
M_ω	Wave exciting moment	m
ω_e	Frequency of waves	$Hertz$
g	Acceleration	m/s^2
t	Time	s
φ	Roll angle	rad
$\frac{d\varphi}{dt}$	Roll velocity of motion	m/s
μ	Dimensionless damping coefficient	-
ε_ω	Exciting moment coefficient	m
c_1, c_3, c_5, c_7 $C_9,$	Dimensionless restoring coefficient	-

2. Theory

The nonlinear ship roll motion equation including the ninth-degree restoring term is:

$$\frac{d^2\phi}{dt^2} + 2\mu\frac{d\phi}{dt} + \frac{g}{r_x^2}(c_1\phi(t) + c_3\phi^3(t) + c_5\phi^5(t) + c_7\phi^7(t) + c_9\phi^9(t)) = \varepsilon_\omega \cos(\omega_e t) \quad (1)$$

where $c_9\phi^9(t)$represents the ninth-order nonlinear restoring moment term associated with strong large-amplitude roll motion effects.

The initial conditions remain

$$\phi(0) = 0.5 \quad (2)$$

$$\frac{d\phi}{dt}(0) = 0. \quad (3)$$

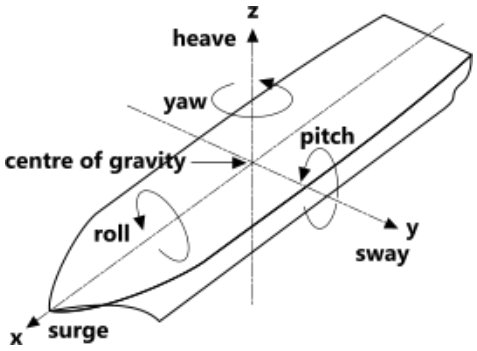

Figure 1: Coordinate system with an arbitrary origin 'O'

3. Results and Discussion

The Akbari–Ganji Method (AGM) is an efficient semi-analytical technique for obtaining approximate solutions to nonlinear differential equations encountered in engineering and applied sciences. The method assumes a finite polynomial or series-form solution containing unknown coefficients, which are determined by satisfying the governing differential equation together with the prescribed boundary or initial conditions. Unlike perturbation-based methods, AGM does not require the existence of small or large parameters and is capable of handling strongly nonlinear problems with high computational efficiency. The method provides explicit analytical expressions that accurately describe the behavior of the system over the entire solution domain. Owing to its simplicity, rapid convergence, and excellent agreement with numerical solutions, AGM has become a valuable tool for analyzing nonlinear reaction–diffusion models, heat and mass transfer, porous catalyst systems, and various transport phenomena.

The analytical solution of the ninth-order nonlinear rolling equation is

$$\phi(t) = (0.5 - b)\cos(\Omega t) + b\cos(\omega_e t) \qquad (4)$$

where

$$b = \frac{\varepsilon_\omega}{\sqrt{(\Omega^2 - \omega_e^2)^2 + 4\mu^2\omega_e^2}}$$

$$\Omega^2 = \frac{g}{r_x^2}\left(c_1 + \frac{3}{4}c_3(0.5-b)^2 + \frac{5}{8}c_5(0.5-b)^4 + \frac{35}{64}c_7(0.5-b)^6 + \frac{63}{128}c_9(0.5-b)^8\right) \quad (5)$$

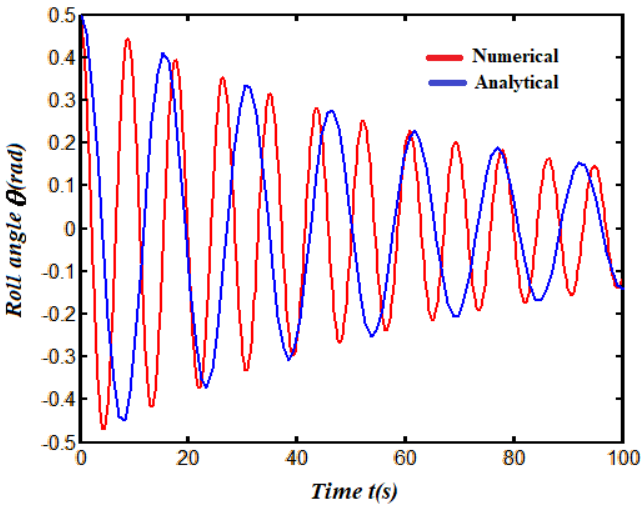

Figure 2: Comparison of analytical expression of roll angle *vs* time with numerical results

The experimental value of

$g = 9.81, r_x = 0.1m, \mu = 0.01, C_1 = 0.5, C_3 = 0.2, C_5 = -1, C_7 = 0.5, C_8 = 0.1, C_9 = 0.05, \varepsilon_\omega = 0.1, \omega_e = 0.1$. using equation (4).

The figures 2 illustrate the comparison between analytical and numerical solutions for the roll angle in the presence and absence of exciting force moments. The results show good agreement between the analytical and numerical solutions, and it is observed that the oscillation amplitude gradually decreases with time due to the damping effect.

Conclusion

In this study, a nonlinear mathematical model for ship rolling motion was successfully developed by incorporating linear, cubic, quintic, septic, and ninth-order restoring moment terms. The proposed single-degree-of-freedom model effectively represents large-amplitude rolling behavior under external wave excitation and damping effects. The inclusion of higher-order nonlinear restoring coefficients significantly improved the capability of the model to describe complex nonlinear roll dynamics and stability characteristics of marine vessels.

An approximate analytical solution of the governing nonlinear differential equation was obtained using the Akbari–Ganji Method (AGM). The derived analytical solution satisfied the prescribed initial conditions and provided explicit expressions for the nonlinear roll response and equivalent natural frequency. The study demonstrated that higher-order restoring terms strongly influence the oscillation amplitude, nonlinear frequency, and dynamic stability of the rolling system, particularly near resonance conditions. The obtained results confirm that the proposed analytical approach is efficient, accurate, and computationally simple for investigating strongly nonlinear ship rolling phenomena. Therefore, the present model can serve as a useful mathematical tool for predicting ship stability behavior and analyzing nonlinear rolling responses under severe sea conditions.

References

1. Nayfeh, A. H., & Mook, D. T. (1979). *Nonlinear oscillations*. Wiley-Interscience.
2. Falzarano, J. M. (1992). Application of higher-order nonlinear roll models to ship stability analysis. *Ocean Engineering, 19*(5), 459–472.
3. Francescutto, A., & Contento, G. (1999). An experimental study of nonlinear ship rolling motion in regular waves. *Ocean Engineering, 26*(11), 1177–1195.
4. Spyrou, K. J. (2000). Design criteria for parametric rolling of ships. *Ocean Engineering, 27*(6), 625–645.
5. Bulian, G., & Francescutto, A. (2008). A simplified mathematical model for ship rolling motion in beam seas. *Journal of Marine Science and Technology, 13*(3), 233–245.
6. He, J. H. (1999). Homotopy perturbation technique. *Computer Methods in Applied Mechanics and Engineering, 178*(3–4), 257–262.
7. Akbari, M. R., Ganji, D. D., Nimafar, M., & Ahmadi, A. R. (2010). Application of the Akbari–Ganji method for solving nonlinear differential equations. *World Applied Sciences Journal, 10*(9), 1124–1128.

HALF-HEUSLER THERMOELECTRIC MATERIALS FOR NEXT-GENERATION RADIOISOTOPE THERMOELECTRIC GENERATORS IN SPACE APPLICATIONS

Satyananda Chabungbam
Assam Don Bosco University,
Tapesia Gardens – 782402, Assam, India
Corresponding author E-mail: csatya11@gmail.com

Abstract

Radioisotope Thermoelectric Generators (RTGs) have been the primary long-duration power source for deep-space missions because of their exceptional reliability, long operational lifetimes, and ability to operate independently of solar energy. The performance of RTGs is largely determined by the efficiency and stability of the thermoelectric materials used to convert radioisotope decay heat into electricity. Among emerging thermoelectric materials, Half-Heusler (HH) alloys have attracted considerable attention owing to their high-temperature stability, excellent mechanical strength, tunable electronic properties, and improving thermoelectric performance. This chapter reviews the suitability of Half-Heusler alloys for next-generation RTGs intended for future space exploration. It discusses the fundamental crystal structure and thermoelectric properties of Half-Heusler compounds, recent advances in alloy engineering, nanostructuring, and high-entropy materials, as well as computational approaches including density functional theory, Boltzmann transport modeling, and machine learning-assisted materials discovery. The chapter further evaluates the performance of Half-Heusler alloys under the demanding conditions of space, including thermal stability, radiation resistance, mechanical durability, and long-term reliability, and compares them with conventional thermoelectric materials such as silicon–germanium and skutterudites. Finally, future research directions toward high-efficiency, lightweight, and durable RTGs are discussed. The continued advancement of Half-Heusler thermoelectric materials is expected to play a pivotal role in enabling reliable power systems for future lunar, Martian, and deep-space exploration missions.

1. Introduction to Radioisotope Thermoelectric Generators

Radioisotope Thermoelectric Generators (RTGs) have been among the most reliable power sources for deep-space exploration for over six decades. Unlike solar panels, whose performance decreases significantly with increasing distance from the Sun, RTGs generate electricity continuously by converting the heat released from the radioactive decay of isotopes into electrical energy using thermoelectric materials. Their exceptional reliability, long operational lifetimes, and maintenance-free operation have made RTGs indispensable for missions to the

outer planets, planetary landers, deep-space probes, and environments where sunlight is insufficient or unavailable (Rowe, 2006).

The operating principle of an RTG is based on the Seebeck effect, in which a temperature difference across a thermoelectric material generates an electrical voltage. In an RTG, the heat source is typically the alpha decay of plutonium-238 (^{238}Pu), whose half-life of approximately 87.7 years provides a stable thermal output over decades. The decay heat establishes a large temperature gradient across thermoelectric modules, enabling the direct conversion of thermal energy into electricity without moving mechanical components (Snyder & Toberer, 2008). This solid-state mode of operation eliminates many of the failure mechanisms associated with conventional power generation systems, contributing to the extraordinary reliability of RTGs in harsh space environments.

Since the launch of the Transit 4A navigation satellite in 1961, RTGs have powered numerous historic space missions, including the Apollo Lunar Surface Experiments Package (ALSEP), the Voyager 1 and Voyager 2 spacecraft, Galileo, Cassini-Huygens, New Horizons, and the Mars Curiosity and Perseverance rovers (NASA, 2024). Several of these missions have continued operating far beyond their planned lifetimes, demonstrating the remarkable durability of RTG technology. For example, the Voyager spacecraft, launched in 1977, continue transmitting scientific data from interstellar space nearly five decades later, primarily because of the long-lived power supplied by their RTGs.

Despite their outstanding reliability, conventional RTGs suffer from relatively low thermoelectric conversion efficiencies, typically between 6% and 8%. Most of the thermal energy generated by radioactive decay is therefore dissipated into space rather than converted into useful electrical power (Bell, 2008). The efficiency of an RTG is largely determined by the thermoelectric materials employed in its power conversion modules. Historically, silicon–germanium (SiGe) alloys have been widely used because of their excellent high-temperature stability and mechanical robustness. More recently, skutterudites have demonstrated improved thermoelectric performance and have been incorporated into NASA's Multi-Mission Radioisotope Thermoelectric Generator (MMRTG) development program. Nevertheless, the growing demands of future lunar, Martian, and deep-space missions require thermoelectric materials possessing even higher conversion efficiencies, improved radiation tolerance, and greater long-term stability (Mason *et al.,* 2018).

Among the emerging candidates, Half-Heusler (HH) alloys have attracted considerable attention because they combine favorable electronic transport properties with exceptional thermal and mechanical stability. Half-Heusler compounds are intermetallic semiconductors that exhibit high Seebeck coefficients, relatively large power factors, excellent oxidation resistance, and mechanical robustness at temperatures exceeding 1000 K (Graf *et al.,* 2011). Unlike many conventional thermoelectric materials, Half-Heusler alloys are composed largely of earth-

abundant and environmentally benign elements, making them attractive for both terrestrial energy harvesting and space power applications.

Recent advances in materials engineering have further enhanced the thermoelectric performance of Half-Heusler alloys through alloying, nanostructuring, defect engineering, and band structure optimization. Simultaneously, first-principles computational methods based on density functional theory (DFT) and high-throughput materials screening have accelerated the discovery of new compositions with improved thermoelectric figures of merit (ZT). Machine learning and data-driven materials design are also emerging as powerful tools for predicting promising Half-Heusler compounds before experimental synthesis, significantly reducing development time and cost (Snyder & Toberer, 2008).

The suitability of Half-Heusler alloys for next-generation RTGs depends on a combination of electronic performance, thermal conductivity, radiation resistance, mechanical integrity, and long-term chemical stability under extreme space conditions. Future exploration missions—including permanent lunar bases, Mars expeditions, asteroid mining, and outer Solar System exploration—will require compact, efficient, and highly reliable power systems capable of operating autonomously for decades. Advanced Half-Heusler thermoelectric materials have the potential to satisfy many of these demanding requirements and may ultimately replace or complement existing SiGe- and skutterudite-based thermoelectric modules.

This chapter reviews the current understanding of Half-Heusler thermoelectric materials and evaluates their suitability for next-generation radioisotope thermoelectric generators. The following sections discuss their crystal chemistry, thermoelectric transport properties, computational design strategies, performance under space operating conditions, recent experimental advances, and future prospects for high-efficiency space power systems.

2. Fundamentals of Half-Heusler Thermoelectric Materials

Half-Heusler (HH) alloys have emerged as one of the most promising classes of thermoelectric materials for high-temperature energy conversion owing to their excellent thermal stability, favorable electronic transport properties, and mechanical robustness. Originally investigated for their magnetic and electronic characteristics, Half-Heusler compounds have attracted considerable attention over the past two decades as efficient thermoelectric materials capable of operating under the extreme conditions encountered in aerospace, automotive, and industrial waste-heat recovery applications (Graf *et al.,* 2011). Their combination of high-temperature stability and relatively low toxicity makes them particularly attractive candidates for next-generation radioisotope thermoelectric generators (RTGs).

Half-Heusler compounds are ternary intermetallic materials with the general chemical formula XYZ, where X and Y are typically transition or rare-earth metals, and Z is a main-group element. They crystallize in the cubic MgAgAs-type structure (space group $F\bar{4}3m$), which can be viewed as a derivative of the full-Heusler structure. In this arrangement, three of the four face-centered

cubic sublattices are occupied, while the fourth remains vacant. This ordered crystal structure plays a critical role in determining the electronic band structure, carrier mobility, and phonon transport properties that govern thermoelectric performance (Casper *et al.,* 2012).

The electronic properties of Half-Heusler alloys depend strongly on their valence electron concentration (VEC). Compounds containing 18 valence electrons generally exhibit semiconducting behavior with narrow to moderate band gaps, making them ideal for thermoelectric applications. Examples include TiNiSn, ZrNiSn, and HfNiSn, which have become model systems for thermoelectric research. Small deviations from the ideal electron count through elemental substitution or doping enable precise control of carrier concentration, allowing researchers to optimize electrical conductivity while maintaining a large Seebeck coefficient (Graf *et al.,* 2011).

The efficiency of a thermoelectric material is commonly measured by its dimensionless figure of merit (ZT), which depends on the Seebeck coefficient, electrical conductivity, thermal conductivity, and operating temperature. An ideal thermoelectric material should simultaneously possess a high Seebeck coefficient and electrical conductivity while exhibiting low thermal conductivity. These requirements are often interdependent because increasing electrical conductivity frequently increases thermal conductivity as well. Consequently, improving thermoelectric performance requires careful engineering of both electronic and phononic transport properties (Snyder & Toberer, 2008).

One of the principal advantages of Half-Heusler alloys is their excellent mechanical and thermal stability at elevated temperatures. Unlike many chalcogenide-based thermoelectric materials, which may undergo phase decomposition or sublimation under prolonged heating, Half-Heusler compounds maintain their crystal structure and transport properties at temperatures approaching 1000–1200 K. This exceptional stability is particularly important for RTGs, where thermoelectric materials must operate continuously for decades under large thermal gradients and intense radiation environments (Zhu *et al.,* 2017).

Another important characteristic of Half-Heusler alloys is their tunability. Their electronic structure can be modified through isoelectronic alloying, carrier doping, and atomic substitution. Replacing Ti with Zr or Hf, or partially substituting Sb for Sn, allows researchers to tailor carrier concentration, band gap, and effective mass while simultaneously introducing phonon scattering centers that reduce lattice thermal conductivity. Nanostructuring, grain refinement, and defect engineering have further enhanced thermoelectric performance by suppressing phonon transport without significantly degrading electrical conductivity (Zhu *et al.,* 2017).

Compared with conventional thermoelectric materials such as silicon–germanium (SiGe), lead telluride (PbTe), and bismuth telluride (Bi_2Te_3), Half-Heusler alloys offer several advantages. They possess superior oxidation resistance, excellent mechanical strength, high melting temperatures, and relatively low environmental toxicity. In addition, many Half-Heusler

compounds consist of earth-abundant elements, making them more sustainable and economically attractive for large-scale production. Although their room-temperature thermoelectric performance is generally lower than that of Bi_2Te_3, Half-Heusler alloys outperform many traditional materials at the elevated temperatures typical of RTG operation (Sakurada & Shutoh, 2005).

In recent years, advances in computational materials science have accelerated the discovery of improved Half-Heusler compounds. Density functional theory (DFT), Boltzmann transport calculations, and high-throughput computational screening are increasingly used to predict electronic structures, phonon spectra, carrier transport properties, and thermodynamic stability before experimental synthesis. These computational approaches, combined with machine learning and data-driven materials discovery, have significantly shortened the development cycle for new thermoelectric materials and continue to identify promising compositions with enhanced figures of merit.

In summary, Half-Heusler alloys combine excellent thermal stability, tunable electronic properties, robust mechanical behavior, and favorable thermoelectric performance, making them strong candidates for next-generation RTGs. Their versatile crystal chemistry allows systematic optimization through alloying and defect engineering, while modern computational techniques continue to accelerate materials discovery. These characteristics establish Half-Heusler alloys as one of the leading thermoelectric material families for long-duration space power applications.

3. Thermoelectric Properties of Half-Heusler Alloys

The suitability of Half-Heusler (HH) alloys for next-generation radioisotope thermoelectric generators (RTGs) depends primarily on their thermoelectric performance under high-temperature operating conditions. Thermoelectric efficiency is governed by the interplay between the Seebeck coefficient, electrical conductivity, thermal conductivity, and operating temperature. These transport properties are strongly coupled, making the optimization of thermoelectric materials a challenging task. Over the past two decades, significant advances in alloy design, carrier engineering, and microstructural control have enabled Half-Heusler alloys to achieve thermoelectric figures of merit (ZT) exceeding 1.5 at elevated temperatures, placing them among the most promising candidates for space power applications (Zhu *et al.,* 2017).

The Seebeck coefficient (S) measures the voltage generated in response to a temperature gradient and is one of the key parameters determining thermoelectric performance. A high Seebeck coefficient enables efficient conversion of thermal energy into electrical energy. In Half-Heusler alloys, the Seebeck coefficient is strongly influenced by the electronic band structure, carrier concentration, and effective mass of charge carriers. Narrow-bandgap semiconducting compounds such as TiNiSn, ZrNiSn, and HfNiSn exhibit relatively large Seebeck coefficients because of their favorable electronic density of states near the Fermi level (Snyder & Toberer,

2008). Careful tuning of carrier concentration through elemental substitution allows optimization of the Seebeck coefficient without excessively compromising electrical conductivity.

The second critical parameter is electrical conductivity (σ), which reflects the ability of charge carriers to transport electrical current. High electrical conductivity is essential for maximizing power output in thermoelectric devices. In Half-Heusler alloys, conductivity depends on carrier concentration, carrier mobility, crystal quality, and defect density. Excessively high carrier concentrations reduce the Seebeck coefficient, whereas insufficient carriers increase electrical resistance. Consequently, achieving optimal thermoelectric performance requires balancing these competing effects through controlled doping and alloying (Sakurada & Shutoh, 2005). Both *n*-type and *p*-type Half-Heusler alloys have demonstrated excellent electrical transport properties suitable for high-temperature thermoelectric generators.

A major challenge in thermoelectric materials is minimizing thermal conductivity (κ) while maintaining excellent electrical transport. Thermal conductivity consists of electronic and lattice contributions, with lattice vibrations (phonons) dominating heat transport in many Half-Heusler compounds. Since high thermal conductivity reduces the temperature gradient across the thermoelectric module, suppressing phonon transport is essential for improving efficiency. Researchers have successfully reduced lattice thermal conductivity through alloy scattering, nanostructuring, grain refinement, and the introduction of point defects and secondary phases that scatter phonons across multiple length scales (Zhu *et al.,* 2017). These approaches have significantly enhanced the thermoelectric performance of modern Half-Heusler materials.

The combined influence of the Seebeck coefficient and electrical conductivity is expressed through the power factor, an important measure of electrical energy conversion capability. Half-Heusler alloys are particularly attractive because they exhibit relatively high power factors compared with many conventional thermoelectric materials. Their excellent carrier mobility, combined with optimized carrier concentrations, enables efficient electrical transport even at temperatures approaching 1000 K. High power factors are especially valuable for RTGs, where maintaining stable electrical output over long mission durations is a primary requirement (He *et al.,* 2017).

One of the most effective methods for improving thermoelectric performance is carrier concentration engineering. Controlled substitution of elements at the X, Y, or Z lattice sites modifies the number of free charge carriers and adjusts the Fermi level. For example, substitution of Sb for Sn or Nb for Ti has been widely employed to optimize *n*-type conductivity, while alloying with transition metals can enhance *p*-type performance. Band convergence strategies, resonant impurity doping, and modulation doping have further increased carrier mobility and improved the power factor without substantially increasing thermal conductivity (He *et al.,* 2017).

Recent years have also witnessed significant progress in nanostructuring and multiscale microstructural engineering. Introducing nanoscale precipitates, grain boundaries, dislocations, and coherent interfaces effectively scatters heat-carrying phonons while preserving electron transport. This selective reduction of lattice thermal conductivity has enabled several Half-Heusler systems to achieve ZT values exceeding 1.5 at temperatures between 800 and 1000 K, approaching the performance required for next-generation RTGs (Zhu *et al.,* 2017). In addition, high-entropy Half-Heusler alloys have recently emerged as promising candidates because their severe lattice distortion further suppresses phonon transport while maintaining favorable electronic properties.

For space applications, high-temperature stability is equally important as thermoelectric efficiency. RTGs operate continuously for decades under large temperature gradients generated by radioisotope decay. Half-Heusler alloys exhibit excellent oxidation resistance, low thermal expansion mismatch, and remarkable structural stability under prolonged high-temperature exposure. These characteristics distinguish them from several conventional thermoelectric materials that suffer from phase instability or chemical degradation during long-term operation (Casper *et al.,* 2012).

Overall, the combination of large Seebeck coefficients, high electrical conductivity, reduced lattice thermal conductivity, and excellent thermal stability makes Half-Heusler alloys among the most promising thermoelectric materials for advanced RTGs. Continued improvements through alloy design, defect engineering, nanostructuring, and computational optimization are expected to further enhance their performance, enabling more efficient and reliable power systems for future deep-space exploration missions.

4. Materials Design and Computational Approaches

The rapid advancement of Half-Heusler (HH) thermoelectric materials has been driven not only by experimental discoveries but also by significant progress in computational materials science. Modern computational techniques enable researchers to predict the structural stability, electronic properties, lattice dynamics, and thermoelectric performance of new materials before experimental synthesis. These approaches considerably reduce the time and cost associated with trial-and-error experimentation and have become indispensable for designing high-performance Half-Heusler alloys for next-generation radioisotope thermoelectric generators (RTGs). The integration of first-principles calculations, transport theory, high-throughput screening, and machine learning has accelerated the discovery of promising thermoelectric materials with enhanced efficiency (Curtarolo *et al.,* 2013). The foundation of computational materials design is Density Functional Theory (DFT), which has become the standard method for investigating the electronic structure of solids. DFT enables accurate calculations of equilibrium crystal structures, formation energies, electronic band structures, density of states, elastic properties, and chemical stability (Hohenberg & Kohn, 1964; Kohn & Sham, 1965). In Half-Heusler alloys, DFT is

widely used to identify stable crystal structures, evaluate band gaps, determine effective carrier masses, and predict the effects of alloying and elemental substitution. Such calculations provide valuable insights into the relationship between crystal chemistry and thermoelectric performance before experimental synthesis is undertaken.

Beyond electronic structure calculations, understanding charge carrier transport is essential for evaluating thermoelectric efficiency. This is commonly achieved using the Boltzmann transport equation (BTE) within the relaxation time approximation. By combining DFT-derived electronic band structures with semiclassical transport theory, researchers can calculate the Seebeck coefficient, electrical conductivity, carrier mobility, and electronic contribution to thermal conductivity over a wide range of temperatures and carrier concentrations (Madsen & Singh, 2006). Computational packages such as BoltzTraP have become standard tools for predicting thermoelectric transport coefficients and identifying compositions with high power factors.

Equally important is the prediction of phonon transport, which governs lattice thermal conductivity. Since reducing lattice thermal conductivity is a key strategy for improving the thermoelectric figure of merit (ZT), accurate modeling of phonon behavior has become an active area of research. Density Functional Perturbation Theory (DFPT) and finite-displacement methods allow the calculation of phonon dispersion relations, phonon density of states, Grüneisen parameters, and anharmonic phonon scattering processes. These calculations provide insight into heat transport mechanisms and help identify alloying strategies that suppress lattice thermal conductivity through enhanced phonon scattering (Togo & Tanaka, 2015).

Another powerful computational strategy is high-throughput materials screening, which enables the rapid evaluation of thousands of candidate compounds using automated first-principles calculations. Large computational databases such as the Materials Project, the Open Quantum Materials Database (OQMD), and the AFLOW repository contain electronic, structural, and thermodynamic information for hundreds of thousands of materials. These databases allow researchers to identify stable Half-Heusler compounds with suitable band gaps, high carrier mobility, and favorable thermoelectric properties before experimental synthesis (Curtarolo *et al.,* 2013). High-throughput screening has significantly accelerated the discovery of previously unexplored Half-Heusler compositions for energy applications.

More recently, machine learning (ML) has emerged as a transformative tool in thermoelectric materials discovery. Instead of performing computationally expensive first-principles calculations for every candidate material, ML models are trained using existing experimental and computational datasets to predict key properties such as formation energy, Seebeck coefficient, thermal conductivity, and ZT. Algorithms including random forests, support vector machines, Gaussian process regression, and deep neural networks have demonstrated remarkable success in identifying promising thermoelectric materials while substantially reducing computational cost

(Schmidt *et al.,* 2019). The combination of DFT and machine learning provides a powerful framework for accelerating materials discovery.

Computational approaches also facilitate defect engineering and alloy optimization. Point defects, vacancies, antisite disorder, and substitutional alloying strongly influence carrier concentration and phonon scattering in Half-Heusler alloys. First-principles defect calculations enable prediction of defect formation energies, equilibrium defect concentrations, and their effects on electronic transport. Such studies guide experimental efforts toward compositions that maximize electrical conductivity while minimizing lattice thermal conductivity. Similarly, computational simulations of nanostructures, grain boundaries, and heterostructures provide valuable insight into microstructural engineering strategies for enhancing thermoelectric performance.

Despite these advances, several challenges remain. Standard DFT often underestimates semiconductor band gaps, requiring hybrid functionals or many-body methods for greater accuracy. Predicting thermal conductivity also remains computationally demanding because of the complex anharmonic interactions among phonons. Furthermore, many computational studies assume ideal crystal structures, whereas experimentally synthesized materials often contain disorder, defects, and secondary phases. Consequently, close collaboration between computational modeling and experimental validation remains essential for developing practical thermoelectric materials.

In summary, computational materials science has become a cornerstone of modern Half-Heusler research. Density functional theory, Boltzmann transport calculations, phonon simulations, high-throughput screening, and machine learning collectively provide a comprehensive framework for understanding and optimizing thermoelectric materials. These computational tools continue to accelerate the discovery of high-performance Half-Heusler alloys and are expected to play an increasingly important role in the development of efficient RTGs for future space exploration missions.

5. Suitability of Half-Heusler Alloys for Space Radioisotope Thermoelectric Generators

The effectiveness of a thermoelectric material for radioisotope thermoelectric generators (RTGs) depends not only on its energy conversion efficiency but also on its ability to operate reliably under the harsh conditions of space for several decades. Unlike terrestrial thermoelectric devices, RTGs are expected to function continuously without maintenance while experiencing intense thermal gradients, vacuum conditions, cosmic radiation, mechanical vibrations during launch, and repeated thermal cycling. Consequently, the selection of thermoelectric materials requires a careful balance between thermoelectric performance, mechanical durability, chemical stability, and long-term reliability. Half-Heusler (HH) alloys satisfy many of these demanding requirements, making them among the leading candidates for next-generation RTGs (Snyder & Toberer, 2008).

One of the greatest advantages of Half-Heusler alloys is their excellent high-temperature stability. Conventional RTGs operate with hot-side temperatures approaching 900–1200 K, depending on the radioisotope heat source and system design. Many high-performance thermoelectric materials, such as bismuth telluride, suffer from thermal degradation or oxidation at elevated temperatures. In contrast, Half-Heusler compounds maintain their crystal structure, electronic properties, and mechanical integrity over prolonged exposure to high temperatures. Their high melting points and strong covalent bonding contribute to excellent thermal stability, making them well suited for long-duration space missions (Casper *et al.,* 2012).

Another critical requirement for RTGs is radiation resistance. The continuous decay of radioisotopes such as plutonium-238 generates alpha particles and secondary radiation that can gradually degrade thermoelectric materials. In addition, spacecraft operating beyond Earth's magnetosphere are exposed to galactic cosmic rays and solar energetic particles. Although systematic radiation studies on Half-Heusler thermoelectric materials remain limited, their robust intermetallic crystal structures and strong atomic bonding suggest good resistance to radiation-induced structural damage compared with many conventional semiconductor thermoelectric materials (Graf *et al.,* 2011). Further experimental investigation under simulated space-radiation environments will be important for validating their long-term performance.

Half-Heusler alloys also exhibit excellent mechanical robustness, an essential characteristic for space hardware. RTGs experience severe mechanical stresses during launch, including intense vibration, shock loading, and rapid acceleration. Mechanical failure of thermoelectric modules could significantly reduce power generation or even terminate an entire mission. Compared with brittle chalcogenide-based thermoelectric materials, Half-Heusler compounds possess relatively high fracture toughness, hardness, and elastic modulus, enabling them to better withstand mechanical loading and repeated thermal cycling (Zhu *et al.,* 2017). Their favorable mechanical properties also simplify module fabrication and improve device reliability.

The long-term chemical stability of Half-Heusler alloys further enhances their suitability for RTGs. Space missions such as the Voyager spacecraft have demonstrated operational lifetimes exceeding four decades, requiring thermoelectric materials with exceptional resistance to oxidation, diffusion, phase separation, and microstructural degradation. Many Half-Heusler compounds remain chemically stable over extended periods at elevated temperatures and exhibit relatively low diffusion rates compared with conventional thermoelectric materials. These characteristics minimize degradation of electrical and thermal transport properties throughout the mission lifetime (Sakurada & Shutoh, 2005).

Compatibility with radioisotope heat sources is another important consideration. Modern RTGs typically employ plutonium-238 oxide encapsulated within robust heat source modules that continuously generate thermal energy. Efficient thermoelectric conversion requires materials capable of sustaining large temperature gradients while maintaining stable electrical transport

properties. Half-Heusler alloys exhibit relatively low coefficients of thermal expansion and good thermal compatibility with structural components used in thermoelectric modules. Their ability to operate efficiently over broad temperature ranges makes them attractive for advanced RTG designs that seek higher conversion efficiencies than current silicon–germanium systems (Bell, 2008).

The performance of Half-Heusler alloys can also be assessed by comparison with other high-temperature thermoelectric materials. Silicon–germanium (SiGe) alloys have historically been the benchmark material for space RTGs because of their exceptional thermal stability and extensive flight heritage. However, their thermoelectric figure of merit is relatively modest compared with modern materials. Lead telluride (PbTe) offers higher thermoelectric efficiency but suffers from chemical instability and toxicity concerns. Skutterudites demonstrate excellent thermoelectric performance and are being explored for advanced RTGs, yet they require complex filler atoms to suppress thermal conductivity. Half-Heusler alloys combine many of the strengths of these materials by offering high-temperature stability, mechanical robustness, environmental compatibility, and steadily improving thermoelectric efficiency (Snyder & Toberer, 2008). Despite these advantages, several challenges remain before Half-Heusler alloys can be widely adopted in space-qualified RTGs. Their lattice thermal conductivity is generally higher than that of leading thermoelectric materials, requiring continued improvements through nanostructuring, alloy disorder, and defect engineering. In addition, large-scale manufacturing, module integration, and long-duration reliability testing under realistic space conditions must be completed before flight qualification.

Overall, Half-Heusler alloys exhibit a unique combination of thermoelectric performance, structural stability, radiation tolerance, and mechanical durability that closely matches the demanding requirements of future RTGs. Continued advances in materials engineering and computational design are expected to further enhance their performance, making them strong candidates for powering future lunar bases, Mars missions, and deep-space exploration.

6. Recent Advances and Experimental Developments

Over the past decade, Half-Heusler (HH) alloys have undergone remarkable development, transforming from moderately efficient thermoelectric materials into one of the leading candidates for high-temperature power generation. Advances in alloy engineering, nanostructuring, defect control, and processing techniques have significantly improved their thermoelectric performance, with several compositions now achieving dimensionless figures of merit (ZT) exceeding 1.5 at temperatures above 900 K. These improvements have strengthened the case for employing Half-Heusler alloys in next-generation radioisotope thermoelectric generators (RTGs), where high efficiency, thermal stability, and long operational lifetimes are essential (Zhu *et al.,* 2017).

One of the most significant breakthroughs has been the development of multicomponent Half-Heusler alloys. Early thermoelectric research focused primarily on simple ternary compounds such as TiNiSn, ZrNiSn, and HfNiSn. More recent studies have shown that partial substitution at the X, Y, or Z atomic sites creates solid-solution alloys that simultaneously optimize electronic transport and suppress lattice thermal conductivity. For example, alloying Ti, Zr, and Hf in varying proportions introduces mass fluctuation scattering, which effectively reduces phonon transport while preserving favorable electrical conductivity. This strategy has produced several *n*-type Half-Heusler systems with substantially improved thermoelectric performance (Fu *et al.,* 2015).

Another major advance is nanostructuring, which has become one of the most effective methods for improving thermoelectric efficiency. By introducing nanoscale precipitates, grain boundaries, coherent interfaces, and dislocations, researchers have significantly reduced lattice thermal conductivity through enhanced phonon scattering while maintaining relatively high carrier mobility. Because phonons possess much shorter mean free paths than electrons, nanostructures selectively scatter heat-carrying phonons without severely degrading electrical transport. This multiscale phonon-scattering approach has enabled several Half-Heusler materials to achieve record thermoelectric performance at temperatures relevant to RTG operation (Snyder & Toberer, 2008).

Recent work has also focused on band structure engineering, which aims to improve the power factor by modifying the electronic density of states near the Fermi level. Techniques such as band convergence, resonant impurity doping, and modulation doping increase the effective density of electronic states while maintaining high carrier mobility. These approaches enhance the Seebeck coefficient without significantly reducing electrical conductivity, thereby improving overall thermoelectric efficiency. Computational studies combined with experimental validation have demonstrated that careful electronic structure engineering can substantially increase the performance of both *n*-type and *p*-type Half-Heusler alloys (He *et al.,* 2017). An emerging area of research involves high-entropy Half-Heusler alloys, which incorporate multiple principal elements within the same crystallographic sublattice. The resulting severe lattice distortion creates strong phonon scattering, dramatically reducing lattice thermal conductivity while preserving crystalline order and electronic transport. High-entropy Half-Heusler compounds have recently demonstrated encouraging thermoelectric performance together with excellent thermal stability, suggesting considerable potential for high-temperature space applications (Fan *et al.,* 2023). Their exceptional structural stability under prolonged heating is particularly attractive for RTGs expected to operate continuously for several decades.

Significant progress has also been made in advanced manufacturing techniques. Spark plasma sintering (SPS) has become one of the preferred fabrication methods for Half-Heusler thermoelectric materials because it enables rapid densification while preserving nanoscale

microstructures. More recently, additive manufacturing and advanced powder-processing techniques have been investigated to fabricate complex thermoelectric modules with improved reproducibility and reduced manufacturing costs. These developments may facilitate the large-scale production of thermoelectric devices required for future space exploration missions (Zhu *et al.,* 2017).

Experimental validation has confirmed many predictions from first-principles calculations and high-throughput computational screening. Modern characterization techniques—including synchrotron X-ray diffraction, transmission electron microscopy, neutron scattering, and atom probe tomography—have provided detailed insight into atomic ordering, defect distributions, and phonon-scattering mechanisms in Half-Heusler alloys. These studies have significantly improved the understanding of structure–property relationships and guided the rational design of higher-performance thermoelectric materials (Casper *et al.,* 2012).

Space agencies have also shown increasing interest in advanced thermoelectric materials for future radioisotope power systems. Although current operational RTGs continue to rely primarily on silicon–germanium alloys, research programs supported by organizations such as the National Aeronautics and Space Administration and the European Space Agency are evaluating higher-efficiency thermoelectric materials for future missions. Improved Half-Heusler alloys offer the possibility of increasing electrical output while reducing radioisotope fuel requirements, thereby improving mission efficiency and lowering system mass. These advantages are particularly important for future lunar habitats, Mars exploration, and deep-space probes where long-duration, maintenance-free power generation is essential.

Despite these advances, several challenges remain before Half-Heusler alloys can be deployed in flight-qualified RTGs. Further improvements in thermoelectric efficiency, long-term thermal aging studies, radiation-resistance testing, and module-level integration are still required. Nevertheless, the rapid progress achieved through alloy design, nanostructuring, computational materials discovery, and advanced manufacturing strongly suggests that Half-Heusler alloys will play an increasingly important role in next-generation space power systems.

7. Future Perspectives and Outlook

Half-Heusler (HH) alloys have evolved into one of the most promising thermoelectric material families for high-temperature energy conversion. Their combination of excellent thermal stability, robust mechanical properties, tunable electronic structures, and steadily improving thermoelectric performance positions them as strong candidates for next-generation radioisotope thermoelectric generators (RTGs). As future space missions become increasingly ambitious—targeting permanent lunar bases, crewed Mars expeditions, asteroid exploration, and deep-space observatories—the demand for highly efficient, reliable, and long-lived power systems will continue to grow. Continued advances in Half-Heusler materials are therefore expected to play a central role in enabling these missions (Snyder & Toberer, 2008).

A major direction for future research is the development of high-ZT Half-Heusler alloys through integrated materials design. Although several compositions have already achieved ZT values greater than 1.5 at elevated temperatures, further improvements are necessary to compete with or surpass the performance of state-of-the-art thermoelectric materials. Strategies such as multicomponent alloying, band convergence, resonant doping, hierarchical nanostructuring, and phonon engineering are expected to remain key approaches for simultaneously enhancing electrical transport and suppressing lattice thermal conductivity. The ability to independently optimize electron and phonon transport remains one of the principal challenges in thermoelectric materials research (Zhu *et al.,* 2017).

Another rapidly developing area is the application of artificial intelligence (AI) and machine learning (ML) to thermoelectric materials discovery. Traditional experimental approaches often require years of synthesis and characterization before identifying promising compositions. Machine learning algorithms trained on computational and experimental databases can rapidly predict formation energies, electronic structures, transport properties, and thermodynamic stability, enabling researchers to prioritize the most promising candidate materials for experimental validation. Coupled with density functional theory (DFT) and high-throughput screening, AI-driven materials discovery is expected to significantly accelerate the development of high-performance Half-Heusler alloys (Schmidt *et al.,* 2019).

Future progress will also depend on advanced computational modeling. Improvements in first-principles methods, anharmonic phonon calculations, and multiscale transport simulations are providing increasingly accurate predictions of thermoelectric performance under realistic operating conditions. Combining electronic structure calculations with atomistic simulations, phase-field modeling, and finite-element analysis will allow researchers to optimize complete thermoelectric modules rather than individual materials. Such integrated computational frameworks are particularly valuable for designing RTGs that maximize efficiency while maintaining long-term structural integrity under extreme thermal and mechanical conditions.

Another important research frontier is the development of high-entropy and compositionally complex Half-Heusler alloys. These materials contain multiple principal elements occupying equivalent lattice sites, creating severe lattice distortions that strongly scatter phonons without significantly degrading electrical transport. Preliminary studies indicate that high-entropy Half-Heusler compounds combine low lattice thermal conductivity with excellent thermal stability, making them attractive candidates for long-duration RTGs. Further experimental investigations are needed to evaluate their radiation tolerance, long-term aging behavior, and manufacturability under realistic aerospace conditions (Fan *et al.,* 2023).

From an engineering perspective, future RTGs will require improved module integration and manufacturing technologies. Advances in spark plasma sintering, additive manufacturing, diffusion bonding, and high-temperature joining techniques will facilitate the fabrication of

reliable thermoelectric modules with improved mechanical integrity and reduced thermal contact resistance. Simultaneously, improved interface engineering between thermoelectric legs, electrodes, and heat exchangers will enhance overall system efficiency. These manufacturing innovations will be essential for translating laboratory-scale materials into flight-qualified power systems.

Future space missions will impose increasingly demanding operational requirements. Lunar night survival systems, autonomous scientific stations on Mars, deep-space probes beyond the heliosphere, and missions to the icy moons of Jupiter and Saturn will require compact power sources capable of delivering continuous electrical power for decades. Because solar energy becomes progressively less effective with increasing distance from the Sun, RTGs will remain indispensable for these missions. Half-Heusler alloys, with their excellent high-temperature stability and improving thermoelectric efficiency, are well positioned to become a core technology for next-generation radioisotope power systems (NASA, 2024).

Despite this promising outlook, several scientific and engineering challenges remain. Long-term thermal aging, radiation damage, thermal fatigue, oxidation resistance, and compatibility with radioisotope heat sources require further investigation. In addition, comprehensive qualification testing under simulated space environments will be necessary before new thermoelectric materials can be incorporated into operational RTGs. International collaboration among universities, research laboratories, space agencies, and industry will play a crucial role in advancing these technologies from laboratory demonstrations to spaceflight applications.

In conclusion, Half-Heusler alloys represent one of the most promising material systems for future radioisotope thermoelectric generators. Their favorable combination of thermoelectric performance, structural stability, mechanical robustness, and environmental compatibility provides a strong foundation for long-duration space power generation. Continued progress in computational materials science, artificial intelligence, advanced manufacturing, and experimental characterization is expected to further enhance their performance, bringing efficient, durable, and lightweight RTGs closer to practical implementation. These developments will contribute significantly to the next generation of space exploration by providing reliable power for missions operating far beyond the reach of conventional solar energy systems.

References

1. Bell, L. E. (2008). Cooling, heating, generating power, and recovering waste heat with thermoelectric systems. *Science, 321*(5895), 1457–1461.
2. Casper, F., Graf, T., Chadov, S., Balke, B., & Felser, C. (2012). Half-Heusler compounds: Novel materials for energy and spintronic applications. *Semiconductor Science and Technology, 27*(6), 063001.

3. Curtarolo, S., Setyawan, W., Hart, G. L. W., Jahnátek, M., Chepulskii, R. V., Taylor, R. H., *et al.* (2013). AFLOW: An automatic framework for high-throughput materials discovery. *Computational Materials Science, 58*, 218–226.
4. Fan, J., Zhu, T., Fu, C., & Zhao, X. (2023). High-entropy thermoelectric materials: Progress and perspectives. *Advanced Functional Materials, 33*, 2300196.
5. Fu, C., Zhu, T., Liu, Y., Xie, H., & Zhao, X. (2015). Band engineering of high-performance *n*-type FeNbSb-based Half-Heusler thermoelectric materials. *Energy & Environmental Science, 8*, 216–220.
6. Graf, T., Felser, C., & Parkin, S. S. P. (2011). Simple rules for the understanding of Heusler compounds. *Progress in Solid State Chemistry, 39*(1), 1–50.
7. He, R., Schierning, G., & Nielsch, K. (2018). Thermoelectric devices: A review of devices, architectures, and contact optimization. *Advanced Materials Technologies, 3*(4), 1700256.
8. Hohenberg, P., & Kohn, W. (1964). Inhomogeneous electron gas. *Physical Review, 136*(3B), B864–B871.
9. Kohn, W., & Sham, L. J. (1965). Self-consistent equations including exchange and correlation effects. *Physical Review, 140*(4A), A1133–A1138.
10. Madsen, G. K. H., & Singh, D. J. (2006). BoltzTraP: A code for calculating band-structure dependent quantities. *Computer Physics Communications, 175*(1), 67–71.
11. Mason, L. S., Schmitz, P. C., & Sutliff, T. J. (2018). *Advanced Radioisotope Power Systems for Space Exploration*. NASA Technical Reports.
12. NASA. (2024). *Radioisotope Power Systems*. National Aeronautics and Space Administration.
13. Rowe, D. M. (Ed.). (2006). *Thermoelectrics Handbook: Macro to Nano*. CRC Press.
14. Sakurada, S., & Shutoh, N. (2005). Effect of Ti substitution on the thermoelectric properties of (Zr,Hf)NiSn Half-Heusler compounds. *Applied Physics Letters, 86*(8), 082105.
15. Schmidt, J., Marques, M. R. G., Botti, S., & Marques, M. A. L. (2019). Recent advances and applications of machine learning in solid-state materials science. *npj Computational Materials, 5*, 83.
16. Snyder, G. J., & Toberer, E. S. (2008). Complex thermoelectric materials. *Nature Materials, 7*(2), 105–114.
17. Togo, A., & Tanaka, I. (2015). First-principles phonon calculations in materials science. *Scripta Materialia, 108*, 1–5.
18. Zhu, T., Fu, C., Xie, H., Liu, Y., & Zhao, X. (2017). High efficiency Half-Heusler thermoelectric materials for energy harvesting. *Advanced Energy Materials, 7*(19), 1700706.

UNDERSTANDING 5G PHYSICAL CHANNELS AND PHYSICAL SIGNALS

Joyanto Roychoudhary
Department of ECE,
Meghnad Saha Institute of Technology, Kolkata
Corresponding author E-mail: joyanto.roychoudhary296@msit.edu.in

What Are Physical Channels in 5G?

In 5G NR, physical channels are responsible for sending user and control information across the air interface. They sit at the lowest level of the protocol stack — the Physical (PHY) layer. Each type of channel is tailored for specific tasks, whether that's broadcasting system info, managing control signals, or transferring user data.

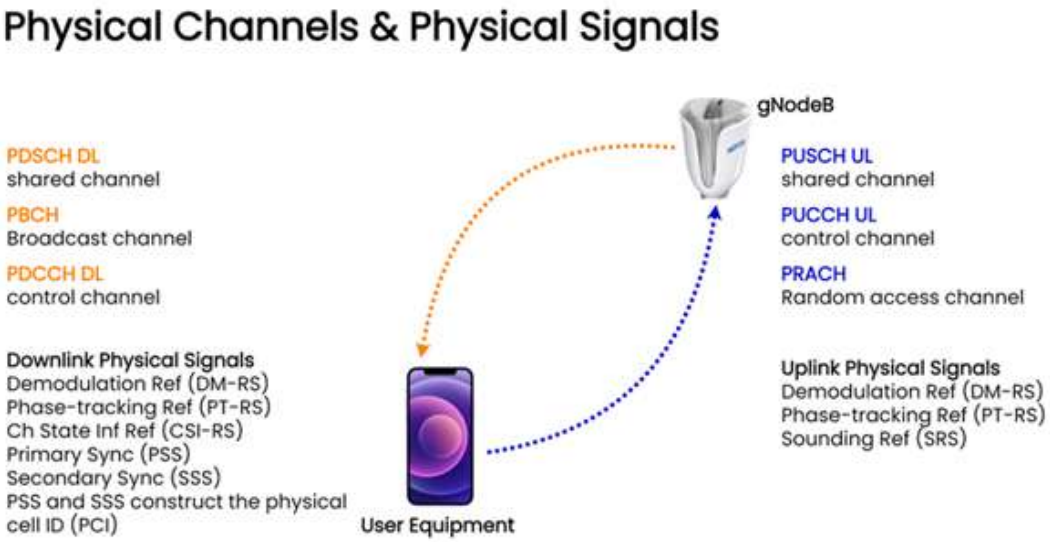

You can categorize physical channels into:

- Downlink Channels (from gNodeB to UE)
- Uplink Channels (from UE to gNodeB)
- Downlink Physical Channels
- Downlink physical channels transmit data and control information from the base station (gNodeB) to the user device (UE).

1. PDSCH (Physical Downlink Shared Channel)

Purpose: This channel carries user data, system info, and higher-layer signaling messages.

Handles multiple users through OFDMA resource allocation.

Transmits both unicast and broadcast data.

Adjusts resources dynamically to optimize bandwidth use.

Key Role: It's essential for high-speed data transfers like streaming videos, browsing, or downloading files.

2. PBCH (Physical Broadcast Channel)

Purpose: This channel broadcasts key system information essential for users to access the network initially.

Transmits the Master Information Block (MIB).

Helps the UE understand parameters like subcarrier spacing and system bandwidth.

Found in the Synchronization Signal Block (SSB), alongside PSS and SSS.

Key Role: It lets devices identify and sync with a 5G network during the cell search and selection process.

3. PDCCH (Physical Downlink Control Channel)

Purpose: This channel sends control info necessary for scheduling communications.

Transmits Downlink Control Information (DCI), informing the UE about where and how to receive or send data.

Offers multiple formats for flexible scheduling of uplink and downlink.

Utilizes techniques like beamforming to enhance reliability.

Key Role: Acts as the command channel between gNodeB and UE, ensuring smooth coordination of data transfers.

Uplink Physical Channels

Uplink physical channels handle data and control information that the UE sends back to the gNodeB.

1. PUSCH (Physical Uplink Shared Channel)

Purpose: Carries user data and control info from UE back to gNodeB.

Supports multiple users using SC-FDMA or DFT-s-OFDM to reduce peak-to-average power ratio (PAPR).

Key for fast data transfers like uploading files or VoNR (Voice over New Radio).

Key Role: The main channel for sending uplink data, maximizing power efficiency in user devices.

2. PUCCH (Physical Uplink Control Channel)

Purpose: This channel transmits uplink control information (UCI), such as acknowledgments and scheduling requests.

Sends Hybrid ARQ acknowledgments (ACK/NACK), CSI reports, and various control signals.

Designed for low-latency transmission of small data packets.

Key Role: Provides accurate feedback to gNodeB, crucial for maintaining transmission reliability and adapting to link changes.

3. PRACH (Physical Random-Access Channel)

Purpose: This channel facilitates initial access and timing synchronization.

Used by UE to connect with gNodeB.

Sends the Random Access Preamble during the connection setup.

Vital for handovers and reconnecting.

Key Role: It's the first step in accessing the network, allowing UE to request communication resources.

Downlink Physical Signals

Physical signals are predefined reference signals that help with synchronization, channel estimation, and tracking.

1. DM-RS (Demodulation Reference Signal)

Helps estimate channels for demodulating data on PDSCH or PUSCH.

Each user has unique DM-RS sequences to ensure precise decoding.

Use Case: It's essential for coherent demodulation and managing interference.

2. PT-RS (Phase-Tracking Reference Signal)

Aids in tracking and correcting phase noise in high-frequency bands like mmWave.

Boosts demodulation accuracy at high data rates.

Use Case: Enhances signal quality under challenging RF conditions.

3. CSI-RS (Channel State Information Reference Signal)

Gives channel quality feedback to gNodeB.

Supports beam management, MIMO optimization, and link adjustment.

Use Case: Essential for advanced features like Massive MIMO and beamforming.

4. PSS and SSS (Primary and Secondary Synchronization Signals)

PSS (Primary Sync Signal): Helps UE find the timing of a 5G cell.

SSS (Secondary Sync Signal): Offers additional details like the physical cell ID (PCI).

Use Case: Critical for initial cell detection and syncing during network access.

Downlink Summary Table

Channel/Signal Full Name Purpose PDSCH Physical Downlink Shared Channel User data & signaling PBCH Physical Broadcast Channel Network information broadcast PDCCH Physical Downlink Control Channel Scheduling & control info DM-RS Demodulation Reference Signal Channel estimation PT-RS Phase Tracking Reference Signal Phase correction CSI-RS Channel State Information RS Channel quality feedback PSS/SSS Sync Signals Cell detection & synchronization

Uplink Physical Signals

Like the downlink, the uplink makes use of reference signals that support synchronization, power control, and channel estimation.

1. DM-RS (Demodulation Reference Signal)

Utilized by gNodeB to assess the uplink channel for data demodulation.

Helps enhance accuracy in scenarios with multiple users.

2. PT-RS (Phase-Tracking Reference Signal)

Fixes phase errors in uplink transmissions, particularly in mmWave bands.

3. SRS (Sounding Reference Signal)

Lets gNodeB measure the quality of the uplink channel across various frequencies.

Helps fine-tune scheduling and beam selection.

Key Role: It's vital for adapting uplink connections and managing interference.

How Physical Channels and Signals Work Together

The way channels and signals interact creates a seamless flow of information in 5G networks:

Cell Discovery: UE uses PSS and SSS to detect and align with a 5G cell.

Network Access: PBCH sends the MIB, while PRACH kicks off random access.

Control Exchange: PDCCH and PUCCH manage scheduling and acknowledgements.

Data Transmission: PDSCH and PUSCH handle user data, with reference signals ensuring link quality.

Optimization: CSI-RS and SRS fine-tune channel understanding for adaptive beamforming and resource management.

5G NR Frame Structure

The 5G NR (New Radio) frame structure, defined by the 3GPP standard, is designed to provide flexibility and scalability for diverse applications, ranging from enhanced mobile broadband (eMBB) to ultra-reliable low-latency communication (URLLC) and massive machine-type communication (mMTC). The frame structure consists of 10 ms radio frames, each divided into 1 ms subframes, which are further segmented into slots. The slot duration varies depending on the selected subcarrier spacing (SCS), enabling adaptable transmission configurations for different deployment scenarios.

Additionally, each slot comprises multiple OFDM symbols, where the number of symbols per slot depends on the numerology (μ) and the chosen SCS.

5G Frame Structure

5G NR supports two frequency ranges:

- FR1 (Sub 6GHz)
- FR2 (millimeter wave range, 24.25 to 52.6 GHz)

NR uses flexible subcarrier spacing derived from the basic 15 KHz subcarrier spacing used in LTE.

A frame has a duration of 10 ms and consists of 10 subframes, each having a 1ms duration, similar to LTE technology. Each subframe can have 2^{μ} slots. Each slot typically consists of 14 OFDM symbols. The radio frames of 10 ms are transmitted continuously, one after the other, as per the TDD topology.

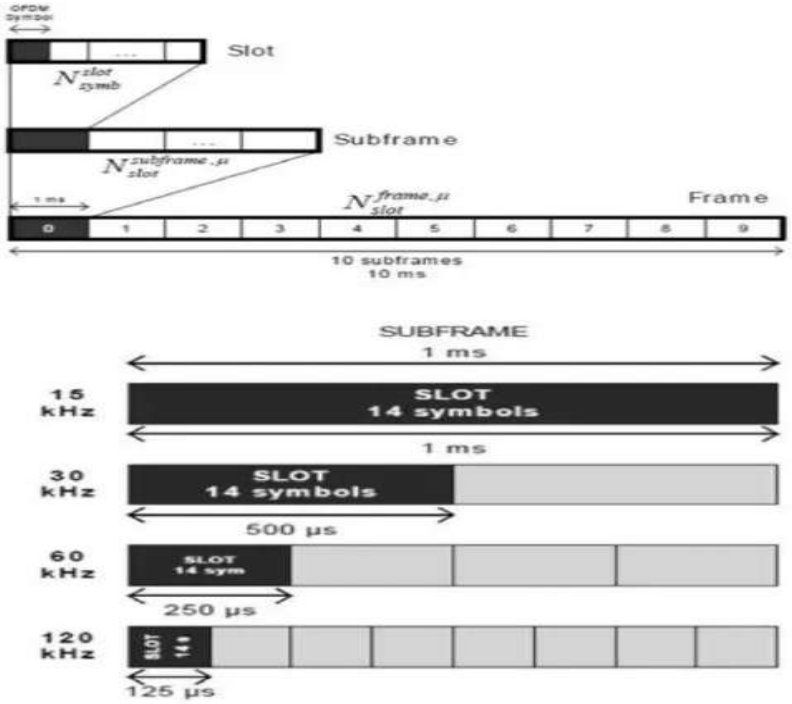

The subframe is of fixed duration (i.e., 1ms), whereas the slot length varies based on the subcarrier spacing and the number of slots per subframe. As shown below, it is 1 ms for 15 KHz, 500 µs for 30 KHz, and so on. A subcarrier spacing of 15 KHz occupies 1 slot per subframe, while a subcarrier spacing of 30 KHz occupies 2 slots per subframe, and so on.

Each slot occupies either 14 OFDM symbols or 12 OFDM symbols based on normal CP and extended CP, respectively.

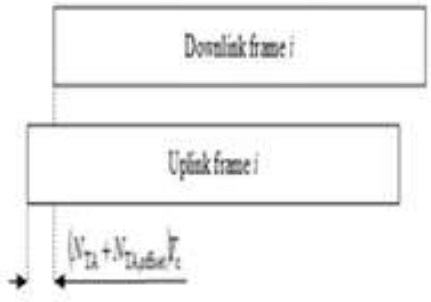

Frequency range and band of cell used for uplink transmission	$N_{TA,offset}$ (Unit: T_c)
FDD in FR1	0
FR1 TDD band	39936 or 25600 (Note 1)
FR2	13792
NOTE 1: The UE identifies $N_{TA,offset}$ based on the information [TBD] according to [TS38.331]	
NOTE 2: The value of $N_{TA,offset}$ that applies to the supplementary UL carrier is determined from the non-supplementary UL carrier.	

Each 5G NR frame is divided into two equal-sized half frames with 5 subframes in each. Half frame-0 consists of subframes 0 to 4, and half frame-1 consists of subframes 5 to 9.

The uplink frame-i starts T_{TA} time duration before the start of downlink frame-i.

$$T_{TA} = (N_{TA} + N_{TA,offset}) * T_c$$

Where:

- Physical layer timing unit, $T_c = 1/(\Delta f_{max} * N_f)$
- $\Delta f_{max} = 480$ KHz, $N_f = 4096$
- $T_c = 0.509$ ns

is defined in TS 38.133 document as per table 1. OFDM symbols in a slot can be classified as 'downlink', 'flexible', or 'uplink'.

- Signaling of slot formats is mentioned in subclause 11.1 of TS 38.213 document.

The table below mentions the same.

Format	Symbol number in a slot													
	0	1	2	3	4	5	6	7	8	9	10	11	12	13
0	D	D	D	D	D	D	D	D	D	D	D	D	D	D
1	U	U	U	U	U	U	U	U	U	U	U	U	U	U
2	F	F	F	F	F	F	F	F	F	F	F	F	F	F
3	D	D	D	D	D	D	D	D	D	D	D	D	D	F
4	D	D	D	D	D	D	D	D	D	D	D	D	F	F
5	D	D	D	D	D	D	D	D	D	D	D	F	F	F
6	D	D	D	D	D	D	D	D	D	D	F	F	F	F
7	D	D	D	D	D	D	D	D	D	F	F	F	F	F
8	F	F	F	F	F	F	F	F	F	F	F	F	F	U
9	F	F	F	F	F	F	F	F	F	F	F	F	U	U
10	F	U	U	U	U	U	U	U	U	U	U	U	U	U
11	F	F	U	U	U	U	U	U	U	U	U	U	U	U
12	F	F	F	U	U	U	U	U	U	U	U	U	U	U
13	F	F	F	F	U	U	U	U	U	U	U	U	U	U
14	F	F	F	F	F	U	U	U	U	U	U	U	U	U
15	F	F	F	F	F	F	U	U	U	U	U	U	U	U
16	D	F	F	F	F	F	F	F	F	F	F	F	F	F
17	D	D	F	F	F	F	F	F	F	F	F	F	F	F
18	D	D	D	F	F	F	F	F	F	F	F	F	F	F
19	D	F	F	F	F	F	F	F	F	F	F	F	F	U
20	D	D	F	F	F	F	F	F	F	F	F	F	F	U
21	D	D	D	F	F	F	F	F	F	F	F	F	F	U
22	D	F	F	F	F	F	F	F	F	F	F	F	U	U
23	D	D	F	F	F	F	F	F	F	F	F	F	U	U
24	D	D	D	F	F	F	F	F	F	F	F	F	U	U
25	D	F	F	F	F	F	F	F	F	F	F	U	U	U
26	D	D	F	F	F	F	F	F	F	F	F	U	U	U
27	D	D	D	F	F	F	F	F	F	F	F	U	U	U
28	D	D	D	D	D	D	D	D	D	D	D	D	F	U
29	D	D	D	D	D	D	D	D	D	D	D	F	F	U
30	D	D	D	D	D	D	D	D	D	D	F	F	F	U
31	D	D	D	D	D	D	D	D	D	D	F	U	U	U
32	D	D	D	D	D	D	D	D	D	D	F	F	U	U
33	D	D	D	D	D	D	D	D	D	F	F	F	U	U
34	D	F	U	U	U	U	U	U	U	U	U	U	U	U
35	D	D	F	U	U	U	U	U	U	U	U	U	U	U
36	D	D	D	F	U	U	U	U	U	U	U	U	U	U
37	D	F	F	U	U	U	U	U	U	U	U	U	U	U
38	D	D	F	F	U	U	U	U	U	U	U	U	U	U
39	D	D	D	F	F	U	U	U	U	U	U	U	U	U
40	D	F	F	F	U	U	U	U	U	U	U	U	U	U
41	D	D	F	F	F	U	U	U	U	U	U	U	U	U
42	D	D	D	F	F	F	U	U	U	U	U	U	U	U
43	D	D	D	D	D	D	D	D	D	F	F	F	F	U
44	D	D	D	D	D	D	F	F	F	F	F	F	U	U
45	D	D	D	D	D	D	F	F	U	U	U	U	U	U
46	D	D	D	D	D	F	U	D	D	D	D	D	F	U
47	D	D	F	U	U	U	U	D	D	F	U	U	U	U
48	D	F	U	U	U	U	U	D	F	U	U	U	U	U
49	D	D	D	D	F	F	U	D	D	D	D	F	F	U
50	D	D	F	F	U	U	U	D	D	F	F	U	U	U
51	D	F	F	U	U	U	U	D	F	F	U	U	U	U
52	D	F	F	F	F	F	U	D	F	F	F	F	F	U
53	D	D	F	F	F	F	U	D	D	F	F	F	F	U
54	F	F	F	F	F	F	F	D	D	D	D	D	D	D
55	D	D	F	F	F	U	U	U	D	D	D	D	D	D
56 – 254	Reserved													
255	UE determines the slot format for the slot based on *tdd-UL-DL-ConfigurationCommon*, *tdd-UL-DL-ConfigurationCommon2*, or *tdd-UL-DL-ConfigDedicated* and, if any, on detected DCI formats													

- In a slot in a downlink frame, the UE shall assume that downlink transmissions only occur in 'downlink' or 'flexible' symbols.
- In a slot in an uplink frame, the UE shall only transmit in 'uplink' or 'flexible' symbols.
- A UE not capable of full-duplex communication is not expected to transmit in the uplink earlier than $N_{Rx-Tx} * T_c$ after the end of the last received downlink symbol in the same cell where N_{Rx-Tx} is given by TS 38.101 document.

Slot Formats in 5G NR Frame Structure (Normal CP)

The table illustrates various slot formats possible within a 5G NR frame structure when using normal Cyclic Prefix (CP). The slots can be entirely downlink, entirely uplink, or a mix of both, with certain symbols being designated as 'flexible' to allow for dynamic allocation.

As mentioned in the description above, a slot can be all downlink, all uplink, or mixed (i.e., a combination of downlink and uplink). Here, mixed refers to static, semi-static, or dynamic configurations.

Slot aggregation is supported in 5G NR; hence, data transmission can be scheduled to span one or multiple slots. Slot format indication informs the UE whether an OFDM symbol is downlink, uplink, or flexible.

The figure below depicts the same.

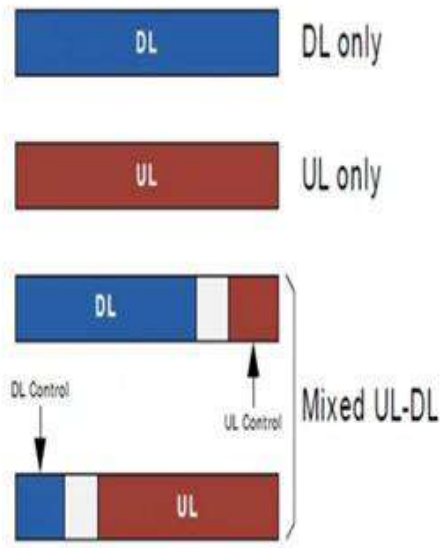

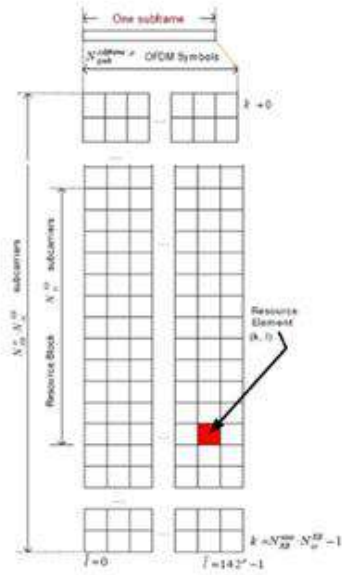

The number of resource blocks per subframe is depicted in the following figure.

The figure depicts the resource grid of 5G NR with symbols on the time axis and subcarriers on the frequency axis. Twelve subcarriers form one PRB (Physical Resource Block). 5G NR supports 24 to 275 PRBs in a single slot. Occupied BW of 34.56 MHz (minimum) and 396 MHz (maximum) can be achieved for 120 KHz subcarrier spacing. One SS/PBCH Block occupies 4 OFDM Symbols in the time domain and 24 PRBs in the frequency domain. 5G NR SS consists of PSS and SSS as specified for LTE.

5G NR Physical Layer Specifications

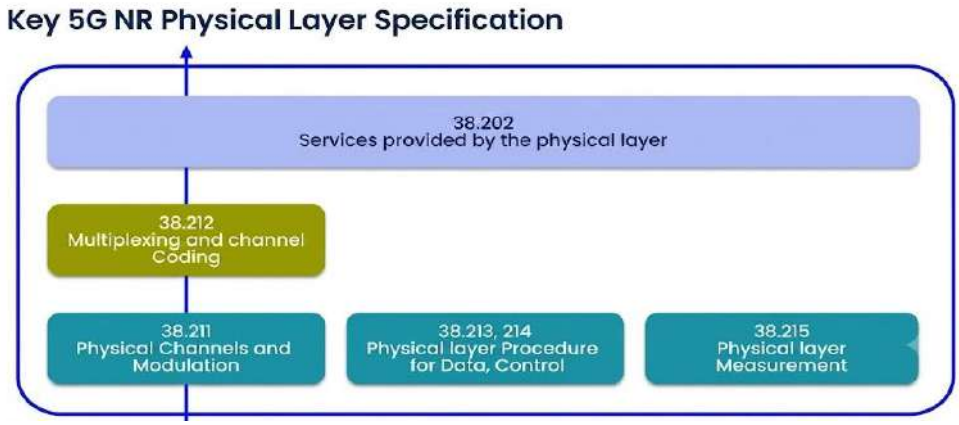

The Backbone of 5G NR Physical Layer

The 5G New Radio (NR) standard marks a significant evolution in wireless communication, enabling lightning-fast data speeds, extensive device connectivity, and remarkably low latency. At the heart of this innovation is the Physical Layer (PHY), which acts as the base for all the higher-layer functionalities.

The 3rd Generation Partnership Project (3GPP) has defined the physical layer to ensure data is transmitted and received efficiently over the air. They've laid out a series of technical specifications (TS) for Release 15 and beyond that detail how the 5G NR PHY works.

The diagram above highlights these essential documents — from TS 38.202 to TS 38.215 — each focusing on different aspects of the physical layer. Together, they cover everything from modulation techniques and coding to physical measurements and procedures.

Overview: 3GPP Specifications for 5G NR Physical Layer

3GPP Specification	Title / Function	Purpose
TS 38.202	Services Provided by the Physical Layer	Defines physical layer (PHY) services and interactions with higher layers.
TS 38.211	Physical Channels and Modulation	Describes modulation schemes, frame structure, and physical channel mapping.
TS 38.212	Multiplexing and Channel Coding	Specifies multiplexing techniques and error correction coding methods.
TS 38.213 / TS 38.214	Physical Layer Procedures for Control and Data	Defines scheduling procedures, HARQ, link adaptation, and other physical layer control mechanisms.
TS 38.215	Physical Layer Measurements	Specifies measurement methods for RSRP, SINR, channel quality, and related performance metrics.

These documents create the technical foundation for the 5G NR radio interface, promoting interoperability, efficiency, and reliability among equipment manufacturers and network providers around the globe.

3GPP TS 38.202 – Services Provided by the Physical Layer

This specification outlines the functional services that the physical layer offers to higher layers, especially the Medium Access Control (MAC) and Radio Resource Control (RRC) layers.

Key Responsibilities:

- Defines the interface between PHY and MAC.
- Manages transport channels (like DL-SCH, UL-SCH, PUSCH, PDSCH).
- Oversees control channels such as PDCCH, PUCCH, and PHICH.
- Ensures synchronization signals (SS/PBCH blocks) for initial access.

Basically, TS 38.202 lays out what the PHY layer does, while the remaining specifications explain how it gets those jobs done.

Purpose in the 5G Stack

It guarantees that all physical layer functions align with the logical and transport channel needs of higher layers, ensuring smooth integration between protocol layers.

3GPP TS 38.211 – Physical Channels and Modulation

TS 38.211 specifies how 5G NR uses Orthogonal Frequency Division Multiplexing (OFDM) to maximize spectral efficiency and flexibility. It outlines the structure and modulation methods of the physical channels.

Main Concepts:

Subcarrier Spacing (SCS): 15, 30, 60, 120, and 240 kHz numerologies.

Slot and Frame Structure: 10 ms frames split into subframes and slots.

Waveforms: * Downlink: CP-OFDM (Cyclic Prefix OFDM) * Uplink: CP-OFDM or DFT-s-OFDM

Modulation Schemes: QPSK, 16QAM, 64QAM, and 256QAM.

Defined Physical Channels:

Channel | Function

PDSCH | Downlink shared channel for user data

PUSCH | Uplink shared channel for user data

PDCCH | Downlink control channel for scheduling

PUCCH | Uplink control channel for feedback

PBCH | Broadcast channel carrying system info

This specification allows flexible bandwidth configuration, enabling 5G NR to operate from sub-1 GHz (FR1) to mmWave (FR2) deployments.

3GPP TS 38.212 – Multiplexing and Channel Coding

Once data is allocated to physical channels, it must be safeguarded against transmission errors. TS 38.212 outlines the coding, rate matching, and multiplexing methods to maintain robustness and reliability.

Core Functions:

Channel Coding: * LDPC (Low-Density Parity Check) for data channels (PDSCH/PUSCH) * Polar Codes for control channels (PDCCH, PUCCH)

CRC Attachment: Provides redundancy for error detection.

Rate Matching: Modifies code rates based on channel conditions.

Code Block Segmentation: Manages large transport blocks.

Why It Matters:

These coding techniques are tailored for 5G's high throughput and low latency needs. LDPC delivers excellent performance at high data rates, while Polar coding ensures efficient control signaling — both are crucial for 5G reliability.

3GPP TS 38.213 and 38.214 – Physical Layer Procedures

These two documents detail the procedures that control the dynamic features of the physical layer — how resources are allocated, how the link adjusts, and how retransmissions are handled.

38.213 – Physical Layer Procedures for Control

Focuses on procedures for:

- Scheduling requests (SR)
- Random access procedures
- Power control strategies
- Timing advance adjustments
- HARQ (Hybrid Automatic Repeat Request) feedback timing
- 38.214 – Physical Layer Procedures for Data

Focuses on:

- Link adaptation (CQI, PMI, RI reporting)
- HARQ retransmission methods
- MIMO precoding and layer mapping
- Resource allocation and time-domain structure

In Practice:

These procedures make the 5G physical layer adaptive and intelligent, reacting in real time to changes in the channel, user movement, and interference. They help ensure the network maintains optimal throughput and reliability across various radio environments.

3GPP TS 38.215 – Physical Layer Measurements

Measurements are essential for maintaining link quality and ensuring network efficiency. TS 38.215 outlines measurement models and metrics that user equipment (UE) and gNodeB rely on to make smart decisions.

Key Measurement Types:

- RSRP (Reference Signal Received Power)
- RSRQ (Reference Signal Received Quality)
- SINR (Signal-to-Interference-plus-Noise Ratio)
- Channel State Information (CSI)
- Timing and frequency accuracy

These metrics are used in higher-layer algorithms for mobility management, beamforming, handover, and link adaptation.

Significance

Accurate measurements are vital for features like beam management in FR2 and massive MIMO systems, where precision directly influences spectral efficiency.

How These Specifications Work Together

All these specifications are interconnected and complementary:

- 38.202 – Defines the services the PHY layer offers.
- 38.211 – Discusses signal structures and modulation.
- 38.212 – Manages error correction and data multiplexing.
- 38.213/214 – Describe operational procedures for data and control.
- 38.215 – Supplies measurement mechanisms for feedback and optimization.

Together, they create the complete physical layer stack, linking theoretical design with real-world application.

Importance of 5G NR PHY Layer for Future Networks

The 5G NR physical layer isn't static; it evolves with each 3GPP release.

Its adaptable design supports:

- Dynamic spectrum sharing (DSS)
- Massive MIMO and beamforming
- Carrier aggregation across FR1 and FR2
- URLLC and eMBB working together

This adaptability allows 5G to easily adjust to new frequency bands, use cases, and device types — an essential base for 6G advancement.

References

1. 3GPP. (2021). *TS 38.213–Physical layer procedures*.
2. Dreifuerst, R. M., & Heath, R. W. (2023). Initial access codebook design and CSI type-II feedback for sub-6GHz 5G NR. *Submission to IEEE Transactions on Wireless Communications*.
3. Giordani, M., et al. (2019). A tutorial on beam management for 3GPP NR at mmWave frequencies. *IEEE Communications Surveys & Tutorials, 21*(1), 173–196.
4. Samsung. (2020). *Massive MIMO for New Radio*. https://www.samsung.com/global/business/networks/insights/white-papers/1208-massive-mimo-for-new-radio/
5. Thelander, M., & Olbrich, E. (2022). In the spirit of giving: Sample results and analysis of a commercial implementation of 8-layer 5G MU-MIMO. *Signals Flash*. https://signalsresearch.com/issue/signals-flash-2/
6. Becirovic, E., Bjornson, E., & Larsson, E. G. (2022, May). Combining reciprocity and CSI feedback in MIMO systems. *IEEE Transactions on Wireless Communications*.

7. ZTE Corporation. (2016). *R1-166222 Meeting 86—Evaluation and analysis on coverage issue of initial access for NR above 6 GHz*.
8. Sim, G. H., et al. (2018). An online context-aware machine learning algorithm for 5G mmWave vehicular communications. *IEEE/ACM Transactions on Networking, 26*(6), 2487–2500.
9. Wang, J., et al. (2009). Beam codebook based beamforming protocol for multi-Gbps millimeter-wave WPAN systems. *IEEE Journal on Selected Areas in Communications, 27*(8), 1390–1399.
10. Choi, J., et al. (2016). Millimeter-wave vehicular communication to support massive automotive sensing. *IEEE Communications Magazine, 54*(12), 160–167.
11. Morozov, G., Davydov, A., & Sergeev, V. (2016, July). Enhanced CSI feedback for FD-MIMO with beamformed CSI-RS in LTE-A Pro systems. In *IEEE Vehicular Technology Conference*.
12. Heath, R. W., Jr., & Lozano, A. (2018). *Foundations of MIMO communication*. Cambridge University Press.
13. Rebato, M., Polese, M., & Zorzi, M. (2018). Multi-sector and multipanel performance in 5G mmWave cellular networks. In *IEEE GLOBECOM* (pp. 1–6).
14. Hussain, M., & Michelusi, N. (2022). Learning and adaptation for millimeter-wave beam tracking and training: A dual timescale variational framework. *IEEE Journal on Selected Areas in Communications, 40*(1), 37–53.

RECENT ADVANCES IN IMIDAZO-THIAZOLE SCAFFOLDS AS ANTICANCER AGENTS

Pravin S. Bhale
Department of Chemistry, Yeshwantrao Chavan Mahavidyalaya,
Tuljapur, Dist-Dharashiv-413601, Maharashtra, India
Corresponding author E-mail: bhale.ps@gmail.com

Abstract
This book chapter provides a concise overview of imidazo-thiazole-based scaffolds as promising anticancer agents, emphasizing their structural diversity, synthetic development, and biological significance. Owing to their fused heterocyclic framework and electron-rich nature, imidazo-thiazole derivatives have emerged as versatile pharmacophores capable of modulating multiple cancer-related molecular targets while addressing key limitations of conventional chemotherapy, including drug resistance, poor selectivity, and systemic toxicity. The chapter also summarizes recent advances in their rational design, synthetic methodologies, and structure–activity relationship (SAR) studies, highlighting the impact of structural modifications on anticancer potency and target selectivity. In addition, key mechanistic pathways such as kinase inhibition, apoptosis induction, and cell-cycle arrest are discussed alongside computational approaches including molecular docking and pharmacokinetic evaluation. Overall, imidazo-thiazole scaffolds are identified as highly promising lead structures for future anticancer drug development.

Keywords: Imidazo-Thiazole, Anticancer Activity, Structure-Activity Relationships.

Introduction

Heterocyclic compounds represent one of the most significant classes of organic molecules in medicinal chemistry because of their remarkable pharmacological properties and broad applicability in diverse scientific disciplines [1]. Nitrogen- and sulfur-containing heterocycles, in particular, have received extensive attention due to their structural diversity, synthetic versatility, and wide spectrum of biological activities. These scaffolds are not only important in pharmaceutical sciences but also find applications in agriculture, material science, supramolecular chemistry, and industrial technologies [2-3]. Over the past few decades, continuous advancements in synthetic methodologies and drug discovery approaches have accelerated the development of heterocyclic systems as promising therapeutic agents. Among these, fused bicyclic heterocycles have emerged as privileged frameworks owing to their enhanced molecular rigidity, improved receptor binding affinity, and favorable pharmacokinetic properties [4-5].

Among sulfur- and nitrogen-containing fused heterocycles, imidazo-thiazole scaffolds have gained considerable attention as important pharmacophores in modern medicinal chemistry. The imidazo-thiazole nucleus consists of the fusion of an imidazole ring with a thiazole moiety, generating a planar and electron-rich bicyclic system capable of interacting effectively with various biological targets [6-7]. The presence of nitrogen and sulfur heteroatoms facilitates hydrogen bonding, π–π stacking, hydrophobic interactions, and metal coordination, thereby enhancing binding affinity toward enzymes, receptors, and nucleic acids. In addition, the imidazo-thiazole framework possesses favorable physicochemical properties such as moderate lipophilicity, electronic tunability, and structural stability, making it highly suitable for the design of biologically active molecules. These characteristics have encouraged researchers to explore imidazo-thiazole derivatives for a wide range of therapeutic applications including antimicrobial, anti-inflammatory, antiviral, antitubercular, antioxidant, and particularly anticancer activities [8-9].

Cancer remains one of the leading causes of mortality worldwide and continues to pose a major challenge to global healthcare systems. Despite substantial progress in chemotherapy, targeted therapy, and immunotherapy, the development of drug resistance, severe side effects, poor selectivity, and tumor recurrence still limit the effectiveness of existing anticancer agents [10]. Consequently, there is an urgent need to identify novel molecular scaffolds capable of selectively targeting cancer cells with improved safety profiles and enhanced therapeutic efficacy. Heterocyclic compounds have played a pivotal role in anticancer drug discovery, and several clinically approved anticancer drugs contain nitrogen- and sulfur-based heterocyclic motifs. In this context, imidazo-thiazole derivatives have emerged as promising candidates because of their ability to interfere with multiple cellular pathways involved in cancer progression, including inhibition of kinases, DNA intercalation, induction of apoptosis, cell cycle arrest, and suppression of angiogenesis [11-13].

Recent studies have demonstrated that structural modification of the imidazo-thiazole scaffold significantly influences anticancer activity and target selectivity. The framework allows substitution at multiple positions across both fused rings, enabling precise modulation of electronic properties, steric effects, hydrophobicity, and pharmacokinetic behavior. Such flexibility has facilitated the rational design of structurally diverse imidazo-thiazole derivatives with enhanced cytotoxic activity against various cancer cell lines [14-15]. Moreover, advances in synthetic chemistry have provided efficient routes for the rapid construction of these scaffolds through methodologies such as condensation reactions, intramolecular cyclizations, multicomponent reactions, microwave-assisted synthesis, and transition-metal-catalyzed cross-coupling reactions. Late-stage functionalization and hybridization strategies have further

expanded the chemical diversity of imidazo-thiazole analogues, enabling the development of multifunctional anticancer agents with improved biological profiles [16-17].

The growing interest in imidazo-thiazole-based anticancer agents has resulted in extensive research focused on their synthesis, biological evaluation, molecular mechanisms, and structure–activity relationship (SAR) studies. Numerous derivatives have shown potent antiproliferative activity against breast, lung, colon, prostate, cervical, and leukemia cancer cell lines, highlighting the therapeutic significance of this scaffold [14,18]. Furthermore, computational approaches including molecular docking, quantitative structure–activity relationship (QSAR) analysis, and in silico pharmacokinetic studies have accelerated the identification of promising lead molecules. In view of these developments, the present book chapter aims to provide a comprehensive overview of recent advances in imidazo-thiazole scaffolds as anticancer agents, emphasizing synthetic strategies, biological activities, molecular targets, SAR investigations, and future perspectives in anticancer drug discovery [19].

Naturally Available Imidazo-Thiazole Scaffolds as Anticancer Agents

Naturally occurring heterocyclic compounds containing imidazole- and thiazole-based frameworks have attracted significant attention in medicinal chemistry because of their remarkable structural diversity and potent biological activities, particularly their anticancer potential. Marine organisms, terrestrial microorganisms, fungi, ascidians, and sponges represent important natural sources of imidazole- and thiazole-containing alkaloids and peptides exhibiting pronounced cytotoxic properties. These naturally derived heterocycles possess unique electronic and conformational features that enable strong interactions with various biological macromolecules, including DNA, enzymes, and cellular receptors. Several naturally occurring thiazole-containing metabolites have demonstrated potent antiproliferative activity through mechanisms such as DNA intercalation, apoptosis induction, inhibition of tubulin polymerization, and suppression of kinase-mediated signaling pathways involved in tumor progression. The broad spectrum of biological activities exhibited by these natural scaffolds has established them as valuable templates for the discovery and development of novel anticancer agents [20].

The therapeutic significance of naturally occurring imidazo-thiazole-related scaffolds has inspired extensive medicinal chemistry efforts focused on the synthesis and structural optimization of novel analogues with improved anticancer efficacy and selectivity. Natural products containing fused imidazole and thiazole pharmacophores have served as lead compounds for the development of synthetic derivatives capable of targeting multiple cancer-related pathways, including kinase inhibition, cell cycle arrest, mitochondrial dysfunction, and angiogenesis suppression. Furthermore, advances in synthetic chemistry and computational drug design have enabled the rational modification of these naturally inspired scaffolds to enhance

pharmacokinetic and pharmacodynamic properties. Consequently, naturally occurring imidazo-thiazole and related thiazole-fused heterocycles continue to play an important role in modern anticancer drug discovery and remain promising molecular frameworks for the development of next-generation anticancer therapeutics [21].

Marketed Anticancer Drugs Containing Imidazo-Thiazole and Related Thiazole Scaffolds

The clinical success of heterocyclic anticancer agents containing thiazole and fused thiazole-based scaffolds has demonstrated the therapeutic significance of these privileged structures in oncology. Although only a limited number of clinically approved drugs possess the exact imidazo-thiazole nucleus, several marketed anticancer agents incorporate structurally related thiazole-containing heterocycles that contribute significantly to their biological activity. These scaffolds provide favorable electronic properties, hydrogen-bonding capability, and optimal molecular geometry for interaction with diverse cancer-related biological targets, particularly kinases, DNA, and microtubules. Consequently, thiazole-based pharmacophores have become important structural motifs in modern anticancer drug discovery [22].

Among the clinically approved agents, Dasatinib is a prominent example of a thiazole-containing anticancer drug widely used for the treatment of chronic myeloid leukemia (CML) and Philadelphia chromosome-positive acute lymphoblastic leukemia (ALL). Dasatinib acts as a potent multi-targeted tyrosine kinase inhibitor against BCR-ABL and SRC family kinases, thereby suppressing cancer cell proliferation and survival. Similarly, Dabrafenib, a thiazole-containing BRAF kinase inhibitor approved for metastatic melanoma harboring the BRAF^V600E mutation, exerts its therapeutic effect by selectively inhibiting aberrant MAPK signaling pathways involved in tumor growth. These examples highlight the importance of thiazole-based scaffolds in kinase-targeted anticancer therapy (Fig. 1) [23].

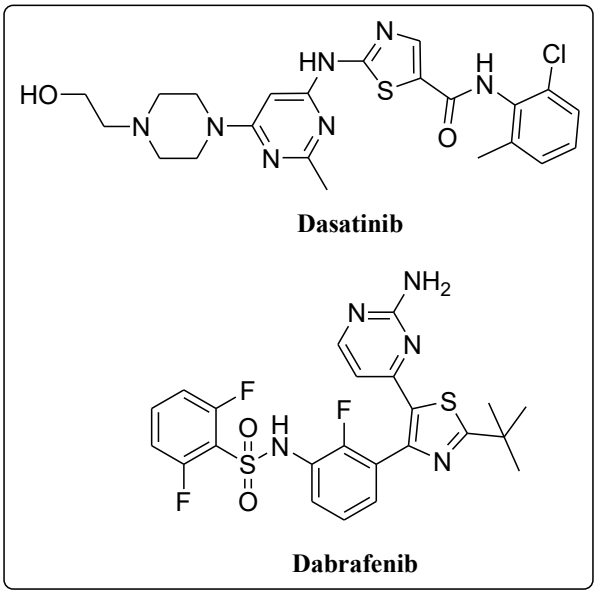

Figure 1: Clinically approved agents of a thiazole-containing anticancer drug

Other clinically significant thiazole-containing anticancer agents include Ixabepilone and Bleomycin. Ixabepilone, a semisynthetic analogue of epothilone B containing a thiazole moiety, functions as a microtubule-stabilizing agent and is approved for the treatment of metastatic or drug-resistant breast cancer. It induces apoptosis by disrupting mitotic spindle formation and inhibiting cell division [24].

Anti-Cancer Potential of Imidazo-Thiazole Derivatives

Shareef *et al.* synthesized a series of aryl hydrazone derivatives containing the imidazo-thiazole scaffold and systematically evaluated their antiproliferative potential against a panel of cancer cell lines. Among the synthesized compounds, derivatives **1-3** demonstrated significant cytotoxic activity, exhibiting IC_{50} values in the range of approximately 1.12–5.20 μM (Fig. 2). Notably, compounds 3 and 2 displayed pronounced antiproliferative potency against the MDA-MB-231 breast cancer cell line, with IC_{50} values of 1.12 μM and 1.65 μM, respectively. Cell cycle analysis further revealed that treatment with compounds 2 and 3 resulted in a substantial increase in the population of cells arrested at the G0/G1 phase compared with untreated control cells, indicating their potential to inhibit cellular proliferation through cell cycle modulation.

Further mechanistic investigations, including Annexin V–FITC apoptosis assay, DAPI staining, DCFH-DA assay, and JC-1 mitochondrial membrane potential analysis, collectively demonstrated that these imidazo-thiazole derivatives induce apoptotic cell death in breast cancer cells. Structure–activity relationship (SAR) analysis indicated that the enhanced anticancer activity of compound **3**, identified as the most potent analogue in the series, could be attributed to the presence of an electron-withdrawing 4-fluoro substituent at the R position along with an electron-donating 3,4,5-trimethoxy group at the R′ position. In comparison, compound **2**, containing electron-donating methoxy substituents at both positions (4-methoxy at R and 3,4,5-trimethoxy at R′), also exhibited remarkable cytotoxic potency. These findings suggest that both electron-withdrawing and electron-donating substituents significantly influence the antiproliferative activity of imidazo-thiazole-based aryl hydrazone derivatives and play a crucial role in optimizing their anticancer efficacy [25].

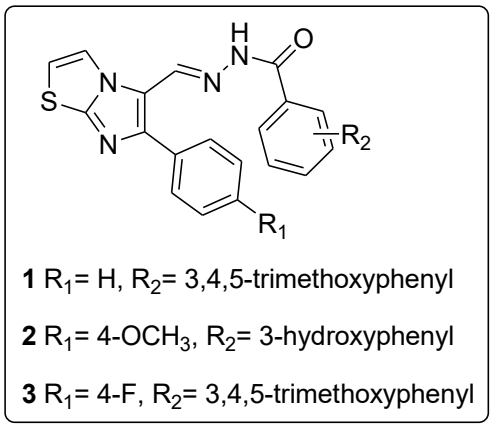

Figure 2: **Imidazo-Thiazole derivatives 1-3**

Rashdan *et al.* reported the synthesis of a series of thiadiazole derivatives incorporating the imidazo-thiazole scaffold using methyl-2-(1-(3-methyl-6-(p-tolyl)imidazo-thiazol-2-yl)ethylidene)hydrazine-1-carbodithioate as a key synthetic intermediate. The developed synthetic strategy efficiently afforded structurally diverse thiadiazole analogues in good to excellent yields, highlighting the synthetic utility and versatility of the intermediate in heterocyclic drug development. Molecular docking and binding affinity studies demonstrated that the synthesized compounds exhibited stronger interactions with the glypican-3 (GPC-3) target protein compared with the reference ligand. In addition, detailed docking analysis revealed the presence of significant noncovalent interactions within the GPC-3 binding cavity, indicating favorable ligand–receptor binding characteristics and suggesting their potential application as therapeutic agents against hepatocellular carcinoma.

The synthesized imidazo-thiazole-based thiadiazole derivatives were further evaluated for their antiproliferative activity against the HepG2 hepatocellular carcinoma cell line. Among the tested compounds, derivative 4 displayed the most promising cytotoxic profile, with IC_{50} values of 12.73 ± 1.36 µg/mL against HepG2 cancer cells and 8.34 ± 1.81 µg/mL against normal cells (Fig. 3). For comparison, the standard anticancer drug doxorubicin exhibited IC_{50} values of 3.56 ± 0.46 µg/mL and 3.21 ± 0.32 µg/mL against HepG2 and normal cell lines, respectively [26]. Although compound 4 demonstrated lower potency than doxorubicin, the results indicate that imidazo-thiazole-containing thiadiazole derivatives possess noteworthy antiproliferative activity and represent promising lead candidates for further optimization in the development of anticancer agents targeting hepatocellular carcinoma.

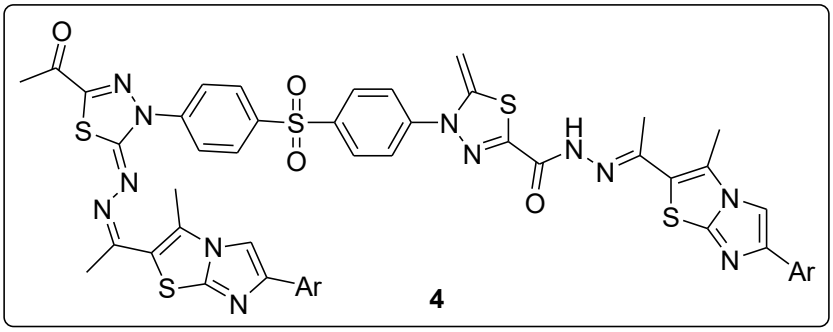

Figure 3: **Imidazo-Thiazole derivative 4**

A series of bromine- and sulfonamide-substituted benzothiazole derivatives was synthesized by Majalakere *et al.,* and the structures of the obtained compounds were confirmed using comprehensive spectroscopic techniques. The synthesized compounds were subsequently evaluated for their in vitro antiproliferative activity against HepG2 hepatocellular carcinoma cells as well as two parental melanoma cell lines. Among them, compounds 5 and 6, each featuring a sulfonamide group with para-substituted phenyl rings (fluoro-substituted in 5 and methyl-substituted in 6), exhibited potent cytotoxicity against HepG2 cells, with IC_{50} values of 0.097 µM and 0.114 µM, respectively. Furthermore, at a concentration corresponding to half of

their IC_{50} values (0.054 μM), both compounds demonstrated a pronounced radiosensitizing effect under hypoxic conditions in HepG2 cells, as confirmed by comet assay analysis, highlighting their potential as dual-function anticancer agents (Fig. 4).

In contrast, compound **7**, a bromine-containing derivative also bearing a fluorine substituent, showed superior potency against both melanoma cell lines, with IC_{50} values of 0.046 μM and 0.052 μM, respectively. When combined with a 2 Gy dose of γ-radiation, **7** further reduced melanoma cell viability to approximately 30–40%, indicating enhanced therapeutic efficacy under combined treatment conditions. The observed biological activities may be rationalized by structure–activity relationships, where fluorine incorporation is known to increase lipophilicity and thereby enhance cellular permeability and target interactions. Similarly, methyl substitution can significantly modulate ADME properties, often leading to improved biological activity, further supporting the enhanced potency observed for these derivatives [27].

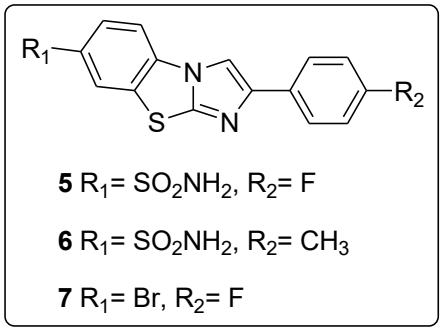

Figure 4: **Imidazo-Thiazole derivatives 5-7**

The novel imidazo-thiazole derivatives were synthesized by Basoglu *et al.* using straightforward and efficient synthetic protocols. Their *in vitro* anticancer activity was assessed with a focus on inhibition of focal adhesion kinase (FAK). A significant proportion of the synthesized analogues, particularly those incorporating a 3-oxo-1-thia-4-azaspiro[4.5]decane scaffold, exhibited notable anticancer potential. Based on the biological evaluation, compound 8 demonstrated the most potent FAK inhibitory activity against the C6 cancer cell line, with 72.55% ± 3.63% inhibition. This was followed by compounds 9 (68.71% ± 0.73%), 10 (47.78% ± 3.93%), and 11 (46.64% ± 8.59%), indicating a clear variation in activity across the series (Fig. 5).

The corresponding IC_{50} values further supported these findings, with 8, 9, 10, and 11 exhibiting values of 16.33 ± 1.52 μM, 28.33 ± 2.88 μM, 10.83 ± 1.25 μM, and 19.66 ± 3.21 μM, respectively. Structurally, these bioactive molecules contain methyl substitution at the eighth position and propyl and phenyl substituents at the second position of the spirothiazolidinone ring, which may contribute to their observed activity profiles. In addition, compound 12 emerged as a promising anticancer candidate due to its high selectivity index and ability to induce apoptosis; however, its antitumor activity does not appear to be mediated through FAK inhibition, suggesting a distinct mechanism of action [28].

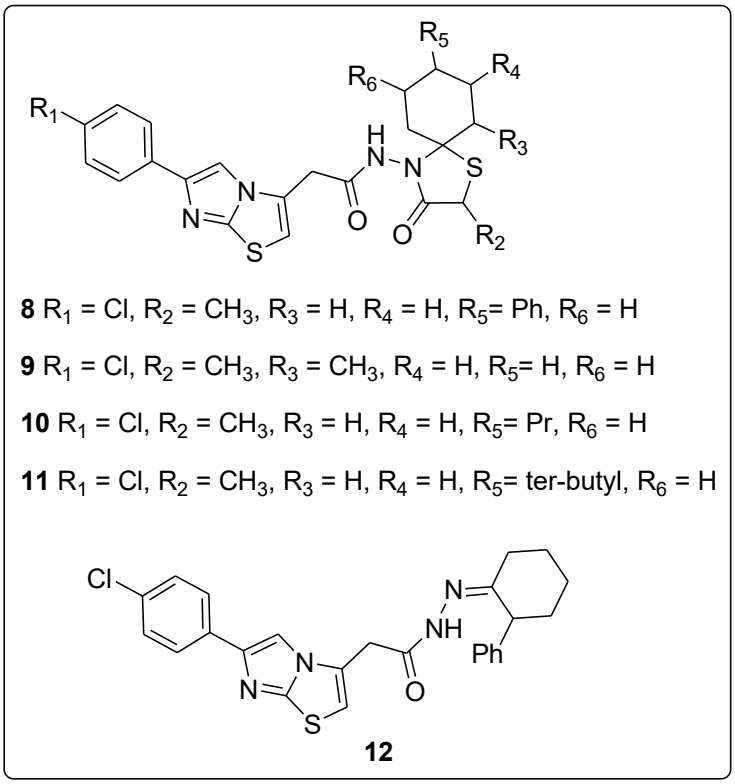

Figure 5: Imidazo-Thiazole derivatives 8-12

Alapati *et al.* designed and synthesized a novel library of isoxazole–imidazo-thiazole amide derivatives, which were subsequently evaluated for their in vitro anticancer activity using the MTT assay against four human tumor cell lines, namely MCF-7, A549, Colo-205, and A2780. The entire series exhibited a broad range of cytotoxicity, with IC_{50} values spanning from 0.17 ± 0.068 μM to 10.6 ± 6.17 μM. In comparison, the positive control (etoposide) showed IC_{50} values in the range of 0.17 ± 0.034 μM to 3.34 ± 0.152 μM across the tested cell lines, indicating that several of the newly synthesized compounds demonstrated comparable or improved antiproliferative activity.

Among the synthesized analogues, five compounds **(**13-17**)** were found to outperform etoposide. Notably, compound 13 exhibited the most potent and broad-spectrum cytotoxic activity across all four cancer cell lines, with IC_{50} values of 0.17 ± 0.068 μM against MCF-7, 0.44 ± 0.039 μM against A549, 1.06 ± 0.56 μM against Colo-205, and 1.12 ± 0.84 μM against A2780, respectively. These findings identify compound 13 as a promising lead structure for further development, owing to its strong and consistent antiproliferative effects across multiple tumor models (Fig. 6) [29].

A novel series of chalcone derivatives incorporating the imidazo-thiazole scaffold was synthesized by Dadou *et al.,* and the compounds were subsequently evaluated for their *in vitro* cytotoxic activity against a panel of human cancer cell lines, including HT-29, A-549, and MCF-7, along with the non-tumorigenic 3T3-L1 cell line. Flow cytometric analysis revealed that compound 18 induces apoptosis in MCF-7 cells predominantly via the intrinsic pathway, as

evidenced by the loss of mitochondrial membrane potential and subsequent activation of the caspase cascade (Fig. 7). These results indicate that the anticancer activity of compound 18 is primarily mediated through mitochondria-dependent apoptotic signaling mechanisms.

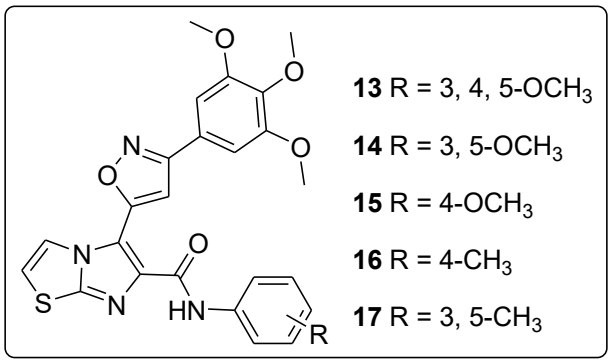

Figure 6: Imidazo-Thiazole derivatives 13-17

Further evaluation using XTT viability assays identified compound 18 as the most potent derivative within the series, demonstrating the lowest IC_{50} values across all tested cancer cell lines and exhibiting improved selectivity toward malignant cells relative to normal cells. In addition, molecular docking studies suggested that compound 18 may interact with both caspase-3 and a DNA dodecamer, implying a potential dual-targeting mode of action. These in silico findings support the hypothesis that simultaneous engagement of apoptotic proteins and DNA could contribute to the observed inhibition of cancer cell proliferation and metastatic progression [30].

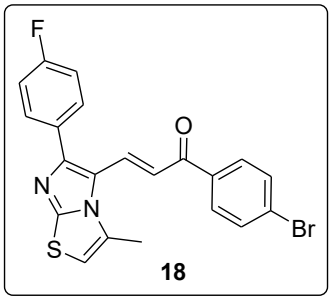

Figure 7: Imidazo-Thiazole derivative 18

A series of novel benzo[d]imidazo-thiazole derivatives was synthesized by Lujing *et al.* employing ethyl acetoacetate and N-bromosuccinimide as key reagents in the synthetic pathway. The resulting analogues were systematically evaluated for their *in vitro* antiproliferative activity against human lung cancer cell lines. Among the synthesized compounds, compound 19 exhibited the most pronounced cytotoxic effect, demonstrating the strongest growth-inhibitory activity within the series (Fig. 8). These findings underscore the successful development of biologically relevant benzo[d]imidazo-thiazole scaffolds with promising anticancer potential.

Quantitative analysis revealed that compound 19 displayed IC_{50} values of 17.63 μM against H2228 cells and 26.32 μM against A549 cells, indicating relatively greater potency toward the H2228 lung cancer cell line. The observed variation in activity suggests a degree of cell line

selectivity, with enhanced efficacy against H2228 cells compared with A549 cells. Overall, these results support compound 19 as a promising lead candidate for further structural optimization and development as a potential therapeutic agent for lung cancer [31].

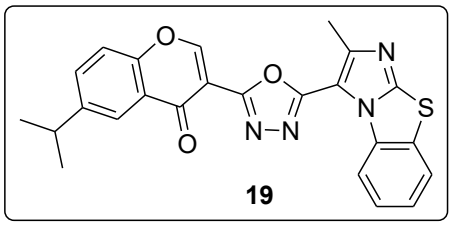

Figure 8: Imidazo-Thiazole derivative 19

Two novel imidazothiazole–chalcone hybrid compounds, designated 20 and 21, were synthesized by Dadou *et al.,* fully characterized, and evaluated for their in vitro cytotoxic activity against A-549, MCF-7, HT-29, and non-tumorigenic 3T3-L1 cell lines (Fig. 9). Both compounds demonstrated notable antiproliferative activity, with a marked degree of potency and selectivity toward MCF-7 breast cancer cells compared with the other tested cancer cell lines. Overall, the two analogues exhibited comparable cytotoxic profiles in MCF-7 cells, indicating a consistent structure–activity relationship within this scaffold. Among them, compound 20 showed the strongest cytotoxic response in MCF-7 cells, with an IC_{50} value of 54.46 mM, while displaying its weakest activity against HT-29 cells (IC_{50} = 17.05 mM). Similarly, compound 21 exhibited its highest potency against MCF-7 cells (IC_{50} = 16.81 mM) and its lowest activity against HT-29 cells, where the IC_{50} value reached 65.66 mM.

Mechanistic investigations in MCF-7 cells using flow cytometry indicated that both 20 and 21 induce apoptosis predominantly via the intrinsic (mitochondrial) pathway, as evidenced by disruption of mitochondrial membrane potential and subsequent activation of caspase enzymes. In silico molecular docking studies further demonstrated favorable binding interactions of both compounds within the active site of caspase-3, as well as with a DNA dodecamer, suggesting potential dual-target engagement. Additionally, drug-likeness and pharmacokinetic properties were evaluated using the Schrödinger 2021–2 QikProp module, providing supportive evidence for their acceptable ADME profiles. Collectively, these findings suggest that imidazothiazole–chalcone hybrids 20 and 21 represent promising scaffolds for further optimization as anticancer agents [32].

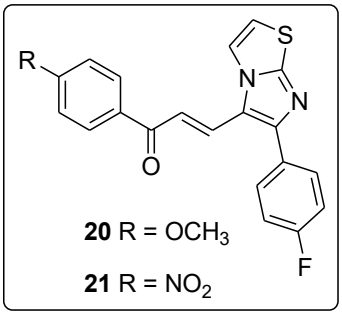

Figure 9: Imidazo-Thiazole derivatives 20 and 21

Deshmukh *et al.* demonstrated the use of PEG-400 as an efficient and environmentally benign green solvent for the synthesis of benzo[d]imidazo-thiazole derivatives, providing a sustainable alternative to conventional organic reaction media. Owing to its unique protic–aprotic nature, PEG-400 enabled the formation of the desired products in excellent yields of up to 92% under mild reaction conditions, while also reducing reaction time and minimizing environmental impact. The developed protocol exhibited broad functional group tolerance, accommodating both electron-donating and electron-withdrawing substituents on phenacyl bromide precursors. In particular, halogen-substituted substrates consistently afforded high yields, underscoring the robustness and general applicability of the synthetic approach across diverse chemical frameworks and highlighting the versatility of benzo[d]imidazo[2,1-b]thiazole scaffolds for medicinal chemistry applications.

Biological evaluation of the synthesized compounds against MCF-7 breast cancer cells revealed that anticancer activity was significantly influenced by the electronic nature of the substituents. Among the tested derivatives, compound 22 exhibited the highest cytotoxic potency with an IC_{50} value of 10.78 ± 0.892 μM, whereas compounds bearing two electron-withdrawing groups showed considerably reduced activity, with IC_{50} values reaching 29.7 ± 2.73 μM (Fig. 10). These findings suggest that electron-donating substituents may enhance anticancer efficacy, potentially by improving interactions with the biological target. Supporting this observation, molecular docking studies identified compound 22 as having the most favorable binding affinity toward epidermal growth factor receptor (EGFR) tyrosine kinase, with a docking score of −6.7 $kcal \cdot mol^{-1}$, which is consistent with its superior cytotoxic profile [33].

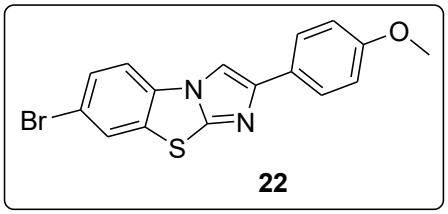

Figure 10: Imidazo-Thiazole derivative 22

Ahmadi *et al.* synthesized a novel series of diaryl benzo[d]imidazo[2,1-b]thiazole derivatives bearing an aminoethoxy side chain and evaluated their *in vitro* cytotoxic activity against the human breast cancer cell line MCF-7. The compounds were systematically assessed using the MTT assay, and all derivatives exhibited significant inhibitory effects on MCF-7 cell proliferation when compared with the reference drug tamoxifen, indicating the potential of this scaffold as a biologically active anticancer framework.

Among the synthesized analogues, compounds 23 and 24 demonstrated the most pronounced antiproliferative activity, with inhibition rates of approximately 73% and 81%, respectively (Fig. 11). These findings highlight these two derivatives as the most promising candidates within the series, suggesting that structural features associated with the aminoethoxy-substituted diaryl

benzo[d]imidazo[2,1-b]thiazole core may play a crucial role in enhancing anticancer potency [34].

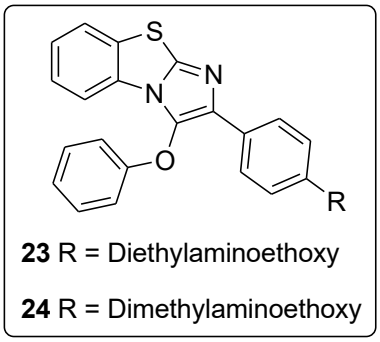

Figure 11: Imidazo-Thiazole derivatives 23 and 24

Three isatin–imidazo[2,1-b]thiazole hybrid derivatives 25-27, linked via a carbohydrazide spacer, were synthesized and evaluated for their anticancer potential using the MTT assay. All compounds demonstrated notable cytotoxic activity, indicating the biological relevance of the hybrid scaffold. Among them, compound 26 emerged as the most potent candidate and was selected for further mechanistic investigations to elucidate its mode of action in cancer cells. To clarify its effects on apoptotic signaling, compound 26 was subjected to gene expression analysis by PCR, focusing on key regulatory markers including Bax, Bcl-2, caspase-8, caspase-9, and cytochrome c, thereby providing insight into its influence on intrinsic and extrinsic apoptotic pathways. Further biological evaluation through cell-cycle and apoptosis assays revealed that 26 induces G2/M phase arrest and promotes apoptosis at levels exceeding those of the reference drug. In addition, molecular docking and ADME studies suggested that these compounds adopt a binding mode comparable to Sorafenib, involving interactions with key residues such as Lys868, Cys1045, Glu885, and Asp1046, thereby supporting their potential as kinase-targeting anticancer agents [35].

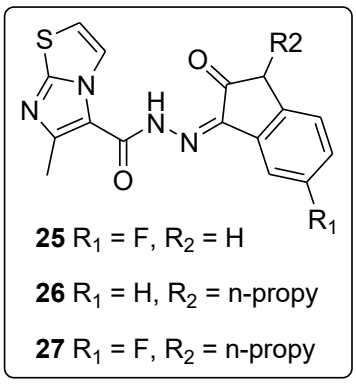

Figure 11: Imidazo-Thiazole derivatives 25-27

Mohammed *et al.* rationally designed, synthesized, and evaluated two series of imidazo-thiazole derivatives within a structure-based optimization program aimed at identifying potent epidermal growth factor receptor (EGFR) inhibitors. The synthesized compounds were screened for their antiproliferative activity against breast cancer cell lines, including MDA-MB-468, MCF-7, and

T-47D, where four analogues exhibited notable growth inhibitory effects. In MTT assays, compound 28 (IC_{50} = 1.46 μM against MCF-7) and compound 29 (IC_{50} = 2.27 μM against MDA-MB-468) showed strong inhibition of cancer cell proliferation, with activities comparable to the reference standard erlotinib (Fig. 12). Furthermore, biological profiling revealed that compounds 28, 29, and 30 possessed favorable tumor selectivity and a promising safety profile, suggesting reduced off-target toxicity.

Enzymatic assays further confirmed that compounds 28 and 29 effectively inhibited EGFR in vitro, with IC_{50} values of 0.099 μM and 0.086 μM, respectively, compared with erlotinib (IC_{50} = 0.046 μM). Cell-cycle analysis demonstrated that both compounds induce cell-cycle arrest, with 28 causing S-phase arrest in MCF-7 cells and 29 producing a similar effect in MDA-MB-468 cells. In addition, in vivo biodistribution studies using a 99mTc-labeled 29 complex in a sarcoma mouse model revealed selective tumor uptake, achieving a tumor-to-normal tissue ratio of approximately 7. Overall, compounds 28 and 29 emerged as promising lead candidates for further optimization as EGFR-targeted anticancer agents with improved selectivity and reduced off-target liabilities [36].

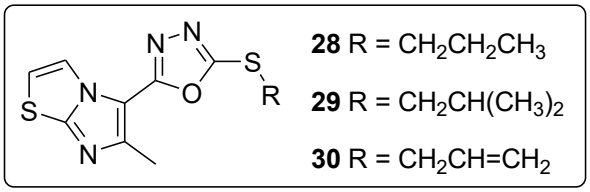

Figure 12: Imidazo-Thiazole derivatives 28-30

Kamboj *et al.* designed and synthesized a novel series of imidazothiazole derivatives incorporating a thiazolidinone fragment through a multistep, reagent-driven synthetic strategy. The resulting compounds were evaluated for their inhibitory activity against epidermal growth factor receptor (EGFR) kinase as well as their in vitro anticancer efficacy. All synthesized derivatives were screened for cytotoxicity against human cancer cell lines A549, MCF-7, and HCT116, along with the normal HEK293 cell line, revealing a range of activities from moderate to potent. Among them, compound 31 emerged as a broad-spectrum antineoplastic candidate, demonstrating strong cytotoxicity with IC_{50} values of 10.74 ± 0.60 μM against A549 cells and 18.73 ± 0.88 μM against MCF-7 cells (Fig. 13). Importantly, compound 31 exhibited comparatively lower toxicity toward HEK293 cells, with an IC_{50} value of 96.38 ± 1.79 μM, indicating a more favorable safety profile than the reference drug erlotinib.

Enzymatic assays further confirmed that compound 31 inhibits EGFR activity with an IC_{50} value of 18.35 ± 1.25 μM, compared with erlotinib (IC_{50} = 6.12 ± 0.92 μM). Mechanistic studies supported its pro-apoptotic potential, as apoptosis induction in A549 cells was validated through DAPI and acridine orange/ethidium bromide (AO/EB) dual staining assays. In addition, safety evaluations indicated that compounds 31 and 32 did not induce notable cardiotoxic or hepatotoxic effects, as evidenced by preserved cellular morphology in cardiomyocytes and

hepatocytes. Structure–activity relationship analysis suggested that electron-withdrawing substituents at the para position of the N-phenyl ring linked to the thiazolidinone moiety significantly enhance anticancer activity. Complementary in silico studies, including molecular docking and molecular dynamics simulations using the EGFR crystal structure (PDB ID: 1M17), demonstrated that compound 20b binds effectively within the active site, forming a key hydrogen bond with Met769, a residue known to be critical for EGFR inhibition [37].

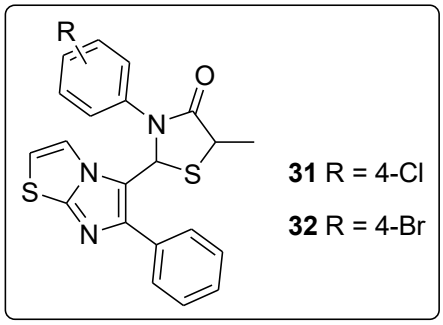

Figure 13: Imidazo-Thiazole derivatives 31-32

Conclusion

Imidazo-thiazole-based scaffolds represent a highly promising class of privileged heterocyclic systems in anticancer drug discovery, exhibiting broad-spectrum activity against diverse cancer types, including breast, lung, colon, hepatocellular carcinoma, and leukemia. Their fused N,S-heterocyclic framework and adaptable substitution patterns enable effective interactions with multiple molecular targets such as EGFR, FAK, caspases, DNA, and key signaling proteins, leading to anticancer effects primarily through apoptosis induction, cell-cycle arrest, and inhibition of oncogenic pathways.

Recent advances in synthetic strategies, including multicomponent reactions, microwave-assisted synthesis, and green chemistry approaches, have significantly enhanced the structural diversity of these compounds. Complementary SAR and computational studies have further facilitated lead optimization by correlating structural features with biological activity and pharmacokinetic properties. Despite notable progress, challenges related to selectivity, toxicity, and in vivo efficacy persist. Overall, imidazo-thiazole scaffolds remain valuable templates for the development of next-generation targeted anticancer agents.

References

1. Wermuth, C. G. (2015). *The practice of medicinal chemistry* (4th ed.). Academic Press.
2. Delost, M. D., Smith, D. T., Anderson, B. J., & Njardarson, J. T. (2018). From oxiranes to oligomers: Architectures of U.S. FDA approved pharmaceuticals containing oxygen heterocycles. *Journal of Medicinal Chemistry, 61*(24), 10996–11020.
3. Vitaku, E., Smith, D. T., & Njardarson, J. T. (2014). Analysis of the structural diversity, substitution patterns, and frequency of nitrogen heterocycles among U.S. FDA approved pharmaceuticals. *Journal of Medicinal Chemistry, 57*(24), 10257–10274.

4. Taylor, R. D., MacCoss, M., & Lawson, A. D. (2014). Rings in drugs. *Journal of Medicinal Chemistry, 57*(14), 5845–5859.
5. Joule, J. A., & Mills, K. (2010). *Heterocyclic chemistry* (5th ed.). Wiley.
6. Kumar, S., & Narasimhan, B. (2018). Therapeutic potential of heterocyclic imidazole derivatives: A review. *European Journal of Medicinal Chemistry, 145*, 248–266.
7. Amrutkar, V. S., Khator, R., & Monga, V. (2025). Recent progress in the synthetic and medicinal perspective of imidazo[2,1-b]thiazole derivatives. *Future Medicinal Chemistry, 17*(17), 2163–2177.
8. Gomtsyan, A. (2012). Chemistry and biology of heterocyclic compounds containing imidazole and thiazole rings. *Chemical Reviews, 112*(1), 275–316.
9. Zhao, Y. (2020). Imidazole- and thiazole-based heterocycles as privileged scaffolds in medicinal chemistry. *Bioorganic & Medicinal Chemistry, 28*(5), 115321.
10. Siegfried, J. M., & Stabile, L. P. (2015). EGFR and cancer: Implications for targeted therapy. *Cancer Research, 75*(7), 1215–1221.
11. Jemal, A., Bray, F., Center, M. M., Ferlay, J., Ward, E., & Forman, D. (2011). Global cancer statistics. *CA: A Cancer Journal for Clinicians, 61*(2), 69–90.
12. Shareef, M. A., Khan, I., Babu, B. N., & Kamal, A. (2020). A comprehensive review on the therapeutic versatility of imidazo[2,1-b]thiazoles. *Current Medicinal Chemistry, 27*(40), 6864–6887.
13. Mohamed, H. A., & Abdel-Wahab, B. F. (2012). Synthetic access to imidazo[2,1-b]thiazoles. *Journal of Sulfur Chemistry, 33*(5), 589–604.
14. Kumari, G., Rani, P., Aneja, D., Dhillon, S., & Kinger, M. (2026). Unlocking the biological potential of novel imidazo[2,1-b]thiazole–2,3-dihydrofuran hybrids: Insights from computational studies. *Results in Chemistry, 28*, 103534.
15. Ahmadi, Y., & Ahmadi, B. (2026). Biological activity of imidazo-thiazole scaffolds: A comprehensive review of 2020–2025 advances. *Results in Chemistry, 26*, 103325.
16. Siwach, A., & Verma, P. K. (2021). Synthesis and therapeutic potential of imidazole containing compounds. *BMC Chemistry, 15*(1), 12.
17. Javahershenas, R., & Nikzat, S. (2023). Recent advances in the multicomponent synthesis of heterocycles using tetronic acid. *RSC Advances, 13*, 16619–16629.
18. Lionta, E., Spyrou, G., Vassilatis, D. K., & Cournia, Z. (2014). Structure-based virtual screening for drug discovery: Principles, applications and recent advances. *Current Topics in Medicinal Chemistry, 14*(16), 1923–1938.
19. Cherkasov, A., Muratov, E. N., Fourches, D., Varnek, A., Baskin, I., Cronin, M., Dearden, J., Gramatica, P., Martin, Y., Todeschini, R., Consonni, V., Kuz'min, V., Cramer, R., Benigni, R., Yang, C., Rathman, J., Terfloth, L., Gasteiger, J., Richard, A., & Tropsha, A.

(2014). QSAR modeling: Where have you been? Where are you going? *Journal of Medicinal Chemistry, 57*(12), 4977–5010.

20. Jin, Z. (2006). Imidazole, oxazole and thiazole alkaloids. *Natural Product Reports, 23*, 464–496.
21. Fascio, M. L., Errea, M. I., & D'Accorso, N. B. (2015). Imidazothiazole and related heterocyclic systems: Synthesis, chemical and biological properties. *European Journal of Medicinal Chemistry, 90*, 666–683.
22. Sbenati, R. M., Semreen, M. H., Semreen, A. M., Shehata, M. K., Alsaghir, F. M., & El-Gamal, M. I. (2021). Evaluation of imidazo[2,1-b]thiazole-based anticancer agents in one decade (2011–2020): Current status and future prospects. *Bioorganic & Medicinal Chemistry, 29*, 115897.
23. Soon, S. S., Goh, S. Y., Bee, Y. M., Poon, J. L., Li, S. C., Thumboo, J., & Wee, H. L. (2010). Audit of Diabetes-Dependent Quality of Life (ADDQoL) [Chinese Version for Singapore] questionnaire: Reliability and validity among Singaporeans with type 2 diabetes mellitus. *Applied Health Economics and Health Policy, 8*(4), 239–249.
24. Berman, E. M., & Werbel, L. M. (1991). The renewed potential for folate antagonists in contemporary cancer chemotherapy. *Journal of Medicinal Chemistry, 34*(2), 479–485.
25. Shareef, M. A., Devi, G. P., Routhu, S. R., Kumar, C. G., Kamal, A., & Babu, B. N. (2020). New imidazo[2,1-b]thiazole-based aryl hydrazones: Unravelling their synthesis and antiproliferative and apoptosis-inducing potential. *RSC Medicinal Chemistry, 11*(10), 1178–1184.
26. Rashdan, H. R., Abdelmonsef, A. H., Shehadi, I. A., Gomha, S. M., Soliman, A. M. M., Mahmoud, H. K., & Abdel-Aziz, H. A. (2020). Synthesis, molecular docking screening and anti-proliferative potency evaluation of some new imidazo[2,1-b]thiazole linked thiadiazole conjugates. *Molecules, 25*(21), 4997.
27. Majalakere, K., Kunhana, S. B., Rao, S., Kalal, B. S., Badiadka, N., Sanjeev, G., & Holla, B. S. (2020). Studies on imidazo[2,1-b][1,3]benzothiazole derivatives as new radiosensitizers. *SN Applied Sciences, 2*(11), 1902.
28. Basoğlu, F., Ulusoy-Güzeldemirci, N., Akalın-Çiftçi, G., Çetinkaya, S., & Ece, A. (2021). Novel imidazo[2,1-b]thiazole-based anticancer agents as potential focal adhesion kinase inhibitors: Synthesis, *in silico* and *in vitro* evaluation. *Chemical Biology & Drug Design, 98*(2), 270–282.
29. Alapati, K. B., Sravani, D., Sailaja, B. B. V., Saritha, B., & Nalla, S. (2024). Synthesis and biological evaluation of amide derivatives of isoxazole-imidazo[2,1-b]thiazole as anticancer agents. *Results in Chemistry, 10*, 101700.
30. Dadou, S., Altay, A., Koudad, M., Türkmenoğlu, B., Yeniceri, E., Çağlar, S., Allali, M., Oussaid, A., Benchat, N., & Karrouchi, K. (2022). Design, synthesis, anticancer evaluation

and molecular docking studies of new imidazo[2,1-b]thiazole-based chalcones. *Medicinal Chemistry Research, 31*(8), 1369–1383.

31. Lujing, H., Ting, H., Longhui, L., Xue, J., Xiaoyan, L., Yuxin, Z., Shengjun, L., Feng, L., Qingsong, Z., Qidong, T., & Jielian, W. (2023). Study on the inhibitory activity of benzo[d]imidazo[2,1-b]thiazole compounds containing chromone in lung cancer cells. *Russian Journal of Organic Chemistry, 59*(Suppl. 1), S94–S100.
32. Dadou, S., Altay, A., Baydere, C., Anouar, E. H., Türkmenoğlu, B., Koudad, M., Dege, N., Oussaid, A., Benchat, N., & Karrouchi, K. (2025). Chalcone-based imidazo[2,1-b]thiazole derivatives: Synthesis, crystal structure, potent anticancer activity, and computational studies. *Journal of Biomolecular Structure and Dynamics, 43*(1), 261–276.
33. Deshmukh, H. S., Adole, V. A., Shah, U., Mali, S. N., Shah, H., Sarkar, R., Pawar, T. B., & Jagdale, B. S. (2025). PEG-400 mediated synthesis of benzo[d]imidazo[2,1-b]thiazoles as bioactive scaffolds: Antibreast cancer potential, EGFR inhibition, antioxidant study, molecular docking, and DFT insights. *ChemistrySelect, 10*(19), e202500521.
34. Ahmadi, N., Shahhosseini, S., Shirazi, F. H., Farnam, G., & Zarghi, A. (2022). Synthesis, structural characterization, and cytotoxic activity of new benzo[d]imidazo[2,1-b]thiazole derivatives against MCF-7 breast cancer cells. *Iranian Journal of Pharmaceutical Research, 21*(1), e127041.
35. Alshaye, N. A., Elgohary, M. K., Elkotamy, M. S., & Abdel-Aziz, H. A. (2024). Design, synthesis and biological assessment of *N′*-(2-oxoindolin-3-ylidene)-6-methylimidazo[2,1-b]thiazole-5-carbohydrazides as potential anti-proliferative agents toward MCF-7 breast cancer. *Pharmaceuticals, 17*(2), 216.
36. Mohammed, E. R., Ezzat, M. A. F., Seif, E. M., Essa, B. M., Abdel-Aziz, H. A., Sakr, T. M., & Ibrahim, H. S. (2024). Synthesis of *S*-alkylated oxadiazole bearing imidazo[2,1-b]thiazole derivatives targeting breast cancer: *In vitro* cytotoxic evaluation and *in vivo* radioactive tracing studies. *Bioorganic Chemistry, 153*, 107935.
37. Kamboj, P., Anjali, Imtiyaz, K., Rizvi, M. A., Nath, V., Kumar, V., Husain, A., & Amir, M. (2024). Design, synthesis, biological assessment and molecular modeling studies of novel imidazothiazole-thiazolidinone hybrids as potential anticancer and anti-inflammatory agents. *Scientific Reports, 14*(1), 8457.

Bhumi Publishing, India
June 2026

QUANTUM ERROR CORRECTION: ENABLING RELIABLE QUANTUM INFORMATION PROCESSING

Satyananda Chabungbam
Assam Don Bosco University, Tapesia Gardens – 782402, Assam, India
Correponding author E-mail: csatya11@gmail.com

Abstract

Quantum error correction (QEC) is a fundamental requirement for realizing reliable and scalable quantum computing in the presence of noise and decoherence. Unlike classical systems, quantum information is highly susceptible to errors arising from interactions with the environment, imperfect gate operations, and measurement inaccuracies, making robust error management indispensable. This chapter provides a comprehensive overview of quantum noise and error correction in qubit-based quantum computing platforms. It begins by introducing the physical origins of quantum noise, including decoherence, relaxation, and dephasing, followed by the principles of quantum error correction, logical qubits, syndrome measurements, and fault-tolerant computation. The chapter then reviews major quantum error-correcting codes, including Shor, Steane, CSS, stabilizer, and surface codes, highlighting their roles in protecting quantum information. Platform-specific noise mechanisms and error correction strategies for superconducting qubits, trapped ions, semiconductor spin qubits, neutral atoms, photonic qubits, and diamond nitrogen-vacancy centers are also discussed. Finally, recent advances in error mitigation, machine learning-assisted quantum control, and emerging fault-tolerant architectures are examined, together with future challenges and research directions. By integrating theoretical concepts with practical implementations, this chapter provides a concise overview of the techniques that underpin reliable quantum computation and the ongoing development of scalable fault-tolerant quantum technologies.

1. Introduction to Quantum Noise and Error Correction

Quantum computing promises to revolutionize information processing by solving certain computational problems exponentially faster than classical computers. Algorithms such as Shor's integer factorization algorithm and Grover's quantum search algorithm have demonstrated the theoretical superiority of quantum computation for selected applications (Nielsen & Chuang, 2010). Unlike classical computers, which process information using binary bits, quantum computers utilize quantum bits, or qubits, that exploit the principles of superposition, entanglement, and quantum interference. These uniquely quantum phenomena enable parallel information processing and provide the computational advantage that underpins quantum technologies. However, the same quantum properties that make quantum computers powerful

also render them exceptionally fragile. Even weak interactions with the surrounding environment can destroy quantum coherence, leading to computational errors that accumulate rapidly during quantum operations (Preskill, 2018).

One of the fundamental obstacles to practical quantum computing is quantum noise. Quantum systems are inherently open systems that continuously interact with their environments through electromagnetic fluctuations, thermal excitations, lattice vibrations, and material defects. These interactions gradually degrade the quantum state through a process known as decoherence, causing the loss of superposition and entanglement that are essential for quantum computation (Breuer & Petruccione, 2002). Unlike classical digital systems, where information can often be recovered using straightforward redundancy techniques, quantum information cannot simply be copied because of the quantum no-cloning theorem (Wootters & Zurek, 1982). This fundamental limitation necessitates entirely new strategies for detecting and correcting errors while preserving the encoded quantum information.

Classical error correction relies on copying information multiple times and comparing redundant copies to identify corrupted bits. For example, a classical bit may be stored three times, allowing majority voting to determine the correct value if one copy is corrupted. Such an approach is impossible in quantum mechanics because an arbitrary unknown quantum state cannot be copied exactly (Wootters & Zurek, 1982). Instead, quantum error correction (QEC) encodes logical quantum information across several entangled physical qubits, allowing errors to be identified indirectly through carefully designed measurements known as syndrome measurements. These measurements reveal the presence and type of error without collapsing the encoded quantum information itself (Gottesman, 1997).

The development of quantum error correction during the mid-1990s represented a turning point in quantum information science. Early pioneering works by Peter W. Shor introduced the first quantum error-correcting code capable of protecting an arbitrary qubit against both bit-flip and phase-flip errors using nine physical qubits (Shor, 1995). Shortly thereafter, Andrew Steane developed a more efficient seven-qubit error-correcting code based on classical coding theory (Steane, 1996). These landmark discoveries demonstrated that reliable quantum computation is theoretically possible despite the presence of noise and decoherence. Subsequent advances by Daniel Gottesman established the stabilizer formalism, providing a unified mathematical framework for constructing and analyzing a broad class of quantum error-correcting codes (Gottesman, 1997).

Modern quantum processors are built using a variety of physical platforms, each exhibiting distinct sources of noise and operational challenges. Superconducting qubits, currently employed by companies such as IBM and Google Quantum AI, are susceptible to dielectric losses, flux noise, microwave control imperfections, and energy relaxation. Trapped-ion qubits experience

decoherence primarily through laser fluctuations and magnetic field instability. Semiconductor spin qubits are affected by charge noise and hyperfine interactions with surrounding nuclear spins, while photonic qubits suffer from photon loss and imperfect optical components (Preskill, 2018). Because the dominant error mechanisms differ substantially among hardware platforms, effective quantum error correction requires platform-specific strategies tailored to the underlying physical processes.

The importance of quantum error correction has become even more evident in the current Noisy Intermediate-Scale Quantum (NISQ) era, characterized by quantum processors containing tens to several hundred physical qubits that are not yet capable of full fault-tolerant computation (Preskill, 2018). Although these devices have demonstrated remarkable experimental progress, computational accuracy remains limited by gate errors, decoherence, and measurement imperfections. Consequently, considerable research efforts are directed toward developing both robust quantum error-correcting codes and complementary error mitigation techniques that improve computational fidelity without requiring the enormous overhead associated with fully fault-tolerant quantum computing.

Beyond its immediate role in protecting quantum information, quantum error correction has profound implications for the future scalability of quantum technologies. The threshold theorem establishes that if physical error rates remain below a certain critical threshold, arbitrarily long quantum computations become possible through recursive error correction (Nielsen & Chuang, 2010). This remarkable result provides the theoretical foundation for constructing large-scale quantum computers capable of solving scientifically and technologically important problems in chemistry, materials science, cryptography, optimization, and artificial intelligence.

This chapter explores the principles, techniques, and practical implementation of quantum error correction in modern qubit platforms. Beginning with the physical origins of quantum noise, subsequent sections examine quantum error-correcting codes, platform-specific error mechanisms, fault-tolerant computation, and emerging error mitigation strategies. Together, these topics illustrate how quantum error correction serves as the cornerstone of scalable and reliable quantum computing.

2. Fundamentals of Quantum Noise in Qubit Systems

Quantum computers derive their computational power from the coherent manipulation of quantum states. Unlike classical bits, which assume one of two well-defined logical states, qubits exploit quantum superposition and entanglement to perform parallel information processing. However, these uniquely quantum properties are extremely sensitive to external disturbances. Every practical quantum computer operates as an open quantum system, interacting continuously with its surrounding environment through electromagnetic fluctuations, thermal excitations, material defects, and control electronics. These unavoidable interactions introduce quantum

noise, degrade coherence, and ultimately limit the accuracy and scalability of quantum computation (Breuer & Petruccione, 2002). Understanding the physical origin and mathematical description of quantum noise is therefore essential for designing robust quantum hardware and effective quantum error-correction protocols.

An ideal quantum computer would evolve solely according to the Schrödinger equation, maintaining perfect coherence throughout a computation. In reality, however, no quantum system is completely isolated from its environment. Interactions with external degrees of freedom gradually transfer quantum information from the system to the environment, producing decoherence. Decoherence causes the loss of quantum superposition and entanglement, effectively transforming quantum states into classical statistical mixtures and reducing computational fidelity (Schlosshauer, 2007). Since quantum algorithms depend critically on maintaining coherent quantum interference, decoherence represents one of the principal obstacles to realizing practical quantum computers.

The dynamics of noisy quantum systems are commonly described using the density matrix formalism, which provides a unified framework for representing both pure and mixed quantum states (Nielsen & Chuang, 2010). While an isolated qubit can often be described completely by a wavefunction, interactions with the environment introduce statistical uncertainty that requires the more general density operator description. The evolution of such open quantum systems is represented mathematically by quantum channels, which characterize how environmental interactions transform the quantum state. These channels provide a convenient framework for analyzing different types of quantum errors and evaluating the performance of quantum hardware under realistic operating conditions (Breuer & Petruccione, 2002).

Among the simplest forms of quantum noise is the bit-flip error, in which the logical state of a qubit changes from $|0\rangle$ to $|1\rangle$ or vice versa. This error is analogous to the inversion of a classical digital bit and may arise from imperfect control pulses, thermal fluctuations, or unintended interactions with neighboring qubits. While relatively straightforward to understand, bit-flip errors alone do not adequately describe the behavior of quantum systems because quantum information is encoded not only in the computational basis states but also in their relative phases (Nielsen & Chuang, 2010).

A uniquely quantum form of error is the phase-flip error, which preserves the logical state of the qubit while altering the relative phase between the basis states. Since quantum algorithms rely heavily on constructive and destructive interference, even small phase errors can significantly affect computational outcomes. Phase noise frequently originates from fluctuations in magnetic fields, charge environments, or microwave control signals and is particularly important in superconducting and spin-based quantum processors (Preskill, 2018). A combination of bit-flip

and phase-flip processes produces bit-phase-flip errors, which represent another fundamental category of quantum noise considered in most quantum error-correcting codes.

In addition to these discrete error models, realistic quantum hardware experiences amplitude damping and phase damping. Amplitude damping describes irreversible energy relaxation, where an excited qubit spontaneously loses energy to its surrounding environment and relaxes toward its ground state. This process is especially important in superconducting circuits, trapped ions, and semiconductor qubits, where spontaneous emission and dielectric losses limit coherence times (Kjaergaard *et al.,* 2020). By contrast, phase damping—often referred to simply as dephasing—does not involve energy exchange but instead randomizes the relative phase of quantum states through interactions with fluctuating environmental fields. Dephasing gradually destroys quantum coherence while leaving the qubit populations largely unchanged, making it one of the dominant error mechanisms in many quantum computing platforms (Schlosshauer, 2007).

Another widely used theoretical model is the depolarizing channel, which represents random quantum errors occurring with equal probability in all directions. Although somewhat idealized, the depolarizing model provides a convenient framework for analyzing the robustness of quantum algorithms and evaluating the performance of quantum error-correcting codes (Nielsen & Chuang, 2010). Many theoretical studies employ depolarizing noise because it captures the combined effects of multiple independent error mechanisms while remaining mathematically tractable.

The performance of qubit platforms is commonly characterized using two fundamental coherence times: the energy relaxation time (T_1) and the phase coherence time (T_2). The relaxation time T_1 measures the average time required for an excited qubit to decay to its ground state through amplitude damping, whereas T_2 quantifies the loss of quantum phase coherence due to dephasing and other environmental interactions. Because quantum computations must be completed before significant decoherence occurs, maximizing both T_1 and T_2 remains a primary objective in quantum hardware development (Devoret & Schoelkopf, 2013). Continuous improvements in materials purification, cryogenic engineering, device fabrication, and electromagnetic shielding have steadily increased coherence times across multiple quantum computing platforms.

The dominant sources of quantum noise vary significantly among different hardware technologies. Superconducting qubits experience dielectric loss, flux noise, quasiparticle generation, and microwave control errors. Trapped-ion systems are affected primarily by laser frequency instability, magnetic-field fluctuations, and motional heating. Semiconductor spin qubits suffer from charge noise and hyperfine interactions with surrounding nuclear spins, whereas photonic qubits are limited by photon loss, imperfect optical components, and detector

inefficiencies (Preskill, 2018). These platform-specific noise mechanisms motivate the development of customized quantum control strategies and error-correction protocols tailored to individual hardware implementations.

Recent advances in quantum characterization techniques have significantly improved the understanding of quantum noise. Methods such as quantum process tomography, randomized benchmarking, and gate-set tomography allow researchers to quantify gate fidelities, identify dominant error sources, and evaluate the performance of quantum processors under realistic operating conditions (Blume-Kohout *et al.,* 2017). More recently, machine learning and artificial intelligence have begun to assist in noise diagnosis, parameter optimization, and adaptive calibration, providing new opportunities for improving quantum hardware performance.

In summary, quantum noise arises from the inevitable interaction between qubits and their surrounding environment, leading to decoherence and computational errors that threaten the reliability of quantum information processing. Bit-flip, phase-flip, amplitude damping, dephasing, and depolarizing noise constitute the principal error models encountered in modern qubit platforms. A thorough understanding of these mechanisms forms the foundation for quantum error correction, fault-tolerant computation, and the development of scalable quantum technologies. As quantum hardware continues to mature, advances in noise characterization and suppression will remain central to achieving practical quantum computation.

3. Principles of Quantum Error Correction

Quantum error correction (QEC) is one of the most significant achievements in quantum information science, providing the theoretical foundation for reliable quantum computation despite the presence of noise and decoherence. Unlike classical computers, where errors can be corrected by simply copying information and comparing redundant copies, quantum systems cannot employ this strategy because of the no-cloning theorem, which prohibits the creation of identical copies of an unknown quantum state (Wootters & Zurek, 1982). Consequently, quantum error correction relies on encoding quantum information across multiple entangled physical qubits rather than duplicating individual quantum states. This approach enables errors to be detected and corrected without directly measuring or destroying the encoded quantum information (Nielsen & Chuang, 2010). A fundamental concept in QEC is the distinction between physical qubits and logical qubits. Physical qubits are the actual quantum systems implemented in hardware, such as superconducting circuits or trapped ions, and are inherently susceptible to environmental noise. A logical qubit, in contrast, is an abstract quantum state encoded across several physical qubits in such a way that the original information can be recovered even if some of the constituent qubits experience errors (Gottesman, 1997). By distributing quantum information over multiple physical qubits, logical encoding introduces redundancy while preserving the principles of quantum mechanics.

The key to quantum error correction lies in syndrome measurement, a process that identifies the presence and nature of errors without revealing the logical quantum information itself. Instead of measuring the encoded state directly, auxiliary qubits, known as ancilla qubits, interact with the logical qubits to extract an error syndrome. This syndrome indicates whether a bit-flip, phase-flip, or combined error has occurred, allowing appropriate corrective operations to be applied. Since the logical state remains undisturbed during syndrome extraction, quantum coherence is preserved throughout the correction process (Shor, 1995).

Quantum error correction typically follows a cyclic procedure consisting of encoding, error detection, correction, and computation. Initially, the logical qubit is encoded into multiple physical qubits using an appropriate error-correcting code. During computation, periodic syndrome measurements monitor the system for errors introduced by decoherence or imperfect gate operations. Once an error is identified, a corresponding recovery operation restores the encoded quantum state before computation continues. Because quantum hardware experiences continuous environmental interactions, these correction cycles must be repeated frequently throughout the execution of a quantum algorithm (Preskill, 2018).

A landmark result in quantum information theory is the threshold theorem, which states that arbitrarily long quantum computations are possible provided the physical error rate remains below a critical threshold and error correction is performed continuously (Aharonov & Ben-Or, 1997). Although the exact threshold depends on the chosen error-correcting code and hardware architecture, this theorem established that scalable quantum computing is theoretically achievable despite the presence of noise. It transformed quantum error correction from a theoretical curiosity into a practical engineering framework for building large-scale quantum computers.

Closely related to QEC is the concept of fault-tolerant quantum computation. Error correction alone is insufficient if the correction process itself introduces additional errors. Fault tolerance therefore requires that every quantum operation—including gate execution, syndrome measurement, and qubit initialization—be designed so that individual hardware errors do not propagate uncontrollably through the quantum circuit (Gottesman, 1997). Modern fault-tolerant architectures employ carefully designed logical gates, transversal operations, and repeated syndrome extraction to ensure that computational errors remain correctable throughout long quantum computations.

Quantum error correction has become indispensable for the development of practical quantum computers. Although current noisy intermediate-scale quantum (NISQ) devices rely primarily on error mitigation techniques, future fault-tolerant quantum processors will require thousands of physical qubits to construct reliable logical qubits capable of executing complex algorithms. Continued improvements in quantum hardware, control techniques, and error-correcting codes

are therefore essential for realizing scalable quantum computation. As research progresses, QEC will remain the cornerstone that bridges today's noisy quantum processors with tomorrow's universal fault-tolerant quantum computers.

4. Quantum Error-Correcting Codes

Quantum error-correcting codes (QECCs) constitute the practical implementation of quantum error correction by encoding a logical qubit into multiple physical qubits. These codes protect quantum information against decoherence, gate imperfections, and environmental noise while preserving the coherence necessary for quantum computation. Since quantum information cannot be copied because of the no-cloning theorem, QECCs employ entanglement and redundancy to detect and correct errors without directly measuring the logical quantum state (Nielsen & Chuang, 2010). Over the past three decades, numerous coding schemes have been proposed, each optimized for different hardware architectures and noise models.

The earliest quantum error-correcting code was introduced by Peter W. Shor in 1995. The Shor nine-qubit code protects a single logical qubit against arbitrary single-qubit errors by combining two types of redundancy: one corrects bit-flip errors, while the other corrects phase-flip errors (Shor, 1995). Although the code requires a relatively large number of physical qubits, it demonstrated for the first time that quantum information could be preserved despite the presence of noise. This pioneering work established the feasibility of fault-tolerant quantum computation and inspired the rapid development of more efficient coding schemes.

A simpler example is the three-qubit repetition code, which protects against either bit-flip or phase-flip errors but not both simultaneously. In this scheme, the logical state is encoded into three identical physical qubits, allowing majority voting to identify and correct a single error. While limited in practical applications, the repetition code provides valuable insight into the basic principles of quantum redundancy and syndrome measurement and remains an important pedagogical example in quantum information theory (Nielsen & Chuang, 2010).

A major improvement was achieved with the introduction of the Steane seven-qubit code, which combines efficient encoding with the ability to correct arbitrary single-qubit errors (Steane, 1996). Based on classical error-correcting codes, the Steane code belongs to the family of Calderbank–Shor–Steane (CSS) codes, which independently address bit-flip and phase-flip errors using two complementary classical linear codes (Calderbank & Shor, 1996; Steane, 1996). CSS codes have become fundamental to quantum information science because of their relatively simple implementation and compatibility with fault-tolerant logical gate operations.

A unifying framework for understanding many quantum error-correcting codes is provided by the stabilizer formalism, developed by Daniel Gottesman (1997). Instead of describing encoded quantum states directly, stabilizer codes characterize them through a set of commuting operators whose measurement reveals the presence of errors without disturbing the logical information.

This elegant mathematical framework encompasses the Shor code, Steane code, CSS codes, and many modern coding schemes. The stabilizer formalism has become the dominant language for designing and analyzing quantum error-correcting codes and forms the basis of most contemporary fault-tolerant architectures.

Among modern QECCs, surface codes have emerged as the leading candidate for large-scale quantum computing. Surface codes arrange qubits on a two-dimensional lattice where each qubit interacts only with its nearest neighbors, making them highly compatible with superconducting and semiconductor quantum processors (Fowler *et al.,* 2012). Their greatest advantage lies in their relatively high error threshold, allowing reliable quantum computation even when individual physical operations remain imperfect. Closely related are color codes, which employ different lattice geometries to support a broader class of fault-tolerant logical operations while maintaining topological protection (Bombín & Martin-Delgado, 2006). Both surface and color codes are actively being investigated by academic researchers and industrial quantum computing companies because they offer realistic pathways toward scalable fault-tolerant quantum processors.

More recently, alternative approaches such as bosonic codes, subsystem codes, and low-density parity-check (LDPC) quantum codes have attracted growing attention. Bosonic codes encode quantum information into harmonic oscillators, such as microwave cavities, reducing the number of physical components required for error correction. LDPC codes aim to minimize qubit overhead while maintaining high error-correction performance, making them promising candidates for future large-scale quantum computers. Although these emerging codes remain under active development, they represent important directions for improving the efficiency and scalability of quantum error correction.

No single quantum error-correcting code is universally optimal. The choice of code depends on factors such as hardware architecture, dominant noise mechanisms, connectivity between qubits, and available computational resources. Consequently, ongoing research seeks to develop more efficient codes that reduce physical qubit overhead while maintaining high fault tolerance. As quantum hardware continues to improve, advances in quantum coding theory will remain essential for bridging the gap between noisy intermediate-scale quantum devices and fully fault-tolerant quantum computers.

5. Noise and Error Correction Across Major Qubit Platforms

The performance of a quantum computer depends not only on the design of quantum algorithms and error-correcting codes but also on the physical characteristics of the underlying qubit technology. Every qubit platform exhibits distinct noise mechanisms arising from its interaction with the surrounding environment, fabrication imperfections, and control electronics. Consequently, the implementation of quantum error correction must be tailored to the dominant

error sources of each hardware architecture. Understanding these platform-specific noise mechanisms is therefore essential for developing scalable and fault-tolerant quantum computers (Preskill, 2018).

Among current technologies, superconducting qubits are the most widely developed and have been adopted by companies such as IBM, Google Quantum AI, and Rigetti Computing. Superconducting qubits are fabricated using Josephson junctions integrated on microchips and operated at millikelvin temperatures. Their principal sources of noise include dielectric losses, charge noise, magnetic flux fluctuations, quasiparticle generation, and microwave control imperfections. These effects limit both energy relaxation (T_1) and phase coherence (T_2), thereby reducing gate fidelity (Kjaergaard *et al.,* 2020). Considerable improvements in fabrication techniques, materials purification, and cryogenic engineering have significantly enhanced coherence times, enabling demonstrations of quantum error correction using surface codes and repeated syndrome measurements (Arute *et al.,* 2023).

Trapped-ion qubits represent one of the most mature quantum computing platforms due to their exceptionally long coherence times and high-fidelity quantum gates. Individual ions are confined using electromagnetic fields and manipulated with laser pulses. The dominant sources of noise include laser intensity fluctuations, magnetic-field instability, spontaneous photon scattering, and motional heating of trapped ions (Monroe *et al.,* 2021). Because trapped ions exhibit relatively low physical error rates, they require fewer rounds of error correction than many solid-state platforms. Recent experiments have demonstrated logical qubits with improved error resilience, highlighting the suitability of trapped ions for fault-tolerant quantum computation.

Another promising platform consists of semiconductor spin qubits, where quantum information is encoded in the spin states of electrons or holes confined within quantum dots or impurity atoms. Their compatibility with existing semiconductor manufacturing technologies makes them attractive for large-scale integration. However, spin qubits are strongly influenced by charge noise, interface defects, and hyperfine interactions with surrounding nuclear spins, all of which contribute to decoherence (Loss & DiVincenzo, 1998). Isotopic purification of semiconductor materials, particularly silicon, has significantly reduced nuclear spin noise and improved coherence, making semiconductor spin qubits increasingly competitive with other leading platforms.

Neutral-atom quantum computers have emerged as a rapidly developing technology for scalable quantum computing. Individual atoms are trapped using optical tweezers or optical lattices and manipulated through laser excitation to highly excited Rydberg states. These systems naturally possess long coherence times and excellent scalability, but their performance is affected by laser phase noise, atom loss, spontaneous emission, and imperfect control of Rydberg interactions (Saffman *et al.,* 2016). Although large-scale quantum error correction has not yet been fully

demonstrated in neutral-atom systems, rapid advances in atom trapping and coherent control are bringing fault-tolerant implementations closer to reality.

In contrast to matter-based qubits, photonic qubits encode quantum information in properties such as polarization, time-bin, frequency, or spatial modes of individual photons. Because photons interact only weakly with their environment, they experience minimal decoherence during transmission, making them ideal for quantum communication and networking. Nevertheless, photon loss, imperfect optical components, detector inefficiencies, and probabilistic two-photon interactions remain major obstacles for photonic quantum computing (O'Brien *et al.,* 2009). Error correction in photonic systems therefore focuses primarily on compensating for photon loss and improving measurement fidelity through redundant encoding and photonic cluster-state architectures.

Another important platform involves nitrogen-vacancy (NV) centers in diamond, where quantum information is stored in the electronic spin associated with a lattice defect. NV centers combine long spin coherence times with optical initialization and readout, making them attractive for quantum sensing, communication, and distributed quantum computing. Their primary sources of decoherence include interactions with nearby nuclear spins, magnetic-field fluctuations, and crystal defects (Jelezko & Wrachtrup, 2006). Recent demonstrations of logical qubit encoding and repeated error correction in diamond have highlighted the potential of this platform for quantum networking applications.

Despite the diversity of hardware technologies, several common themes emerge. All platforms require continuous improvements in qubit coherence, gate fidelity, state preparation, and measurement accuracy. Furthermore, the choice of quantum error-correcting code often depends on hardware connectivity and dominant noise mechanisms. For example, surface codes are particularly well suited to superconducting architectures with nearest-neighbor interactions, whereas trapped-ion systems can exploit their all-to-all connectivity to implement more flexible coding schemes (Fowler *et al.,* 2012). These differences underscore the importance of hardware–software co-design in future fault-tolerant quantum computers.

Overall, no single qubit platform has yet emerged as the definitive solution for scalable quantum computing. Instead, each technology offers distinct advantages and faces unique challenges. Continued advances in materials science, quantum control, fabrication, and error correction are steadily improving the performance of all major platforms. As quantum hardware matures, platform-specific noise mitigation combined with efficient quantum error correction will be essential for realizing reliable, large-scale quantum computation.

6. Error Mitigation, Fault Tolerance, and Emerging Techniques

Although quantum error correction provides the theoretical foundation for reliable quantum computation, current quantum processors remain far from the scale required for fully fault-

tolerant operation. Present-day quantum devices belong to the Noisy Intermediate-Scale Quantum (NISQ) era, characterized by tens to a few thousand physical qubits with limited coherence times and imperfect gate operations (Preskill, 2018). Because implementing complete quantum error correction requires a substantial overhead of physical qubits, researchers have developed complementary strategies known as quantum error mitigation. Unlike error correction, which actively detects and corrects errors during computation, error mitigation aims to reduce the impact of noise on computational outcomes without introducing large redundancy (Temme *et al.,* 2017).

One of the most widely studied error mitigation methods is zero-noise extrapolation (ZNE). The basic idea is to deliberately amplify the noise present in a quantum circuit and then extrapolate the measured results back to the ideal zero-noise limit (Temme *et al.,* 2017). Since no additional qubits are required, ZNE has become an attractive technique for improving the performance of NISQ devices. Experimental demonstrations on superconducting and trapped-ion quantum processors have shown that zero-noise extrapolation can significantly improve the accuracy of quantum simulations and variational quantum algorithms.

Another important approach is probabilistic error cancellation (PEC). This technique first characterizes the noise affecting individual quantum gates and then mathematically compensates for these errors during post-processing. In principle, probabilistic error cancellation can completely remove the effects of noise, although its computational cost increases rapidly as circuit size grows (Endo *et al.,* 2018). Consequently, PEC is currently most suitable for small- and medium-scale quantum circuits but continues to serve as an important benchmark for evaluating quantum hardware.

A complementary strategy for suppressing decoherence is dynamical decoupling, which employs carefully designed sequences of control pulses to average out unwanted interactions between qubits and their environment. Originally developed in nuclear magnetic resonance, dynamical decoupling has become an effective tool for extending coherence times in superconducting circuits, trapped ions, semiconductor spin qubits, and nitrogen-vacancy centers in diamond (Viola *et al.,* 1999). Unlike quantum error correction, dynamical decoupling does not require additional qubits and can often be integrated directly into existing quantum control protocols.

Another emerging technique is randomized compiling, in which random gate sequences are inserted into quantum circuits to convert coherent control errors into stochastic errors that are easier to characterize and correct. Because coherent errors accumulate systematically during computation, transforming them into random errors substantially improves the performance of conventional quantum error-correcting codes (Wallman & Emerson, 2016). Randomized compiling is particularly attractive because it requires relatively minor modifications to existing quantum software while providing measurable improvements in computational fidelity.

The long-term objective of quantum computing remains fault-tolerant quantum computation, where logical qubits are protected continuously against errors throughout arbitrarily long computations. Fault tolerance requires that every quantum operation—including gate implementation, qubit initialization, syndrome extraction, and measurement—be designed to prevent the uncontrolled propagation of errors (Gottesman, 1998). Modern fault-tolerant architectures rely heavily on surface codes because of their comparatively high error thresholds and compatibility with nearest-neighbor hardware connectivity (Fowler *et al.,* 2012). Achieving fault tolerance will require physical gate fidelities well above 99.9%, together with efficient logical gate implementations and scalable quantum hardware.

Recent years have witnessed the growing integration of artificial intelligence (AI) and machine learning (ML) into quantum control and error management. Machine learning algorithms are increasingly being used to optimize pulse sequences, calibrate quantum gates, identify dominant noise sources, and predict hardware drift before computational errors occur. Reinforcement learning has also shown promise for designing adaptive quantum control strategies capable of improving gate fidelities without requiring explicit physical models of the underlying hardware (Bukov *et al.,* 2018). These AI-assisted approaches are expected to become increasingly important as quantum processors continue to grow in size and complexity.

Future quantum computing systems are likely to combine error mitigation, quantum error correction, and intelligent quantum control within unified hardware–software frameworks. Near-term NISQ processors will continue to rely primarily on mitigation techniques, while future large-scale processors will gradually transition toward fully fault-tolerant architectures supported by logical qubits and continuous syndrome correction. This hybrid approach provides a practical roadmap from current experimental devices to universal quantum computers capable of solving scientifically and technologically important problems.

In conclusion, error mitigation and fault tolerance represent complementary approaches to improving quantum computational reliability. While error mitigation enables useful computations on today's noisy hardware, fault-tolerant quantum error correction remains the ultimate objective for scalable quantum computing. Continued advances in quantum control, optimized error-correcting codes, machine learning, and hardware engineering are steadily reducing the gap between present-day NISQ devices and future universal quantum computers.

7. Future Perspectives and Outlook

Quantum error correction has evolved from a theoretical concept into one of the foundational pillars of modern quantum computing. Over the past three decades, remarkable advances in quantum hardware, coding theory, and quantum control have demonstrated that reliable quantum computation is achievable despite the unavoidable presence of noise and decoherence. Nevertheless, building large-scale fault-tolerant quantum computers remains one of the greatest

scientific and engineering challenges of the twenty-first century. Continued progress in quantum error correction will determine the pace at which quantum computing transitions from laboratory demonstrations to practical technologies capable of solving real-world problems (Preskill, 2018).

A major challenge is the large hardware overhead required for fault-tolerant quantum computation. Current quantum processors typically operate with physical qubits that exhibit error rates several orders of magnitude higher than those acceptable for reliable long-duration computations. Consequently, thousands of physical qubits may be required to encode a single high-fidelity logical qubit using present-day surface code architectures (Fowler *et al.,* 2012). Reducing this overhead through improved quantum codes, higher-fidelity hardware, and more efficient decoding algorithms remains an active area of research. Advances in low-density parity-check (LDPC) quantum codes and bosonic error-correcting codes offer promising pathways toward significantly reducing resource requirements while maintaining fault tolerance.

Another important direction involves improving qubit quality rather than relying solely on increasingly sophisticated error correction. Continuous improvements in superconducting circuits, trapped ions, semiconductor spin qubits, neutral atoms, and photonic systems have steadily increased coherence times and gate fidelities over the past decade (Kjaergaard *et al.,* 2020). Progress in materials science, nanofabrication, cryogenic engineering, and quantum control is expected to further suppress noise at its physical origin. As physical error rates decrease, the overhead required for quantum error correction will likewise diminish, making scalable quantum computing more economically and technologically feasible.

The future of quantum error correction is also closely tied to advances in quantum software and decoding algorithms. Efficient decoding is essential because syndrome measurements generated during error correction must be interpreted rapidly enough to apply corrective operations before additional errors accumulate. Classical decoding algorithms based on minimum-weight perfect matching have proven highly effective for surface codes, but they become increasingly computationally demanding as quantum processors grow larger (Dennis *et al.,* 2002). Recent research has therefore explored machine learning-based decoders capable of identifying error patterns with improved speed and accuracy. Neural networks, reinforcement learning, and graph-based learning algorithms have demonstrated encouraging performance in syndrome decoding and adaptive error correction, suggesting that artificial intelligence will become an integral component of future fault-tolerant quantum computers (Baireuther *et al.,* 2018).

Another emerging trend is the development of modular and distributed quantum computing. Rather than constructing a single monolithic quantum processor containing millions of qubits, future architectures may interconnect smaller fault-tolerant quantum modules through quantum communication channels. Such distributed systems require reliable quantum networking protocols together with error correction capable of protecting quantum information during

transmission. Quantum repeaters, entanglement purification, and network-level error correction will therefore become increasingly important as researchers move toward realizing a global quantum internet (Kimble, 2008). In these architectures, quantum error correction extends beyond individual processors to encompass communication links connecting geographically separated quantum devices.

The growing involvement of industry is another defining feature of the current quantum landscape. Companies such as IBM, Google Quantum AI, Quantinuum, IonQ, PsiQuantum, and Rigetti Computing are investing heavily in quantum hardware and fault-tolerant architectures. Recent experimental demonstrations of logical qubits outperforming their constituent physical qubits represent important milestones toward scalable quantum computing (Google Quantum AI, 2023). These achievements indicate that quantum error correction is gradually moving from theoretical validation to practical implementation.

Looking ahead, quantum error correction is expected to enable transformative applications across numerous scientific disciplines. Reliable quantum processors will accelerate discoveries in quantum chemistry, allowing accurate simulation of molecular electronic structures and catalytic reactions beyond the reach of classical supercomputers. In materials science, fault-tolerant quantum computers may facilitate the discovery of high-temperature superconductors, novel quantum materials, and energy-efficient catalysts. Other important applications include optimization, secure communications, financial modeling, drug discovery, climate science, and artificial intelligence. None of these large-scale applications will be feasible without robust quantum error correction capable of supporting long computational sequences with extremely low logical error rates.

Future progress will likely depend on the close integration of hardware, software, and intelligent control systems. Rather than treating error correction as an isolated layer, next-generation quantum processors are expected to incorporate hardware-aware coding schemes, adaptive calibration, machine learning-assisted noise diagnosis, and real-time quantum feedback. Such hardware–software co-design approaches will maximize computational efficiency while minimizing resource overhead, accelerating the transition from noisy intermediate-scale devices to universal fault-tolerant quantum computers.

In conclusion, quantum error correction remains the enabling technology upon which the future of quantum computing depends. Although significant challenges remain in reducing hardware overhead, improving qubit fidelity, and implementing efficient decoding algorithms, remarkable progress over the past decade demonstrates that these obstacles are steadily being overcome. Continued advances in quantum information theory, materials science, quantum engineering, artificial intelligence, and device fabrication are expected to transform quantum error correction from a specialized research topic into a mature engineering discipline. As scalable logical qubits

become a practical reality, quantum error correction will provide the essential foundation for the next generation of quantum technologies, enabling reliable computation, secure communication, and scientific discoveries that are beyond the capabilities of classical computing.

References

1. Aharonov, D., & Ben-Or, M. (1997). Fault-tolerant quantum computation with constant error. *Proceedings of the 29th Annual ACM Symposium on Theory of Computing*, 176–188.
2. Arute, F., *et al.* (2023). Suppressing quantum errors by scaling a surface code logical qubit. *Nature, 614*, 676–681.
3. Baireuther, P., O'Brien, T. E., Tarasinski, B., & Beenakker, C. W. J. (2018). Machine-learning-assisted correction of correlated qubit errors in a topological code. *Quantum, 2*, 48.
4. Blume-Kohout, R., Gamble, J. K., Nielsen, E., *et al.* (2017). Demonstration of qubit operations below a rigorous fault-tolerance threshold with gate set tomography. *Nature Communications, 8*, 14485.
5. Bombín, H., & Martin-Delgado, M. A. (2006). Topological quantum distillation. *Physical Review Letters, 97*(18), 180501.
6. Breuer, H. P., & Petruccione, F. (2002). *The Theory of Open Quantum Systems*. Oxford University Press.
7. Bukov, M., Day, A. G. R., Sels, D., *et al.* (2018). Reinforcement learning in different phases of quantum control. *Physical Review X, 8*(3), 031086.
8. Calderbank, A. R., & Shor, P. W. (1996). Good quantum error-correcting codes exist. *Physical Review A, 54*(2), 1098–1105.
9. Dennis, E., Kitaev, A., Landahl, A., & Preskill, J. (2002). Topological quantum memory. *Journal of Mathematical Physics, 43*(9), 4452–4505.
10. Devoret, M. H., & Schoelkopf, R. J. (2013). Superconducting circuits for quantum information: An outlook. *Science, 339*(6124), 1169–1174.
11. Endo, S., Benjamin, S. C., & Li, Y. (2018). Practical quantum error mitigation for near-future applications. *Physical Review X, 8*(3), 031027.
12. Fowler, A. G., Mariantoni, M., Martinis, J. M., & Cleland, A. N. (2012). Surface codes: Towards practical large-scale quantum computation. *Physical Review A, 86*(3), 032324.
13. Google Quantum AI. (2023). Suppressing quantum errors by scaling a surface code logical qubit. *Nature, 614*, 676–681.
14. Gottesman, D. (1997). *Stabilizer Codes and Quantum Error Correction*. Ph.D. Thesis, California Institute of Technology.
15. Gottesman, D. (1998). Theory of fault-tolerant quantum computation. *Physical Review A, 57*(1), 127–137.

16. Jelezko, F., & Wrachtrup, J. (2006). Single defect centres in diamond: A review. *Physica Status Solidi (A), 203*(13), 3207–3225.
17. Kimble, H. J. (2008). The quantum internet. *Nature, 453*(7198), 1023–1030.
18. Kjaergaard, M., Schwartz, M. E., Braumüller, J., *et al.* (2020). Superconducting qubits: Current state of play. *Annual Review of Condensed Matter Physics, 11*, 369–395.
19. Loss, D., & DiVincenzo, D. P. (1998). Quantum computation with quantum dots. *Physical Review A, 57*(1), 120–126.
20. Monroe, C., *et al.* (2021). Programmable quantum simulations of spin systems with trapped ions. *Reviews of Modern Physics, 93*, 025001.
21. Nielsen, M. A., & Chuang, I. L. (2010). *Quantum Computation and Quantum Information* (10th Anniversary ed.). Cambridge University Press.
22. O'Brien, J. L., Furusawa, A., & Vučković, J. (2009). Photonic quantum technologies. *Nature Photonics, 3*, 687–695.
23. Preskill, J. (2018). Quantum computing in the NISQ era and beyond. *Quantum, 2*, 79.
24. Saffman, M., Walker, T. G., & Mølmer, K. (2016). Quantum information with Rydberg atoms. *Reviews of Modern Physics, 82*, 2313–2363.
25. Schlosshauer, M. (2007). *Decoherence and the Quantum-to-Classical Transition*. Springer.
26. Shor, P. W. (1995). Scheme for reducing decoherence in quantum computer memory. *Physical Review A, 52*(4), R2493–R2496.
27. Steane, A. M. (1996). Error correcting codes in quantum theory. *Physical Review Letters, 77*(5), 793–797.
28. Temme, K., Bravyi, S., & Gambetta, J. M. (2017). Error mitigation for short-depth quantum circuits. *Physical Review Letters, 119*(18), 180509.
29. Viola, L., Knill, E., & Lloyd, S. (1999). Dynamical decoupling of open quantum systems. *Physical Review Letters, 82*(12), 2417–2421.
30. Wallman, J. J., & Emerson, J. (2016). Noise tailoring for scalable quantum computation via randomized compiling. *Physical Review A, 94*(5), 052325.
31. Wootters, W. K., & Zurek, W. H. (1982). A single quantum cannot be cloned. *Nature, 299*, 802–803.

SYNTHETIC APPROACHES AND BIOLOGICAL IMPLICATIONS OF HYDRAZIDE-BASED COMPOUNDS IN DRUG DISCOVERY

Kuldeep Singh and Raman Singh*
Department of Applied Chemistry,
Amity University Madhya Pradesh, Gwalior, Madhya Pradesh, India.
*Corresponding author E-mail: bhadauria.raman@gmail.com

Abstract

Hydrazides and their derivatives have versatility in their chemical structures and having various biological properties, such as anti-inflammatory, analgesic, anticonvulsant, anti-tuberculous, antitumor, anti-HIV and other pharmacological activity (Rollas & Küçükgüzel, 2007)(Chimenti *et al.,* 2005) (Loganathan *et al.,* 2025) (Natorska-Chomicka *et al.,* 2026)(Wu *et al.,* 2026). These hydrazides containing compounds attracts researchers for drug design due to their property of forming metal complexes, organo catalysis and also the genesis of different heterocyclic compounds. The ease of preparation, increase hydrolytic stability relative to imines, and tendency towards crystallinity are all desirable characteristics of hydrazides**.**

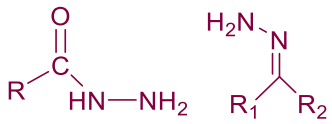

Basic Structure of (1) Hydrazide (2) Hydrazone

Due to these positive traits, hydrazides have been under study for long time, but much of their basic chemistry remains unexplored. Hydrazides (1) in organic chemistry are a class of organic compounds with the formula $R{-}NR^1{-}NR^2R^3$ where R is acyl (R'−C(=O)−), sulfonyl (R'−$S(=O)_2$−), phosphoryl ($(R'-)_2P(=O)-$), phosphonyl ($(R'-O-)_2P(=O)-$), etc. and R^1, R^2, R^3 and R' are any groups (typically hydrogen or organyl). Among the various derivatives of hydrazides, hydrazones are particularly important because they are readily obtained by the condensation of hydrazides with aldehydes or ketones. Hydrazones **(2)** contain two connected nitrogen atoms of different nature and a carbon - nitrogen double bond that is conjugated with a lone pair of the electron of the terminal nitrogen atom. Both nitrogen atoms of the hydrazone group are nucleophilic, although the amino type of nitrogen is more reactive. The carbon atom of hydrazone group has both electrophilic and nucleophilic character. The introduction of functional groups in the hydrazide molecules expands the scope of use of the latter in organic synthesis including medicinal chemistry. Moreover, the combination of the hydrazide group with other functional groups leads to compounds with unique physical and chemical properties. We are here highlighting synthesis, and biological activity of compound containing hydrazides.

Introduction

Hydrazides

Hydrazides are organic compounds contain functional group which is characterized by N to N covalent bond with at least one of them being an acyl group. Due to diverse chemical features and various pharmacological applications hydrazides fascinate the organic chemists.

Ajoy Saha, *etal* developed the green synthesis of hydrazides (Ajoy Saha, Rajesh Kumar*, 2010). Here, a carboxylic acid (RCOOH) reacts with hydrazine hydrate ($NH_2NH_2{\cdot}H_2O$) to form an acid hydrazide (Scheme 1)

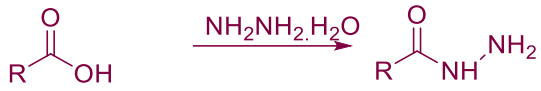

Scheme 1 Synthesis of Acid Hydrazides

Clinically used drugs:

One example of Drug containing hydrazide moiety is Hydrochlorothiazide. Hydrochlorothiazide is known as water pill because of its characteristic to prevent hypertension and fluid retention. It causes the kidneys to get rid of unneeded water and from the body into the urine salt.

Methods of synthesis of Hydrazides:

N-alkyl hydrazine derivatives were syntshesized in one pot manner by using the direct reductive alkylation of hydrazine derivatives with α-picoline-borane. This method was applied to the synthesis of active pharmaceutical ingredients of therapeutic(Kawase *et al.,* 2014) drugs.

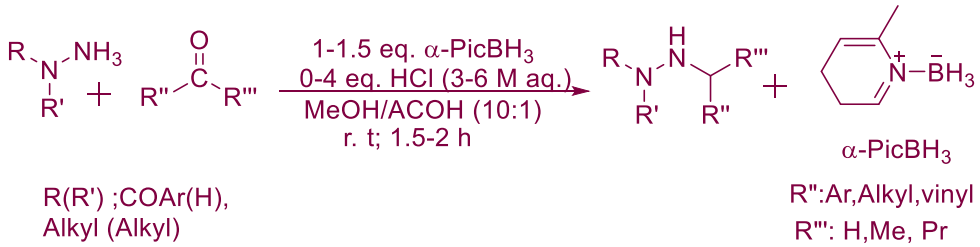

Scheme 2 Synthesis of N,N-Disubstituted Hydrazines

The direct reductive hydrazination promoted by lewis base enables a straightforward and facile synthesis of 1,1-disubstituted hydrazines (Wang *et al.,* 2016) with very good yields. Under the catalysis of *N,N*-dimethylacetamide (DMAc) and hexamethyl phosphoramide (HMPA) various ketones and aldehydes reacted with phenylhdrazines.

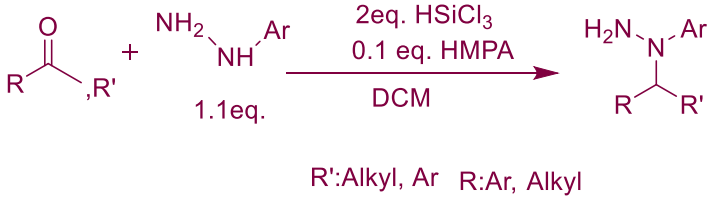

Scheme 3 Synthesis of N-Arylhydrazines

CuI may act as a catalyzed in which coupling of *N*-acyl-*N*′-substituted hydrazines will be occur with aryl iodides affords *N*-acyl-*N*′,*N*′-disubstituted hydrazines regioselectively. *N*-Acyl-*N*′-substituted hydrazines(Xiong *et al.,* 2012) can also react with 2-bromoarylcarbonylic compounds in the presence of 4-hydroxy-L-proline as ligand to provide 1-aryl-1*H*-indazoles.

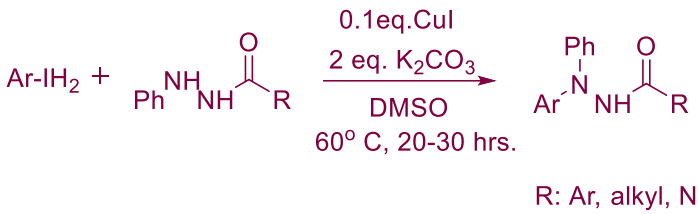

Scheme 4 CuI-Catalyzed Synthesis of N-Acyl-N,N'-Disubstituted Hydrazides

Biological Activities of Hydrazides

Hydrazides as AnticancerAgents

The anticancer properties (Hasdemir *et al.,* 2026) of the Novel N-Acyl Sulfonohydrazides Derived From β-Hydroxy Esters were investigated, along with a complementary study evaluating their antioxidant and antimicrobial properties. The cytotoxicity against HCT116 and PANC1 cancer cell lines revealed generally low antiproliferative effects; however, some compounds demonstrated relatively higher pro-apoptotic potential in HCT116 cells compared to the other compounds.

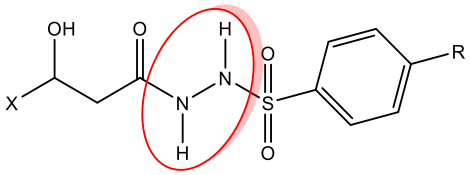

(1)

Hydrazides as Antimycobacterial Agents

Tuberculosis (TB) is caused to the bacterium Mycobacterium tuberculosis. Tuberculosis(Scribner *et al.,* 2008) become associating factor for AIDS infections.The simultaneous presence of HIV infection, the spread of drug resistant strains of *Mycobacterium tuberculosis* (MTB) and the poor compliance with the lengthy complex therapies often complicate the treatment of tuberculosis(Bedia *et al.,* 2006).

Therefore, there is a need to develop new, potent and fast-acting antimycobacterial drugs with low toxicity. In this context new hydrazide derivatives of imidazole[1,2-a]pyridine were synthesized and evaluated for antituberculosis activity. The reaction of 2-[(2-carboxyimidazo[1,2-*a*]pyridine-3-yl) sulfonyl]acetic acid hydrazide with various benzaldehydes gave *N*-(arylidene)-2-[(2-carboxyimidazo[1,2-*a*]pyridine-3-yl)sulfanyl]acetic acid hydrazide derivatives. (Kaplancikli *et al.,* 2008). Joshi *et al.* synthesized a new series of 4-pyrrol-1-yl benzoic acid hydrazide analogs, 5-substituted-2-thiol-1,3,4 oxadiazoles, 5-substituted-4-amino-1,2,4-triazolin-3-thione and 2,5-dimethyl pyrroles and tested for their *in vitro* anti mycobacterial activity against *M. tuberculosis* H_{37}Rv. The results indicated that compound 5-(4-pyrrol-1-yl-

phenyl)-[1,3,4]oxadiazole-2-thiol (**2**), showed potent activity (MIC = 16.0 µg/ml) against *M. tuberculosis* $H_{37}Rv$ as compared to other synthesized derivatives(Joshi *et al.,* 2008).

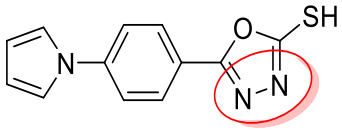

(2)

Hydrazides as Antiplatelet Agents

Cardiovascular diseases are the major cause of natural death all over the world. Some of them are Platelet adhesion and aggregation are key events in homeostasis and thrombosis, which lead to the thrombotic processes, inflammation, immunological diseases and tumor metastasis(McGregor, 2006).Clinical studies reveal that antiplatelet therapy is useful for preventing thrombotic disorders and peripheral vascular diseases(Jackson & Schoenwaelder, 2003). Keeping this view in mind Brito *et al.* synthesizes some derivatives and screen for the antiplatelet activity. Compound (2-thienylidene) 3,4-methylenedioxybenzoylhydrazine) (**3**) showed potent antiplatelet activity among the series (Brito *et al.,* 2010).

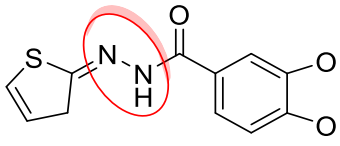

(3)

Hydrazides as Vasodilator Agents

Vasodilator agents are used for the treatment of hypertension. Several vasodilators were synthesized but none of them shows activity without adverse effect. So, It is important to find new vasodilators with a maximum activity and less adverse effects. Inspired by this facts Silva *et al.* were synthesized various *N*-acylhydrazone derivatives and evaluated for their *in vivo* vasodilatory activity. Results showed that Benzo [1,3]dioxole-5-carboxylic acid *N*-methyl-*N*'-(3*H*thiophen-2-ylidene)-hydrazide (4) was found to be seven times more potent than the reference compound LASSBio-294 (IC50 = 74M) in producing an endothelium-independent vasodilator effect(Silva *et al.,* 2005).

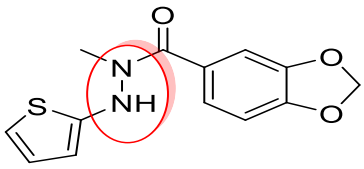

(4)

Hydrazides as Diuretic Agents

Diuretics are used to increase the amount of water and salt expelled from the body as urine. Mainly theses are used to manage hypertension. In this context, Smirnov *et al.* synthesized 3-sulfamoyl-4-chlorobenzoylhydrazone derivatives and tested them for their diuretic activities. The study showed that most of the synthesized hydrazones(Lebedev *et al.,* 1988) exhibits increase in the level of diuresis natri uresis and kali uresis. Compound (5) showed a high kali uretic activity

in the experiments on dogs, exceeding the effect of hypothiazide. The natriuretic and diuretic activities of compound (5) and hypothiazide was comparable.

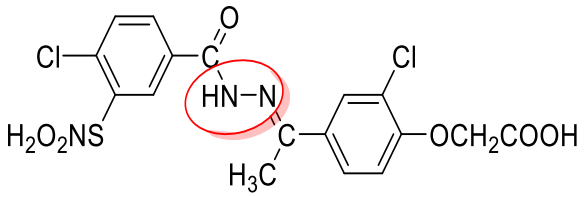

(5)

Hydrazides as Hypoglycemic Agent

Hypoglycemics are the compound which are used to manage diabetes. In this field Several new aryl substituted pyrazole-3-one derivatives were prepared by the reaction of substituted phenyl hydrazine with diethyl ethoxymethylene malonate. Synthesized compounds(Das, N., Verma, A., Shrivastava, P. K., & Shrivastava, 2008) were tested for hypoglycemic activity and among the tested compounds ethyl-2-para nitrophenyl-2,3-dihydro-1H-pyrazole-3-one-4-carboxylate (6) were identified potent hypoglycemic agents. Compound (**6**) showed activity to the standard drug, metformin.

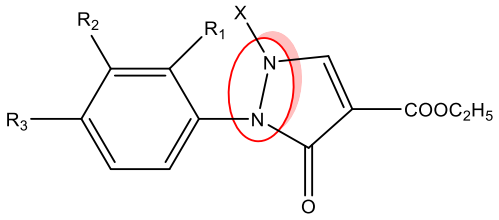

(6)

Hydrazides as Anti-Trypanosomal Agent

Parasite *Trypanosomacruzi* causes Chaga's disease, which lead to the significant mortality. In view of above Hernandes *et al.* synthesized a new series of thiazolyl hydrazones and thiosemicarbazone derivatives and evaluated for their *in vitro* activity against both the epimastigote and trypomastigote forms of *T. cruzi* were identified. Studies showed that 2-{[3-(4-Chloro-phenylsulfanyl)-propylidene]-hydrazono}-5-methylthiazolidin- 4-one (7) and 5-methyl-2-[(3-phenylsulfanylpropylidene)- hydrazono]-thiazolidin-4-one (8)(Hernandes *et al.,* 2010) were found to be the most potent anti trypanosomal agents.

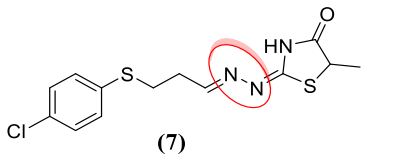

(7)

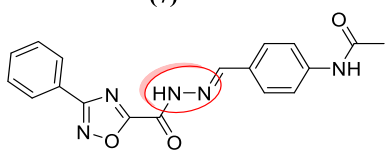

(8)

De Oliveira *et al.* were the synthesized two new series of 3-(4- substituted-aryl)-1,2,4-oxadiazole-*N*-acylhydrazones and evaluated against epimastigote and trypomastigote forms of

T.cruzi. Among the series *N*-{4-[(3-phenyl-[1,2,4]oxadiazole-5-carbonyl)-hydrazonomethyl]-phenyl}-acetamide **(9)** exhibited potent activity(De Oliveira *et al.,* 2012).

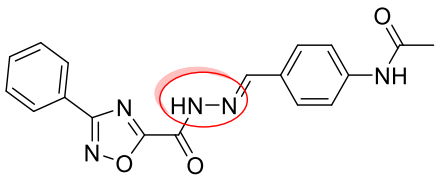

(9)

Hydrazides as Antimalarial Agents

Malaria is a life-threatening blood disease caused by parasites transmitted to humans through the bite of the Anopheles mosquito. A series of N^1-arylidene-N^2-quinolyl- and N^2-acrydinylhydrazones(Gemma *et al.,* 2006) were synthesized and tested *in vitro* against a series of *Plasmodium falciparum* (*Pf*) strains, The results revealed that *N*-(6-chloro-2- methoxy-acridin-9-yl)-*N*'-(1*H*-imidazol-2-ylmethylene)-hydrazine (**10**) and *N*-(7-chloro-quinolin-4-yl)-*N*'-(4-pyrrolidin-1-ylmethylbenzylidene)-hydrazine (**11**) were most active compounds.

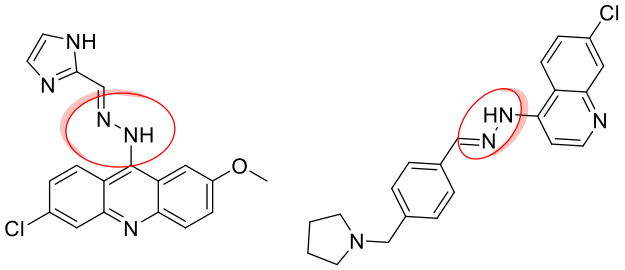

(10) (11)

Hydrazides as Antioxidant and Neuroprotective Activity

Pyrrole-based hydrazide-hydrazones **(12)** are promising complexes that may be effective for treating neurodegenerative diseases. Karatchobanov *et al.* (2026) synthesized ten new pyrrole-based hydrazide-hydrazone compounds and assessed their biological activities. Among these, compounds few compounds showed the strongest antioxidant and neuroprotective effects with the lowest neurotoxicity. Their pharmacokinetic properties were predicted using computer-based methods, and DFT analysis was performed to study their stability and chemical reactivity (Karatchobanov *et al.,* 2026).

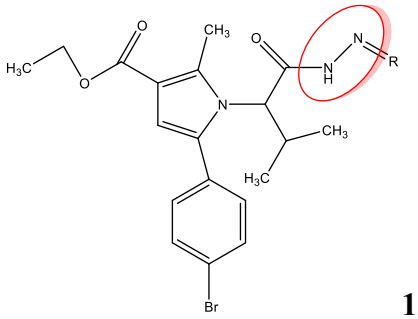

12

References

1. Saha, A., Kumar, R., R. K., & C. D. (2010). Development and assessment of green synthesis of hydrazides. *Indian Journal of Chemistry, Section B, 49B*, 526–531.

https://www.researchgate.net/publication/216046147_Development_and_Assessment_of_Green_Synthesis_of_Hydrazides

2. Bedia, K.-K., Elçin, O., Seda, U., Fatma, K., Nathaly, S., Sevim, R., & Dimoglo, A. (2006). Synthesis and characterization of novel hydrazide–hydrazones and the study of their structure–antituberculosis activity. *European Journal of Medicinal Chemistry, 41*(11), 1253–1261. https://doi.org/10.1016/j.ejmech.2006.06.009
3. Brito, F. C. F., Kummerle, A. E., Lugnier, C., Fraga, C. A. M., Barreiro, E. J., & Miranda, A. L. P. (2010). Novel thienylacylhydrazone derivatives inhibit platelet aggregation through cyclic nucleotides modulation and thromboxane A2 synthesis inhibition. *European Journal of Pharmacology, 638*(1–3), 5–12. https://doi.org/10.1016/j.ejphar.2010.04.003
4. Chimenti, F., Maccioni, E., Secci, D., Bolasco, A., Chimenti, P., Granese, A., Befani, O., Turini, P., Alcaro, S., Ortuso, F., Cirilli, R., La Torre, F., Cardia, M. C., & Distinto, S. (2005). Synthesis, molecular modeling studies, and selective inhibitory activity against monoamine oxidase of 1-thiocarbamoyl-3,5-diaryl-4,5-dihydro-(1H)-pyrazole derivatives. *Journal of Medicinal Chemistry, 48*(23), 7113–7122. https://doi.org/10.1021/jm040903t
5. Das, N., Verma, A., Shrivastava, P. K., & Shrivastava, S. (2008). Synthesis and biological evaluation of some new aryl pyrazol-3-one derivatives as potential hypoglycemic agents. *Indian Journal of Chemistry, Section B, 47B*(10), 1555–1558. https://www.scirp.org/reference/referencespapers?referenceid=3779768
6. De Oliveira, C. S., Lira, B. F., Barbosa-Filho, J. M., Lorenzo, J. G. F., & De Athayde-Filho, P. F. (2012). Synthetic approaches and pharmacological activity of 1,3,4-oxadiazoles: A review of the literature from 2000–2012. *Molecules, 17*(9), 10192–10231. https://doi.org/10.3390/molecules170910192
7. Gemma, S., Kukreja, G., Fattorusso, C., Persico, M., Romano, M. P., Altarelli, M., Savini, L., Campiani, G., Fattorusso, E., Basilico, N., Taramelli, D., Yardley, V., & Butini, S. (2006). Synthesis of N1-arylidene-N2-quinolyl- and N2-acrydinylhydrazones as potent antimalarial agents active against CQ-resistant *P. falciparum* strains. *Bioorganic & Medicinal Chemistry Letters, 16*(20), 5384–5388. https://doi.org/10.1016/j.bmcl.2006.07.060
8. Hasdemir, B., Yıldız, T., Yaşa, H., Küçük, H. B., Kara, E. M., Yıldırım, S., Kocabaş, F., & Can, Z. (2026). Design, synthesis, and biological evaluation of novel N-acyl sulfonohydrazides derived from β-hydroxy esters: Anticancer, antioxidant, and antimicrobial activities. *Chemical Biology & Drug Design, 107*(6), e70344. https://doi.org/10.1111/cbdd.70344
9. Hernandes, M. Z., Rabello, M. M., Leite, A. C. L., Cardoso, M. V. O., Moreira, D. R. M., Brondani, D. J., Simone, C. A., Reis, L. C., Souza, M. A., Pereira, V. R. A., Ferreira, R. S.,

& McKerrow, J. H. (2010). Studies toward the structural optimization of novel thiazolylhydrazone-based potent antitrypanosomal agents. *Bioorganic & Medicinal Chemistry, 18*(22), 7826–7835. https://doi.org/10.1016/j.bmc.2010.09.056

10. Jackson, S. P., & Schoenwaelder, S. M. (2003). Antiplatelet therapy: In search of the "magic bullet." *Nature Reviews Drug Discovery, 2*(10), 775–789. https://doi.org/10.1038/nrd1198
11. Joshi, S. D., Vagdevi, H. M., Vaidya, V. P., & Gadaginamath, G. S. (2008). Synthesis of new 4-pyrrol-1-yl benzoic acid hydrazide analogs and some derived oxadiazole, triazole and pyrrole ring systems: A novel class of potential antibacterial and antitubercular agents. *European Journal of Medicinal Chemistry, 43*(9), 1989–1996. https://doi.org/10.1016/j.ejmech.2007.11.016
12. Kaplancikli, Z. A., Turan-Zitouni, G., Ozdemir, A., & Teulade, J. (2008). Synthesis and antituberculosis activity of new hydrazide derivatives. *Archiv der Pharmazie, 341*(11), 721–724. https://doi.org/10.1002/ardp.200800048
13. Karatchobanov, V., Mateev, E., Valkova, I., Kondeva-Burdina, M., & Georgieva, M. (2026). Novel pyrrole-based hydrazide-hydrazones: Synthesis, *in vitro* evaluation of antioxidant and neuroprotective activity, *in silico* ADME, and DFT studies. *Antioxidants, 15*(6). https://doi.org/10.3390/antiox15060666
14. Kawase, Y., Yamagishi, T., Kato, J., Kutsuma, T., Kataoka, T., Iwakuma, T., & Yokomatsu, T. (2014). Reductive alkylation of hydrazine derivatives with α-picoline-borane and its applications to the syntheses of useful compounds related to active pharmaceutical ingredients. *Synthesis, 46*(4), 455–464. https://doi.org/10.1055/s-0033-1340484
15. Lebedev, A. A., Smirnov, V. A., Posokhov, V. P., & Simerzina, L. V. (1988). Synthesis and diuretic activity of 3-sulfamoyl-4-chlorobenzoyl hydrazones of aromatic aldehydes. *Pharmaceutical Chemistry Journal, 22*(9), 683–685. https://doi.org/10.1007/BF00763662
16. Loganathan, V., Manilal, A., & Akbar, I. (2025). Design and synthesis of vanillin-mediated hydrazine derivatives as multi-bioactive drug development. *Future Medicinal Chemistry, 17*(23), 2851–2862. https://doi.org/10.1080/17568919.2025.2580927
17. McGregor, L. (2006). Platelet-leukocyte aggregates and derived microparticles in inflammation, vascular remodelling and thrombosis. *Frontiers in Bioscience, 11*(1), 830. https://doi.org/10.2741/1840
18. Natorska-Chomicka, D., Gawrońska-Grzywacz, M., Patrejko, P., Herbet, M., Piątkowska-Chmiel, I., Iwan, M., Dudka, J., & Popiołek, Ł. (2026). Novel experimental therapeutic approaches in glioma—New hydrazide-hydrazones as chemical agents sensitizing

glioblastoma cell line to radiotherapy. *International Journal of Molecular Sciences, 27*(12). https://doi.org/10.3390/ijms27125459

19. Rollas, S., & Küçükgüzel, S. G. (2007). Biological activities of hydrazone derivatives. *Molecules, 12*(8), 1910–1939. https://doi.org/10.3390/12081910
20. Scribner, A., Dennis, R., Lee, S., Ouvry, G., Perrey, D., Fisher, M., Wyvratt, M., Leavitt, P., Liberator, P., Gurnett, A., Brown, C., Mathew, J., Thompson, D., Schmatz, D., & Biftu, T. (2008). Synthesis and biological activity of imidazopyridine anticoccidial agents: Part II. *European Journal of Medicinal Chemistry, 43*(6), 1123–1151. https://doi.org/10.1016/j.ejmech.2007.09.013
21. Silva, A. G., Zapata-Sudo, G., Kummerle, A. E., Fraga, C. A. M., Barreiro, E. J., & Sudo, R. T. (2005). Synthesis and vasodilatory activity of new N-acylhydrazone derivatives, designed as LASSBio-294 analogues. *Bioorganic & Medicinal Chemistry, 13*(10), 3431–3437. https://doi.org/10.1016/j.bmc.2005.03.003
22. Wang, T., Di, X., Wang, C., Zhou, L., & Sun, J. (2016). Reductive hydrazination with trichlorosilane: A method for the preparation of 1,1-disubstituted hydrazines. *Organic Letters, 18*(8), 1900–1903. https://doi.org/10.1021/acs.orglett.6b00675
23. Wu, L., Tian, H., Zhang, Y., Ma, W., Zhang, Q., Chen, R., & Chen, X. (2026). A new and efficient synthesis of substituted 2-amino-1,3,4-oxadiazoles from isothiocyanates and hydrazides. *BMC Chemistry*. https://doi.org/10.1186/s13065-026-01845-7
24. Xiong, X., Jiang, Y., & Ma, D. (2012). Assembly of *N,N*-disubstituted hydrazines and 1-aryl-1H-indazoles via copper-catalyzed coupling reactions. *Organic Letters, 14*(10), 2552–2555. https://doi.org/10.1021/ol300847v

Bhumi Publishing, India
June 2026

ADVANCES IN CHEMISTRY AND FUNCTIONAL MATERIALS: FROM INNOVATION TO APPLICATION

S. Umarani
Department of Chemistry (Science and Humanities),
Hindusthan Institute of Technology, Coimbatore-641032, Tamil nadu, India
Corresponding author E-mail: umarani.kalidas@gmail.com

Abstract
Over the past few decades, chemistry and materials science have seen significant transformation. This is due to people's desire to create environmentally friendly and useful products. We need technologies that are sustainable and we need to make healthcare better. We also need to make energy systems that're efficient and manufacturing processes that are smart. Chemistry and materials science have made a lot of progress because of discoveries in nanotechnology, smart materials, green chemistry and biomaterials. Now we have materials that can sense things respond to things heal themselves and adapt to changes in the environment. Green chemistry is equally vital since it ensures that we manufacture in an environmentally friendly manner. The current chapter focuses on the advancements in chemistry and material science. It also talks about trends, technologies and applications.

Keywords: Chemical Innovation, Materials Science, Nanotechnology, Smart Materials, Green Chemistry, Functional Materials, Biomaterials, Sensors and Sustainable Materials.

1. Introduction

The foundation of technology is chemistry and materials science. They improve our lives and contribute to the expansion of our economy. They are used in the production of electronics, medications, and many other items. We can now create materials that do more than just support us. Thanks to developments in computational material design, molecular engineering, and nanotechnology, we can make them perform tasks.

Green chemistry principles also allow us to create environmentally friendly products. Green nanotechnology enables us to create environmentally friendly and sustainable nanomaterials.

2. Advanced Nanomaterials and Nanotechnology

2.1 Synopsis of Nanomaterials

Nanomaterials are minuscule. They possess unique qualities. They have applications in energy storage, medicine, and environmental cleaning.

There are some frequently used nanomaterials which include metal nanoparticles, metal oxide nanoparticles, carbon nanotubes, graphene, and quantum dots.

2.2 Graphene and Two-Dimensional Materials

The graphene is an interesting material that has good electrical conductivity and is very strong with a large surface area.

Other materials including molybdenum disulfide, black phosphorous and MXenes are also very important and have great potential for use in sensors, flexible electronics, batteries, and biomedical devices.

2.3 Green Nanomaterials

Green nanomaterials are produced through processes that are environmentally friendly. Materials obtained from plants, microbial species, and biopolymers are employed for their feedstock materials.

The advantages of such materials include non-toxicity, energy efficiency, and sustainable production.

3. Intelligent Materials and Smart Structures

Intelligent materials change due to variations in environmental parameters such as temperature, pressure, and light intensity.

3.1 Types of Smart Materials

There are types of smart materials like shape memory alloys, piezoelectric materials, electrochromic materials and self-healing materials.

They can be applied to robotics, aircraft, and medical devices, among other fields.

In industries like intelligent systems, environmental monitoring, and healthcare, smart materials are crucial.

4. Innovation in Green Chemistry

Green chemistry is the idea of creating ecologically friendly processes and products.

4.1 Principles of Green Chemistry

The process of chemical synthesis involves shorter reaction time, energy consumption and waste creation.

4.2 Chemical Synthesis

We have made many new ways to synthesize chemicals, like solvent-free reactions microwave-assisted synthesis and ultrasonic synthesis.

These techniques lower energy use, reaction times, and the production of hazardous waste.

5. Cutting Edge Functional Materials

Features that allow them to be used for many purposes make up functional materials.

5.1 Conductive Polymers

Conductive polymers are employed in electronic devices and biosensors for energy storage purposes.

5.2 Metal-Organic Frameworks (MOFs)

Metal-organic frameworks represent porous materials that are capable of gas storage and carbon capture as well as drug delivery

5.3 Hybrid Nanocomposites

Inorganic components are combined in hybrid materials to produce better qualities. They can be utilized in biomedical devices, structural materials, and water purification.

6. Innovations in Biomedical Materials

Materials science has transformed healthcare through the development of advanced biomaterials.

6.1 Systems for Drug Delivery

Drug delivery can be highly targeted thanks to Nano carriers, which boosts their efficacy and reduces any potential side effects.

6.2 Engineering Tissue

Biomaterials may be used to construct organs and rejuvenate tissues.

6.3 Diagnostics and Biosensors

Biosensors are contemporary gadgets that use fluorescence, electrochemical methods, and nanomaterials to monitor the environment and identify diseases.

7. Energy-Related Materials

Our world faces a problem with energy.

7.1 Cutting-Edge Battery Materials

We have created new battery materials, such as sodium-ion, solid-state, and lithium-ion batteries.

7.2 Materials for Hydrogen Storage

Energy innovations benefit from the effective storage of hydrogen by nanostructured materials.

7.3 Materials for Solar Energy

For the creation of cells, cutting-edge materials like organic photovoltaics, quantum dots, and perovskites are being used.

8. Applications in the Environment

8.1 Purification of Water

Advanced materials can remove metals, dyes and pathogens from water.

8.2 Pollution Control

Materials are now capable of absorbing carbon dioxide, volatile organic compounds, and other pollutants from industries.

8.3 Circular Economy Materials

Our goal is to create materials that can be repurposed and recycled.

9. Chemical and Material Science Artificial Intelligence

Artificial intelligence is increasingly being used to find new materials.

AI may be used to develop materials, forecast properties, and optimise manufacturing processes.

It can even aid in the development of new materials and drugs.

10. Difficulties and Prospects

Even after all the achievements, challenges lie ahead of us

11. Chemistry and materials science are changing our world

They are helping us make technologies, better healthcare and more efficient energy systems.

Our ability to collaborate and apply our expertise to produce new discoveries will determine the future.

12. Current Chemistry and Materials Science Case Studies

12.1 Case Study 1: Healthcare Wearable Biosensors Based on Graphene

Graphene is a useful material that can be utilised to create body-worn biosensors.

These biosensors have the ability to track health and identify illnesses.

They have a high degree of sensitivity. can identify even the smallest changes in the body.

The development of graphene-based biosensors has advanced somewhat. Biosensors could help with real-time health monitoring. Graphene is an excellent electrical conductor. It is adaptable. We can use it in our bodies without risk. Because of this, graphene is ideal for health tracking devices. Scientists have developed graphene-based sensors that can monitor blood sugar levels, examine perspiration, and identify cardiac issues. These gadgets provide us with quick and highly accurate non-invasive monitoring. Graphene and intelligence work together to improve data analysis. These graphene-based technologies can provide you with individualised medical recommendations.

12.2 Case Study 2: Perovskite Solar Cells to Efficiently Convert Energy

Perovskite cells produce energy using the same methodology as solar cells. They have achieved power conversion efficiencies of over 26% which's close to traditional silicon-based solar cells. Perovskite materials have advantages, including production costs, lightweight structures and easy fabrication methods. Currently researchers are working on improving their long-term stability resistance to factors and large-scale commercialization of solar cells.

12.3 Case Study 3: Carbon Capture Using Metal Organic Frameworks

The Metal Organic Frameworks have been widely used in the capturing of carbon dioxide based on the porosity characteristic and capacity of pore size manipulation. Metal-Organic Frameworks for Carbon Capture work very well at carbon dioxide capture because of their porosity and customized pores. Several MOF-based systems have shown potential for capturing carbon dioxide from emissions after combustion. These materials offer selectivity, low energy requirements for regeneration and significant potential for reducing greenhouse gas emissions from metal- frameworks.

12.4 Case Study 4: Synthesis of Nanoparticles for Water Treatment

We can now produce metal nanoparticles using green synthesis approaches that utilize plant extracts. Nanoparticles based on silver, iron oxide, and zinc oxide produced via such processes have been efficient in removing heavy metals, dyes, and microbes from water. These sustainable technologies reduce chemical waste. Make green nanoparticles environmentally friendly.

12.5 Case Study 5: AI and Materials Discovery

Use of AI is one major breakthrough in the field of materials discovery due to their desired properties. Recent AI platforms have successfully predicted battery materials, catalysts and drug-delivery nanostructures from intelligence. Autonomous laboratories that integrate robotics and machine learning can conduct thousands of experiments with intervention significantly reducing development time and costs of artificial intelligence-driven materials discovery.

13. Comparison of Emerging Materials and Their Applications

S. No.	Material/System	Key Properties	Major Applications	Advantages	Current Challenges
1	Graphene	High conductivity, strength, flexibility	Sensors, electronics, batteries	Excellent electrical performance	Large-scale production
2	MXenes	High conductivity, surface functionality	Supercapacitors, sensors	Fast charge transport	Oxidation stability
3	MOFs	High porosity, tunable structures	Carbon capture, gas storage	Exceptional adsorption capacity	Moisture sensitivity
4	Conductive Polymers	Electrical conductivity, flexibility	Flexible electronics, biosensors	Lightweight and processable	Long-term stability
5	Hydrogels	High water content, biocompatibility	Tissue engineering, drug delivery	Excellent biological compatibility	Mechanical weakness
6	Perovskites	High photovoltaic efficiency	Solar cells	Low-cost fabrication	Stability concerns
7	Smart Alloys (Nitinol)	Shape memory effect	Medical devices, aerospace	Self-actuation capability	High manufacturing cost
8	Green Nanomaterials	Eco-friendly synthesis	Environmental remediation	Sustainable production	Scale-up limitations

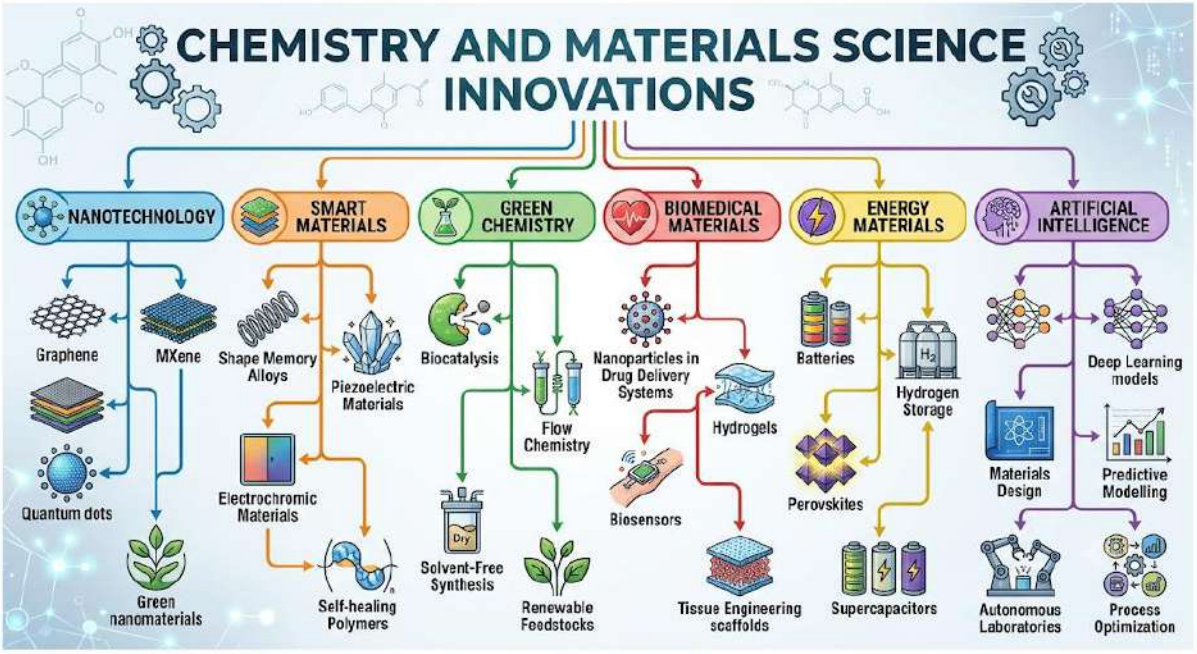

References

1. Martins, R., & Kaczerewska, O. (2021). Green nanotechnology: The latest innovations, knowledge gaps and future perspectives. *Applied Sciences*.
2. Kumar, A., *et al.* (2024). Integrating green nanotechnology with sustainable development goals: A pathway to sustainable innovation.
3. Thakur, S., *et al.* (2026). Graphene oxide as smart sustainable nanomaterial. *npj Materials Sustainability*.
4. Singh, H., *et al.* (2026). Next-generation nanomaterials for environmental remediation. *Frontiers in Chemistry*.
5. Nag, A., & Chaudhuri, D. (2026). Advances in nanomaterials for energy and sensing applications. *Discover Electronics*.
6. Ramakrishnan, T., Senthil Kumar, S., Chelladurai, S. J. S., Gnanasekaran, S., Sivananthan, S., Geetha, N. K., Arthanari, R., & Assefa, G. B. (2022). Recent developments in stimuli responsive smart materials and applications: An overview. *Journal of Nanomaterials*, 2022, 4031059.
7. *Materials Today Communications: Recent trends in green nanomaterials: Synthesis, properties and applications*. (2024). *SSRN First Look*.
8. Sharma, K., Dahiya, Y., & Ichikawa, T. Recent advances in nanomaterials: Synthesis, properties, and applications.
9. Geim, A. K., & Novoselov, K. S. (2007). The rise of graphene. *Nature Materials, 6*(3), 183–191.
10. Bhushan, B. (Ed.). (2017). *Springer handbook of nanotechnology* (4th ed.). Springer.

11. Kharissova, O. V., Dias, H. R., Kharisov, B. I., Pérez, B. O., & Pérez, V. M. J. (2013). The greener synthesis of nanoparticles. *Trends in Biotechnology, 31*(4), 240–248.
12. Ahmed, S., Ahmad, M., Swami, B. L., & Ikram, S. (2016). A review on plant extract mediated synthesis of silver nanoparticles for antimicrobial applications: A green expertise. *Journal of Advanced Research, 7*(1), 17–28.
13. Iravani, S. (2011). Green synthesis of metal nanoparticles using plants. *Green Chemistry, 13*(10), 2638–2650.
14. Novoselov, K. S., Mishchenko, A., Carvalho, A., & Castro Neto, A. H. (2016). 2D materials and van der Waals heterostructures. *Science, 353*(6298).
15. Chhowalla, M., Shin, H. S., Eda, G., Li, L.-J., Loh, K. P., & Zhang, H. (2013). The chemistry of two-layered transition metal dichalcogenide nanosheets. *Nature Chemistry, 5*(4), 263–275.
16. Naguib, M., Mochalin, V. N., Barsoum, M. W., & Gogotsi, Y. (2014). MXenes: A family of two-dimensional materials. *Materials Today, 26*(7), 992–1005.
17. Otsuka, K., & Wayman, C. M. *Shape memory materials*. Cambridge University Press.
18. Hager, M. D., Greil, P., Leyens, C., van der Zwaag, S., & Schubert, U. S. (2010). Self-healing materials. *Advanced Materials, 22*(47), 5424–5430.
19. Hu, J., Meng, H., Li, G., & Ibekwe, S. I. (2012). A review of stimuli-responsive polymers. *Smart Materials and Structures, 21*(5), 053001.
20. Addington, D. M., & Schodek, D. L. *Smart materials and new technologies*. Elsevier.
21. Anastas, P. T., & Warner, J. C. *Green chemistry: Theory and practice*. Oxford University Press.
22. Sheldon, R. A. (2016). Green chemistry and resource efficiency. *Green Chemistry, 18*(11), 3180–3183.
23. Poliakoff, M., Fitzpatrick, J. M., Farren, T. R., & Anastas, P. T. (2002). Green chemistry: Science and politics of change. *Science, 297*(5582), 807–810.
24. Clark, J. H., & Tavener, S. J. (2007). Alternative solvents. *Organic Process Research & Development, 11*(1), 149–155.
25. Furukawa, H., Cordova, K. E., O'Keeffe, M., & Yaghi, O. M. (2013). The applications of metal-organic frameworks. *Science, 341*(6149), 1230444.
26. Li, J.-R., Kuppler, R. J., & Zhou, H.-C. (2009). Selective gas adsorption and separation in MOFs. *Chemical Society Reviews, 38*(5), 1477–1504.
27. Yaghi, O. M., Kalmutzki, M. J., & Diercks, C. S. *Introduction to reticular chemistry*. Wiley-VCH.
28. Skotheim, T. A., & Reynolds, J. R. *Handbook of conducting polymers*. CRC Press.

29. Langer, R., & Tirrell, D. A. (2004). Designing materials for biology and medicine. *Nature, 428*, 487–492.
30. Ratner, B. D., Hoffman, A. S., Schoen, F. J., & Lemons, J. E. *Biomaterials science*. Academic Press.
31. Peppas, N. A., Hilt, J. Z., Khademhosseini, A., & Langer, R. (2006). Hydrogels in biology and medicine. *Advanced Materials, 18*(11), 1345–1360.
32. Farokhzad, O. C., & Langer, R. (2009). Impact of nanotechnology on drug delivery. *ACS Nano, 3*(1), 16–20.
33. Goodenough, J. B., & Park, K.-S. (2013). The Li-ion rechargeable battery. *Journal of the American Chemical Society, 135*(4), 1167–1176.
34. Tarascon, J.-M., & Armand, M. (2001). Issues and challenges facing lithium batteries. *Nature, 414*, 359–367.
35. Manthiram, A. (2020). A reflection on lithium-ion battery cathode chemistry. *Nature Communications, 11*, 1550.
36. Kojima, A., Teshima, K., Shirai, Y., & Miyasaka, T. (2009). Organometal halide perovskites as light sensitizers. *Journal of the American Chemical Society, 131*(17), 6050–6051.
37. Shannon, M. A., Bohn, P. W., Elimelech, M., Georgiadis, J. G., Marinas, B. J., & Mayes, A. M. (2008). Science and technology for water purification. *Nature, 452*, 301–310.
38. Wang, Z., Dai, Z., & Lin, S. Advanced nanomaterials for water treatment and environmental remediation. *Environmental Science & Technology, 57*, 11245–11268.
39. Geyer, R., Jambeck, J. R., & Law, K. L. (2017). Production, use and fate of plastics. *Science Advances, 3*(7), e1700782.
40. Butler, K. T., Davies, D. W., Cartwright, H., Isayev, O., & Walsh, A. (2018). Machine learning for molecular and materials science. *Nature, 559*, 547–555.
41. Stach, E., DeCost, B., Kusne, A., Hattrick-Simpers, J., & Brown, K. (2021). Autonomous experimentation systems for materials development. *Nature Reviews Materials, 6*, 9–18.
42. Schmidt, J., Marques, M. R. G., Botti, S., & Marques, M. A. L. (2019). Recent advances and applications of machine learning in solid-state materials science. *npj Computational Materials, 5*, 83.
43. Jain, A., Shin, Y., & Persson, K. A. (2016). Computational predictions of energy materials using materials databases. *Nature Reviews Materials, 1*, 15004.

Bhumi Publishing, India
June 2026

NICKEL SULFIDE THIN FILMS: SYNTHESIS, OPTICAL, ELECTRICAL, AND THERMOELECTRIC PROPERTIES

Prashant A. Chate[1] and Dattatray J. Sathe[2]

[1]Department of Chemistry, J. S. M. College, Alibag (M.S.) India

[2]Department of Chemistry, KIT College of Engg (Autonomous), Kolhapur (M.S.) India.

Corresponding author E-mail: pachate04@rediffmail.com, djsathe77@gmail.com

1. Introduction

Transition metal chalcogenides (TMCs) have attracted considerable scientific and technological interest over the past few decades due to their rich structural chemistry and diverse physical properties. These compounds, formed between transition metals and group VI elements (S, Se, Te), exhibit a wide range of electronic behaviors spanning from metallic and semiconducting to semimetallic characteristics. Among them, nickel sulfide (NiS) has emerged as a particularly intriguing material due to its complex phase behavior, variable stoichiometry, and multifunctional properties [1-3].

NiS belongs to the family of nickel chalcogenides, which includes NiS, NiS_2, Ni_3S_2, Ni_3S_4, and Ni_7S_6. Each of these phases exhibits distinct crystallographic structures and electronic properties, making nickel sulfides highly tunable materials [4]. The Ni–S system is especially notable for its non-stoichiometric nature, where slight variations in composition can significantly alter electrical conductivity, optical response, and catalytic activity. This tunability makes NiS a versatile material for applications in energy storage, catalysis, sensing, and optoelectronic devices. In thin film form, NiS becomes even more attractive because its properties can be engineered through controlled deposition parameters such as substrate temperature, precursor concentration, pH of the reaction bath, and post-deposition annealing conditions. These parameters strongly influence crystallite size, grain boundary density, defect states, and phase formation, all of which determine the functional performance of the film [5-7].

One of the most fascinating aspects of NiS is its structural diversity. NiS primarily exists in two important crystallographic forms: the hexagonal millerite structure (commonly referred to as α-NiS) and the rhombohedral heazlewoodite-related structure (β-NiS). The α-phase is stable at higher temperatures and exhibits metallic behavior, while the β-phase is more stable at lower temperatures and displays semiconducting characteristics. The phase transition between these structures is accompanied by significant changes in electrical resistivity and lattice arrangement. This metal–semiconductor transition is a subject of extensive research, as it provides insights into correlated electron systems and defect-driven conductivity mechanisms. Furthermore, the presence of intrinsic defects such as nickel vacancies and sulfur interstitials plays a crucial role

in defining the electronic structure of NiS thin films. From a crystallographic perspective, NiS typically exhibits hexagonal symmetry with lattice parameters that vary depending on synthesis conditions. The degree of crystallinity, preferred orientation, and grain size are strongly influenced by the deposition technique employed. In thin film systems, texture development is often observed along specific crystallographic planes, which can enhance charge transport and catalytic activity [8-10].

The fabrication of NiS thin films has been achieved using a variety of physical and chemical techniques, each offering unique advantages in terms of film quality, cost, and scalability. Common deposition methods include: chemical bath deposition (CBD) [11], spray pyrolysis [12], Electrodeposition [13], successive ionic layer adsorption and reaction [14], sol–gel processing [15], chemical vapor deposition, atomic layer deposition. Among these, solution-based methods such as CBD, successive ionic layer adsorption and reaction, and electrodeposition are widely preferred due to their simplicity, low processing temperature, and ability to coat large-area substrates. These methods allow precise control over nucleation and growth processes by adjusting reaction kinetics and ionic concentrations in the solution. Post deposition treatments, such as annealing in inert or sulfur rich atmospheres, further influence the crystallinity and phase purity of NiS films. Annealing often improves grain connectivity, reduces structural defects, and enhances electrical conductivity, although excessive heat treatment may lead to phase transformation or sulfur loss.

NiS thin films exhibit interesting optical and electronic properties that make them suitable for a variety of device applications. The material typically shows strong absorption in the visible region, making it a potential candidate for photovoltaic and photoelectrochemical systems. The optical band gap of NiS thin films varies depending on phase composition, crystallite size, and defect concentration, generally lying in the range of narrow band gap semiconductors. Quantum confinement effects may also influence the band gap in nanostructured films.

Electrically, NiS can behave as either a semiconductor or a near-metallic conductor. This dual nature arises from its complex band structure and high density of defect states. The conductivity is strongly dependent on temperature, phase purity, and stoichiometric ratio. In many cases, NiS exhibits p-type conductivity due to nickel vacancies acting as acceptor states.

This chapter provides a comprehensive overview of NiS thin films, including their, synthesis approaches, and functional properties.

2. Synthesis of NiS Thin Films

The synthesis of NiS thin films plays a decisive role in determining their structural, morphological, optical, and electrochemical properties. Because NiS exhibits multiple phases, variable stoichiometry, and strong defect sensitivity, careful control of deposition conditions is essential to obtain phase-pure and high-performance films. Over the past few decades, both

physical and chemical deposition techniques have been developed to fabricate NiS thin films with tailored properties for applications in energy storage, catalysis, sensing, and optoelectronics. In general, NiS thin film growth involves the controlled reaction of nickel ions (Ni^{2+}) with sulfur precursors such as thiourea, thioacetamide, sodium sulfide, or elemental sulfur sources under suitable thermodynamic and kinetic conditions. The nucleation and growth behavior depends strongly on substrate nature, solution chemistry, temperature, and deposition time. These parameters determine grain formation, crystallite size, film thickness, and phase evolution.

2.1 Chemical Bath Deposition (CBD)

Chemical bath deposition is one of the most widely used techniques for synthesizing NiS thin films due to its simplicity, low cost, and ability to coat large-area substrates at relatively low temperatures. In CBD, the substrate is immersed in an aqueous solution containing nickel salts such as $NiCl_2$, $NiSO_4$, or $Ni(NO_3)_2$ and a sulfur source like thiourea or thioacetamide. Controlled release of S^{2-} ions occurs through thermal decomposition of the precursor in an alkaline medium, leading to the gradual formation of NiS on the substrate surface. The growth process typically follows three stages: ion-by-ion deposition on the substrate surface, nucleation of NiS clusters, coalescence into a continuous thin film. The deposition rate is governed by pH, complexing agents such as ammonia, triethanolamine, or citrate ions, temperature, and precursor concentration. Complexing agents are particularly important as they regulate the free Ni^{2+} ion concentration, preventing rapid precipitation in solution and promoting uniform film formation. CBD offers excellent control over thickness and morphology, but challenges include poor adhesion in some cases, long deposition times, and difficulty in achieving precise phase control when multiple NiS phases coexist.

2.3 Successive Ionic Layer Adsorption and Reaction (SILAR)

The SILAR method is a highly effective layer-by-layer deposition technique used for fabricating nanostructured NiS thin films. SILAR involves alternate immersion of the substrate in cationic (Ni^{2+}) and anionic (S^{2-}) precursor solutions. Each cycle results in the adsorption of ions followed by chemical reaction on the substrate surface, forming a thin layer of NiS. Each deposition cycle consists of four steps: immersion in Ni^{2+} solution (adsorption of Ni ions), rinsing in deionized water (removal of loosely bound ions), immersion in sulfur source solution (reaction with S^{2-}), and final rinsing step. By controlling the number of cycles, film thickness can be precisely tuned at the nanometer scale. The advantages of this method are excellent thickness control, low-temperature deposition, high uniformity over large areas, suitable for nanostructured films. However, film adhesion and crystallinity may require post-deposition annealing.

2.4 Electrodeposition Method

Electrodeposition is a powerful electrochemical technique for synthesizing NiS thin films directly onto conductive substrates such as FTO glass, stainless steel, or graphite. In this method,

Ni^{2+} ions are reduced at the cathode surface in the presence of sulfur species, forming NiS through electrochemical reactions. The process is governed by applied potential or current density. A simplified reaction pathway can be expressed as $Ni^{2+} + S^{2-} \rightarrow$ NiS (solid film on electrode surface). Sulfur ions are often generated in situ from thiourea or sodium thiosulfate under cathodic polarization. Key parameters for synthesis process are applied potential/current density, electrolyte composition, pH of solution, temperature, deposition time. The advantages of this method are strong adhesion to substrate, good electrical connectivity, easy control of film thickness, and suitable for electrochemical applications. Electrodeposited NiS films are widely used in supercapacitors and hydrogen evolution reaction studies due to their excellent electroactive surface area.

2.5 Spray Pyrolysis Technique

Spray pyrolysis is a simple and scalable method used to deposit NiS thin films on heated substrates. A precursor solution containing nickel salts and sulfur compounds is atomized into fine droplets and sprayed onto a heated substrate. Upon contact, the droplets undergo thermal decomposition, forming NiS thin films. Process parameters are substrate temperature, spray rate and nozzle distance, precursor concentration, and carrier gas pressure. Advantages of this method are suitable for large-area coatings, low cost and simple setup, and good reproducibility. However, film uniformity and stoichiometric control can be challenging due to rapid solvent evaporation and thermal gradients.

2.6 Sol–Gel Method

The sol–gel technique offers molecular-level control over NiS film formation. In this method, a colloidal solution (sol) containing nickel precursors is prepared, followed by gelation and deposition on substrates through spin coating, dip coating, or drop casting. Subsequent annealing in a sulfur-rich atmosphere converts the gel into crystalline NiS. Key features are high purity films, excellent compositional control, low processing temperature, ability to form uniform coatings. However, there are certain limitations of this method like shrinkage during drying and annealing, multi-step processing, possible cracking in thick films.

2.7 Chemical Vapor Deposition (CVD) and Advanced Methods

CVD and atomic layer deposition (ALD) are advanced techniques used to fabricate high-quality NiS thin films with precise thickness control and superior crystallinity. In CVD, volatile nickel and sulfur precursors react at elevated temperatures to form NiS on the substrate surface. This method produces highly crystalline and dense films, suitable for electronic applications. Atomic layer deposition allows atomic-scale control of film thickness through sequential self-limiting surface reactions. Although expensive and complex, ALD provides exceptional uniformity and conformality, especially for nanoelectronics.

2.8 Post-Deposition Treatments

Post-deposition annealing plays a critical role in improving NiS thin film properties. Annealing in inert medium like argon, nitrogen or sulfur-rich atmospheres enhances crystallinity, reduces defects, and stabilizes phase composition. Typical effects include: grain growth and improved crystallinity, reduction of structural defects, phase transformation control, enhanced electrical conductivity. However, excessive annealing may lead to sulfur loss and formation of secondary phases, affecting film performance.

3. Optical properties of NiS Thin Film

The optical properties of NiS thin films are among the most important characteristics governing their suitability for optoelectronic, photovoltaic, and photoelectrochemical applications. These properties arise from the interaction of electromagnetic radiation with the electronic structure of the material and are strongly influenced by factors such as crystallite size, phase composition, film thickness, and defect density. Because NiS is a narrow band gap semiconductor with significant defect states, it exhibits strong absorption in the visible region, making it a promising candidate for solar energy harvesting and related applications.

Optical studies of NiS thin films are typically carried out using UV–Visible spectroscopy in the wavelength range of 300–1100 nm. From the measured absorbance and transmittance spectra, important optical constants such as absorption coefficient, band gap energy, extinction coefficient, refractive index, optical conductivity, and Urbach energy can be determined. These parameters collectively describe how NiS thin films interact with light and how effectively they can be used in energy conversion systems. One of the most significant optical features of NiS thin films is their strong absorption in the visible region. This behavior arises due to electronic transitions between the valence band, which is mainly composed of sulfur 3p orbitals, and the conduction band, dominated by nickel 3d orbitals. In addition, defect levels introduced by vacancies and non-stoichiometry also contribute to sub-band gap absorption, further enhancing light absorption.

The absorption coefficient (α), which represents how strongly a material absorbs light of a given wavelength, is calculated using absorbance data and film thickness. For NiS thin films, the absorption coefficient is typically high, indicating efficient photon harvesting capability. For example, when a film shows an absorbance of 1.2 at 500 nm with a thickness of 300 nm, the calculated absorption coefficient is of the order of 10^4 cm^{-1} [16]. Such a high value confirms that even thin layers of NiS can effectively absorb a large fraction of incident light, which is advantageous for photovoltaic and photoelectrochemical devices where efficient light absorption is required.

Another important parameter is the optical band gap, which defines the minimum energy required to excite an electron from the valence band to the conduction band. The band gap of

NiS thin films is generally evaluated using the Tauc plot method, where a linear extrapolation of the $(\alpha h\nu)^2$ versus photon energy plot is used to determine band gap. Experimental studies show that NiS thin films typically exhibit a band gap in the range of 1.4 to 1.8eV [17-18]. This relatively narrow band gap enables strong absorption of visible light, particularly in the red and near-infrared regions of the solar spectrum. The extinction coefficient, which is related to the loss of intensity of light as it propagates through the material, further describes the optical response of NiS thin films. A moderate extinction coefficient indicates that the material not only absorbs light efficiently but also has significant interaction with electromagnetic radiation. This property is particularly important in applications such as photodetectors and electrochemical solar cells, where light–matter interaction directly influences device performance.

In addition to absorption-related parameters, the refractive index of NiS thin films provides insight into their optical density and polarization response. Typically, NiS films exhibit refractive index values in the range of 2 to 3.5, indicating relatively high optical density compared to many conventional semiconductors. This high refractive index is associated with strong electronic polarizability due to the presence of transition metal ions and defect states. Optical conductivity is another important parameter that reflects the ability of the material to conduct electricity under the influence of incident light. NiS thin films generally show enhanced optical conductivity in the visible region, which is directly linked to photon-induced charge carrier generation. Higher optical conductivity indicates improved photoresponse and is beneficial for applications in optoelectronic devices and energy conversion systems. An additional feature observed in NiS thin films is the presence of an exponential absorption edge known as the Urbach tail. This region is associated with localized states in the band gap arising from structural disorder, grain boundaries, and defects such as vacancies and interstitials. The width of this tail, known as Urbach energy, provides a quantitative measure of disorder in the material. Higher Urbach energy values indicate increased defect density and structural imperfections, which are commonly observed in chemically deposited NiS thin films due to their nanocrystalline nature. Although excessive disorder may negatively affect electronic transport, moderate defect levels can enhance optical absorption and improve photoelectrochemical activity by providing additional active sites.

The electrical and thermoelectric properties of nickel sulfide (NiS) thin films are of considerable importance for their application in energy conversion, sensing, and thermoelectric devices. These properties are strongly influenced by crystallite size, phase composition, defect density, and carrier concentration. Due to the non-stoichiometric nature of NiS and its transition metal chalcogenide character, it exhibits complex charge transport behavior and moderate thermoelectric response.

4. Electrical and Thermoelectric Properties of NiS thin film

The electrical behavior of NiS thin films is primarily governed by their semiconducting nature, defect chemistry, and nanocrystalline structure. In most cases, NiS exhibits p-type conductivity, which originates from nickel vacancies acting as acceptor states. These vacancies generate holes in the valence band, which serve as the main charge carriers responsible for electrical conduction. The conductivity (σ) of NiS thin films is described by the fundamental relation: $\sigma = nq\mu$, where conductivity depends on carrier concentration (n), charge of electron (q), and mobility (μ). In NiS thin films, carrier concentration is strongly affected by intrinsic defects, while mobility is influenced by grain boundaries and structural disorder. Because chemically deposited NiS thin films are typically nanocrystalline, grain boundaries play a dominant role in limiting charge transport. These boundaries act as potential barriers, causing carrier scattering and resulting in reduced mobility. As a result, charge transport in NiS thin films often deviates from ideal band conduction and instead follows hopping or thermally assisted tunneling mechanisms. Temperature has a strong influence on electrical conductivity. In most cases, conductivity increases with temperature, indicating semiconducting behavior. This is due to thermal excitation of charge carriers from localized defect states into the conduction process. At higher temperatures, the increased thermal energy reduces the effect of grain boundary barriers, thereby enhancing conductivity. Resistivity values of NiS thin films typically vary over a wide range depending on deposition conditions. Highly crystalline films show relatively low resistivity due to improved charge transport pathways, whereas defect-rich or poorly crystalline films exhibit higher resistivity due to increased scattering effects. Hall effect measurements confirm that NiS thin films generally exhibit p-type conduction [19]. The positive Hall coefficient indicates holes as the majority charge carriers. Carrier concentration typically lies in the range of 10^{16} to 10^{19} cm^{-3}, while mobility values are relatively low due to structural disorder. Despite low mobility, sufficient conductivity is maintained due to moderately high carrier concentration.

Thermoelectric properties describe the ability of a material to convert temperature gradients into electrical energy. NiS thin films have attracted attention in this context due to their semiconducting nature, moderate electrical conductivity, and defect-induced carrier transport. The most important thermoelectric parameter is the Seebeck coefficient (S), which represents the magnitude of thermoelectric voltage generated per unit temperature difference. In NiS thin films, the Seebeck coefficient is generally positive, confirming p-type conduction. This positive value arises due to the dominance of hole transport. The Seebeck coefficient is defined as: $S = \Delta V / \Delta T$, where ΔV is the thermoelectric voltage generated and ΔT is the applied temperature difference [20]. In NiS thin films, the Seebeck coefficient is positive, confirming p-type conduction. The typical values of Seebeck coefficient lie in the range of +20 to +180 μV/K,

depending on film quality and microstructure. Poorly crystalline or highly conductive films generally show lower values (+20 to +60 μV/K), while nanocrystalline and defect-engineered films exhibit higher values in the range of +80 to +150 μV/K, and in optimized cases it may reach up to about +180 μV/K. For NiS thin films, conductivity typically lies in the range of 10^2 to 10^4 S/m. Lower conductivity values are usually observed in highly defective or amorphous films, whereas better crystallinity and improved grain connectivity increase conductivity toward the upper limit. This wide variation clearly reflects the strong dependence of electrical transport on microstructural features. The combined effect of Seebeck coefficient and electrical conductivity is expressed through the power factor ($PF = S^2\sigma$), which represents the useful electrical power generated from a temperature gradient. For NiS thin films, the power factor typically ranges from 10^{-6} to 10^{-4} W/m·K². Lower values correspond to disordered films with poor charge transport, while higher values are obtained in nanostructured films where an optimal balance between carrier concentration and mobility is achieved. Thermal conductivity (κ) is also a crucial parameter in thermoelectric materials, as it determines how efficiently a material can maintain a temperature gradient. NiS thin films generally exhibit relatively low thermal conductivity, typically in the range of 1 to 3 W/m·K. This low value is mainly due to strong phonon scattering at grain boundaries, lattice defects, and nanocrystalline interfaces. Such reduced thermal conductivity is beneficial for thermoelectric applications because it helps maintain a temperature difference across the material. The overall thermoelectric efficiency is described by the dimensionless figure of merit (ZT), given by $ZT = S^2\sigma T/\kappa$. For NiS thin films, the ZT value at room temperature is generally in the range of 0.01 to 0.1, indicating moderate thermoelectric performance. In optimized nanostructured or doped systems, this value can approach 0.1 to 0.2 at elevated temperatures, although it is still lower than that of high-performance thermoelectric materials.

Reference:

1. Wagh, R., Yewale, C., Deshmane, V., Tupe, U., Mandawade, S., Naeem, S., & Patil, A. (2025). *Total Chemistry, 2*, 100023.
2. Gul, M., Ahmad, K., Thomas, A., & Tighezza, A. (2024). *Chemical Papers, 78*, 4143.
3. Sun, C., Duan, D., Chen, X., & Ge, X. (2026). *Ionics, 32*, 5425.
4. Jung, M., Park, Y., Lee, C., Song, D., Park, S., Park, C., Kim, J., Myung, S., Park, J., Kim, C., & Lim, J. (2025). *Applied Surface Science, 709*, 163873.
5. Chen, Y., Cheng, Y., Zhang, T., Zhang, H., & Zhong, S. (2024). *International Journal of Hydrogen Energy, 77*, 184.
6. Patil, A., Lokhande, A., Chodankar, N., Kumbhar, V., & Lokhande, C. (2016). *Materials & Design, 97*, 407.

7. Slatnia, R., Lakel, A., Sengouga, N., Tibermacine, T., & Meddas, H. (2025). *Journal of Sol-Gel Science and Technology, 116*, 656.
8. Luo, L., Liu, L., Zhao, C., Li, W., Wang, X., Wang, D., Huang, J., Dong, P., Zhang, Y., & Duan, J. (2025). *Ionics, 31*, 4027.
9. Boughalmi, R., Rahmani, R., Boukhachem, A., Amrani, B., Driss-Khodja, K., & Amlouk, M. (2015). *Materials Chemistry and Physics, 163*, 99.
10. Ruan, H., Li, Y., Qiu, H., & Wei, M. (2014). *Journal of Alloys and Compounds, 588*, 357.
11. Selvanathan, V., Rokonuzzaman, M., Razali, S., Chelvanathan, P., Islam, M., Su'ait, M., Akhtaruzzaman, M., & Kiong, T. (2025). *International Journal of Energy Research, 15*, 8895957.
12. Gahtar, A., Benramache, S., Ammari, A., Boukhachem, A., & Ziouche, A. (2022). *Inorganic and Nano-Metal Chemistry, 52*, 112.
13. Bharathi, B., Thanikaikarasan, S., Chandrasekar, P., Kollu, P., Mahalingam, T., & Ixtlilco, L. (2014). *Journal of New Materials for Electrochemical Systems, 17*, 167.
14. Ubale, A., & Bargal, A. (2011). *Materials Research Bulletin, 46*, 1000.
15. Nalage, S., Chougule, M., Sen, S., Joshi, P., & Patil, V. (2012). *Thin Solid Films, 520*, 4835.
16. Suresh, S., Anand, S., Arul, R., & Isha, D. (2016). *Chalcogenide Letters, 13*, 291.
17. Kotei, P., Boadi, N., Saah, S., & Mensah, M. (2022). *Advances in Materials Science and Engineering, 10*, 6587934.
18. Balayeva, O., Azizov, A., Muradov, M., Maharramov, A., Eyvazova, G., Alosmanov, R., Mamiyev, Z., & Aghamaliyev, Z. (2016). *Materials Research Bulletin, 75*, 155.
19. Sartale, S., & Lokhande, C. (2001). *Materials Chemistry and Physics, 72*, 101.
20. Chen, Y., Kuo, Y., Hsiao, V., & Huang, C. (2025). *Materials Chemistry and Physics, 339*, 130769.

CELLULOSE NANOCRYSTALS IN MODERN DRUG DELIVERY: PREPARATION, STRUCTURAL CHARACTERISTICS AND BIOMEDICAL APPLICATIONS

Pawan P. Kalbende
Department of Chemistry,
Jagadamba Mahavidyalaya, Achalpur, Dist- Amaravati (India)
Corresponding author E-mail: pawankalbende@gmail.com

Abstract
Cellulosic materials are converted into cellulose nanocrystals by a variety of mechanical and chemical procedures (CNCs). As the need for eco-friendly, biodegradable, and biocompatible materials develops throughout the globe, CNCs have emerged as an appealing sustainable material due to their increased functions. Novel extraction processes, procedures, and resources are now being developed to meet the expanding demand for cellulose nanocrystals-based products on an industrial scale. Cellulose Nanocrystals are a potential biomaterial for a variety of applications, including medication delivery, catalysis, food processing, environmental investigations, and heat transmission. In the present review article, a short summary of the structural aspects, isolation techniques (reaction conditions), and application in the drug delivery system is offered after a review of the existing literature.

Keywords: CNCs, Acid Hydrolysis, Nanocrystal.

1. Inroduction

Cellulose (Figure 1) is a common and naturally occurring polymer that may be found in a variety of resources [1].

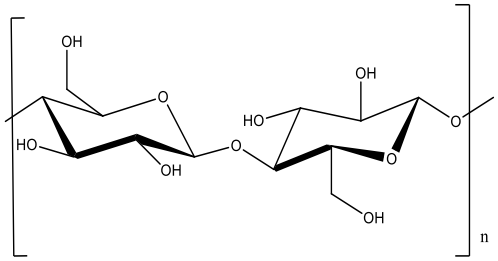

Figure 1: Structure of Cellulose molecule

Worldwide funding agencies, governments, and research communities are currently stressing the importance of nanotechnology and nanoscience, particularly for exceedingly crystalline nanoscale biomaterials, such as cellulose nanocrystals (CNCs), also known as cellulose nanowhiskers and cellulose nanoparticles [2-5]. In the last decade, cellulose nanocrystals have gotten a lot of attention from a lot of research organisations, as seen by the rising number of scientific research articles published in the area of Nanocellulose [5-12]. Materials derived from

bio-resources have piqued researchers' attention in recent years owing to their considerable potential for manufacturing a variety of sustainable goods with little environmental impact [13-19]. Because of its well-organized structure and crystalline composition, cellulosic material has the potential to develop a diverse assortment of nanomaterials. [5,8]. Table 1 shows many biosources, including tunicate, wood cotton, bacterial cellulose, microcrystalline cellulose (MCC) and sisal, were used to produce a variety of nanocrystalline cellulose (NCC) products with various dimensions [18].

Table 1: Dimensions of NCCs from various sources obtained via different techniques

Source	L (nm)	d (nm)	Aspect ratio (L/d)	Method
Ramie	50–150	5–10	5–30	TEM
MCC	∼500	10	50	AFM
Sisal	100–500	3–5	20–167	TEM
Bacterial	100–1000	10–50	2–100	TEM
Wood	100–300	3–5	20–100	AFM
Cotton	100–150	5–10	10–30	TEM
Tunicate	1160	16	73	DDLS

Table 2: CNC producers with annual production capacity

Company/Research Institute	Country	Production (tons/year)
Cellu Force	USA	400
GranBio Inc.	USA	200
Alberta-Pacific Forest Industries Inc.	Canada	180
Anomera Inc.	Canada	11
Forest Products Laboratory (USDA)	USA	5
University of Maine Orono, Maine.	USA	4
Blue Goose Biorefineries Inc.	Canada	4
Cellulose Lab	Canada	4
Advanced Cellulosic Material Inc.	Canada	1
FPInnovations	Canada	0.5
InnoTech Alberta	Canada	0.3
National Nanotechnology Laboratory for Agriculture	Brazil	Pilot Project
Melodea Bio Based Solution	Israel	Pilot project
Indian Council of Agricultural Research	India	Pilot Project

The dimensions of CNC are dictated by the kind of cellulosic material supply as well as the hydrolysis conditions that are utilised during extraction [20]. It was found that the nanocrystalline cellulose that was obtained from bacterial cellulose and tunicate had dimensions that were typically larger than those of the nanocrystalline cellulose that was derived from wood and cotton. [21,22]. Because they have a greater axial elastic modulus than strength in addition to an elastic modulus that is equivalent to that of traditional reinforcing materials, CNCs are the perfect materials for the emerging industry of biopolymer composites [23-25]. As can be seen in Table 2, several research projects and companies from all around the globe have only lately started the process of manufacturing cellulose nanocrystals that will be ready for purchase on the market.

This review article begins with an overview of recent developments in the structure of CNCs, followed by a detailed discussion of the primary techniques for isolating CNCs from bioresources, focusing particularly on reaction conditions and their applications in drug delivery. Finally, the article concludes with some conclusions and recommendations.

2. Structure of CNCs

The sugar units that make up the CNC structure are connected to one another by -H and -OH groups with the removal of water molecule [26]. It is presumed to be in the α configuration if the OH group that is attached to the first carbon is on the same side of the ring as the carbon that is attached to the sixth carbon. The first carbon of the cellulose molecule is oriented in the opposite way, resulting in a structure known as β configuration [27].

The origin of cellulose was intrigued by the crystal size and degree of crystallinity of primary fibrils from various cellulose samples. Algae and tunicate cellulose microfibrils produce nanocrystals that are hundreds of micrometres long, while wood microfibrils produce a lot of shorter nanocrystals [28, 29]. Cellulose is a linear chain of aldohexose molecules in which the continuation unit is made up of two anhydroglucose rings [$(C_6H_{10}O_5)_n$;n= 10000-15000, n is determined by the cellulose supply material] linked together by a chemical element covalently attached to C1 of the aldohexose ring and C4 of the conterminous ring (1 - 4 linkage) and then referred to as the β 1–4 glucosidic bond [30]. The –OH group on the first carbon is an aldehyde hydrate group with increased activity. On the other hand, the –OH group on the fourth carbon on the other side of the chain is non-reducing [31].

Although cellulose does not exist as a single entity, a number of cellulose molecules (about 30 to 100 chains) may be assembled to create a chain conformation by Van der Waals conformation by Van der Waals forces of attraction and hydrogen bonding to form the basic unit of cellulose fibres and protofibrils, at the nanoscale, with diameters ranging from 2 to 20 nm [32]. Due to the presence of three -OH groups in equatorial regions all along its length, the cellulose chain was discovered to be easily accessible for the formation of hydrogen bonds. [7, 8]. The cellulose

molecules may be arranged and stabilised in their crystalline packing by forming a strong and intricate network of hydrogen bonds between the –OH groups of distinct cellulose chains. The cellulose microfibril, a highly crystalline cellulose microfibril, may be separated using a combination of chemical, enzymatic, and mechanical processes, resulting in the production of desirable cellulose nanocrystals [33].

Surface modifications such as 2, 2, 6, 6-tetramethylpiperidine-1-oxyl (TEMPO) regioselective type oxidation, silane treatments, sulphonation, acetylation, carboxylation, polymer grafting, and polyelectrolyte adsorption may be used to achieve surplus particle functionality [34-39]. Natural sources and isolation techniques of cellulose influence CNC properties such as degree of crystallinity and size of crystalline areas. For example, crystallinity varies from roughly 50% in certain plants to 60% in bacterial cellulose, 90% in some algae, and 80% in tunicates [40]. Because of hierarchical structural design that spans the nanoscale to macroscopic range of dimensions, biomaterials generate flexibility and great mechanical strength. It does this by constructing the structures using thin and almost limitless rods of crystalline material running parallel to the cellulose microfibril [41, 42]. The hierarchical structure of plant cellulose is depicted schematically in Figure 1[43].

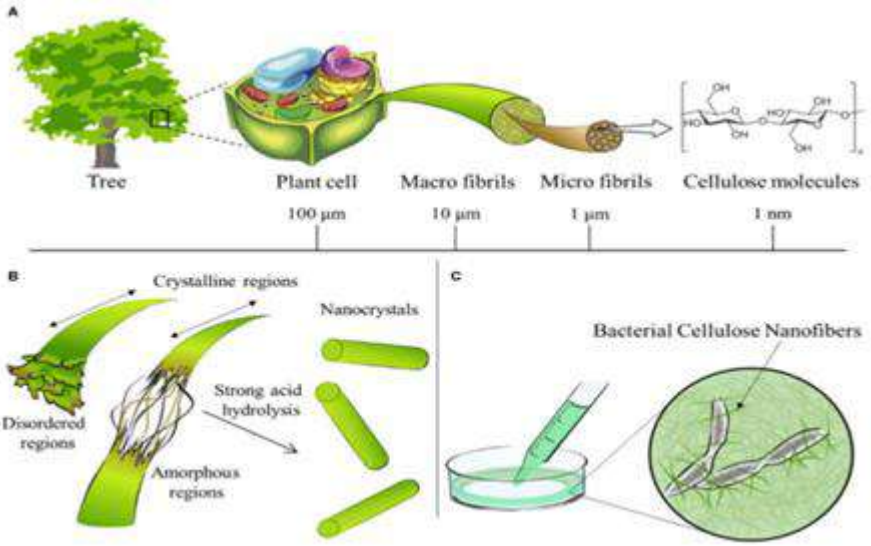

Figure 1: Plant based cellulose hierarchical structure from meter to nanometer scale (a). Schematic diagram of acid hydrolysis to obtain nanocellulose (b). Bionanocellulose cultured from cellulose synthesizing bacteria (c)[43]

3. Methods of Isolation

Pre-treatment methods, which include completely or partially removing the matrix elements from the raw material in order to get individual cellulose fibres, are included among the approaches that may be used to isolate CNCs. Updating extraction techniques and making improvements in combined processes by combining two or more of the below-mentioned approaches might be the

most effective way to enhance CNC's qualities and overcome the problem of limited percent yields.

3.1. Acid Hydrolysis

Following a chemical process known as mild acid hydrolysis, cellulose fibres were converted into cellulose nanocrystals. During hydrolysis, concentrated sulfuric acid enters amorphous regions of cellulose chains, where it then digests the chains to separate out their crystalline components [44]. Because the amorphous domain of the cellulose fibre is oriented in a random pattern, it causes the fibre to have a lower density. Because of this, it is more susceptible to acid hydrolysis, particularly from hydronium ions H_3O+, which results in the hydrolytic breakage of glycosidic bonds [45]. Figure 2 displays a schematic illustration of the hydrolysis of cellulose fibre that was carried out by sulfuric acid. After the amorphous domain has been removed, the subsequent step of sonication will lead to the isolation of CNCs that have half sulphate ester groups on their surface. These charges are produced as a consequence of an interaction between sulfuric acid and the hydroxyl groups found in cellulose.

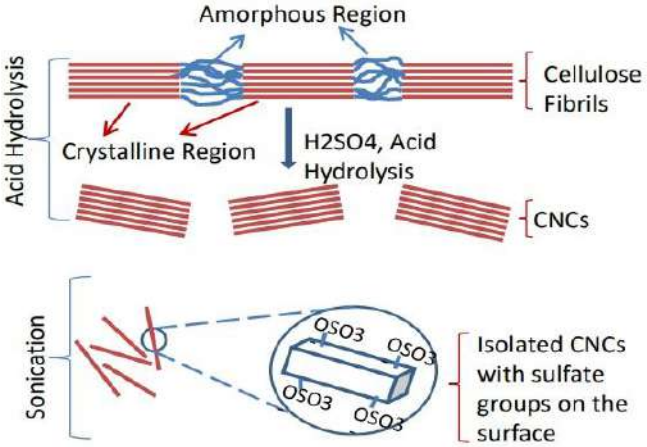

Figure 2: Schematic representation of sulfuric acid hydrolysis of cellulose fiber

This process triggers repulsion between negatively charged CNC and fascilited colloidal stability in water, which causes the charges to be produced [46]. Other organic and mineral acids, such as hydrochloric acid, phosphoric acid, and hydrobromic acid, have been the subject of investigation by a few researchers. These acids, however, produce suspensions that are less stable [47-50]. Table 3 is a representation of some of the reaction conditions for the acid hydrolysis technique.

3.2 Mechanical Method

The mechanical treatment is a physical approach that is usually employed for the manufacturing of CNC. It comprises of four different ways: freeze crushing, fine grinding, microfluidization, and homogenization [57]. In the freezing smashing approach, liquid nitrogen was used as the freezing medium, and the structure of the frozen fibres was broken down into nanosize fragments as a result of the tremendous impact caused by the mechanical smashing [58]. The fibres are divided into nanosize fragments using the fine grinding process, which involves relative motion

between the two discs of a commercial grinder. This allows the grinder to crush, grind, rip, and shear the fibres [59]. Figure 3 provides an illustration of the microfluidization under high pressure approach for the production of nanomaterials. The fabrication of the nanoparticle begins with the raw material being subjected to a pressure of around 4000 bars and then being compelled into an interactive tank. This results in the production of a tremendous shear force [60].

Table 3: Reaction conditions for acid hydrolysis method of isolation

Raw Material	Purification	Treatment Procedure	Post-Treatment	Ref.
Pineapple leaf	Grinding, NaOH, acetic acid, sodium chlorite treatments	Grinding, H_2SO_4 64% at 45 °C hydrolysis, dilution	Centrifugation, dialysis, ultrasonication	[51]
Whatman filter paper	Blending	4N HCl solution at 100 °C for 120 min	Centrifugation, dialysis, ultrasonication	[52]
	Blending	H_3PO_4 85% at 60 °C hydrolysis, dilution	Centrifugation, dialysis, ultrasonication, lyophilization	
Pseudostems of banana plants	Soxhlet extraction, bleaching with H_2O_2 and acetic acid	Dilution, blending, H_2SO_4 at 50 °C hydrolysis	Centrifugation, dialysis, lyophilization	[53]
Recycled Newspaper	Grinding, NaOH, sodium chlorite treatments at 125 °C	H_2SO_4 65% at 45 °C hydrolysis, dilution	Centrifugation, dialysis, sonication	[54]
Bleached kraft eucalyptus dry lap pulp	Soaking in water, disintegrating, drying	Anhydrous organic acid hydrolysis at 90–120 °C, dilution, filtration	Washing, centrifugation, dialysis	[55]
Bacterial cellulose	Washing, homogenization, drying, grinding	H_2SO_4/HCl mixture at 45 °C, dilution	Centrifugation, dialysis, ultrasonication	[56]

3.3 TEMPO Oxidation Method

In order to extract the CNC, TEMPO was used since it is an effective and environmentally friendly reagent. The typical reaction scheme comprised of TEMPO, NaBr, and NaClO [62]. According to the most recent study published in this field, the C6-formyl group on cellulose undergoes a transformation into the C6-carboxyl group when it is exposed to TEMPO [63]. The NaBr was transformed into NaBrO by the presence of NaClO and TEMPO was oxidised into

nitrosonium as a result. Upon oxidation, nitrosonium changed the hydroxyl group of the alcoholic compound into aldehyde or carboxylic acid. Saito et al. observed that the aldehyde groups congregated in the newly generated CNC surface obtained from the reaction system of the TEMPO/NaBr/NaClO, which did not occur in the TEMPO/NaClO/NaClO2 system. This was discovered when Saito et al. added $NaClO_2$ instead of NaBr in the reaction system of the TEMPO/NaBr/Na [64].

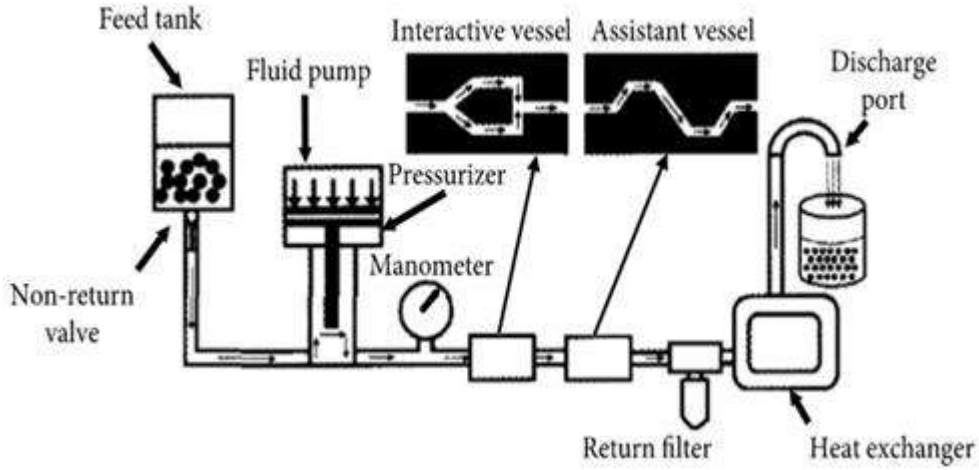

Figure 4: Schematic of microfluidization under high pressure method [61]

Figure 5 illustrates the mechanism for the oxidation of the primary hydroxyl to the carboxyl by the TEMPO/NaClO/NaClO2 system. The TEMPO/NaClO/NaClO2 system had a few benefits, but it also had some obvious drawbacks, such as a sluggish rate of reaction and a relatively low concentration of carboxyl groups in newly produced CNC. Even though this system had a few advantages, these drawbacks were unavoidable [65]. Table 4 outlines a few of the requirements that must be satisfied for oxidation and mechanical treatment.

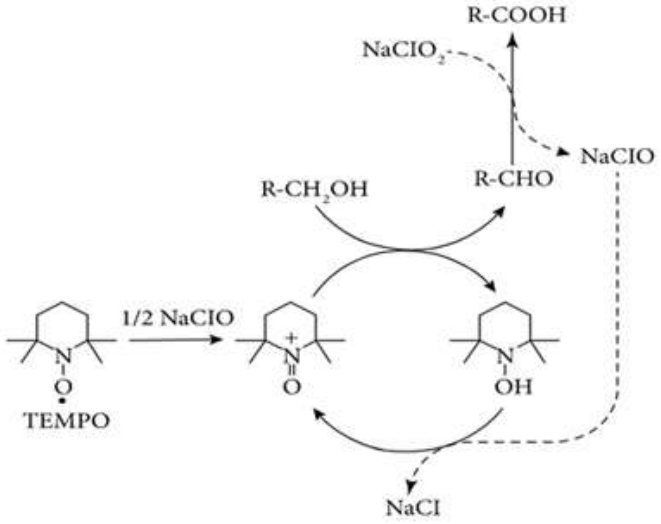

Figure 5: Mechanism of Oxidation of primary hydroxyl to carboxyl by TEMPO/NaClO/$NaClO_2$ system [64]

Table 4: Reaction conditions for Mechanical Treatment and Oxidation Methods

Raw Material	Purification	Treatment Procedure	Post-Treatment	Ref.
Microcrystalline cellulose	No	Swilling in water, ultrasonication at power of 1500 W	Centrifugation, freeze drying	[66]
Microcrystalline cellulose	No	Dispersion in water, ultrasonication for 50 minutes at an output of 500 W, frequency of 20 kHz	Decantation, freeze drying	[67]
		Dispersion in water, high-energy bead milling		
Wood	Ethanol solvothermal treatment, alkaline hydrogen peroxide treatment	Soaking in distilled water, ultrasonication	Washing, drying	[68]
Jute fibers	Grinding, Sodium hydroxide, washing, dimethylsulfoxide treatments	Treatment with TEMPO/NaClO/NaBr system	Centrifugation, sonication, drying	[69]
Bleached kraft hardwood pulp	No	Lithium chloride-assisted sodium metaperiodate oxidation at 75 °C	Washing, dispersion, homogenization	[70]

3.4 Enzymatic Hydrolysis

The enzymatic production of CNCs is a less costly alternative to the preparatory process of mechanical fibrillation and heating. This method also removes the demand for the use of toxic chemicals and requires less energy overall [71]. The crystalline portions of the cellulose fibres are not digested to a significant degree by the enzymes, which results in CNCs that maintain a hydroxyl group surface chemistry. Enzymes preferentially breakdown the amorphous domains of the cellulose fibres. In the first stage, referred to as step I, the source material is subjected to pretreatment in order to disrupt the connectivity between the lignin and the amorphous area using a mechanical process combined with washing procedures [72]. Controlled enzymatic hydrolysis, in which the pretreatment material is solubilized in buffer solution with an enzyme cocktail, is the second stage (II), which is followed by the third step (III), which is known as homogenization [73]. Table 5 illustrates some of the reaction parameters for enzymatic hydrolysis, which is performed in order to isolate CNCs.

4. Application in Drug Delivery System

The hydrophilic drugs tetracycline and doxorubicin were able to be bound by CNCs, and once bound, they were promptly and totally released within a single day. Because of the neutralizing CTAB-modified CNCs are able to bind significant quantities of hydrophobic anticancer medicines, such as etoposide and docetaxel. This is because CTAB was delivered in a regulated way over the course of many days [80]. Cationic polysaccharide at the surface of CNCs (Binding chitosan) generated the novel polyelectrolyte macro-ion complex (PMC), which is essential for drug delivery applications [81]. The hydrophobic drug curcumin may be encapsulated by CD/ CNCs complexes, which are generated by binding Cationic b-cyclodextrin (CD) to the surface of CNCs by ionic association. These complexes can then enclose the drug. 82 The attachment of folic acid molecules to the surfaces of CNCs serves as an additional efficient way for the ease of targeted delivery of chemotherapeutic molecules to cancer cells that express folate receptors [83]. Figure 5 depicts the electrostatic and hydrophobic interactions of surfactant molecules with cellulose nanocrystals, and its mechanism emphasises drug adsorption. Table 4 provides a summary of the numerous drug carrier systems that are based on CNCs. Through electrostatic interactions, several water-soluble medicines may be bonded to and released from CNCs. The large specific surface area of CNC enables for high specific drug delivery. Additionally, a large variety of medicines may bind to CNC following straightforward chemical changes to its surface. Controlled release of different medications is possible when the CNCs surface is chemically changed or physically manufactured properly. CNCs in calcium cross-linked alginate microspheres boost theophylline drug loading efficiency and permit prolonged drug release [86].

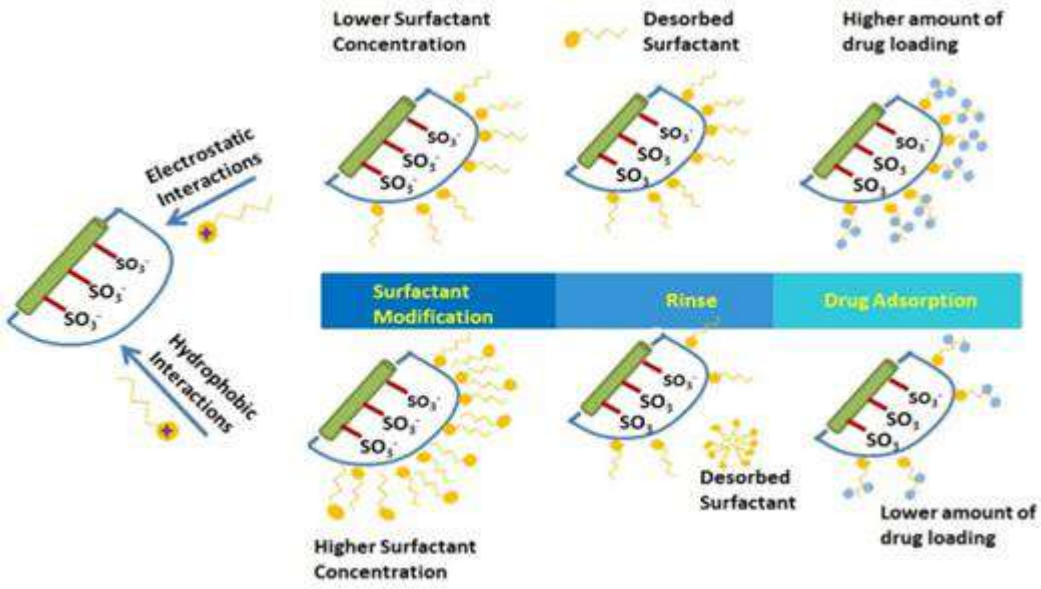

Figure 6: Schematic representation of the surfactant and nanocrystalline cellulose mechanism and its effect on drug adsorption [84]

It was hypothesised that the CNC may prevent a sudden release of the medication during the early stage while yet maintaining the steady release of the drug over an extended period of time. The nanocellulose component was used in the development of a hydrogel that is constituted of beta-cyclodextrin (-CD), CNCs, and Pluronic polymer. The nanocellulose component served as a cross-linking junction [87]. When inserted into the hydrogel mesh, the CNC was thought to inhibit the release of the anticancer drug. In another investigation, an aromatic linker was added to the CNC surface to enable effective binding of amine-containing medicines and regulated release [88].

Table 5: Reaction conditions for enzymatic hydrolysis methods

Raw material	Description of Treatment	Enzymes	Enzyme Concentration	Conditions of Hydrolysis (pH, Temp., Time)	Ref.
Bleached Craft Eucalyptus pulp	Enzymatic hydrolysis followed by microfluidization	EG & CBH	15 FPU/grams of substrate	(4.8, 50 ℃, 48 hr)	[74]
Recycled Pulp	Enzymatic hydrolysis with microwave and conventional heating	EG	420 EGU/grams of substrate	(6.8, 50 ℃, 1 hr)	[75]
Wood fiber pulp	Enzymatic hydrolysis followed by mechanical shearing	EG	0.02%–3%	(7, 50 ℃, 2 hr)	[76]
Orange waste residue	Enzymatic hydrolysis followed by bleaching	BG & Commercial enzymes	3.4 mg pulpzyme HA, 3.4 mg celluclast & 0.6 mg β-galactosidase per gram of substrate	(4, 50 ℃, 48 hr)	[77]
Sugarcane Bagasse	Pretreatment with liquid hot water followed by enzymatic hydrolysis	EG & BG	7, 12 & 22 mg of protein per gram of cellulose	(5, 50 ℃, 24 hr)	[78]
Soybean Straw	Enzymatic hydrolysis followed by pretreatment with NaOH & H_2O_2	BG & CBH	93 µL of Optimash VR per gram of substrate	(4, 50 ℃, 42 hr)	[79]

In order to direct the anticancer drugs specifically toward cancer cells, one investigating team coupled folic acid to CNCs. Using fluorescence imaging, researchers were able to determine that CNCs quickly attached to the cells and were then swallowed via the process of endocytosis [89]. It was discovered that positively charged pharmaceuticals like tetracycline hydrochloride and doxorubicin easily link (via the process of ionic bonding) to sulfated CNCs that were generated by the hydrolysis of sulfuric acid. Under physiological settings (10 mM PBS, 37°C), the majority of these medicines were discharged out from CNCs after 4 hours. This discharge may have been caused by ion interactions [90].

Table 6: Drug carrier systems based on CNCs [85]

Carrier Form	Matrix	Model Drug	Release Time and Medium	Mechanism Model
Microsphere or bead	EA; MMA; BMA	Propranolol hydrochloride	12 h in pH 6.8 PBS	–
	Sodium alginate	Theophylline	16 h in pH 7.4, pH 6.8, pH 1.0 PBS	Ritger–Peppas equation
Suspension	CTAB	Paclitaxel; docetaxel; DOX; TET; etoposide	1–4 d in PBS	–
	Chitosan oligosaccharide	Procaine hydrochloride	100 min in pH 8 NaCl solution	–
Hydrogel or gel	Cyclodextrin/Pluronic	DOX	6.5 d in water	Ritger–Peppas equation
	Cyclodextrin/Pluronic	Bovine serum albumin	20 h in pH 7.4 PBS	–
	Regenerated cellulose	Bovine serum albumin	48 h in simulated body fluid	Fickian diffusion law
Nanofiber	Poly(lactic acid)	Columbia blue	48 h in water	Higuchi equation
	Hordein/zein	Riboflavin	24 d in pH 7.4 PBS	–

5. Future Perspective and Conclusion

The process of extracting CNCs from the biomaterials from which they are derived may cause damage to the crystal structure of the CNCs, which in turn causes changes in the characteristics of the resultant CNC when compared to the attributes that are anticipated for perfect cellulose crystal structures. A more streamlined approach to the production of prototypes for the design

of more environmentally friendly goods will result from structural identifications of CNCs. Nano mechanics of discrete CNC is still a very difficult problem to solve due to the fact that the tiny size scale drives the constraints of sensitivity of current techniques. As a consequence of this, additional investigation is required immediately in order to remove any ambiguity from the measurements. Researchers looked at a number of different chemical functionalization processes and discovered that the majority of those processes focused on compatibilization. Despite the significant effort that has been put in, this problem is still only partially fixed. CNCs are still not compatible with matrix materials. Improving the dispersion of CNCs in polymer matrices, fortifying the interfacial characteristics of the composite, and increasing the strength and stiffness of the material without sacrificing its toughness are all major difficulties that still need to be addressed. The high cost of manufacturing that results from the poor yield of CNC synthesis when beginning with plant-, animal-, or tunicate-based raw materials and other bio sources is one of the most significant obstacles that CNC chemistry must overcome. This may result in excessive waste output and energy consumption, in addition to higher manufacturing costs. The cellulose pulp and paper business is particularly price sensitive; hence, if this problem is not solved, it will create hurdles for the commercialization of the process in the near future. Cellulose is considered to be a material that is efficient in terms of cost, and the industry itself is quite price sensitive.

Acknowledgement

The author is grateful to Principal, Jagadamba Mahavidyalaya, Achalpur for constant encouragement and support.

References

1. Cunha, A. G., Mougel, J. B., Cathala, B., Berglund, L. A., & Capron, I. (2014). Preparation of double Pickering emulsions stabilized by chemically tailored nanocellulose. *Langmuir, 30*, 9327–9335.
2. Bledzki, A. K., & Gassan, J. (1999). Composites reinforced with cellulose based fibres. *Progress in Polymer Science, 24*, 221–274.
3. Kumar, A., Vemula, P. K., Ajayan, P. M., & John, G. (2008). Silver-nanoparticle-embedded antimicrobial paints based on vegetable oil. *Nature Materials, 7*, 236–241.
4. Lendlein, A., Jiang, H., Jünger, O., & Langer, R. (2005). Light-induced shape-memory polymers. *Nature, 434*, 879–882.
5. Pappu, A., Patil, V., Jain, S., Mahindrakar, A., Haque, R., & Thakur, V. K. (2015). Advances in industrial prospective of cellulosic macromolecules enriched banana biofibre resources: A review. *International Journal of Biological Macromolecules, 79*, 449–458.
6. Sturcová, A., Davies, G. R., & Eichhorn, S. J. (2005). Elastic modulus and stress-transfer properties of tunicate cellulose whiskers. *Biomacromolecules, 6*, 1055–1061.

7. Shaabani, A., Keshipour, S., Hamidzad, M., & Seyyedhamzeh, M. (2014). Cobalt (II) supported on ethylenediamine-functionalized nanocellulose as an efficient catalyst for room temperature aerobic oxidation of alcohols. *Journal of Chemical Sciences, 126*, 111–115.
8. Bandura, A. V., & Lvov, S. N. (2006). The ionization constant of water over wide ranges of temperature and density. *Journal of Physical and Chemical Reference Data, 35*, 15–30.
9. Abitbol, T., Kam, D., Levi-Kalisman, Y., Gray, D. G., & Shoseyov, O. (2018). Surface charge influence on the phase separation and viscosity of cellulose nanocrystals. *Langmuir, 34*, 3925–3933.
10. Ahlen, M., Tummala, K. G., & Mihranyan, A. (2018). Nanoparticle-loaded hydrogels as a pathway for enzyme-triggered drug release in ophthalmic applications. *International Journal of Pharmaceutics, 536*(1), 73–81.
11. Araki, J., Wada, M., Kuga, S., & Okano, T. (1998). Low properties of microcrystalline cellulose suspension prepared by acid treatment of native cellulose. *Colloids and Surfaces A, 142*, 75–82.
12. Schyrr, B., Pasche, S., Voirin, G., Weder, C., Simon, Y. C., & Foster, E. J. (2014). Biosensors based on porous cellulose nanocrystal-poly(vinyl alcohol) scaffolds. *ACS Applied Materials & Interfaces, 6*, 12674–12683.
13. Sun, B., Zhang, M., Hou, Q., Liu, R., Wu, T., & Si, C. (2016). Further characterization of cellulose nanocrystal (CNC) preparation from sulfuric acid hydrolysis of cotton fibers. *Cellulose, 23*, 439–450.
14. Bai, W., Holbery, J., & Li, K. (2009). A technique for production of nanocrystalline cellulose with a narrow size distribution. *Cellulose, 16*, 455–465.
15. Beck-Candanedo, S., Roman, M., & Gray, D. (2005). Effect of reaction conditions on the properties and behavior of wood cellulose nanocrystal suspensions. *Biomacromolecules, 6*, 1048–1052.
16. Bondeson, D., & Oksman, K. (2007). Polylactic acid/cellulose whisker nanocomposites modified by polyvinyl alcohol. *Composites Part A: Applied Science and Manufacturing, 38*, 2486–2492.
17. Braun, B., & Dorgan, J. R. (2009). Single-step method for the isolation and surface functionalization of cellulosic nanowhiskers. *Biomacromolecules, 10*, 334–341.
18. Cirtiu, C. M., Dunlop-Brière, A. F., & Moores, A. (2011). Cellulose nanocrystallites as an efficient support for nanoparticles of palladium: Application for catalytic hydrogenation and Heck coupling under mild conditions. *Green Chemistry, 13*, 288–291.
19. Zhou, C., Shi, Q., Guo, W., Terrell, L., Qureshi, A. T., Hayes, D. J., & Wu, Q. (2007). Electrospun bio nanocomposite scaffolds for bone tissue engineering by cellulose

nanocrystals reinforcing maleic anhydride grafted PLA. *ACS Applied Materials & Interfaces, 5*, 3847–3854.

20. Cao, X. D., Habibi, Y., & Lucia, L. A. (2009). One-pot polymerization, surface grafting, and processing of waterborne polyurethane-cellulose nanocrystal nanocomposites. *Journal of Materials Chemistry, 19*, 7137–7145.
21. Cheng, M., Qin, Z., Hu, J., Liu, Q., Wei, T., Li, W., Ling, Y., & Liu, B. (2020). Facile and rapid one step extraction of carboxylated cellulose nanocrystals by H_2SO_4/HNO_3 mixed acid hydrolysis. *Carbohydrate Polymers, 231*, 115701.
22. Coelho, C. C., Michelin, M., Cerqueira, M. A., Gonçalves, C., Tonon, R. V., & Pastrana, L. M. (2018). Cellulose nanocrystals from grape pomace: Production, properties and cytotoxicity assessment. *Carbohydrate Polymers, 192*, 327–336.
23. Nascimento, D. M., Almeida, J. S., Dias, A. F., Figueirêdo, M. C. B., Morais, J. P. S., Feitosa, J. P., & Rosa, M. D. F. (2014). A novel green approach for the preparation of cellulose nanowhiskers from white coir. *Carbohydrate Polymers, 110*, 456–463.
24. De Souza Lima, M. M., Wong, J. T., Paillet, M., Borsali, R., & Pecora, R. (2003). Translational and rotational dynamics of rodlike cellulose whiskers. *Langmuir, 19*, 24–29.
25. Dominic, M., Joseph, R., Begum, P. S., Kanoth, B. P., Chandra, J., & Thomas, S. (2020). Green tire technology: Effect of rice husk derived nanocellulose (RHNC) in replacing carbon black (CB) in natural rubber (NR) compounding. *Carbohydrate Polymers, 230*, 115620.
26. Dong, S., Cho, H. J., Lee, Y. W., & Roman, M. (2014). Synthesis and cellular uptake of folic acid conjugated cellulose nanocrystals for cancer targeting. *Biomacromolecules, 15*, 1560–1567.
27. Dong, X., Revol, J., & Gray, D. (1998). Effect of microcrystallite preparation conditions on the formation of colloid crystals of cellulose. *Cellulose, 15*, 19–32.
28. Fortunati, E., Peltzer, M., Armentano, I., Torre, L., Jiménez, A., & Kenny, J. M. (2012). Effects of modified cellulose nanocrystals on the barrier and migration properties of PLA nano-biocomposites. *Carbohydrate Polymers, 90*, 948–956.
29. Errokh, A., Magnin, A., Putaux, J. L., & Boufi, S. (2018). Morphology of the nanocellulose produced by periodate oxidation and reductive treatment of cellulose fibers. *Cellulose, 25*, 899–3911.
30. Beltramino, F., Roncero, M. B., Torres, A. L., Vidal, T., & Valls, C. (2016). Optimization of sulfuric acid hydrolysis conditions for preparation of nanocrystalline cellulose from enzymatically pretreated fibers. *Cellulose, 23*, 1777–1789.
31. Favier, V., Chanzy, H., & Cavaille, J. (1995). Polymer nanocompsoites reinforced by cellulose whiskers. *Macromolecules, 28*, 6365–6367.

32. Foster, E. J., Moon, R. J., Agarwal, U. P., Bortner, M. J., Bras, J., & Camarero-Espinosa, S. (2018). Current characterization methods for cellulose nanomaterials. *Chemical Society Reviews, 47*, 2609–2679.
33. Fujisawa, S., Togawa, E., & Kuroda, K. (2017). Nanocellulose-stabilized Pickering emulsions and their applications. *Science and Technology of Advanced Materials, 18*, 959–971.
34. Chen, G., Roy, I., Yang, C., & Prasad, P. N. (2016). Nanochemistry and nanomedicine for nanoparticle-based diagnostics and therapy. *Chemical Reviews, 116*, 2826–2885.
35. Guhados, G., Wan, W. K., & Hutter, J. L. (2005). Measurement of the elastic modulus of single bacterial cellulose fibers using atomic force microscopy. *Langmuir, 21*, 6642–6646.
36. Fiore, G. L., Rowan, S. J., & Weder, C. (2013). Optically healable polymers. *Chemical Society Reviews, 42*, 7278–7288.
37. Ndong Ntoutoume, G. M. A., Granet, R., Mbakidi, J. P., Brégier, F., Léger, D. Y., Fidanzi-Dugas, C., Lequart, V., Joly, N., Liagre, B., Chaleix, V., & Sol, V. (2016). Development of curcumin-cyclodextrin/cellulose nanocrystals complexes: New anticancer drug delivery systems. *Bioorganic & Medicinal Chemistry Letters, 26*, 941–945.
38. Wei, G., Zuo, H., Guo, Y., & Pan, Q. (2016). Applications of cellulose nanocrystals: A review. *BioResources, 11*, 6244–6253.
39. Gan, P., Sam, S., Abdullah, M. F., & Omar, M. F. (2020). Thermal properties of nanocellulose-reinforced composites: A review. *Journal of Applied Polymer Science, 137*, 48544.
40. Gao, A., Chen, H., Hou, A., & Xie, K. (2019). Preparation of high-aspectratio cellulose nanocrystals by solvothermal synthesis followed by mechanical exfoliation. *Cellulose, 26*, 5937–5945.
41. Gebald, C., Wurzbacher, J. A., Tingaut, P., Zimmermann, T., & Steinfeld, A. (2011). Amine-based nanofibrillated cellulose as adsorbent for CO2 capture from air. *Environmental Science & Technology, 45*, 9101–9108.
42. Goussé, C., Chanzy, H., Excoffier, G., Soubeyrand, L., & Fleury, E. (2002). Stable suspensions of partially silylated cellulose whiskers dispersed in organic solvents. *Polymer, 43*, 2645–2651.
43. Miyashiro, D., Hamano, R., & Umemura, K. (2020). A review of applications using mixed materials of cellulose, nanocellulose and carbon nanotubes. *Nanomaterials, 10*, 186.
44. Le Gars, M., Douard, L., Belgacem, N., & Bras, J. (2019). Cellulose nanocrystals: From classical hydrolysis to the use of deep eutectic solvents. In *Smart Nanosystems for Biomedicine, Optoelectronics and Catalysis*. IntechOpen, France.

45. de Souza Lima, M. M., & Borsali, R. (2004). Rodlike cellulose microcrystals: Structure, properties, and applications. *Macromolecular Rapid Communications, 25*, 771–787.
46. Habibi, Y., Lucia, L. A., & Rojas, O. J. (2010). Cellulose nanocrystals: Chemistry, self-assembly, and applications. *Chemical Reviews, 110*, 3479–3500.
47. Camarero Espinosa, S., Kuhnt, T., Foster, E. J., & Weder, C. (2013). Isolation of thermally stable cellulose nanocrystals by phosphoric acid hydrolysis. *Biomacromolecules, 14*, 1223–1230.
48. Chen, L., Wang, Q., Hirth, K., Baez, C., Agarwal, U. P., & Zhu, J. Y. (2015). Tailoring the yield and characteristics of wood cellulose nanocrystals (CNC) using concentrated acid hydrolysis. *Cellulose, 22*, 1753–1762.
49. Viet, D., Beck-Candanedo, S., & Gray, D. G. (2007). Dispersion of cellulose nanocrystals in polar organic solvents. *Cellulose, 14*, 109–113.
50. Yu, H., Qin, Z., Liang, B., Liu, N., Zhou, Z., & Chen, L. (2013). Facile extraction of thermally stable cellulose nanocrystals with a high yield of 93% through hydrochloric acid hydrolysis under hydrothermal conditions. *Journal of Materials Chemistry A, 1*, 3938–3944.
51. Liu, D. G., Zhong, T. H., Chang, P. R., Li, K. F., & Wu, Q. L. (2010). Starch composites reinforced by bamboo cellulosic crystals. *Bioresource Technology, 101*, 2529–2536.
52. Hubbe, M., Rojas, O., Lucia, L., & Sain, M. (2008). Cellulosic nanocomposites: A review. *BioResources, 3*, 929–980.
53. Bercea, M., & Navard, P. (2000). Shear dynamics of aqueous suspensions of cellulose whiskers. *Macromolecules, 33*, 6011–6016.
54. Tamo, A., Doench, I., Helguera, A., Hoenders, D., Walther, A., & Madrazo, A. O. (2020). Biodegradation of crystalline cellulose nanofibers by means of enzyme immobilized-alginate beads and microparticles. *Polymers, 12*, 1522.
55. Kaushik, M., Li, A. Y., Hudson, R., Masnadi, M., Li, C.-J., & Moores, A. (2016). Reversing aggregation: Direct synthesis of nanocatalysts from bulk metal. Cellulose nanocrystals as active support to access efficient hydrogenation silver nanocatalysts. *Green Chemistry, 18*, 129–133.
56. Lima, M. M. D., & Borsali, R. (2004). Rodlike cellulose microcrystals: Structure, properties, and applications. *Macromolecular Rapid Communications, 25*, 771–787.
57. Geng, L., Chen, B., Peng, X., & Kuang, T. (2017). Strength and modulus improvement of wet-spun cellulose I filaments by sequential physical and chemical cross-linking. *Materials & Design, 136*, 45–53.

58. Ma, J., Yu, F., & Wang, J. N. (2010). Preparation of water-dispersible single-walled carbon nanotubes by freeze-smashing and application as a catalyst support for fuel cells. *Journal of Materials Chemistry, 20*, 5742–5747.
59. Li, J., & Liu, Z.-m. (2016). Preparation and hydrophobic modification of *Phyllostachys heterocycla* cv. *Pubescens* NFC/SiO2 aerogel. *Cellulose Chemistry and Technology, 1*, 8.
60. Yang, Y., Chen, Z., Zhang, J., Wang, G., Zhang, R., & Suo, D. (2019). Preparation and applications of the cellulose nanocrystal. *International Journal of Polymer Science, 5*, 1–10.
61. Song, S., Guo, J., Chen, X., et al. (2013). Progress in application of high pressure microfluidization in preparation of nanomedicines. *Chinese Journal of New Drugs, 22*, 2388–2391.
62. Saito, T., Shibata, I., Isogai, A., Suguri, N., & Sumikawa, N. (2005). Distribution of carboxylate groups introduced into cotton linters by the TEMPO-mediated oxidation. *Carbohydrate Polymers, 61*, 414–419.
63. Saito, T., & Isogai, A. (2006). Introduction of aldehyde groups on surfaces of native cellulose fibers by TEMPO-mediated oxidation. *Colloids and Surfaces A: Physicochemical and Engineering Aspects, 289*, 219–225.
64. Saito, T., Hirota, M., & Tamura, N. (2009). Individualization of nano-sized plant cellulose fibrils by direct surface carboxylation using TEMPO catalyst under neutral conditions. *Biomacromolecules, 10*, 1992–1996.
65. Saito, T., Hirota, M., Tamura, N., & Isogai, A. (2010). Oxidation of bleached wood pulp by TEMPO/NaClO/NaClO2 system: Effect of the oxidation conditions on carboxylate content and degree of polymerization. *Journal of Wood Science, 56*, 227–232.
66. Karim, Z., Mathew, A. P., Grahn, M., Mouzon, J., & Oksman, K. (2014). Nanoporous membranes with cellulose nanocrystals as functional entity in chitosan: Removal of dyes from water. *Carbohydrate Polymers, 112*, 668–676.
67. Kang, X., Kuga, S., Wang, C., Zhao, Y., Wu, M., & Huang, Y. (2018). Green preparation of cellulose nanocrystal and its application. *ACS Sustainable Chemistry & Engineering, 6*, 2954–2960.
68. Mariano, M., El Kissi, N., & Dufresne, A. (2014). Cellulose nanocrystals and related nanocomposites: Review of some properties and challenges. *Journal of Polymer Science Part B: Polymer Physics, 52*, 791–806.
69. Klemm, D., Kramer, F., Moritz, S., Lindström, T., Ankerfors, M., Gray, D., & Dorris, A. (2011). Nanocelluloses: A new family of nature-based materials. *Angewandte Chemie International Edition, 24*, 5438–5466.

70. Brinchi, L., Cotana, F., Fortunati, E., & Kenny, J. (2013). Production of nanocrystalline cellulose from lignocellulosic biomass: Technology and applications. *Carbohydrate Polymers, 94*, 154–169.
71. Chen, L., Zhu, J., Baez, C., Kitin, P., & Elder, T. (2016). Highly thermal-stable and functional cellulose nanocrystals and nanofibrils produced using fully recyclable organic acids. *Green Chemistry, 18*, 3835–3843.
72. Camargo, L. A., Pereira, S. C., Pereira, S. C., Correa, A. C., Farinas, C. S., Marconcini, J. M., & Mattoso, L. H. C. (2016). Feasibility of manufacturing cellulose nanocrystals from the solid residues of second generation ethanol production from sugarcane bagasse. *BioEnergy Research, 9*, 894–906.
73. Barcelos, C. A., Rocha, V. A., Groposo, C., Castro, A. M., Pereira, N., Jr., (2015). Enzymes and accessory proteins involved in hydrolysis of lignocellulosic biomass for bioethanol production. *Mycology: Current and Future Developments, 1*, 23–56.
74. Zhu, J. Y., Sabo, R., & Luo, X. (2011). Integrated production of nanofibrillated cellulose and cellulosic biofuel (ethanol) by enzymatic fractionation of wood fibers. *Green Chemistry, 13*, 1339–1344.
75. Filson, P. B., Dawson-Andoh, B. E., & Schwegler-Berry, D. (2009). Enzymatic-mediated production of cellulose nanocrystals from recycled pulp. *Green Chemistry, 11*, 1808–1814.
76. Henriksson, M., Henriksson, G., Berglund, L. A., & Lindstrom, T. (2007). An environmentally friendly method for enzyme-assisted preparation of microfibrillated cellulose (MFC) nanofibers. *European Polymer Journal, 43*, 3434–3441.
77. Tsukamoto, J., Duran, N., & Tasic, L. (2013). Nanocellulose and bioethanol production from orange waste using isolated microorganisms. *Journal of the Brazilian Chemical Society, 24*, 1537–1543.
78. Camargo, L. A., et al. (2016). Feasibility of manufacturing cellulose nanocrystals from the solid residues of second generation ethanol production from sugarcane bagasse. *BioEnergy Research, 9*, 894–906.
79. Martelli-Tosi, M., Torricillas, M. da S., Martins, M. A., Assis, O. B. G. de, & Tapia-Blacido, D. R. (2016). Using commercial enzyme to produce cellulose nanofibers from soybean straw. *Journal of Nanomaterials, 2016*, 8106814.
80. Hamid, S. B. A., Zain, S. K., Das, R., & Centi, G. (2016). Synergic effect of tungstophosphoric acid and sonication for rapid synthesis of crystalline nanocellulose. *Carbohydrate Polymers, 138*, 349–355.
81. Espinosa, S. C., Kuhnt, T., Foster, E. J., & Weder, C. (2013). Isolation of thermally stable cellulose nanocrystals by phosphoric acid hydrolysis. *Biomacromolecules, 14*, 1223–1230.

82. Dong, S., Cho, H. J., Lee, Y. W., & Roman, M. (2014). Synthesis and cellular uptake of folic acid conjugated cellulose nanocrystals for cancer targeting. *Biomacromolecules, 15*, 1560–1567.
83. Iwamoto, S., Nakagaito, A. N., & Yano, H. (2007). Nano-fibrillation of pulp fibers for the processing of transparent nanocomposites. *Applied Physics A, 89*, 461–466.
84. Bundjaja, V., Sari, T. M., Soetaredjo, F. E., Yuliana, M., Angkawijaya, A. E., Ismadji, S., Cheng, K.-C., & Santoso, S. P. (2020). Aqueous sorption of tetracycline using rarasaponin-modified nanocrystalline cellulose. *Journal of Molecular Liquids, 301*, 112433.
85. Lin, N., & Dufresne, A. (2014). Nanocellulose in biomedicine: Current status and future prospect. *European Polymer Journal, 59*, 302–325.
86. Plackett, D., Letchford, K., Jackson, J. K., & Burt, H. M. (2014). A review of nanocellulose as a novel vehicle for drug delivery. *Nordic Pulp & Paper Research Journal, 29*, 105–118.
87. Lin, N., & Dufresne, A. (2013). Supramolecular hydrogels from *in situ* host-guest inclusion between chemically modified cellulose nanocrystals and cyclodextrin. *Biomacromolecules, 14*, 871–880.
88. Dash, R., & Ragauskas, A. J. (2012). Synthesis of a novel cellulose nanowhisker-based drug delivery system. *RSC Advances, 2*, 3403–3409.
89. Dong, S., Cho, H. J., Lee, Y. W., & Roman, M. (2014). Synthesis and cellular uptake of folic acid-conjugated cellulose nanocrystals for cancer targeting. *Biomacromolecules, 15*, 1560–1567.
90. Jackson, J. K., Letchford, K., Wasserman, B. Z., Ye, L., Hamad, W. Y., & Burt, H. M. (2011). The use of nanocrystalline cellulose for the binding and controlled release of drugs. *International Journal of Nanomedicine, 6*, 321–330.

Innovations in Chemical and Materials Science

(ISBN: 978-81-688266-7-0)

About Editors

Dr. Aarti Dwivedi is an Assistant Professor Grade III with more than 15 years of teaching, research, and academic experience in the field of Chemistry. She holds an M.Sc., B.Ed., and a Ph.D. in Chemistry. Her research interests include Green Chemistry, Corrosion Science, Materials Chemistry, and Sustainable Chemical Technologies. Dr. Dwivedi has published numerous research papers in reputed national and international journals and contributed chapters to edited books. She has also served as an editor of academic publications, reflecting her dedication to advancing scientific knowledge. Her academic pursuits focus on promoting innovative research, interdisciplinary collaboration, and excellence in higher education. She has been honoured with the Society Impact Award in Chemistry, the Indian Inspiration Award, and the Naari Shakti Samman for her outstanding contributions to education, women's welfare, and scientific excellence. She is committed to fostering quality education through research.

Ms. Pratiksha is an experienced educator with more than 15 years of teaching experience in higher education. She completed her M.Sc. in Chemistry from Bareilly College, Bareilly, and is currently pursuing her Ph.D. in Chemistry at Maharaja Agrasen Himalayan Garhwal University, Uttarakhand. She is an Assistant Professor in the Department of Chemistry at Rajshree Group of Institutions, Bareilly. She has published five research papers in reputed international journals and participated in numerous national and international conferences. Her academic interests include environmental studies, chemical sciences, sustainable research practices, and innovative approaches to quality education. She is committed to promoting scientific research, academic excellence, and student development through effective teaching, mentorship, innovation, and lifelong learning.

Dr. Balasaheb Pathare is an Associate Professor in the Department of Chemistry at B. K. Birla College (Empowered Autonomous Status), Kalyan, with 16 years of teaching experience. He holds an M.Sc. in Organic Chemistry, a Ph.D. in Synthetic Chemistry, and has qualified GATE and NET in Chemical Sciences. He has completed one university-sponsored minor research project and supervised 15 student research projects. His research interests focus on the synthesis of heterocyclic compounds. Dr. Pathare has published four research papers in international journals and presented his work at national and international conferences. He has actively participated in numerous seminars, workshops, training programmes, Faculty Development Programmes, and refresher courses, demonstrating his commitment to academic excellence, scientific research, and professional development.

Dr. Satish Piplode is an Assistant Professor at SBS Government Post Graduate College, Pipariya, District Narmadapuram, affiliated with Barkatullah University, Bhopal. He earned his Ph.D. in Physical Chemistry and M.Phil. in Organic Chemistry from Vikram University, Ujjain, and was awarded the UGC National Fellowship for his M.Phil. and Ph.D. studies. He completed his Bachelor's and Master's degrees from Government Holkar Science College, Indore (NAAC A++). With over nine years of experience in research and academia, his expertise includes Nanotechnology, Wastewater Treatment, and Photocatalysis. Dr. Piplode has published more than 40 research papers and two patents. He received the Best Academician Award from the ELSEVIER SSRN Network in 2022. He has also served as Principal of Government College, Bankhedi, and currently supervises one Ph.D. scholar.

Bhumi Publishing

Bhumi Publishing,
Kolhapur, Maharashtra, India
bhumipublishing@gmail.com
www.bhumipublishing.com

ISBN 978-81-688266-7-0